THE EFFECTS OF CROSSLINKING IN POLYMER MISCIBILITY

by

Gabriela Rueda de la Garza, B.Sc., M.Sc.

A thesis submitted for the degree of Doctor of Philosophy of the University of London and for the Diploma of Membership of Imperial College.

Department of Chemical Engineering and Chemical Technology
Imperial College of Science and Technology
London SW7 2BY

December 1987

ABSTRACT

The effect of crosslinking one of the component polymers of a binary blend was studied; particular emphasis was paid to miscibility and phase separation behaviour. The blends selected are based on sulphochlorinated polyethylene (SCPE), a polymer which is easily crosslinkable via its SO_2Cl groups. A total of six blends were examined. SCPEs of different chlorine content were mixed with either a copolymer of ethylene-vinylacetate or two poly(butyl acrylates) of different molecular weight or poly(methyl methacrylate).

After mixing with the second polymer, the SCPE was crosslinked by diffusing the curing agent (diethylenetriamine) into a cast film. The resultant products are semi-IPNs. The degree of crosslinking was determined by swelling and when applicable was derived from static and dynamic moduli. All systems were found to be lightly crosslinked.

The miscibilities of the blends before and after being crosslinked were investigated using the glass transition criteria. With the exception of the blend containing poly(methyl methacrylate), which was miscible for all compositions, the rest of the blends were one phase up to 50 or 60% SCPE content and partially miscible above these compositions. Each of the two phases present in the partially miscible samples was itself a blend with appropriate composition of both polymers. Crosslinking did not alter the number of T_gs observed for each sample; but small shifts in the T_gs for the partially miscible samples suggested slight intermixing between the two phases.

In most systems the phase separation behaviour was measured using the cloud point temperature obtained with various scattering methods. On crosslinking, the cloud point curves shifted to higher temperatures. This phenomenon is a result of a kinetic effect and not thermodynamic. The scattering data also showed that the size of the domains usually decreased after curing.

TO MY FATHER:

WITH ALL MY LOVE,

GRATITUDE

AND

ADMIRATION

As a small measure of my gratitude I want to thank in a very special way **Mr. Richard N. Sheppard**, Senior Research Officer at the Department of Chemistry. He encouraged, supported and guided me continuously since the beginning of my doctoral work. For helping me in the use of several analytical techniques, fundamental to this project. For his numerous and very helpful discussions, for revising and proof-reading this thesis. I truly believe that his support has been essential for the completion of this thesis.

ACKNOWLEDGEMENTS

I also wish to thank:

Mr. Francisco Villaseñor, whose professional quality was a source of inspiration during my studies. I also want to thank him for all his moral support and for his invaluable help in the use of the Apple-Macintosh and the editing of this thesis

Dr. Julia S. Higgins, Reader in Polymer Science and Ph.D. supervisor, my present supervisor, whose assistance, guidance and support proved invaluable for the completion of this work.

Dr. David J.Walsh, former Lecturer and Ph.D. supervisor, my original supervisor, for all his support since the beginning to the completion of this work. He introduced me to the field of Polymer Blends and originated this project.

Dr. John M. Hodgkinson, Senior Research Officer in the Composite Materials Centre, who kindly had numerous and very helpful discussions on mechanical behaviour of polymer blends and other aspects of this thesis and also proof-read it.

Dr. Ann Maconnachie, Senior Research Officer in the Department of Chemical Engineering. For helping me to determine the molecular weight of the polymers studied in this work using the gel permeation chromatograph.

Mr. Ian W. Drummond, Senior Research Officer in the Department of Chemical Engineering. For his guidance with the elemental analysis and gas chromatography. For proof-reading some chapters of this thesis. For his great moral support and encouragement during most stages of my doctoral work.

Dr. Hans J. Michels, Departmental Postgraduate Tutor, for his confidence and great support.

Dr. James A. Barrie, Senior Lecturer and Ph.D. Supervisor at the Department of Chemistry, for his helpful discussions on various aspects of this thesis.

Mrs. Lizbeth Rogel (Lyon Playfair Library) and **Mrs. Elizabeth Corbett**, (Chemical Engineering Departamental Library), for all the help which they provided me so efficiently at these libraries.

Miss Sue Johnson, Mssrs. Chris Murray, John Bilton, Terry Stephenson, Albert Lucas (now retired), Ken Gurney, Bob King, Colin Smith, Dick Wood, Ken Grose, Perminder Amrit, Malcolm Dix, Ron Lewis, for being such charming friends and providing me with all the technical support that I required.

Dr. Alan Freundlich, of Biophysics in the Physics Department, for all his patience and very skillful instruction in the use of the LKB ultramicrotome.

Dr. Peter Prentice, former Research Assistant in the Department of Mechanical Engineering, for helping me in the use of the Nikon Optiphot Universal Microscope and in the processing of some photographic material.

Mr. Sanjoy Ray, postgraduate student and **Dr. David Webb**, Researcher at the BP Research Centre (Sunbury), for their encouragement and support, and for helping me to proof read this thesis.

Financial support is greatly acknowledged from the **National Autonomous University of Mexico, CONACYT**, the **Old Centralians** and **Imperial College**.

Lastly but not the least my **father**, my sisters and brothers: **María Luisa, Patricia, Manuel** and **Mauricio, Mr. Abraham Cruz Ortiz** and **all my friends**, who encouraged me always and made my staying at IC a memorable, very happy and fruitful experience.

TABLE OF CONTENTS

LIST OF TABLES

LIST OF FIGURES

CHAPTER 1
INTRODUCTION

Materials composed of several components are replacing natural materials, metals and homopolymers in increasing amounts. Manufacturers of multicomponent polymer systems are modifying the properties of homopolymers to obtain superior materials. These materials are either stronger, tougher, more flexible, will withstand environmental influences, or have other desirable characteristics. At the present time, the scientific and patent literature describes over 150 distinguishable ways of organizing two kinds of polymers in mixtures [158]. Graft, block copolymers, polymer blends and interpenetrating polymer networks (IPNs) are the main types of polymer mixtures [2, 3, 158]. Figure 1.1 illustrates the topologies of all these polymer mixtures [13].

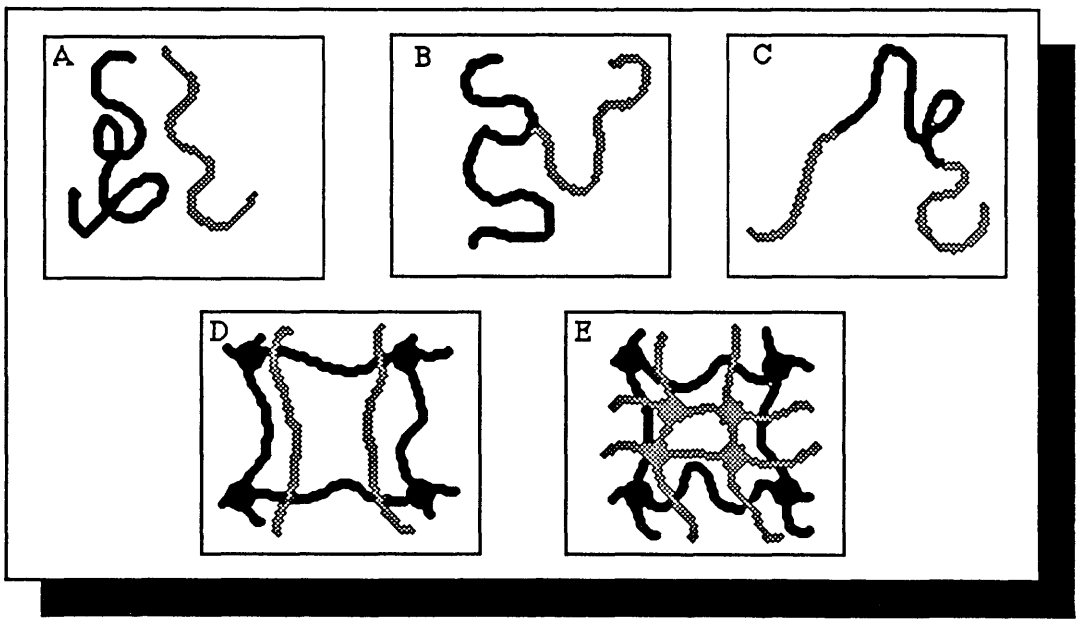

Figure 1.1 Schematic diagram of some two-polymer combinations: (A) a polymer blend; (B) a graft copolymer; (C) a block copolymer; (D) a semi-IPN; (E) an IPN.

As shown in this figure a blend is a combination of two polymers without any chemical bonding between them (figure 1.1A). In a graft copolymer two different

polymers are in a single molecule, but do not form a linear chain (figure 1.1B). Block copolymers contain two different polymer subunits in a single linear molecule (figure 1.1C). IPNs are a mixture of two polymers in which one or both components are in a network form, in the first case they are called semi-IPN (fig. 1.1D), the second case constitutes a true IPN.

In this work a study is made of the ways in which the original properties of a binary blend are affected by crosslinking one of the components. When one component is crosslinked the resulting blend is a type of semi-IPN: the major areas of concern in this project will therefore be the properties of polymer blends and IPNs. There are many aspects of interest to discuss which relate to these two types of polymer mixtures (preparation methods, miscibility behaviour, phase separation, thermodynamic theories, etc.) which will be discussed in chapter 2. At this point it will be sufficient to discuss some basic ideas about these subjects.

One of the first properties to determine in any type of mixture is its miscibility behaviour. In classical thermodynamics two substances are considered to be miscible when their mixture behaves as a one phase system. In this context one phase means that the chemical composition and the physical properties are uniform throughout [5]. This concept, which is generally applied to mixtures of substances of low molecular weight, cannot strictly be applied to polymer mixtures as the level of molecular mixing achieved by the two polymers is related to the macroscopic properties used in the determination of the single phase behaviour [2, 3]. Fortunately thermodynamics offers the most powerful criterion of miscibility: the composition dependence of the Gibb's free energy of mixing which requires that

$$(\partial^2 \Delta G_m / \partial \phi^2)\, T, P > 0 \qquad 1.1$$

where ϕ is the volume fraction of one of the components and ΔG_m is the Gibbs free energy of mixing.

With this criterion there is no need for a detailed knowledge of the scale of mixing of the molecules, so the above problem can be solved in principle. Unfortunately its use is quite restricted because of difficulty in its experimental determination. Other criteria are therefore used for determining polymer-polymer miscibility. Among the most commonly used are: glass transition, microscopy, scattering methods, ternary solution methods and methods based on thermodynamic properties.

Although a host of miscible systems have been identified [3, 8], miscibility of polymer mixtures is more an exception than a rule. This is mainly a consequence of the large molecular weight of the polymers. If $\Delta G_m < 0$ (see equation 1.1) is chosen as a criterion for miscibility (this is a necessary criterion but not sufficient) and

$$\Delta G_m = \Delta H_m - T\Delta S_m \qquad 1.2$$

the value of ΔS_m (the entropy of mixing) will be almost negligible as a consequence of the large molecular weights of the polymers and so ΔH_m (the enthalpy of mixing) will be almost entirely responsible for miscibility. According to the above criterion, then, there are three cases in which one phase systems may be achieved: (1) In polymers of low molecular weight, where ΔS_m is not negligible. (2) In polymer mixtures in which both components are very similar in composition (this minimizes values for ΔH_m). (3) In polymers with favourable ΔH_m arising from specific interactions between them [7].

As miscibility in polymer blends is rather uncommon, it is not surprising to see that there has been considerable research into methods of improving miscibility in polymer mixtures. If the components of a blend are close to miscibility and it is suspected that ΔG_m is not greatly positive, minor changes in the structure of the polymer may render the mixture miscible.The following modifications have been found to enhance miscibility: the introduction of strong specific interactions, permanent attachment of the components of the blend via block and graft copolymers, crosslinking and formation of IPNs [3, 11, 12].

Crosslinking appears to be the most drastic method for increasing the miscibility between the components of a blend as covalent links are introduced between the components. Examples are SBR-BR and NR-BR, these systems are blended and then crosslinked. There are various methods of introducing crosslinks in a polymer mixture (via peroxides, radiation, polymerization of a monomer in the presence of the second polymer component (*insitu* polymerization), etc [3]). The method used depends on the characteristics of the components in the blend. Higher levels of molecular mixing have been achieved by forming IPNs, which may be prepared via *insitu* polymerization and crosslinking techniques. Interesting examples are: poly(urethane)/poly(acrylate)[11] and poly(ethyl acrylate)/poly(styrene-co-methylmethacrylate) IPN [12].

Before using a blend for any specific application it is important to know its miscibility behaviour. If the blend is miscible then it is also convenient to know its phase boundary. Miscible blends are thermodynamically stable and can only become phase separated by driving forces which are thermodynamic in origin. Phase separation in polymer mixtures is generally brought about by variations in temperature, pressure and / or composition.

In a similar way to liquid-liquid mixtures of low molecular weight components, polymer blends may have different types of phase behaviour. These phase boundaries may look like those shown in figure 1.2

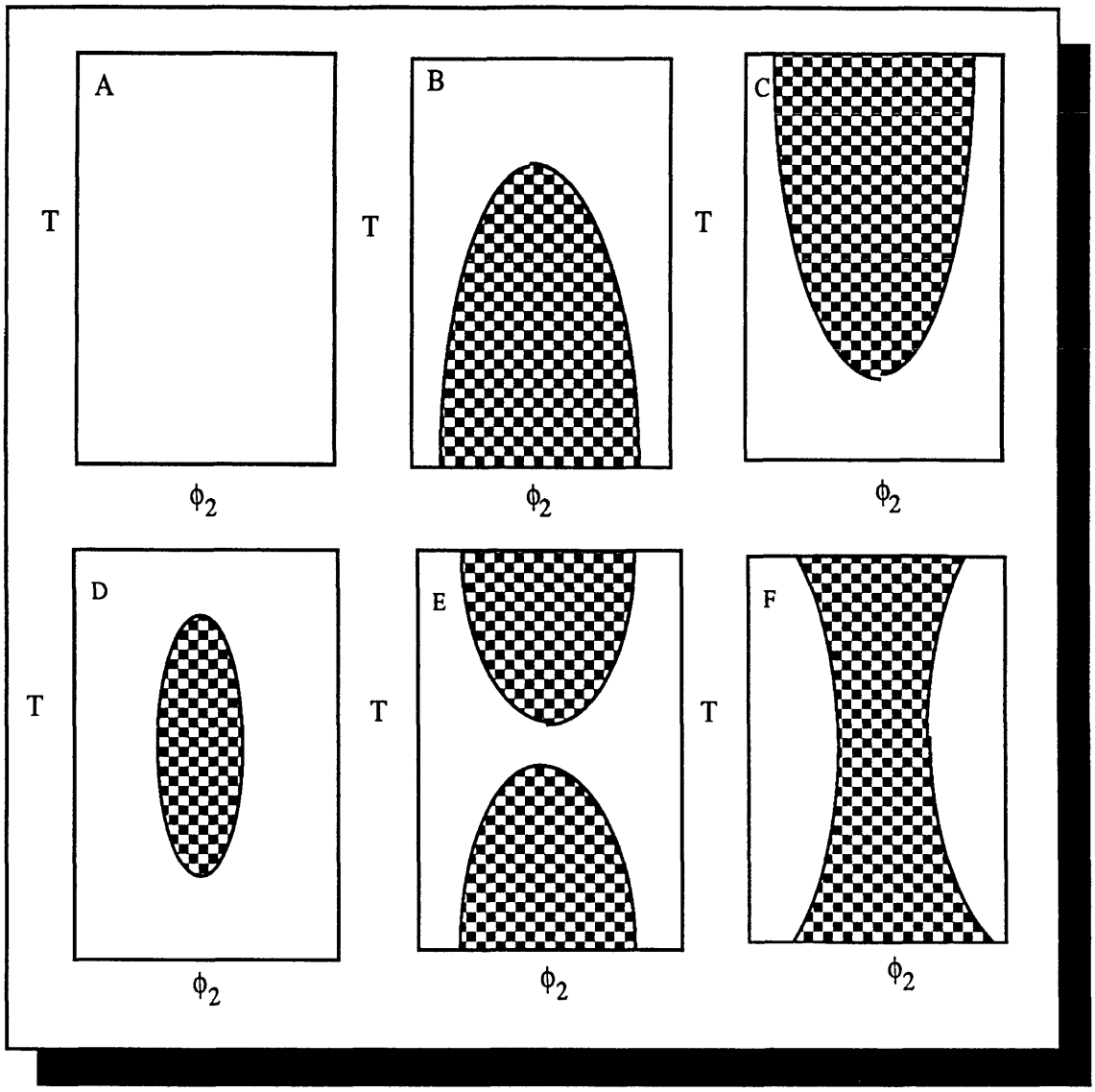

Figure 1.2 Liquid-liquid temperature-composition phase diagrams. Shaded areas represent the temperature-composition regimes of a solution where phase separation occurs.

Figure 1.2A illustrates the behaviour of a mixture which is completely miscible. Figure 1.2B shows the behaviour of mixtures that phase separate on cooling, these systems have an Upper Critical Solution Temperature (UCST). This is observed in liquids and in polymer mixtures of modest molecular weight. Figure 1.2C represents the behaviour of a mixture which phase separates on heating. This is typically observed in mixtures of polymers of high molecular weight. These systems have a Lower Critical Solution Temperature (LCST). Figure 1.2D shows a mixture with the UCST above the LCST (closed phase diagram). In 1.2E the system exhibits both an UCST and a LCST. Figure 1.2F shows an hourglass shaped phase diagram [2] sometimes seen in polymer solvent systems. The phase boundaries of mixtures of monodisperse polymers may

look very similar to those in figure 1.2, but in reality polymers are polydisperse and their phase boundaries may be more complicated. They might even show bimodalities, as pointed out by Allen [9] and Koningsveld[10].

1.1 PROBLEMS AND OBJECTIVES OF THIS WORK

In this work the crosslinking of one of the components of a blend produces a semi-IPN and, as previously mentioned, the main interest is to see how this affects the original miscibility behaviour of the system. The blends under study are based on sulphochlorinated polyethylene (SCPE) of different degrees of chlorination mixed either with ethylene-vinyl acetate copolymer (EVA), or with poly(butyl acrylate) (PBA) or with poly(methyl methacrylate) (PMMA).

Due to its industrial importance, PVC is one of the most extensively investigated components for polymer blends. At the present moment there are around a hundred different types of blends based on this polymer [3, 8]. However, in spite of PVC's capability of being miscible with a great number of polymers and its unquestionable practical significance, it is not a very convenient polymer to use in miscibility studies. The reasons are: (a) PVC's morphology is not yet fully understood and (b) its complex semicrystalline structure has been found to persist even in polymer blends which are ostensibly miscible. This fact makes the interpretation of the miscibility of PVC blends uncertain and difficult [21]. Chlorinated polyethylenes (CPE) and sulphochlorinated polyethylenes (SCPEs) at 30% chlorine content do not contain crystalline regions because the chlorine atoms are randomly distributed and make the structure less regular. These polymers are therefore a better choice for miscibility studies. Besides this, CPEs and SCPEs offer extra advantages; their chlorine content can be varied easily, which is very useful for studies of specific interactions, and in the case of the SCPE the SO_2Cl groups enable it to be crosslinked.

As CPEs and SCPEs are very similar in chemical structure to PVC it is expected that their miscibility behaviour will resemble that exhibited by PVC blends. Many polymers which are miscible with PVC (e.g. syndiotactic PMMA [16], ethylene-vinyl acetate copolymer [17], poly(ε-caprolactone)[18], some poly(acrylates) [19] and poly(methacrylates) [20]) have the carbonyl unit as common entity. It is therefore expected that the SCPEs studied in this project should be miscible with the polymers chosen, as these also contain carbonyl groups.

CPEs and SCPEs of varying degrees of chlorination have been blended with several

polymers and copolymers [3,8]. CPE with 30% chlorine has been reported to be miscible with chlorinated poly(isoprene) and with chlorinated poly(vinyl chloride) (except at 1 to 1 composition) but immiscible with PVC, poly(ethyl acrylate), PMMA and copolymers of poly(vinyl chloride-co-vinyl acetate) [22, 23]. Blends of PVC/CPE (CPE containing 30% Cl) and PVC/SCPE (SCPE containing 29.5% Cl and 1.6%S) were found to be immiscible [22]. Doubé and Walsh [24] found that PVC and SCPE were miscible, when the SCPE contained 43% Cl and 1% S as SO_2Cl. The blend exhibits a phase diagram with a LCST around 120°C. The heat of mixing was found to be negative and in agreement with the low values of the interaction parameter between both polymers [25]. In further research, Walsh [21] showed that the dimensions of the chain length for this blend are consistent with a single phase system. It is thought that due to the chemical similarity between PVC and SCPE, there are only dipole-dipole interacions and London dispersion forces, but no specific interactions.

Chai and Walsh [26] found that the blend CPE/PMMA was miscible when the CPE contained from 50 % of Cl upwards. The blends showed a LCST. Heats of mixing were measured using CPE and PMMA analogues of low molecular weight. When the analogue contained less than 50% Cl, the ΔH_m values were positive. With increasing Cl content, ΔH_m became less positive until it finally became negative for a chlorine content around 50%. CPE/poly(butyl acrylates) blends behave in a similar way. They were found to be miscible and exhibit a LCST for CPEs with chlorine contents around and above 50% [27]. The values of ΔH_m for PBA with analogues of CPE of low molecular weight were found to disagree with the miscibility of the blends. After some adjustment of the thermodynamic parameters, it was found that the theoretical simulations of the phase boundaries of this system closely matched the experimental ones.

In the case of blends of CPE or SCPE with the copolymer of ethylene-co-vinyl acetate (EVA), the miscibility was again found to be dependent on the chlorine content of CPE and SCPE and on the vinyl acetate (VA) content of EVA. A CPE containing 52.65% Cl and two commercial SCPEs, containing 1% of S and 40% and 43% Cl respectively, were mixed with two commercial EVAs, one containing 40% VA and the other 45% VA. It was found that all these blends were miscible and that the polymers with a higher concentration of functional groups, chlorine or acetate respectively, showed a higher LCST and were hence more compatible [28,29]. Measurements of the ΔH_m and the interaction parameter for the blend of CPE with 52.65% Cl and EVA with 45% VA confirmed the experimental behaviour [29].

Although these blends have been studied in great detail, there are interesting aspects which have not yet been considered. One of these provides the framework of the present

research; this is the effect on miscibility and phase separation behaviour when one of the components of these blends has been crosslinked. As mentioned earlier, after crosslinking one of the components of a blend the product is a semi-IPN. Several researchers have previously studied the miscibility and phase separation behaviour of semi-IPNs and IPNs. Donatelli and coworkers [107] studied IPNs and semi-IPN of the copolymer styrene-butadiene with poly(styrene). In the semi-IPN, the poly(styrene) was the crosslinked polymer; phase separation was observed in this system. Nishi and Kwei[140] studied the miscible blend poly(vinyl methyl ether)/poly(styrene). They found that after crosslinking, phase separation occured at higher temperature. Allen and coworkers[150] investigated a semi-IPN of PMMA/poly(urethane) where the poly(urethane) was crosslinked. By analysing the dynamic mechanical and dielectric relaxation data they found that the miscibility of the system increased after crosslinking. Coleman and coworkers[157] studied semi-IPNs of phenolic resin/EVA_{70} (70 wt% VA). Using Fourier transform infrared spectroscopy they found that the systems were phase separated. Miscible IPNs and semi-IPNs have been reported by Frish and coworkers[154], who prepared blends, semi-IPNs and IPNs of polystyrene and poly(2,6-dimethyl-1,4-phenylene oxide) which exhibited single T_gs that varied systematically with composition. In addition, no evidence of phase separation was seen by electron microscopy.

In the case of a single polymer, crosslinking introduces several changes with respect to its original properties, such as an increase in the values of T_g, Young's modulus (Y) and loss modulus (E'), and a decrease in the level of swelling by solvents. In the case of a polymer blend, besides changes in its miscibility and phase separation behaviour, it is also expected that by crosslinking one of the components, changes in its overall behaviour must occur. The goal of this research was to examine all these modifications. To achieve this goal it was necessary :

(1) To select a suitable curing agent to be able to crosslink the polymer when blended.

(2) To determine and to compare the miscibility and phase separation behaviour of the blends before and after being crosslinked.

(3) To quantify the degree of crosslinking of the polymer when blended using swelling and shear modulus measurements.

(4) To measure and compare E and E' of the blends before and after crosslinking.

(5) To compare the size of the domains after crosslinking after phase separation has taken place in uncrosslinked and crosslinked blends.

(6) To elucidate if possible the mechanism of phase separation of the unmodified and

crosslinked blends.

In order to undertake this research, systems similar to those described above containing one component which is easily crosslinkable had to be selected. Both of these conditions are successfully met if SCPEs are used in the blends. With this in mind the blends chosen for this project were:

(a) SCPE containing 43% Cl and 1% S as SO_2Cl ($SCPE_{43}$) mixed with PVC ($SCPE_{43}$/PVC): this is the same system as studied by Doubé and Walsh [24,25].

(b) $SCPE_{43}$ mixed with EVA containing 45 % VA ($SCPE_{43}/EVA_{45}$). This blend was studied by Walsh and coworkers under the name of H_{48}/EVA_{45} [28, 29].

(c) A sulphochlorinated poly(ethylene) containing 54% Cl and 0.98% S as SO_2Cl groups ($SCPE_{54}$) mixed with EVA_{45} ($SCPE_{54}/EVA_{45}$). This system was selected as similar to CPE3/EVA45 (CPE3 contained 52.65 Cl)[28,29].

(d) $SCPE_{54}$ mixed with a PBA of M_n=27,000 ($SCPE_{54}/PBA_{LMW}$). This system was the most similar to PBA/CPE_{20} studied by Walsh and coworkers [27]. (CPE_{20} contains 62.1% Cl).

(e) $SCPE_{54}$ mixed with a PBA of higher molecular weight (M_n = 183,000) than that in (d) ($SCPE_{54}/PBA_{HMW}$).

(f) $SCPE_{54}$ mixed with a commercial PMMA ($SCPE_{54}/PMMA_{1.4}$) which is very similar to PMMA/CPE16, studied by Chai and Walsh [26]. (CPE16 contains 51.6% Cl).

Besides offering the possibility of studying the effect of crosslinking the $SCPE_{43}$ or $SCPE_{54}$ on their miscibility and phase behaviour, these blends were chosen because they offer other aspects of interest. In the system (a), it is feasible to prepare the blend by two different procedures, therefore the influence of the preparation method on the miscibility behaviour of the system may also be studied. The blends (b) and (c) are very similar, only differing in the chlorine content of the SCPE used. As previously shown in similar blends containing CPE, those with the highest chlorine content are more miscible with EVA, it is therefore interesting to determine whether the same behaviour occurs in (b) and (c). The chemical structure of the two components in systems (d) and (e) is very similar, the only difference being the higher molecular weight of the PBA in (e). Hence, thermodynamically, the blend with the PBA of higher M_n should be less miscible than that containing the other PBA. It will be possible to determine whether that occurs in these two systems. The blend (f) was chosen because PMMA has a higher density of carbonyl groups than PBA and therefore PMMA should have a stronger specific interaction with the acidic proton of the $SCPE_{54}$ than that between the SCPE and PBA in the blends (d) and (e). This suggested that (f) should be more miscible than (d) and (e).

CHAPTER 2
SUBJECT REVIEW

As mentioned in chapter 1, the main objective of this research is to study the effect of crosslinking on the miscibility and phase separation behaviour of some blends based on sulphochlorinated polyethylene. Central to this problem is the study of the miscibility of these polymers, their phase separation behaviour, crosslinking reactions, the determination of their degree of crosslinking and the mechanical properties of these blends before and after being crosslinked. The purpose of this chapter is to provide a brief revision of the basic theories and principal experimental methods.

2.1 PRINCIPAL THERMODYNAMIC THEORIES OF POLYMER MISCIBILITY

Polymer solution theories are closely related to the development of general solution theory. Between 1880 and 1920, the basis of solution theory was established by such workers as Van't Hoff (the concept of osmotic pressure), Raoult (Raoult's law), and Van der Waals (equation of state for pure components and mixtures) [32]. In the late 1920's increasing experimental evidence showed that the liquid state had many features in common with crystals, and mainly for this reason many attempts have since been made to explain the behaviour of liquid solutions based on lattice models [30]. Gugenheim[30] produced the clearest and most complete formulation in 1952. The lattice method was developed from two points of view: in the first, a simplified lattice model was derived from a purely statistical approach; the second method was developed from the statistical mechanical partition function and includes cell theories, hole theories, tunnel theories and the Monte Carlo and molecular dynamic models [3]. In the 1930s, Fowler and Rushbroke [3, 34], using the simplified lattice model, were the first to extend the concept of a regularly arranged set of rigid lattices to polymer solutions. T.S. Chang[3] used this concept to derive an expression for the entropy of athermal mixing. In 1942, Flory [3, 32, 33] and Huggins [3, 32, 43], simultaneously but independently, extended Chang's formalism to the evaluation of the combinatorial factor for polymer solutions.

As this formulation is based on a very simple model, it fails to account for the real contribution of the entropy of mixing (ΔS_m) to the Gibbs free energy of mixing (ΔG_m) and is unable to predict the change on mixing of quantities related to the equation of state, such as volume, compressibility, etc. Prigogine [3, 35, 37] extended the Lennard-Jones and Devonshire cell model to polymer solutions deriving a principle of corresponding states. As this approach was found to disagree with experimental results, Flory [3, 35, 37] developed a new approach based on Eyring and Hirschfelder's cell model. Because this approach is simple, it is very frequently used in polymer mixtures. However it too fails where the cell model fails. In the 1960's, the hole theories were extended to polymer solutions overcoming some of the problems which the cell model could not handle. Among the most important of these new theories is the lattice fluid theory of Sanchez and Lacombe [40, 41, 42], which has been extended to polymer mixtures.

In the next sections the Flory-Huggins lattice theory and the Flory equation of state will be reviewed. Before introducing these theories, it is convenient to remember some of the basic concepts of the classical theories for solutions of small molecules, i.e. the ideal and the regular solution theories.

2.1.1 THERMODYNAMICS OF SOLUTIONS OF LOW MOLECULAR WEIGHT

2.1.1.1 IDEAL SOLUTIONS [1, 3, 31]

A solution behaves ideally when the molecules of the components are sufficiently alike to be under the same forces in the mixture as in the pure components. Ideal solutions follow Raoult's law. Substituting Raoult's law into the appropirate expressions it can be easily shown that

$$\Delta G_m = NRT\Sigma x_i \ln x_i \qquad 2.1$$

and as

$$\Delta S_m = (\partial \Delta G_m / \partial T)_{P,Ni} \qquad 2.2$$

then

$$\Delta S_m = NR\Sigma x_i \ln x_i \qquad 2.3$$

where x_i is the mole fraction of the ith component and N is the total number of moles.

In ideal solutions ΔH_m is zero, therefore ΔG_m is only a function of ΔS_m and is always negative. This implies that the components of an ideal solution are completely miscible. As ΔG_m is, in this case, independent of P and T the change in volume of

mixing (ΔV_m) will be zero:

$$\Delta V_m = (\partial \Delta G_m / \partial P)_{T, Ni} = 0 \qquad 2.4$$

Although, in practice, solutions seldom behave ideally, it is convenient to use the ideal solution model as a standard for comparison.

2.1.1.2 REGULAR SOLUTIONS

In 1906 Van Laar [32] expressed the heat of mixing by

$$\Delta H_m = [(x_1 x_2 V_1 V_2) / (x_1 V_1 + x_2 V_2)][(a_1^{1/2} / V_1) - (a_2^{1/2} / V_2)]^2 \qquad 2.5$$

where V_1 and V_2 are the molar volumes of component 1 and 2, a_1 and a_2 come from Van der Waals expression for the parameter "a":

$$a = x_1^2 a_1 + 2 x_1 x_2 a_{12} + x_2^2 a_2 \qquad 2.6$$

Equation 2.5 is known as the Van der Waals-Van Laar equation for ΔH_m and is important because it expresses a basic thermodynamic property of a mixture in terms of the properties of its pure components [32].

In 1931 G. Scatchard [3, 32] derived the following expression in terms of the "cohesive energy density" of the pure components:

$$\Delta H_m = (N_1 + N_2) z \Delta w x_1 x_2 \qquad 2.7$$

where z is the coordination number and Δw is the exchange energy:

$$\Delta w = (1 / 2) \varepsilon_{11} + (1 / 2) \varepsilon_{22} - \varepsilon_{12} \qquad 2.8$$

where ε_{ij} is the energy of contact between components i and j.

In 1933 Hildebrand and Wood [3, 32] derived the same equation and a simplified version appeared in 1970:

$$\Delta H_m = RT \ln (a_2 / x_2) = V_2 \phi_1^2 (\delta_1 - \delta_2)^2 \qquad 2.9$$

or

$$\Delta H_m = V_m (\delta_1 - \delta_2)^2 \phi_1 \phi_2 \qquad 2.10$$

where $a_2 = p_2 / p_2^o$, V_2 is the molar volume of component 2; V_m is the total molar volume; ϕ_1, ϕ_2 are the volume fraction of each component and δ_1, δ_2 are the solubility parameters of each component. This parameter is defined as

$$\delta = (\Delta E^V / V)^{1/2} \qquad 2.11$$

where ΔE^V is the energy of vaporization.

The ΔS_m is the same as for ideal solutions and so substituting equations. 2.7 or 2.9 and 2.2 into 1.2 (p. 3) the following expression for ΔG_m is obtained :

$$\Delta G_m = (N_1 + N_2) z \Delta w x_1 x_2 + kT (N_1 + N_2)(x_1 \ln x_1 + x_2 \ln x_2) \qquad 2.12$$

This equation predicts UCST behaviour and is restricted to non polar systems with equivalent molar volume ($\Delta V_m = 0$) and positive ΔH_m [32].

2.1.2 THE FLORY-HUGGINS LATTICE THEORY

2.1.2.1 SOLUTIONS OF POLYMERS WITH LOW MOLECULAR WEIGHT SOLVENTS

Solutions with components that differ widely in molar volume are not properly described by the Ideal or Regular Solution theories; the reason being that they use the mole fraction as a composition variable which is not representative for this type of mixture. In 1941 Flory [1, 3, 32, 33] and Huggins [3, 32, 43] calculated the ΔS_m for a chain in a solvent using the volume fraction ϕ as a composition variable:

$$\phi_1 = N_1 / [N_1 + (V_2 / V_1) N_2] \qquad 2.13$$

where V_1 and V_2 are molar volumes of components 1 and 2 respectively.

In their statistical analysis they calculate Ω, that is the total number of possible ways of arranging N_2 polymer molecules in a lattice. In such a calculation the polymer molecules are divided into r segments of size equal to that of the solvent molecule.The polymer segments are arranged in contiguous sites of the lattice because of their chain like characteristics. The resultant expression for Ω is:

$$\Omega = [N! / (N - rN_2)! N_2!] [(z - 1) / N]^{N(r-1)} \qquad 2.14$$

which after being substituted and simplified into the following expression

$$S_c = k \ln \Omega \qquad 2.15$$

yields:

$$S_c = -k [N_1 \ln(N_1 / (N_1 + rN_2) + N_2 \ln(N_2 / N_1 + rN_2) - N_2 (r - 1) \ln(Z-1) / e] \qquad 2.16$$

where S_c is the configurational entropy of mixing a perfectly ordered pure polymer and a pure solvent; k is the Boltzmann constant and Z is the number of neighbours next to an occupied cell.

The third term in expression 2.16 is the ΔS of disorientation of the molecules during mixing (ΔS_d). This term is difficult to evaluate but fortunately it is of little quantitative significance compared with the rest of the terms in the equation which constitutes the Flory-Huggins expression for ΔS_m:

$$\Delta S_m = -k\{N_1 \ln [N_1 /(N_1 + rN_2)] + N_2 \ln[N_2 /(N + rN_2)]\} \qquad 2.17$$

where $V_1 / V_2 = r$

Equation 2.17 can also be expressed as

$$\Delta S_m = -k(N_1 \ln\phi_1 + N_2 \ln\phi_2) \qquad 2.18$$

Equations 2.17 or 2.18 are used for monodisperse polymers. For polydisperse polymers the following generalized expression can be applied:

$$\Delta S_m = -k(N_1 \ln\phi_1 + \Sigma' N_i \ln\phi_i) \qquad 2.19$$

The first term represents the solvent, the second the polydisperse polymer.

The ΔH_m expression is similar to that of the regular lattice theory but has some modifications because: (a) in this case the interactions are between the segments of the polymers and (b) the number of dissimilar contact neighbours (p_{12}) vary with each arrangement. The ΔH_m is then:

$$\Delta H_m = \Delta w_{12} \tilde{p}_{12} \qquad 2.20$$

where Δw_{12} is the same as in equation 2.8 and p_{12} is given by:

$$\tilde{p}_{12} = z r_2 N_2 \phi_1 = z r_1 N_1 \phi_2 \qquad 2.21$$

where $z r_2 N_2$ is the total number of contacts betwen polymer molecules in the solution.

The probability that an adjacent site to a polymer molecule is occupied by a solvent molecule is proportional to ϕ_1 (volume fraction of the solvent). The term r_1 is introduced as a generalization that allows the extension of the expression to polymer mixtures. If 2.21 is introduced into 2.20 a new expression for ΔH_m is obtained

$$\Delta H_m = \Delta w_{12} z N_1 \phi_2 r_1 \qquad 2.22$$

If 2.22 is multiplied by kT/kT it becomes:

$$\Delta H_m = kT \chi N_1 \phi_2 \qquad 2.23$$

where χ is the interaction parameter (this parameter measures the interaction energy per solvent molecule) and is equal to

$$\chi = z \Delta w_{12} r_1 / kT \qquad 2.24$$

Introducing equations 2.23 and 2.20 into 1.2 (see p. 3) a new expression for ΔG_m is then obtained:

$$\Delta G_m = kT (\chi N_1 \phi_2 + N_1 \ln\phi_1 + N_2 \ln\phi_2) \qquad 2.25$$

This expression is used for monodisperse polymers; for polydisperse polymers the following expression is applicable:

$$\Delta G_m = kT (\chi N_1 \phi_2 + N_1 \ln\phi_1 + \Sigma' N_i \ln\phi_i) \qquad 2.26$$

where the term $N_1 \ln\phi_1$ corresponds to the solvent and $\Sigma' N_i \ln\phi_i$ is for the polydisperse polymer.

By differentiating 2.25 with respect to N_1, the change in chemical potential during mixing is obtained

$$\mu - \mu_1^o = RT \{ \ln (1 - \phi_2) + [1 - (1/r)\phi_2] + \chi \phi_2^2 \} \qquad 2.27$$

Solving 2.27 for χ yields

$$\chi = [(\mu - \mu_1^o) / RT \phi_2^2] - \{ \ln(1 - \phi_2) + [1 - (1/r)] \phi_2 \} / \phi_2^2 \qquad 2.28$$

where χ is assumed to be independent of composition and inversely proportional to temperature.

2.1.2.2 POLYMER-POLYMER MIXTURES [3]

The extension of the Flory-Huggins lattice theory for solutions of polymers with solvents of low molecular weight to polymer blends gives rise to serious conceptual problems as the same lattice model has to be applied to the latter case. Fortunately these problems are easily overcome as the lattice parameters do not need to be taken into consideration in the final expressions for ΔG_m. In order to give a more realistic approach it is convenient to express ΔG_m on a volume basis which can be easily achieved by dividing 2.26 by

$$V = N_1V_1 + N_2V_2 \qquad 2.29$$

giving

$$\Delta G_m / V = kT [(\phi_1 / V_1) \ln\phi_1 + (\phi_2 / V_2) \ln\phi_2] + (z\Delta w\phi_1\phi_2) / V_2 \qquad 2.30$$

where the term in square brackets correspond to ΔS_m and the last term is ΔH_m. Due to the large values of V_1 or V_2, ΔS_m tends to contribute very little to ΔG_m, so ΔH_m is almost entirely responsible for the value of ΔG_m.

The Flory-Huggins theory has many advantages over the ideal or regular solution theories as it describes the behaviour of polymer-solvent solutions and polymer blends in a more realistic way. It can predict the UCST and provides a framework for fractionation studies [1]. However the theory can not predict LCST behaviour, and the interaction parameter is considered to be concentration independent and to contribute only to ΔH_m whilst in fact it also contributes to ΔS_m [39]. Since it is based on the Regular solution theory it is unable to predict the change in any quantity related to the equation of state such as ΔV_m [39]. It is important to point out that the Flory-Huggins theory is not applicable at high dilutions; the above relationships are only applicable at concentrations in which the randomly coiled molecules overlap one another extensively[1].

2.1.3 FLORY EQUATION OF STATE THEORY

As mentioned before, Prigogine [3, 35, 37] developed the first equation of state for chain molecules. This equation proved to be of little value because it assumes quasicrystalline order which suppresses randomness, a foremost characteristic of the liquid state. However he was able to produce a law of corresponding states for chain molecules wich was quite successful. This fact encouraged Flory and coworkers [35] to develop an equation of state theory which could overcome the limitation in Prigogine's equation of state, and which was capable of being extended to polymer mixtures [36-38].

The Flory equation of state [39] was based on Eyring and Hirschfelder's cell model[37]. The derivation considers the number of ways that particles of volume v* can be placed into a configurational space of cells of volume v. As v* is always less than v, additional volume is accessible to the system. The intermolecular energy E_0 is considered to be only a function of the volume ($E_0 \alpha 1/v^n$). The intersegmental energy is assumed to arise from interactions between the surfaces of adjoining segments. In the development of the equation of state, Flory and coworkers [35-38] first calculated a statistical mechanical partition function Z from which they determined the equation of state.

2.1.3.1 THE PARTITION FUNCTION AND EQUATION OF STATE

The generalized function chosen by Flory and coworkers [37, 38] was of the form:

$$Z = \Omega e^{(-Eo / KT)} \qquad 2.31$$

where Ω is the partition function of N non-interacting molecules in a volume V and E_0 is the mean intermolecular energy of the system per molecule.

The Ω in 2.31 is based on the analysis by Tonks [37, 38] of a unidimensional system of N hard and non-attractive particles arranged on a line of length L

$$\Omega = [(1 - l^*) e^N] \qquad 2.32$$

where l^* is the hard-core length of a particle, $l = L / N$ and e^N is the communal entropy.

Tonks extended equation 2.32 to three dimensions and then Flory and coworkers adapted the resultant expression to polymer liquids by the introduction of the concept of a "polymer segment" (r), which is an arbitrarily chosen isometric portion of the chain molecule:

$$\Omega = [\gamma e^3 (v^{1/3} - v^{*1/3})^3]^{Nrc} \qquad 2.33$$

where $\gamma = l^{*3} / l$ is a geometric factor, $v = V / rN$, v^* is the hard core volume, c is a term originally introduced by Prigogine [34, 35, 37, 38] which is related to chain interconnectivity, 3Nr is the number of degrees of freedom related to internal motions.

E_0 in 2.31 takes a Van der Waals form (inversely proportional to the volume) and due to the short range of the forces between molecules is represented by [38]:

$$E_0 = - Nrs\eta / 2v \qquad 2.34$$

where s is the number of intermolecular contact sites per segment, η is a constant characterizing the energy of interaction for a pair of neighbouring sites, v is the volume per segment.

Introducing equation 2.34 and 2.33 into 2.31 the partition function for a chain molecule is obtained:

$$Z = Z_{comb} [\gamma (v^{1/3} - v^{*1/3}) ^3]^{rNc} e^{-Nrs\eta / 2v} \quad 2.35$$

where Z_{comb} is the combinatorial factor which takes into account the number of ways of arranging rN elements among one another without regard to the precise location of each relative to its chosen neighbour. This term absorbs e^N.

Equation 2.35 can be expressed in reduced variables as:

$$Z = Zcomb (\gamma v^*)^{Nrc} (v^{1/3} -1)^{3Nrc} e^{(Nrc/\tilde{v}\tilde{T})} \quad 2.36$$

where

$$\tilde{v} = v / v^* \quad 2.37$$

$$\tilde{T} = T / T^* = 2v^*ckT / s\eta \quad 2.38$$

$$\tilde{p} = p / p^* = 2pv^{*2} / s\eta \quad 2.39$$

$$p^* = ckT^* / v^* \quad 2.40$$

$$p^*v^* / \tilde{v} = -E_o / rN \quad 2.41$$

where the starred quantities are the parameters of the equation of state.

The equation of state can be derived from 2.35 or 2.36 using either of the following relationships:

$$p = kT (\partial \ln Z / \partial v)_T \quad 2.42$$

or in reduced variables:

$$\tilde{p} = \tilde{T} / xNc (\partial \ln Z / \delta \tilde{v})_T \quad 2.43$$

Introducing equation 2.36 into 2.43 and after suitable mathematical manipulation the following equation of state expressed in reduced variables is obtained:

$$\tilde{p}\tilde{v} / \tilde{T} = [\tilde{v}^{1/3} / (\tilde{v}^{1/3} -1)] - (1 / \tilde{v}\tilde{T}) \quad 2.44$$

Equations 2.35 or 2.36 and 2.44 are practically identical to Eyring and Hirschfelder's expressions for the partition function and equation of state [37], the only differences are the parameter " c" and the way T* is defined [34].

Equation 2.44 takes a simple form when p = 0:

$$\tilde{T} = (\tilde{v}^{1/3} -1) / \tilde{v}^{4/3} \quad 2.45$$

from which it follows that:

$$\tilde{v}^{1/3} - 1 = (\alpha T / 3) / (1 + \alpha T) \quad 2.46$$

where α is the thermal expansion coefficient ($\alpha = \partial \ln v / \partial T)_{p=0}$

If equation 2.44 is differentiated and equations 2.39 and 2.40 are substituted into it the following expression is obtained:

$$p^* = \nu T \tilde{v}^2 \quad 2.47$$

where ν is the thermal pressure coefficient ($\partial \ln v / \partial T)_{p=0}$

If the value of α is known, it is possible to determine $\tilde{v}$ and $\tilde{T}$ using equations 2.45 and 2.46. Then, using expression 2.38, and the calculated values of $\tilde{v}$ and $\tilde{T}$, T* may be calculated. From v and $\tilde{v}$, v* is obtained, using equation 2.37. If ν is

known p* can be obtained from 2.46 and so the pure liquid is completely characterized[38]. The parameter c and $s\eta$ can be computed from equations 2.40 and 2.38 or 2.39.

2.1.3.2 BINARY MIXTURES

Flory and coworkers [36] extended the above treatment to polymer-polymer mixtures adopting the following combining rules [34, 37, 38].

1) As the segments are chosen arbitrarily to be of the same size then

$$v_1^* = v_2^* = v_3^* \qquad 2.48$$

2) The hard core volume of the pure components are additive:

$$v^* = r_1N_1v_1^* + r_2N_2v_2^* = rNv^* \qquad 2.49$$

where

$$N = N_1 + N_2 \qquad 2.50$$

$$x_1 = 1\text{-}x_2 = N_1 / N_2 \text{ (mole fraction)} \qquad 2.51$$

$$\bar{r} = x_1r_1 + x_2r_2 \text{ (segment fraction)} \qquad 2.52$$

$$\bar{c} = (r_1x_1c_1 + r_2x_2c_2) / rN \qquad 2.53$$

3) The total number of pair interactions in the mixture is equal to the sum of the pure component pair interactions.

$$(s_1r_1N_1 + s_2r_2N_2) = (\bar{s}\bar{r}N) / 2 \qquad 2.54$$

$$= N_{11} + N_{12} + N_{22} \qquad 2.55$$

where s is the number of contact sites and N_{ij} are the number of i, j pairs.

$$\bar{s} = \phi_1s_1 + \phi_2s_2 \qquad 2.56$$

$$\phi_1 = 1\text{-}\phi_2 = (r_1N_1) / rN = N_1v_1^* / (N_1v_1^* + N_2v_2^*) \qquad 2.57$$

ϕ_1, ϕ_2 are segment or core volume fractions.

The partition function for a binary mixture will be very similar to that for pure polymer liquids in equation 2.36, the only differences being that for binary mixtures, N is given by 2.49, r by 2.52, $\bar{c}$ by 2.53 and E_o has a different definition which will be given below. As a consequence the equation of state of the mixture will be similar to that of the pure polymer in 2.44, only that in this case p* and T* are given by expressions 2.66 and 2.69 respectively.

The mean intermolecular energy E_o is defined in a similar way to that in equation 2.34 [37, 38].

$$E_{om} = - [(A_{11}\eta_{11} / v) + (A_{22}\eta_{22} / v) + (A_{12}\eta_{12} / v)] \qquad 2.58$$

where E_{om} is the internal energy of the mixture, A_{ij} are the number of contact pairs between species and η_{ij} / v is the energy associated with each.

The above expression can be rewritten after suitable mathematical manipulation and defining

$$\Delta\eta = \eta_{11} + \eta_{22} - 2\eta_{12} \quad 2.59$$

$$E_o = -1/2\ [\ s_1r_1N_1\ (\eta_{11}/v) + s_2r_2N_2(\eta_{22}/v) - A_{12}(\Delta\eta/v)\ ] \quad 2.60$$

where

$$s_1r_1N_1 = 2A_{11} + A_{12} \quad 2.61$$

$$s_2r_2N_2 = 2A_{22} + A_{12} \quad 2.62$$

Equation 2.60 may be expressed in terms of site fractions θ_i where

$$\theta_2 = 1-\theta_1 = (\ s_2r_2N_2 / srN\ ) \quad 2.63$$

and

$$A_{12} = s_1r_1N_1\theta_2 = s_2r_2N_2\theta_1 = s_1r_1N_1s_2r_2N_2 / \bar{s}\bar{r}N \quad 2.64$$

yielding the following expression:

$$E_{om} = -\ \bar{s}\bar{r}N / 2v\ (\ \theta_1\eta_{11} + \theta_2\eta_{22} - \theta_1\theta_2\Delta\eta\ ) \quad 2.65$$

Equation 2.41 can be extended to a mixture:

$$-E_{om} = rNp^*v^* / v \quad 2.66$$

where the p* for each component is:

$$p_i^* = s_i^*\eta_{ij} / 2v^{*2} \quad 2.67$$

An interaction parameter X_{ij} with the dimensions of pressure may be defined as

$$X_{12} = s_1\Delta\eta / 2v^{*2} \quad 2.68$$

Combination of equations 2.65, 2.66 and 2.67 leads to the following expression

$$p^* = p_1^*\phi_1 + p_2^*\phi_2 - \phi_1\theta_2X_{12} \quad 2.69$$

where ϕ_i is the segment fraction

E_{om} in 2.65 can be written in terms of the usual thermodynamic parameters yielding

$$E_{om} = -\ (\ \bar{s}\bar{r}N / 2v\ )\ (\ p_1^*\phi_1 + p_2^*\phi_2 - \phi_1\theta_2X_{12}\ ) \quad 2.70$$

T* for binary mixtures can be obtained by substituting the expressions for c from 2.53, p* from 2.66 and ϕ_1 from 2.57 into 2.40 yielding the following expression:

$$T^* = p^* / [\ \phi_1p_1^*(\ T^*_1\ )^{-1} - \phi_2p^*_2(\ T^*_2\ )^{-1}\ ] \quad 2.71$$

2.1.3.3 ENTHALPY OF MIXING

In condensed systems (solids and liquids) at low pressures, ΔH is similar to ΔE and so:

$$\Delta H_m = E_{om} - (\ E_{o1} - E_{o2}\ ) \quad 2.72$$

If E_{o1} and E_{o2} are given according to expression 2.41 and E_{om} by 2.70 then equation 2.72 may be rewritten as:

$$\Delta H_m = rNv^* [(\phi_1 p^*_1 / v_1) + (\phi_2 p^*_2 / v_2) - p^* / v] \quad 2.73$$

If the expression for p* in 2.69 is introduced into 2.73 then

$$\Delta H_m = rNv^* [\phi_1 p^*_1 (v_1^{-1} - v^{-1}) + \phi_2 p^*_2 (v_2^{-1} - v^{-1}) + (\phi 1 \theta_2 X_{12} / v)] \quad 2.74$$

where the first two terms are the equation of state terms and the last one is the contact interaction term.

The contribution of the equation of state terms to the ΔH_m is a function of the difference between the reduced volume of the solution and the reduced volume of the components. These differences may dominate the ΔH_m [37].

$$\Delta v_m = v^E \quad 2.75$$

where v^E is the excess reduced volume. The contact interaction term contains X_{12} which as seen from 2.59 and 2.69 is a function of the contact interaction energy of like and unlike species [37].

2.1.3.4 FREE ENERGY OF MIXING

As the Gibbs free energy is very similar to the Helmholtz free energy (A) for condensed systems, it is possible to calculate G using the following relationship [37]:

$$A = -kT\ln Z \sim G \quad 2.76$$

The ΔG_m may be obtained if the Z for the mixture and for the components are substituted into 2.76 yielding after some mathematical manipulation:

$$\Delta G_m = KT(N_1 \ln\phi_1 + N_2 \ln\phi_2) + 3rNv^* \{ \phi_1 p^*_1 T_1 \ln[(v_1^{1/3}-1) / (v_1^{1/3}-1)] + \phi_2 p^*_2 T_2 \ln[(v_2^{1/3}-1) / (v_2^{1/3}-1)]\} + rNv^*[\phi_1 p^*_1 (v_1 - v) + \phi_2 p^*_2 (v_2 - v) + (\phi_1 \theta_2 X_{12} / v)] \quad 2.77$$

where the first term is the ΔS_{comb}, the second is the so called residual entropy (S_R) which contains the equation of state parameters and the third is the ΔH_m, previously obtained in expressions 2.73 or 2.74, which contains the contact terms. S_R and ΔH_m may be gathered together in one term called the residual Gibbs free energy (G_R), and the ΔS_{comb} will constitute the ΔG_{comb}. Equation 2.77 may then be simply represented as[37,38].

$$\Delta G_m = \Delta G_{comb} + G_R \quad 2.78$$

Flory [37] used the term "residual function" in an analogous way to that of "excess function" [30] (an excess function is the difference between the thermodynamic function of mixing in the actual system and the value corresponding to a perfect solution at the same T, P and composition) but in the case of the residual function it will include the equation

of state and contact terms without limitation on the nature of the expression for ΔS_{comb}:

Excess property = Residual property + $(\Delta S_{comb} - \Delta S_{ideal})$ 2.79

and

$\Delta S_{comb} = \Delta S_{ideal}$ if $r_1 = r_2$ 2.80

2.1.3.5 PARTIAL MOLAR PROPERTIES [37, 38]

The partial molar quantities of interest for polymer solutions are $\mu - \mu_{1o}$, H_R and S_R. $\Delta\mu_m$ can be obtained by differentiating ΔG_m in equation 2.77 with respect to N_1 or N_2 obtaining the following relationship:

$$\Delta\mu_{1m} = (\partial\Delta G_m / \partial N_1)_{T, v, N2} = (\mu_1 - \mu_{1o})_{conf} + (\mu_1 - \mu_{1o})_R \quad 2.81$$

$$= RT\{\ln (1- \phi_2) + [1- (1 / x)] \phi_2\} + p^*_1 v^*_1 \{ 3T_1 \ln [(v_1^{1/3} - 1)/(v^{1/3}-1) + (v_1^{-1} - v^{-1}) + (v^*_1 X_{12} \theta_2^2 / v) \} \quad 2.82$$

The first term in brackets corresponds to $(\mu_1 - \mu_{1o})_{conf}$ and the second is $(\mu_1 - \mu_{1o})_R$. ΔG_m can be differentiated with respect to component 2 giving a similar equation to 2.82. $\Delta\mu_1$ and $\Delta\mu_2$ are very important, as it is possible to calculate from them the binodal and spinodal curves and the critical point.

H_R can be obtained from 2.74 giving the following relationship:

$$H_R = H_1 - H_{1o} = (\partial\Delta H / \partial N_1)_{T1,P1,N2}$$
$$= P_1 * V_1 * \{ v_1^{-1} - v^{-1}) + (\alpha T / v)[(T_1 - T / T)] + v_1 * X_{12} v^{-1} (1+\alpha T) \theta^2 \} \quad 2.83$$

where α is related to v by equation 2.46.

S_R can be obtained from the second term in 2.77 giving:

$$S_R = -P_1 * V_1 * \{ (3T_1 / T) \ln [(v_1^{1/3} - 1) /(v^{1/3} - 1)] - (\alpha / v) [(T_1 - T) / T] + \alpha v^{-1} v^*_1 X_{12} \theta_2^2 \quad 2.84$$

The term $(\mu_1 - \mu_{1o})_R$ in 2.82 can also be obtained from 2.83 and 2.84.

The Flory equation of state [39] represents a step in the right direction. It demonstrates that the thermodynamic properties of mixtures depend on the thermodynamic properties of the pure components which are the equation of state parameters T*, p* and v*. It can explain the LCST and UCST as being due to free volume effects. At low temperature the intermolecular energy dissimilarities cause the UCST and at high temperatures the free volume dissimilarities cause the LCST behaviour [3]. However the Flory equation of state is not entirely successful from the quantitative point of view, for example it does not take

into account the variation of the scaling parameters with temperature and pressure and the contact interactions between neighbours are only considered to contribute to the enthalpy, although they also affect the entropy [39]. The theory does not consider the role of polydispersity [3] in the determination of the shape and the location of the spinodal curve.This effect was described later by Huggins [3] and Koningsveld [3]. Huggins considers that chain flexibility between polymers is the important factor, Koningsveld believes that the radius of gyration is the major factor.

In order to overcome the limitations of this equation of state several modifications have been introduced. Flory and Eichinger [38] added an entropic term to the existing contact term in equation 2.77: $-T\tilde{v}Q_{ij}$, where Q_{ij} is an empirical parameter which corresponds to the entropy of interaction between unlike segments. Q_{ij} is equivalent (but not equal) to the c in Flory-Huggins lattice theory. McMaster [39] found that the effect of pressure was incorrectly predicted at any non zero pressure if the term $(\partial \Delta G_m / \partial v)_{T1, N2}(\partial v / \partial N)_{T1, V1, N2}$ was not introduced into the derivation of $\Delta\mu_m$ in equation 2.75. He found a great improvement in the theoretical calculations if the correction for c, formulated originally by Lin, was introduced[39]:

$$\bar{c} = \sum_{i=1}^{n} \phi_i c_i - \sum_{j=2}^{n} \sum_{i=1}^{j=1} \phi_i \phi_j c_{ij} \qquad 2.85$$

where c_{ij} are quadratic correction coefficients to a linear variation in the number of external degrees of freedom.

The limitations of the Flory equation of state are mainly a consequence of the cell model on which it is based [3]. This fact encouraged the development of new equations of state based on different solution theories. One of the most useful is the lattice fluid theory of Sanchez and Lacombe (LFT) [40,41,42] which is based on the Hole theory. In this theory the molecules are arranged in a lattice with holes, which allows the prediction of changes in volume on mixing, UCST and LCST behaviour. The LFT has much in common with the Flory equation of state as both require three equation of state parameters to characterize the pure components, and at low temperatures both reduce to the Flory-Huggins equation. In spite of the great ability that this theory has for predicting changes in the volume of mixing, LCST and UCST, it still has some disadvantages: (1) the predictions of the ΔV_m are based on close-packed densities, (2) the predicted values of ρ^* are smaller than the corresponding known crystalline densities and (3) the model needs the introduction of an entropic term.

2.2 PHASE SEPARATION BEHAVIOUR

Phase separation in a miscible blend can be caused by variations in temperature, pressure and / or composition [3]. The resultant phases coexist on a curve called the binodal which delimits the region of stability and metastability in the phase diagram of the mixture. Besides the stable and metastable regions there is an unstable region which is delimited from the metastable region by the spinodal curve. These regions are shown clearly in figure 2.1. The illustration shows the typical phase diagram of a polymer mixure presenting a LCST behaviour. The illustration also displays the free energy vs composition behaviour corresponding to that phase diagram.

At temperatures below the binodal curve the mixture is homogeneous. The point T_0 in the binodal curve corresponds to a minimum of free energy. At this temperature the chemical potential of each component in the two phases is the same:

$$\mu_1 = \mu_1' \quad \mu_2 = \mu_2' \qquad 2.86$$

where the prime designates the second phase.

In the spinodal curve the point T_0 corresponds to an inflection point in the free energy curve, at this point

$$\partial^2 \Delta G / \partial \delta\phi_1 \partial\phi_2 = 0 \qquad 2.87$$

The binodal and the spinodal curves meet at the critical point α where:

$$\partial^2 \Delta G / \partial \phi^2 = \partial^3 \Delta G / \partial \phi^3 = 0 \qquad 2.88$$

For monodisperse polymers the binodal curve can be identified with the cloud point curve (the cloud point (CP) is the temperature at which incipient phase separation starts in a homogeneous mixture when heated or cooled at an infinitesimally slow rate). For polydisperse polymers the binodal and the CP curve are not identical [39]. The CP curve associated with a UCST is convex upward; its maximum shifts to higher temperatures with increasing molecular weight. As shown in figure 2.1 the CP curve associated with an LCST is convex downwards and generally shifts to lower temperatures with increasing molecular weight, however the opposite effect has also been observed. Nishi and Kwei [140], studying (PS/PVME), observed that the CP curve decreases until a certain value of molecular weight, above which the molecular weight dependence of the CP levels off or even reverses.The UCSTs reported in the literature are usually for low molecular weight polymers; UCSTs are difficult to observe in high molecular weight polymers, if they exist at all, because of the very slow diffusion of polymers at lower temperatures[3,44].

The binodal and spinodal curves and the critical point may be simulated using equations 2.86, 2.87 and 2.88 respectively and the corresponding expressions for ΔG_m

derived from a particular thermodynamic solution theory (see section 2.1 pp 9-22) . In practice, there are two complicating factors: the polydispersity of the polymers and the selection of the model on which the calculation of ΔG_m is based. Koningsveld and coworkers [44] extended the Flory-Huggins model by introducing variables that will take into account the polydispersity of the polymers in mixtures. They were able to explain at

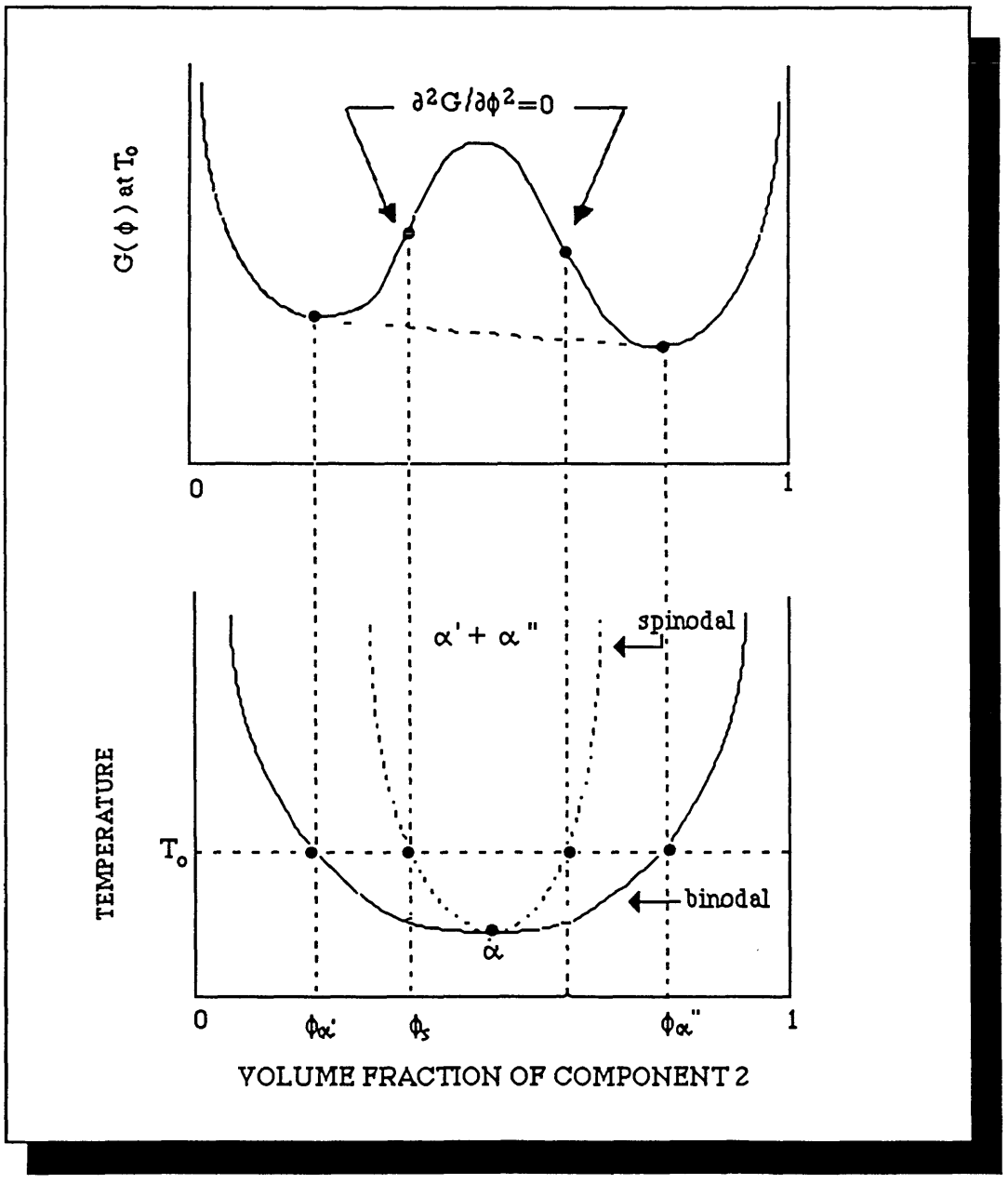

Figure 2.1 The lower graph is a typical temperature-composition diagram for a polymer blend showing the binodal (solid line) and the spinodal curves (dashed line). The upper graph illustrates the corresponding free energy vs composition diagram.

least qualitatively the experimental behaviour of polydisperse mixtures, such as the skewness of the phase boundary shifting towards the higher weight concentration of the polymer with greater polydispersity. They were also able to predict two peaks in the CP curve due to the dependence of χ on ϕ. The predicted binodal and spinodal curves and critical point will depend on the theoretical expression used to predict ΔG_m; selection of a particular model will take into consideration its accuracy and simplicity. As mentioned before, the Flory equation of state, despite its limitations, is quite frequently used because it is able to predict in a quite realistic way the behaviour of polymer mixtures. McMaster [3, 39, 44] tested the predictions of the Flory equation of state theory by computing a set of binodal and spinodal curves for a representative pair of polymers. He was able to study the effects of chain length, thermal expansion coefficient, thermal pressure coefficient, interaction parameter and polydispersity. In the following paragraphs some of his conclusions are summarized.

(1) The most important parameter controlling phase separation is the thermal expansion coefficient. In polymers of molecular weights close to 200,000 where energy interactions between them are negligible, differences in α larger than 4% cause immiscibility between both components.

(2) Polymer mixtures which exhibit strong hydrogen bonding or acid base interactions have negative interaction parameters. For small positive values of χ_{23} the UCST and LCST can be observed simultaneously. With larger positive values, the LCST and UCST merge to yield hour glass shaped binodal and spinodal curves.

(3) The LCST usually increases with pressure. Large differences in the thermal pressure coefficient decrease LCST, however if pressure is increased the reverse behaviour is observed.

(4) With increasing positive values of Q_{12} solubility increases. Negative values can lead to LCST and UCST.

(5) Miscibility decreases with differences in the average chain length of any of the two polymers. This behaviour is expected because ΔS_m decreases monotonically with increasing molecular weight.

(6) For quasibinary polymer mixtures the spinodals remain unchanged. The binodals and the critical point depend on the ratio of the Z average to weight average chain length of each component (a_i). The critical point will shift to the side of the component with bigger a_i, so for example if $a_1 > a_2$, the critical point will shift to the side of component 1.

(7) Negative values of degrees of freedom c_{12} (a modification introduced by McMaster, see section 2.1.3 p. 21) increase solubility, positive values decrease

solubility.

(8) The effect of increasing n in the expresssion $E_i(o) \alpha 1/v^n$ from 1 to 1.25, increases solubility and the binodal and spinodal curves also flatten somewhat.

2.2.1 PHASE SEPARATION MECHANISMS

Polymer mixtures may phase separate by two different phase separation mechanisms: nucleation and growth or spinodal decomposition. The mechanism followed depends on the thermodynamic stability of the system. When the blend is in the metastable region it will phase separate by nucleation and growth, if it is in the unstable region it will phase separate by spinodal decomposition [44].

In nucleation and growth large clusters (nuclei) are formed. These clusters are unstable because an increase in free energy is required during their formation. The composition of each nucleus and that of the immediate vicinity remains constant until the phase separation is completed. The growth in size of nuclei is initially a function of the concentration gradient set up between them and their immediate vicinity; later on it will depend on coarsening or ripening [3, 44, 46].

In spinodal decomposition the growth originates from composition fluctuations. In this case the effective attraction between like species is so large that the flux of the molecules is against the concentration gradient. This kind of growth, which is usually thermodynamically unfavourable, is possible in this unstable region because such change causes a decrease in free energy [45]. The molecules in the gradient move toward the cluster of their species leaving a depleted zone around it. The molecules in the outer edge of the depleted zone sense the concentration gradient and move away from it forming a new cluster [46]. The major and minor phases of the decomposed system are interconnected at the beginning, but afterwards, they tend to minimize their interfacial energy by coarsening [44]. Depending on the viscosity of the system, the resultant phase separated blend may resemble the original interconnected structure, (high viscosity) or it may be dispersed in small droplets (as in nucleation and growth) or it may consist of two layers of each of the components (low viscosity) [46]. A system in the stable region also has concentration fluctuations, but in this case the molecules execute a nearly random walk to favourable clusters that have no permanence as they tend to form and disappear[46]. The main difference between nucleation and growth and spinodal decomposition is that in the latter the diffusion flux is against the concentration gradient (negative diffusion coefficient), and in nucleation and growth the molecules move in the same direction (positive diffusion coefficient).

2.2.2 KINETICS OF PHASE SEPARATION

Gibbs [45,46] in the 1880's was the first to realize that there were logical rules about the conditions when the spinodal decomposition and nucleation and growth occur. Little attention was paid to both until the mid 1920's when the theory of nucleation and growth was revived [44]. In the mid 1950's M. Hiller [44-46] gave the basis for understanding spinodal behaviour simply by solving a diffusion equation modified by thermodynamic requirements. This idea was fully extended by Cahn [47] to three dimensional isotropic solids and generalized to any type of solution free from structural imperfections. Cahn's approach is directly applicable to isotropic polymer mixtures because it is based on phenomenological assumptions [44]. In the theoretical treatment the free energy is a function of concentration and concentration gradients [44-47].

$$G = \int [\, G(c) + K(\nabla c)^2 \,]\, dv \qquad 2.89$$

where G(c) is the free energy-density of an homogeneus material of composition c; $K(\nabla c)^2$ is the additional free energy density associated with a composition gradient, K measures energy contributions from incipient surfaces between regions differing in composition.

If equation 2.89 is differentiated with respect to c, μ_A-μ_B can be obtained:

$$\mu_A - \mu_B = (\partial G / \partial c) = (\partial G / \partial c_A) - 2k\nabla^2 c_A \qquad 2.90$$

In this equation, non linear terms have been already eliminated and so it is applicable during the early stages of spinodal decomposition.

It is possible to relate thermodynamics with a simple diffusion equation by relating the interdiffusional flux ($\tilde{J}$) of two species ($\tilde{J} = \tilde{J}_A = -\tilde{J}_B$) with ($\mu_A - \mu_B$):

$$-\tilde{J} = M\nabla (\mu_A - \mu_B) \qquad 2.91$$

where M is the diffusion mobility

If equation 2.90 is substituted into 2.91 it is possible to obtain Cahn's diffusion equation

$$(dc / dt) = M[(\partial^2 G / \partial c^2)\nabla^2 c - 2k\nabla^4 c] \qquad 2.92$$

where $M(\partial^2 G / \partial c^2)$ is the Cahn - Hilliard [48] diffusion coefficient D. The sign of D depends on $(\partial^2 G / \partial c^2)$ which can be either positive or negative depending on the position in the phase diagram.

The solution of 2.92 gives [44, 45]:

$$c - c_0 = \sum_{all\ \beta} [\, \exp R (\beta)t \,][\, A(\beta)\cos(\beta r) + B(\beta)\sin(\beta r)] \qquad 2.93$$

where c_0 is the average composition, $\beta = 2\pi / \lambda$ (λ is the wavelength of a concentration fluctuation), $R(\beta)$ is the kinetic amplification factor, A and B are constants that can be determined from the existing composition fluctuations in the one phase system.

$$R(\beta) = -M\beta^2[(\partial^2 G / \partial c^2) + 2K\beta^2] \quad 2.94$$

The second term can be neglected for small values of β. Because of the exponential dependence on R(β) any fluctuation from the average will decay or grow rapidly depending on whether R(β) is positive or negative. In the metastable region $(\partial^2 G/\partial c^2)>0$ consequently R(β) < 0 and any fluctuation will decay. In the spinodal region $(\partial^2 G/\partial c^2) < 0$; R(β) is a nonmonotonic function of β and vanishes at β = 0 and at

$$\beta = \beta_c = [-(\partial^2 G / \partial c^2) / 2K]^{1/2} \quad 2.95$$

and reaches a maximum at

$$\beta = \beta_c / 2^{1/2} \quad 2.96$$

$$\beta = \beta_m = \beta_c / 2^{1/2} = 1/2[-(\partial^2 G / \partial c^2)k]^{1/2} \quad 2.97$$

The Fourier transform of this situation gives rise to a scattering pattern which shows a peak at a wave vector (Q_m) where [48]

$$Q_m = (4\pi / \lambda)\sin(\theta / 2) \quad 2.98$$

where θ is the scattering angle, λ: the wavelength of the incident light, η: refractive index.

If equation 2.97 and the Cahn -Hilliard diffusion coefficient $\tilde{D}$ are combined it can be seen that the $\tilde{D}$ can be calculated from the growth rate of the wave vector maximum β_m [48]:

$$\tilde{D} = -2R(\beta_m) / \beta_m^2 \quad 2.99$$

It is possible to measure R(β_m) from the time dependent scattered intensity (I) because

$$I(Q) \alpha e^{2R(Q)t} \quad 2.100$$

2.3 BLEND PREPARATION AND ITS INFLUENCE ON MISCIBILITY

The final properties of a polymer blend are strongly dependent on the method of preparation and the time and the temperature to which the mixture was subjected.There are various ways of preparing blends, among the most important are: melt mixing, solvent casting, freeze drying, mixing polymer emulsions and via reaction (this last includes *insitu* polymerization, co-crosslinking and IPNs).

Melt mixing [49] is frequently used in industry because it is fast, efficient, economic and does not introduce an extra compound to the mixture. The method consists simply of mixing molten polymers in a mechanical mixer (Banbury, Brabender, two roll mill, extruder, rheometer or Minimax mixer). The method has some disadvantages (a) due to

the low diffusion of polymer it usually produces heterogeneous blends (b) the polymer may degrade due to the high temperatures employed, (c) it is costly for academic research because of the equipment and the large quantities of material employed.

In solvent casting [7,49] the components are dissolved in a common solvent which after a careful and thorough evaporation leaves a film that may be immediately characterized by calorimetric and dynamic methods, infrared analysis and microscopic techniques. Solvent casting is the simplest and the most commonly used blending method for academic work because it is inexpensive, requires small quantities of material and contamination of the resulting blend can easily be precluded by careful manipulation of the materials. However this method has some disadvantages: (a) not all polymers are readily soluble in common solvents, (b) the nature of the solvent and the casting history of the blend may influence the miscibility of the final mixture, as is the case for crystalline polymers [50] or glassy systems with high T_g components. The latter are very susceptible to "cast in" memory of any irregular ternary phase behaviour (if at any point during casting a biphasic ternary system develops, then the cast film will also be biphasic even though the blend should be miscible [51]). This behaviour is explained in figure 2.2. In this figure a ternary system of polymer 1, polymer 2 and a solvent is represented. The solvent starts to evaporate at point A where it is one phase, but arriving at B phase separation takes place. When the system leaves the two phase region at C, the phases have grown too large and due to the low diffusion of polymers the resultant polymer blend of composition D will be two phase [52]. As pointed out by Robbard *et al*[52], this behaviour may be a result of a large difference between the interaction parameter of the common solvent with each component (χ_{12} and χ_{13}) even though the interaction parameter of both polymers (χ_{23}) indicates miscibility. This is known as the $\Delta\chi$ effect, where

$$\Delta\chi = \chi_{12} - \chi_{13} \qquad 2.101$$

References 26, 28, 49 and 53 provide information of methods for casting thin, bubble free and uniform films together with some procedures used to eliminate the solvent from cast films most efficiently.

In freeze drying a small volume of a solution is quenched down to a very low temperature so that the solvent freezes and the blend will collect randomly throughout the solvent, which is removed by sublimation. This method has some disadvantages: (a) only small volumes can be frozen at one time (b) the freeze drying may affect the miscibility of the blend [54] and (c) the blend has to be reshaped afterwards.

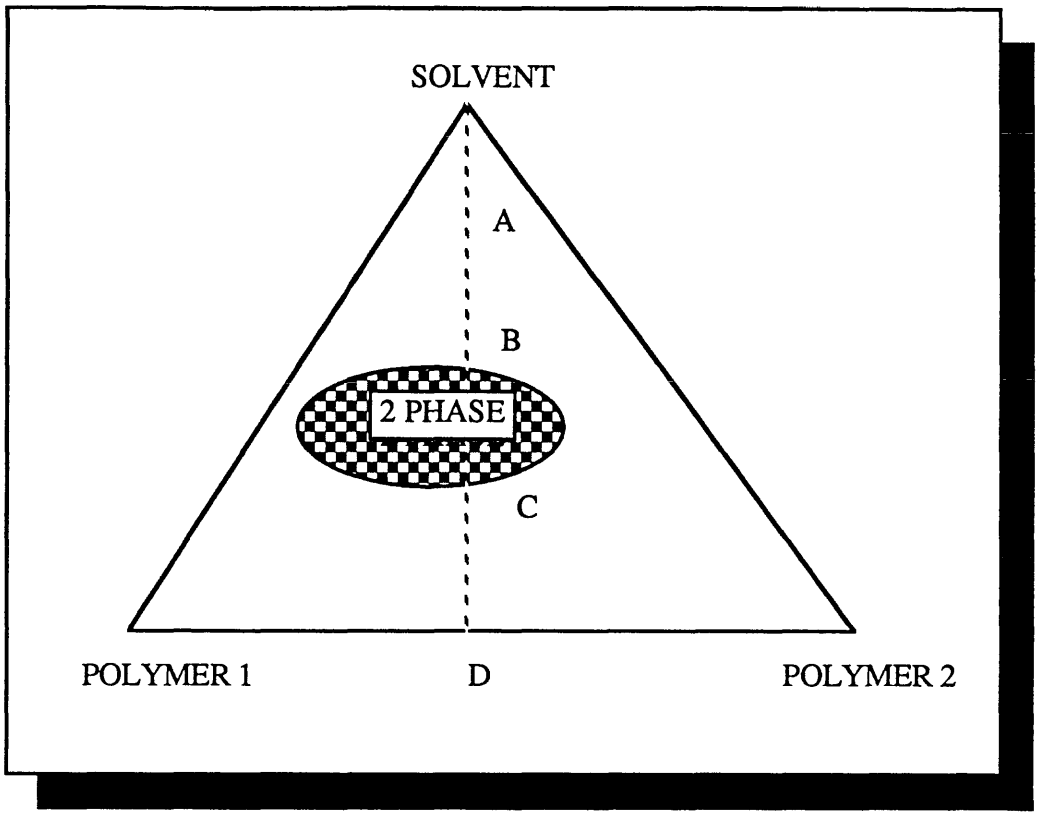

Figure 2.2 Biphasic behaviour of a blend caused by interference of the solvent used for casting.

Blending polymers in emulsion [49] has the same advantages as solvent casting, however polymer emulsions are not always available or easy to prepare and they may affect the state of the blend [55].

Mixing via reaction comprises *insitu* polymerization, co-crosslinking and IPN formation. In *insitu* polymerization [7] a monomer is polymerized in the presence of another polymer. This method is very convenient in the case of polymers with poor thermal stability or high T_g and it also avoids the problem of the interference of the solvent with miscibility. However it can not ensure homogeneous blends as two phase regions may exist within the polymer 1/polymer 2/monomer mixture [20, 27].

In co-crosslinking and IPN formation simultaneous mixing and crosslinking occur. This may help to increase the degree of miscibility between the two components of the blend [4]. Some of the most important methods for preparing this special type of blend will be discussed in secion 2.4.3.1 (p. 37-39).

2.4 POLYMER NETWORKS AND INTERPENETRATING NETWORKS

Polymers may be synthesized as linear, branched and crosslinked entities or a mixture of the three [4]. In the crosslinked polymers, the molecules are joined together at one or more points named crosslinks, forming eventually a giant molecule [71]. As the crosslinking reaction progresses the solubility of the polymer decreases until it reaches a point of complete insolubility, named the gel point. Despite insolubility, polymer networks can swell in the presence of solvents, the degree of which depends on the crosslinking density and the affinity between the polymer and the solvent [74]. The number of crosslinks cannot be computed from the amount of curing agent added as it enters wasteful reactions [71], however the swelling behaviour and the tensile properties of the network may be used to determine the degree of crosslinking (see section 2.4.2 pp 32-7).

The physical properties of crosslinked polymers are influenced by their degree of crosslinking, the regularity of the network, the presence or absence of crystallinity and at intermediate degrees of crosslinking by the molecular weight of the polymer before crosslinking [71, 72]. In amorphous polymers, as the crosslink density increases the T_g, the rigidity, and the tensile strength increase while the elongation, the swelling by solvents and the creep behaviour decrease. In crystalline polymers, small amounts of crosslinking will reduce crystallinity yielding a softer, more elastic and lower melting material. In both cases, highly crosslinked polymers are extremely rigid and intractable[72]. Crosslinking is important in the production of polymers in general because it leads to stiffer, stronger products usually with enhanced heat and abrasion resistance[31]. In the case of elastomers the high mobility of the chains is restricted producing a material that can regain its original shape when the stress is released [85].

2.4.1 PREPARATION OF NETWORKS FROM PREFORMED POLYMERS

There are two types of crosslinks that may be introduced in a polymer: physical and chemical [4, 71]. Physical crosslinks are non permanent and may be broken by raising the temperature or by shearing stress. Chemical crosslinks are permanent and can be introduced in two ways: (a) simultaneously during the step reaction polymerization of polyfunctional monomers or through reaction with a reactive site on the backbone during polycondensation and (b) by formation of covalent bonds between preformed linear

polymers which may be carried out by irradiation, vulcanization and by miscellaneous chemical reactions [71, 72, 74].

There are a great variety of chemical reactions which may introduce crosslinks into a polymer: (a) graft copolymerization (b) reaction of the backbone carbons with various reagents and (c) reactions of functional groups in or pendant to the backbone of the polymers. Crosslinking by grafting may be carried out by polymerizing a vinyl monomer in the presence of a linear unsaturated condensation polymer or by chain transfer in which some radical species present in the media are able to abstract a hydrogen from the backbone [72]. Crosslinking involving functional groups involves as many reactions as the specific organic structure of the polymer under study allows. Frequently a difunctional reagent may be applied to link a group from one chain with a group from the second. The reactive groups may be pendant or in the backbone. Formation of linkages may be through an addition or condensation reaction between labile groups pendant to different polymer backbones. Common examples are [72, 74]: (a) ring opening reactions of epoxy groups by difunctional nucleophilic agents (diamines or dibasic acids) (b) the reactions of diisocyanates with a great diversity of functional groups (hydroxyls, amines, amides, urethanes, ureas etc.) and (c) halogen removal in polymers such as butyl rubbers containing 1.1-1.3 % chlorine by weight, fluorinated and chlorinated polyethylenes.

2.4.1.1 CROSSLINKING METHODS FOR CHLOROSULPHONATED POLYETHYLENES

Polyethylene (PE) was synthesized for the first time in 1930. A few years later it was found that chlorinating PE yielded an elastomeric product with no tendency to crystallize[75]. In 1940 McQueen introduced sulphur dioxide and chlorine simultaneously to PE (Reed reaction [76]).

$$RH + SO_2 + Cl_2 \xrightarrow{h\nu} RSO_2Cl + HCl \qquad 2.102$$

yielding a PE containing chlorine and sulphonyl chloride pendant groups known as sulphochlorinated polyethylene SCPE. McAlevy [77, 78] crosslinked SCPEs of different Cl and SO_2Cl content. He found that SCPEs with a Cl content lower than 20% give waxy and tacky products, between 20-45% they give rubbery polymers and at higher Cl contents stiff and virtually inflexible glass like products were obtained. He also found that in order to achieve satisfactory vulcanizable rubber like products the sulphur content must be within 0.4 to 3%. In the following years a great variety of crosslinking reactions for SCPE were studied. It was found that besides the RSO_2Cl groups there are other sites for crosslinking SCPE such as the Cl atoms in the chain (mainly those adjacent to

SO_2Cl), tertiary C atoms (if present), unsaturation in the molecule due to splitting out of SO_2 and HCl and active hydrogen atoms on the chains [76, 79]. All these possibilities together with the high reactivity of SO_2Cl enable SCPE to be crosslinked with a great variety of reactive compounds. Common examples are:

(a) Metal oxide systems [75, 80] based on magnesia or lead bases, an organic acid and a sulphur accelerator which provides sulphur crosslinks through chain unsaturation arising from dehydrochlorination. The organic acid is the source of water for SO_2Cl hydrolysis, the metal oxide acts as a crosslinking agent and an acid acceptor [75, 83].

(b) Solutions of polyfunctional alcohols and SCPE in the presence of organic bases or inorganic hydroxides crosslink SCPE by the formation of sulphonate esters [76, 79, 83]. Primary polyols show excellent curing activity (pentaerythritol, poly(vinyl alcohol)), secondary polyols give poor vulcanizates [76]. Monofunctional alcohols do not crosslink.

(c) Bifunctional amines and imines combine crosslinking and acid accepting capabilities. Simple aliphatic and aromatic diamines react too rapidly to be used in solid polymer compounding. Sterically hindered amines or complexed amines give safe curing but with poor states of curing and resistance to water swelling [76, 79, 81-83]. Ammonium hydroxide crosslinks SCPE forming polysulphonamide crosslinks.

(d) Quinoxalines with unhindered alkyl substituents in position 2 and 3, aziridines and organotin oxides serve both as acid acceptors and crosslinking agents. Quinoxalines offer delayed curing giving excellent vulcanizates, however with the disadvantage of a tendency to swelling by water. Aziridines react too rapidly to be used on a practical basis. Organic oxides act in a similar way to metal oxides with no extra advantage [83].

2.4.2 DEGREE OF CROSSLINKING DETERMINATIONS

The most important methods for determination of the degree of crosslinking are measurement of the modulus of elasticity and swelling measurements. Both methods measure the molecular weight between crosslinks ($\bar{M}_c$) and are based on some type of deformation of the network. In the first method the network is deformed mechanically and in the second the deformation is caused by swelling the network with solvent [84].

2.4.2.1 MODULUS OF ELASTICITY MEASUREMENTS

When an ideal rubber is stretched isothermally and in a reversible way its chains uncoil. As this is a less probable configuration, the entropy of the system decreases with a minor change in internal energy. In stretching, the system does work (w) which is

equal to a change in the Helmholtz free energy (A) [71]:

$$w = \Delta A = fdL = T\Delta S \qquad 2.103$$

where f is the force and L is the unstretched length.

If one end of the chain is placed at the origin of a system of coordinates as shown in figure 2.3, then the probability that the other end lies within a volume element located at x, y, z is:

$$\Omega(x, y, z)\, dxdydz = (\beta^3 / \pi^{3/2}) \exp[-\beta^2(x^2 + y^2 + z^2]\, dxdydz \qquad 2.104$$

where β is a parameter that depends on the length of the chain and its flexibility Expression 2.104 considers an idealized chain with units joined by bonds having no volume about which there is free rotation.

The entropy of the unstretched rubber is:

$$S = (\beta^3 / \pi^{3/2}) - k\beta^2(x^2 + y^2 + z^2) \qquad 2.105$$

and for the stretched rubber:

$$S' = (\beta^3 / \pi^{3/2}) - k\beta^2(\lambda_1^2 x^2 + \lambda_2^2 y^2 + \lambda_3^2 z^2) \qquad 2.106$$

The change in entropy ΔS will be:

$$\Delta S = 1/2\, kN(\lambda_1^2 + \lambda_2^2 + \lambda_3^2 - 3) \qquad 2.107$$

where N is the number of chains per unit volume and λ_1, λ_2, λ_3 are the ratio of the stretched (L) and unstretched (L_o) length in the x,y, z directions.

If equation 2.107 is substituted into equation 2.103 the following expression for the work done when stretching the rubber is obtained:

$$w = \Delta A = 1/2\, TkN(\lambda_1^2 + \lambda_2^2 + \lambda_3^2 - 3) = 1/2\, G(\lambda_1^2 + \lambda_2^2 + \lambda_3^2 - 3) \qquad 2.108$$

where G is the elastic modulus and is equal to:

$$G = TkN = \rho RT / M_c \qquad 2.109$$

Equation 2.108 completely defines the properties of a rubber in the Gaussian region and it allows the derivation of any type of stress-strain relationships. As G depends on the structure of the material it can be used to determine M_c [86]. In a simple elongation

$$\lambda_1 = \lambda \text{ and } \lambda_2 = \lambda_3 = \lambda^{-1/2} \qquad 2.110$$

and so

$$f = G(\lambda - \lambda^{-2}) \qquad 2.111$$

James and Guth [87] and simultaneously Flory [87] working with swollen rubbers calculated that the function Ψ defined by 2.112 is independent of both elongation and degree of crosslinking

$$\Psi = fA_o^{-1}T^{-1}v_r^{1/3}(\lambda - \lambda^2)^{-1} = \rho RM_c^{-1} \qquad 2.112$$

where f is the load required to extend the rubber to an extension ratio λ, A_o is the cross-sectional area of dry sample, T is the absolute temperature, v_r is the volume

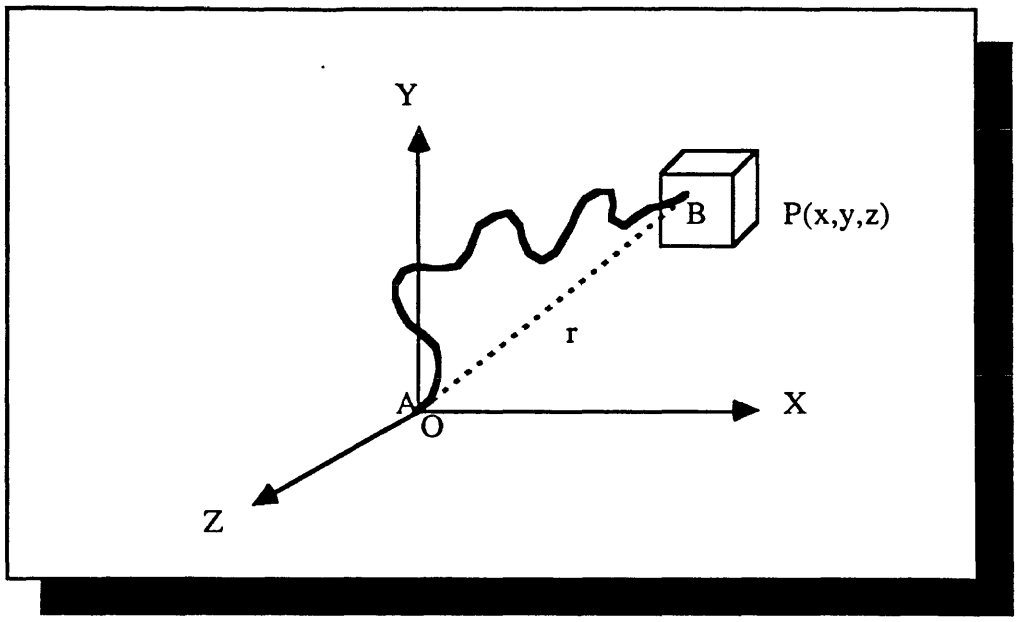

Figure 2.3 The statistically kinked chain. Specification of probability that the end B of a chain, whose end A is fixed in the origin of a Cartesian coordinate system, will be found at any instant within the volume element dxdydz.

fraction of the rubber in the swollen vulcanizate.

Gee [86, 87] found that the stress strain properties of dry and swollen rubber were different, that as the degree of swelling increases the rubber will follow closely the prediction of equation 2.112 and that in dry or lightly swollen rubber Ψ will decrease with elongation and swelling. Rivlin and Saunders [87] found that in the region in which the stress strain curve is reversible the behaviour of dry rubber in simple extension may be described by:

$$C_1 + \lambda^{-1}C_2 = 1/2\,[\,fA_0^{-1}\,(\lambda - \lambda^{-2})^{-1}\,] \qquad 2.113$$

where C_1 and C_2 are constants at a given temperature and degree of crosslinking.

For swollen rubbers 2.113 becomes:

$$C_1 + \lambda^{-1}C_2 = 1/2\,[\,fA_0^{-1}\,v_r^{1/3}(\lambda - \lambda^{-2})^{-1}\,] = \phi \qquad 2.114$$

where

$$\phi = 1/2T\Psi \qquad 2.115$$

C_2 accounts for the non ideal behaviour and tends to zero at high degrees of swelling [86] and so

$$C_1 = 1/2\rho RT\bar{M}_c^{-1} \qquad 2.116$$

At high extensions equation 2.113 deviates strongly from experimental results due to the finite extension of the chains. Mullins [88] showed that equation 2.114 even deviates for swollen polymers at low elongations. This and the oversimplifications made in order to adopt the Gaussian distribution in equation 2.104 such as "phantom chains" and

networks with no defects make this theory rather inadequate. Flory [86] considered the presence of defects in the network by introducing the following correction factor into equation 2.109:

$$G = g\rho RT(1 - 2\bar{M}_c / \bar{M}) / \bar{M}_c \qquad 2.117$$

where g takes account of interlooping or entanglements in the chains and closed loops and is approximately equal to 3 [71] and $(1 - 2\bar{M}_c / \bar{M})$ is the correction for free ends.

Treloar [88] proposed a modified stress strain relationship which is difficult to use. Mullins [88] in colaboration with Moore and Watson [91] were able to correlate $\bar{M}_{c\ physical}$ with $\bar{M}_{c\ chemical}$ ($\bar{M}_{c\ physical}$ = Effective $\bar{M}_n$ of the network chain segments. This includes chemical crosslinks and chain entanglements, $\bar{M}_{c\ chemical} = \bar{M}_n$ of chain segments bounded by chemical crosslinks at both ends):

$$\bar{M}_c^{-1}{}_{physical} = \bar{M}_c^{-1}{}_{chemical} + 0.68x10^{-4} \qquad 2.118$$

Walsh [84] pointed out that the determination of the degree of crosslinking based on the above relationships is open to question, that in using them it is important to consider if the equation used is applicable to the system under study and that the accuracy of the M_c obtained is such that it should only be used in comparative studies. Despite these limitations it is very common to measure the degree of crosslinking from the value of G determined from tensile experiments and the following relationships:

$$G = 1/2fA_o^{-1}(\lambda - \lambda^{-2})^{-1} \qquad 2.119$$

$$G = \rho RT\bar{M}_c^{-1}(1 - 2\bar{M}_c\bar{M}^{-1}) \qquad 2.120$$

a detailed explanation of these methods will be given in section 3.5.2, p. 79-81.

2.4.2.2 SWELLING MEASUREMENTS

When a crosslinked polymer is immersed in a liquid of similar chemical structure, the former absorbs solvent until the osmotic forces tending to swell the network are just balanced by the elastic forces of the network. At this point the gain in entropy by mixing the polymer network with the solvent (ΔS_m) is equal to the decrease in entropy by deforming the network (ΔS_{el}) (swelling the network is analogous to deformed it, the differerence being that in the former case the network is extended isotropically in three directions [92]). At this point the chemical potential of the solvent μ_1 is the same inside and outside the network [71, 92]. Flory and Rehner [93] conclude that μ_1 may be expressed as:

$$\mu_1 = \mu_m + \mu_{el} \qquad 2.121$$

In this expression μ_m, is given by the Flory-Huggins equation (see equation 2.28)(p. 13)) and μ_{el} by equation 2.108 (p. 33). If this last expression is applied to a simple isotropical expansion in three dimensions it yields the following equation :

$$\Delta A = w = 1 / 2NkT(3\lambda^2 - 3) = 1 / 2\rho RT(3\lambda^2 - 3) = 3 / 2\rho RTM_c^{-1}(\phi_2^{-2/3} -1) \quad 2.122$$

where $\lambda^3 = \phi_2^{-1}$ is the volume fraction of the polymer in the swollen state.

As $\Delta G = \Delta A + P\Delta V$, where P is the surrounding pressure and ΔV is assumed to be zero: $\Delta A = \Delta G$ and so

$$\mu_{el} = dA / dn_1 = \rho RTM_c V_1 \phi_2^{1/3} \quad 2.123$$

where V_1 is the molar volume of the swelling liquid, M_c is the number-average molecular weight of the chains between crosslinks, ρ is the density of the swollen polymer, ϕ_2 is the volume fraction of polymer in the swollen state and χ is the Flory interaction parameter.

At equilibrium swelling, $\mu_1 = 0$ and so $\mu_m = \mu_{el}$ 2.124

Substituting equation 2.28 and 2.123 into 2.124, the Flory-Rehner equation is obtained:

$$-\ln (1-\phi_2) - \phi_2 - \chi\phi_2^2 = V_1\rho_2 M_c^{-1}\phi_2^{1/3} \quad 2.125$$

This equation was later modified to [71]:

$$-\ln (1-\phi_2) - \phi_2 - \chi\phi_2^2 = V_1\rho_2 M_c^{-1}[q_o^{2/3}\phi_2^{1/3} - \phi_2/2] \quad 2.126$$

Equations similar to that in 2.126 were also provide by Hermans [71, 143, 144] and James and Guth [71, 143]. Hermans calculated ΔS_{el} by a different method, leading to a similar equation to 2.133:

$$-\ln (1-\phi_2) - \phi_2 - \chi\phi_2^2 = V_1\rho_2 M_c^{-1}[q_o^{2/3}\phi_2^{1/3} - \phi_2] \quad 2.127$$

Experimentally the difference between both equations may be detected only when the polymers are crosslinked in dilute solution. The equation by James and Guth was based on a different type of distribution function :

$$-\ln (1-\phi_2) - \phi_2 - \chi\phi_2^2 = V_1\rho_2 M_c^{-1}[q_o^{2/3}\phi_2^{1/3}] \quad 2.128$$

In all these expressions, if the networks are formed in an amorphous, disordered state in the absence of a solvent and then are swollen at the same temperature, q_o is equal to the unity and $\phi_2^{1/3}$ is

$$\phi_2^{1/3} = (r_1^2/r_o^2)^{1/2} \quad 2.129$$

where r_o is the end-to-end distance of a chain segment between crosslink sites in the network and r_1 is the equivalent free chain end-to-end distance [4].

If the network is formed in the presence of solvent then:

$$(r_1^2/r_o^2)_o^{1/2}\phi_2^{-1/3} = (r_1^2/r_o^2)^{1/2} \quad 2.130$$

and

$$q_o = 1/(r_1^2/r_o^2)_o \quad 2.131$$

where $(r_1^2/r_o^2)_o$ is the value of (r_1^2/r_o^2) in the absence of solvent.

Equations 2.125 and 2.128 may be used to determine M_c by measuring swelling volumes provided that χ is known. Conversely, as pointed out by Gumbrell et al [87], it is

possible to evaluate χ from swelling measurements if M_c is known.($\bar{M}_c$ may be obtained from force extension measurements) [74, 90].

It is important to mention that equations 2.133 to 2.135 were derived for a perfect network, which is composed entirely of chains joined to one another at tetrafunctional junction points. Real polymer networks have many imperfections such as dangling chain ends, wasted loops and interpenetrating loops. Flory took this into account by replacing $\bar{M}_c^{-1}$ with

$$\bar{M}_c^{-1} g'''(1-2\bar{M}_c\bar{M}_n^{-1}) \qquad 2.132$$

where $\bar{M}_n$ is the number average molecular weight of the polymer before it was crosslinked, g''' is an empirical constant approximately equal to three.

A detailed explanation of the experimental procedure followed to determine $\bar{M}_c$ using swelling measurements and equations 2.126 to 2.128 where the Flory correction has been considered is given in section 3.5.1 (pp.76-9).

2.4.3 INTERPENETRATING NETWORKS

As mentioned in chapter 1, an IPN is a combination of two polymers in network form of which one at least is synthesized and / or crosslinked in the immediate presence of the other. The main difference between IPNs and polymer blends, blocks and grafts is that the first ones swell but do not dissolve. Most IPNs are phase separated to a greater or lesser extent, however some level of interpenetration exists between the components. Truly molecular interpenetration exists only when both polymers are miscible. In an IPN both or only one component may be crosslinked, the former case constitutes the so called IPNs, the latter are named semi-IPNs [4, 13].

2.4.3.1 PREPARATION OF IPNs AND SEMI-IPNs

There are many ways of preparing IPNs, each method yields a special topology. Sperling [4] provides an exhaustive review of a number of IPNs and related materials prepared in the last two decades. He classified them according to the synthetic procedure used in the following groups: IPNs, interpenetrating elastomeric networks (IENs), latex IPNs, simultaneous interpenetrating networks (SINs), AB crosslinked polymers and thermoplastic IPNs.

IPNs are prepared by the method called sequential interpenetration where the polymer network I (N_I) is formed by simultaneous polymerization and crosslinking. Monomer II (M_{II}) with crosslinker and initiatior is swollen into N_I and then it is

polymerized *insitu*. The composition of the IPN is determined by the time polymer I (P_I) is left imbibing M_{II}. Some examples are: poly(ethyl acrylate)/polystyrene[94] (polystyrene may be replaced by PMMA or copolymers of polystyrene-co-PMMA [12]), castor oil urethanes/polystyrene [95] and styrene butadiene rubber/polystyrene [96].

In the IENs two latexes of linear polymers are mixed together along with crosslinkers and catalysts and then are crosslinked simultaneously. Two of the following latexes may be mixed together : poly(acrylates), poly(chloroprene), poly(styrene-co-butadiene) and silicone [4].

In the latex IPNs, a crosslinked polymer I in latex form is used as the seed latex. MII plus crosslinker and activator are then added and polymerized yielding the IPN [4,97]. Common examples are: poly(ethyl methacrylate)/poly(n-butyl acrylate) [4], PVC/Nitrile rubber [4], methacrylic/acrylic compositions [97] and some latex semi-IPNs of commercial interest known as ABS plastics [4].

In the case of the SINs, two monomers or prepolymers or even linear polymers are mixed with crosslinkers and activators until they form a homogeneous fluid, then both components are simultaneously polymerized by independent non interfering reactions. Three subcases must be distinguished in SINs: (a) simultaneous gelation of both polymers such as an epoxy/acrylic mix [98], (b) sequential polymerization of the prepolymer mix, one example being polyurethane / PMMA [99] and (c) the introduction of a greater or lesser number of graft sites between the two polymers.

The AB crosslinked polymers are close relatives of the IPNs, in this case two polymers are grafted together yielding a monolithic network. Two types may be distinguished: (a) both ends of P_{II} are bound to different chains of P_I . (b) The P_{II} chains grow across P_I forming a series of tetrafunctional graft linkages. Some examples of AB crosslinked polymers are: AB crosslinked polymers of conjugated dienes [4], rubber toughened epoxy resins such as those based on the diglycidyl ether of bisphenol A and a carboxyl-terminated butadiene-acrylonitrile rubber [4].

In the thermoplastic IPN's the crosslinks are of physical nature. They offer the advantage over any of the other types of IPNs of being able to be processed and reprocessed at any time. There are three ways of introducing physical crosslinks; (a) ABA block copolymers in which the end block forms a discrete phase physically crosslinking the system (b) introduction of ionic groups which, when segregation takes place, form a discrete phase crosslinking the system and (c) crystalline regions in a partially crystalline material serve as physical crosslinks. Common examples are: crystalline/ crystalline mechanical blends such as poly(ester)/poly(carbonate) [4].

With respect to the semi-IPNs, they can be prepared sequentially or simultaneously.

In the first case N_I (or N_{II}) is formed by simultaneous polymerization and crosslinking and then it is swollen with M_{II} (or M_I). If the polymerizations are sequential in time, four semi-IPNs may be distinguished: if P_I is crosslinked and P_{II} is linear, the product is called a semi-IPN of the first kind, or semi-I. If P_I is linear and P_{II} is crosslinked a semi-II results. An example of a semi-II is SBR/PS, here the uncrosslinked SBR which contains the crosslinking agent, was dissolved in a styrene monomer solution followed by the thermal polymerization of the styrene [107]. The other two types correspond to the products obtained by inverting the order of polymerization. In a simultaneous semi-IPN either two monomers or prepolymers of linear polymers are mixed with a crosslinking agent specific for one of them. In this case only two semi-IPNs or semi-SINs may be distinguished [4]. An example is poly(4-vinyl phenol)/EVA (EVA contains 70% by weight of VA). After mixing both polymers the phenolic resin was crosslinked with hexamethylenetetramine [157].

2.4.3.2 THE RUBBERY MODULUS EQUATION FOR IPNs AND THE THIELE-COHEN EQUATION

There are two equations which relate the modulus and swelling behaviour to the double-network composition and crosslink level: the rubbery modulus equation for IPNs and the Thiele-Cohen equation. Both equations were deduced from the supposition that both components are identical.

SEQUENTIAL IPN MODULUS [4].

The following equation that is a simple average of the moduli of each of the networks in an IPN can not predict correctly the modulus of an IPN:

$$G = G_1 + G_2 = 3(\nu_1\phi_1 + \nu_2\phi_2)RT \qquad 2.133$$

where $\nu_1 = \rho\bar{M}c^{-1}$

To described G correctly it is necessary to consider that N_I dilutes N_{II} while N_{II} always swells and dilutes N_I.This can be accounted for by introducing the factor r_0^2/r_1^2 into 2.133 yields:

$$G = 3\,(r_0^2/r_1^2)\,(\nu_1\phi_1 + \nu_2\phi_2)\,RT \qquad 2.134$$

In the case of N_I, the concentration of the ν_1 chains is reduced to $\nu_1\phi_1$ and the factor is equal to $\phi_1^{-2/3}$ so G_1 is given by:

$$G_1 = 3\phi_1^{1/3}\nu_1 \qquad 2.135$$

In the case of N_{II}, sufficient continuity is preserved and so $r_0^2/r_1^2 = 1$ and G_2 may

be represented by the first term in 2.134. So G for the IPN is:

$$G = G_1 + G_2 = 3 (\phi_1^{1/3} \nu_1 + \phi_2 \nu_2) RT \qquad 2.136$$

Although this equation represents an improvement with respect to 2.134, it is still not able to account for the presence of physical crosslinks, which may result during the formation of the IPN, and the domination of N_I over N_{II}.

THE THIELE-COHEN EQUATION [4, 101].

The change in free energy for an IPN during swelling is:

$$\Delta G = \Delta G_m + \Delta G_{el\,(1)} + \Delta G_{el\,(2)} \qquad 2.137$$

where $\Delta G_{el(1)}$ and $\Delta G_{el(2)}$ are the elastic contribution of N_I and N_{II} respectively.

This equation may be written in terms of chemical potential as:

$$\Delta\mu = N_A (\partial \Delta G_m / \partial n_S)_{T,P} + N_A (\Delta \partial G_{el(1)} / \partial \lambda_1)_{T,P} (d\lambda_1 / \partial n_2)_{T,P} + N_A (\partial \Delta G_{el(2)} / \partial \lambda_2)_{T,P} (\partial \lambda_2 / \partial n)_{T,P} \qquad 2.138$$

The first term is given by the Flory-Huggins expression (see equation 2.25, p.13), except that the volume fraction of both components (ϕ_1 and ϕ_2) must be taken into account:

$$\mu_m = RT\{ \ln[1 - (\phi_1 + \phi_2)] + (\phi_1 + \phi_2) + \chi_s (\phi_1 + \phi_2)^2 \} \qquad 2.139$$

The second term is derived from the theory of rubber elasticity 2.108 (p. 33)

$$\Delta G_{el\,(1)} = (\nu_1 RT / 2) (3\lambda_1^3 - 3 - \lambda_1^3) \qquad 2.140$$

where

$$\lambda_1^3 = V / V_o = (V_o + n_s \phi_s / N_A + n_2 \phi_2 / N_A) / V_o \qquad 2.141$$

where ϕ_s is the molar volume of the solvent, ϕ_2 is the specific volume of P_{II}, V_o is the initial unswollen volume of N_I and V is the total volume of the swollen IPN

so

$$N_A (\partial \Delta G_{el1} / \partial \lambda_1)_{T,P} (\partial \lambda_1 / \partial n_2)_{T,P} = RT \phi_s (\nu_1 / V_o) (\phi_1^{1/3} - \phi_1 / 2) \qquad 2.142$$

For the third term, due to the fact that N_{II} is crosslinked in the presence of N_I, which acts as a diluent, the ΔS_{el} derived by Herman [4, 71] is used:

$$\Delta S_{el2} = \nu_2 R \{ 1 / 2 \ln (\lambda_2 / \lambda_2^o)^3 - 3/2 [(\lambda_2 / \lambda_2^o)^2 - 1] \} \qquad 2.143$$

where

$$\lambda_2 = (1 / \phi_2)^{1/3} = [v / (V^o - V_o)]^{1/3} = [(V^o + n_s \phi_s / N_A / (V^o - V_o)]^{1/3} \qquad 2.144$$

and λ_2^o (the deformation ratio in the unswollen state) is:

$$\lambda_2^o = (1 / \phi_2^o)^{1/3} = [v^o / (V^o - V_o)]^{1/3} \qquad 2.145$$

v^o is the unswollen volume of the IPN.

so

$$N_A(\partial\Delta G_{el2}/\partial\lambda_2)_{T,P}(\partial\lambda_2/\partial n_s)_{T,P}=[RT\phi_s\nu_2/(V^o-V_o)](\phi_2^{o\,2/3}\phi_2^{1/3}-\phi_2/2) \quad 2.146$$

If equations 2.139, 2.140 and 2.146 are substituted into 2.138 and supposing the system is in equilibrium so $\Delta\mu=0$, the following equation, which is the Thiele-Cohen equation, will be obtained:

$$\ln(1-\phi_1-\phi_2)+\phi_1+\phi_2+\chi_s(\phi_1+\phi_2)^2 = V_s\nu'_1(\phi_1^{1/3}-\phi_1/2)-V_s\nu_2'(\phi_2^{o\,2/3}\phi 2^{1/3}-\phi_2/2) \quad 2.147$$

where ν_1' and ν_2'correspond to the single networks and can be determined from the Flory-Rehner equation (see equation 2.125 p. 36). Galanti and Sperling[4] modified equation 2.147 by multiplying the first term on the right hand side by $(1/\phi_{01})^{1/3}$ which accounts for internal energy changes on swelling. The experimental quantity of interest in 2.147 is the volume of swollen IPN (ϕ, where $\phi = \phi_1+\phi_2$).

2.4.3.3 IPNs AND THE MOLECULAR CONTROL OF MORPHOLOGY

Most IPN and related materials investigated to date show, in a lesser or greater degree, phase separation. The size, phase and composition of the phase domains constitute the morphology of the material [4]. There are several factors which control the morphology in IPNs: (a) chemical compatibility, (b) interfacial tension, (c) crosslink densities of the networks (d) polymerization method and (e) IPN composition [13]. Kim *et al* [102] claimed that compatibility between the polymers composing the IPN is necessary because monomers or prepolymers must form solutions or swell networks during the synthesis. Beside this, compatibility between the components yields IPNs with smaller domain sizes as proved by Huelk *et al* [12] in a series of IPNs of poly(ethyl acrylate)/PMMA and poly(ethyl acrylate) with copolymers of PMMA-co-styrene. With respect to the degree of crosslinking it has been shown that the domain size of N_{II} decreases inversely with the degree of crosslinking, the tighter the initial network the greater the restriction to growth of the regions in P_{II} during phase separation. Donatelli *et al* [103] rationalized this behaviour with a semiempirical thermodynamic model that is explained in the next section. They were also able to show that even in semi-IPN's such as SBR-PS (PS is linear), crosslinking the SBR decreases the final size of domains [96, 104, 105]. Allen *et al* [104, 105] saw the same effect working with polyurethane/PMMA in which the polyurethane was crosslinked at different levels; the tighter the crosslinks the smaller the domain size.

The polymerization method also plays an important role in the morphology of the resulting product. In the case of IPNs, semi-IPNs and SINs in which the rate of formation is not the same, the first network formed is the one that controls the morphology. With respect to composition, N_{II} sets the upper limit of the amount of M_{II} swelled and an increase in the amount of the second component will result in an increase of the domain sizes [105-109].

2.4.3.4 A QUANTITATIVE EXPRESSION FOR PHASE DOMAIN SIZE

Donatelli *et al* [4, 13, 103] derived a semi-empirical equation for the phase domain sizes of semi-IPNs of the first kind. The development of the equation is done following a hypothetical path: (1) at the beginning P_I and P_{II} are completely separated, (2) then P_{II} swells N_I and (3) P_{II} phase separates in spherical domains within N_I, with no change in the volume of the system. The total change in free energy involved here is:

$$\Delta G_d = \Delta G_{12} + \Delta G_{23} \qquad 2.148$$

where ΔG_{12} and ΔG_{23} are the changes in free energy from state 2 to 1 and from state 3 to 2 respectively and ΔG_d is the free energy involved for the domain formation.

ΔG_{12} and ΔG_{23} are given by

$$\Delta G_{12} = \Delta G_m + \Delta G_{el} \qquad 2.149$$

$$\Delta G_{23} = \Delta G_{dm} + \Delta G_s \qquad 2.150$$

where ΔG_m is the free energy of mixing N_I with P_{II}, ΔG_{el} is the elastic free energy change of P_{II} swelling N_I, ΔG_{dm} is the free energy of demixing (phase separation taking place) and ΔG_s is the surface free energy for domain formation.

After substituting the expressions for ΔG_m, ΔG_{el}, ΔG_{dm} and ΔG_s in 2.149 and 2.150, the resulting expressions for ΔG_{12} and ΔG_{23} are substituted into ΔG_d in 2.148. Finally the domain size of P_{II} (D_2) that yields a minimum of ΔG_d, can be calculated from $d\Delta G_d / dD_2$ which is equated to zero, yielding the following equation:

$$(\nu_1 / C^2K^2)[\nu_1 / (1-w_2) + 2 / \bar{M}_1]D_2^3 + [(w_2 / \bar{M}_2) - (\nu_1 / 2)]D_2 = 2\gamma w_2 / RT \qquad 2.151$$

where ν_1 is the crosslink density of P_I, $\bar{M}_1$ is the primary molecular weight of P_I, D_2 is the domain size of P_{II}, $\bar{M}_2$ is the molecular weight of P_{II}, w_2 the mass fraction of P_{II}, γ is the interfacial energy, C is a constant of the order of $2^{1/2}$ and $k = (r_0 / \bar{M}^{1/2})$ for P_I (r_0 is the unperturbed root-mean-square end-to-end distance). This equation may be applied to IPNs taking $\bar{M}_2 = \infty$.

2.4.3.5 PHYSICAL AND MECHANICAL BEHAVIOUR OF IPNs AND BLENDS[13].

The properties of IPNs and blends depend on the properties of the components, and if two phases are present, which is very often the case, on the phase morphology and interactions between the phases. In two phase materials some properties are a simple average of the component polymers, however several other properties depart completely from such a simple average [13]. In heterogeneous blends and two phase IPNs the glass transition and small deformation mechanical properties (viscoelastic behaviour) reflect the molecular relaxation processes characteristic of each constituent. Inhomogeneous blends and IPNs containing an elastomeric component, exhibit considerable toughness. In the case of IPNs this is attributed to a cellular type morphology and the probable dual phase continuity.

A careful interpretation of the mechanical and dynamic mechanical properties of these mixtures may provide a great deal of information about blends and IPNs. For example in the case of the two phase mixtures it may give some insight into their morphology, volume fraction of inclusions, etc [110]. It is then of interest to be able to predict the properties of any type of mixture (blends, IPNs, semi-IPNs, etc). In determining the physical and mechanical behaviour of any of them it is necessary to consider their degree of miscibility. If miscible, it is important to know the interactions between the molecules and how they pack. If two phases, it is important to know which is the continuous phase and which is dispersed, the shape of the particles, if the particles are not spherical their orientation, the morphology of the system, the way the particles pack and the type of interaction occuring at the interfaces.

If the mixture is behaving as one phase its properties may be predicted by either of the following expressions[149]:

$$p = p\phi_1 + p\phi_2 \qquad 2.152$$

$$1/p = \phi_1/p_1 + \phi_2/p_2 \qquad 2.153$$

where p is any property and ϕ_1 and ϕ_2 are the concentrations of both components. These concentration terms may be weight fractions, volume fractions, or mole fractions.

Equation 2.152 is the simplest mixture rule and is called "the rule of mixtures". Equation 2.153 is the "inverse rule of mixtures". Both expressions simply provide the bounds or limits where the values of the properties of one phase mixtures may be expected.

In the two phase system category it is possible to find systems with a continuous phase and a dispersed or discontinuous phase (suspensions, semi-IPNs), or mixtures in

which two separate or discrete continuous phases are present (IPNs, mats and felts filled with air or some other material, etc.). For all these systems there are a number of theories and equations in the literature which try to predict or simulate their mechanical and dynamic behaviour [110, 148, 149, 150]. One of these equations is the well known Kerner equation,which was developed by considering the effect of hydrostatic compression and tension on a single, typical, filler particle.The Kerner equation requires spherical particles and perfect adhesion between the matrix and the filler particles [150]. The equation was first developed to predict the shear moduli (G) of two phase systems. Later on it was extended to predict their viscoelastic behaviour using the correspondence principle (this principle states that expressions for the complex moduli of composites may be obtained by replacement of phase elastic moduli by phase complex moduli in exact expressions for the corresponding elastic moduli [150]). The equation for the storage modulus G'can be written as [148]:

$$G' = G_m' (A / C) - G_m'' (B / C) \qquad 2.154$$

where

$$A = (1- \phi)(1 + \alpha\phi)\gamma(G_m^{2'} + G_m^{2''}) + (1 - \phi)(a + \phi)\alpha\beta^2\gamma(G_i^{2'} + G_i^{2''}) + [(1 - \phi)^2\alpha+(\alpha + \phi)(1 + \alpha\phi)]\beta\gamma(G_m'G_i' + G_m''G_i'') \qquad 2.155$$

$$B = \beta\gamma(\alpha + 1)^2\phi(G_i''G_m' - G_m''G_i') \qquad 2.156$$

$$C = (1 + \alpha\phi)^2(G_m^{2'} + G_m^{2''}) + (1 - \phi)^2\alpha^2\beta^2(G_i^{2'} + G_i^{2''}) + 2(1+ \alpha\phi) (1 - \phi) \alpha\beta (G_i'G_m' + G_m''G_i'') \qquad 2.157$$

where m denotes the matrix and i the inclusion, ϕ_i is the volume fraction of the inclusion, γ, β =1 and $\alpha = 2 (4-5\mu_1) / (7-5\mu_1)$ (μ_1 is the Poisson ratio of the continuous phase).

These equations are used in the evaluation of the dynamic mechanical behaviour of the blends and semi-IPNs studied in this work.

2.5 DETERMINATION OF THE MISCIBILITY AND PHASE SEPARATION BEHAVIOUR IN BLENDS AND IPNs

Some of the main goals of polymer blends and IPNs characterization are to determine the miscibility, the degree of interaction of the components and, in the case of two phase systems, to study their morphology and the compositon of the phases [58]. There are many methods for carrying out such characterization. In table 2.1 a list of some of these is given. In the paragraphs below a brief description will be given of some of the most frequently used methods.

A. One or two phases

1. Opacity (light scattering)
2. Glass transition
   a. DSC, DTA, TMA, TOA*
   b. Dynamic Mechanical
   c. Dielectric
   d. Volumetric
3. Microscopy (visible, phase contrast, electron)
4. Diffusion (Permeability)
5. Excimer Fluorescence
6. Mechanical rheological response.

B. Composition of equilibrium phases

1. NMR
2. Glass transition
3. Phase equilibria (using any method in A by varying during the experiment T, P or concentration)

C. Thermodynamic Parameters

1. Phase equilibria
2. Inverse gas chromatography
3. Vapour sorption
4. Neutron scattering
5. Heats of solution
6. Freezing point depression
7. Ternary (polymer 1 + polymer 2 + solvent) phase behaviour.

*DSC = Differential Scanning Calorimetry, DTA = Differential Thermal Analysis, TMA = Thermomechanical analysis, TOA = Thermo-optical Analysis

Table 2.1. Methods for the determination of the miscibility and phase separation behaviour in polymer blends

2.5.1 GLASS TRANSITION TEMPERATURE

The glass transition temperature (T_g) can be defined in a number of ways. One of the simplest definitions is the following: the T_g is the temperature below which a polymer is glassy and above which it is rubbery. In terms of molecular motion, the T_g is the temperature at which large scale molecular motions of chain segments start. Although there is no enthalpy change at the T_g, the heat capacity and the mechanical properties change abruptly at this temperature.

The detection of a single T_g, whose temperature is intermediate between those

corresponding to the two component polymers is very frequently used to determine polymer blend miscibility.This criterion guarantees molecular homogeneity within the limits of detection of the technique used to measure the T_g [6].

In binary systems a miscible blend will exhibit a single glass transition which is usually intermediate between the T_gs of the two components. Blends of incompatible polymers, that separate completely into two distinct phases, exhibit two glass transitions similar in temperature and width to those of the parent polymers. In cases of intermediate miscibility, such as partial mixing between components or small size of the dispersed phase, the T_g analysis is more complex. In these cases, the T_gs of the individual components may appear as a broad single peak or as two peaks shifted towards each other with respect to the T_gs of the homopolymers [6]. There is substantial evidence to suggest that in such systems significant amounts of both component molecules may intermix in interfacial regions between the dispersed phase and the matrix. It is possible that this interfacial mixing may involve the lower molecular weight molecules of both components for which the thermodynamic driving force for compatibility is the greatest [6].

Many compatible blends exhibit T_g composition dependence which can be predicted by any of the well known equations such as the Fox, the Kelley-Bueche, the Gordon Taylor, Gibbs-DiMarzio or Kanig expressions [3, 6]. These equations, which may be theoretical or empirical, are derivable from only a few simple but very general mixture rules. Of all these expressions the Fox equation is the simplest:

$$1 / T_{gb} = w_1 / T_{g1} + w_2 / T_{g2} \qquad 2.158$$

where w_1, w_2 are the weight fractions of components 1 and 2 respectively, T_{gb}, T_{g1} and T_{g2} are the T_gs of the blend and component 1 and 2 respectively.

This equation is empirical and as it is basically an inverse rule of mixtures relationship it predicts a limiting behaviour. This expression applies most accurately to miscible polymer blends where the components do not interact strongly [133].

The use of the T_g criterion for the determination of miscibility has the following limitations: (1) the T_gs of the components should at least be 20 degrees apart and it must be possible to differentiate between them (such differentiation depends on the sharpness of the T_gs, the proximity of the phase boundaries, instrumental characteristics and possible transitional smearing in the mixture), (2) small concentrations (usually less than 10%) of any of the two components may not be detected, (c) the analysis of crystalline material is nearly always difficult as glass transitions and melting processes may overlap.

There are many methods for the determination of the T_gs, among the most widely used are: the calorimetric determination of the heat capacity as a function of temperature

(and related techniques) and dynamic mechanical testing.

2.5.1.1 CALORIMETRIC TECHNIQUES

Calorimetric techniques have evolved from older differential thermal analysis techniques which have been used for a variety of applications. Commercial production of more sensitive apparatus using a variety of cell designs led to the widespread use of differential calorimetry for detecting T_g by detecting the corresponding change in heat capacity. One family of designs e.g. Perkin Elmer DSC provides an absolute calorimetric measurement. Other systems e.g. Du Pont are modified DTA cells which may be calibrated with known transitions. In DSC a change in enthalpy between the sample and the reference is measured as a function of temperature (dH/ dT = Cp in mcal / seg). In DTA the difference in temperatures (ΔT) between the sample and the reference is measured as a function of T. The magnitude of ΔT is proportional to the change in enthalpy, the specific heat capacity (Cp), and the thermal resistance to the flux of heat (R). DTA presents some inconveniences for quantitatve measurements because it requires knowledge of the variation of Cp, R and the calibration constant of the equipment with temperature, inconveniences that are overcome quite successfully by DSC. However for qualitative determination of T_gs either of the two techniques will be suitable as the change in Cp produces a step in the signal.

These calorimetric techniques have the following advantages: (a) they require small samples (5-30 mg) [6]. (b)The measurements are relatively rapid and are performed with high sensitivity [60]. (c) It is possible to do a qualitative determination of the composition of unknown multiphase or compatible blends from the measurement of the height and position of the T_gs [62]. There are, however, the following disadvantages: (a) the sample needs to have a homogeneous presentation (film, fine powder, etc.) in order to achieve the best contact with heating and detection elements [61], and (b) the results have to be cautiously interpreted since the technique may present artifactual phenomena [59].

2.5.1.2 DYNAMIC MECHANICAL ANALYSIS (DMA)

The determination of elastic and viscoelastic properties of polymers by subjecting them to small amplitude cyclic deformations is known as dynamic mechanical analysis. These measurements can be accomplished using various experimental techniques of which free and forced vibrational methods are the most widely used [6]. Forced vibrational techniques use a sample rigidly clamped at both ends to which a small sinusoidal strain

(ε) is applied at a constant frequency (ω) by an external power source. As a response, a sinusoidal stress (σ) will be observed with a lag or phase angle δ with respect to ε (linear viscoelastic behaviour) [31]. This phase lag results from the necessary time for molecular strain rearrangements to occur and is associated with relaxation phenomena [7].

In order to introduce the time dependance of ε and σ, it is possible to express them in their Fourier components:

$$\varepsilon^* = \varepsilon_0 e^{iwt} \qquad 2.159$$

$$\sigma^* = \sigma_0 e^{[iwt - \delta(\omega)]} \qquad 2.160$$

where ε_0 and σ_0 are the peak strain and stress respectively.

The ratio σ^* / ε^* yields the dynamic modulus G* which describes completely the dynamic mechanical behaviour of a material for the case of small strain.

$$G^* = (\sigma_0 / \varepsilon_0)\, e^{[-i\delta(\omega)]} = Go\, e^{[-i\delta(\omega)]} \qquad 2.161$$

where $\sigma_0 / \varepsilon_0 = G_0$

Equation 2.161 can be expressed as:

$$G^* = G_0 (\cos\delta - i\sin\delta) \qquad 2.162$$

where $G_0\cos\delta$ (real part) is the storage modulus G' (related to the stored elastic energy) and $G_0\sin\delta$ (imaginary part) is the loss modulus G" (related to the viscous loss of energy). The ratio of these two quantities is called $\tan\delta$ or the dissipation factor:

$$\tan\delta = \sin\delta / \cos\delta = G'' / G' \qquad 2.163$$

These properties are directly affected by molecular processes and their study over a wide range of temperature and frequency provides the most sensitive means of studying glass and secondary transitions, and of quantitatively determining the effects of phase type and morphology of such phases [64]. The relationship between mechanical properties and the corresponding molecular processes can be explained as follows: when a polymer is heated through a transition temperature, new modes of molecular motion are initiated; the frequency of these motions increases rapidly with temperature. If the sample is simultaneously subjected to an alternating stress of fixed frequency, energy will be transfered from the external force field to the new molecular motions when their correlation times coincide with the applied frequency and G" will therefore increase. The maximum of G" will occur at a temperature where the maximum number of molecular motions have the appropriate correlation time. At higher temperatures all the molecular motions increase in frequency, and the energy absorption from the external force field decreases rapidly, as does G". In the region of the glass transition G" will maximize and G' will present an inflection point at essentially the same temperature; their ratio, $\tan\delta$, will show a maximum close at a temperature close to this. The maximum in $\tan\delta$ is more easily measured and is therefore often used to measure T_g.

There are many methods for measuring tanδ, G' and G", and the Rheovibron Dynamic viscoelastometer has been one of the most popular and widely used. A brief description of this method and the Dynamic Mechanical Thermal Analyser (DMTA) (Polymer Laboratories) will be presented in section 3.2.2 (p. 63).

One disadvantage of DMA compared with calorimetric methods (section 2.5.1.1 (p. 47)) is that the first technique can only study samples as films or fibres. Despite this limitation, DMA is more sensitive than the calorimetric methods and can easily detect secondary transitions.

Dielectric relaxation and dilatometry are not so frequently used to measure T_gs because they present greater experimental difficulties than calorimetric and DMA techniques [6, 59]. Dielectric relaxation, which is very similar to DMA, can only be used with blends of polar polymers and makes possible the study of the dynamic dielectric constants ε', ε" and tanδ as a function of temperature over a wide range of frequencies. In dilatometric methods, a volumetric determination of the T_g is made by detecting a discontinuity in the expansion coefficient α. It is possible to use this technique for the determination of the volume change of mixing in binary blends [59].

2.5.2 OPTICAL CLARITY

Visual confirmation of the presence of one or two phases has been used as a preliminary indication of miscibility [3]. When two polymers are mutually miscible they are optically clear. It has been shown that only a very small amount of a second incompatible polymer is required to cause opacity in the blend [6]. However this criterion must not be used as an absolute judgement as immiscible polymers may be optically clear as is the case of (a) very thin films, (b) films in which both components distribute in two layers (one on top of the other), (c) blends in which the two polymers have a difference in refractive indices of ≤ 0.01 and (d) blends in which the dispersed phase has smaller dimensions than the wavelength of visible light (6000 Å).

2.5.3 MICROSCOPY

Microscopy is the best method for detailed characterization of phase morphology in blends. It depends on the development of contrast between phases, a requirement that is quite often difficult to meet in polymer blends. Efforts to increase the contrast in the sample may lead to spurious results. In optical microscopy contrast may arise from colour, opacity, refractive index, orientation absorption and dichroic differences. If

ultraviolet illumination is used differences in fluorescence characteristics may be used. In transmission electron microscopy (TEM) contrast is due to electron scattering differences. In scanning electron microscopy (SEM), contrast depends on the surface texture. To enhance contrast in this technique polishing, etching or cryofracture are commonly used.

2.5.3.1 LIGHT MICROSCOPY

Transmitted light and phase contrast microscopy are the two types of light microscopy most frequently used in polymer blends. For contrast both techniques rely on sufficient difference of refractive index. Transmitted light microscopy also relies on differences in opacity or colour. Phase contrast is preferred over transmitted light because it gives contrast in transparent samples, avoiding the necessity of staining the sample which may cause spurious results. Good optical microscopes are capable of resolution down to 0.2 μm.

Image formation in microscopy is always based on interference phenomena. Basically the microscopic samples diffract the illuminating light and, depending on the aperture of the objective, a number of diffracted wave fronts reaching the objective take part in image formation by interference between those wavefronts [66].

Phase contrast techniques can be applied to samples with regions of different refractive index or thickness called phase objects. Such phase objects (A) diffract the light in all directions. The resulting wavefronts called "diffracted waves" will have a phase difference (φ) with respect to the light rays passing through the medium (M) called direct waves.φ is a function of the path difference δ, defined as

$$\delta = (\eta - \eta')\, e \qquad 2.164$$

where η, η' are the refractive indices of M and A and e is the thickness of A. The direct and diffracted waves will be collected by an objective lens and then will interfere with each other so as to form the final image. The interference and the resulting contrast of the image are direct functions of φ [67]. There are a great variety of phase contrast microscopes, each based on a different way of interfering the diffracted and direct waves. A brief description of the Carl Zeiss Jena and the Nikon Optiphot Universal microscopes will be given in section 3.6.2, p. 84.

2.5.3.2 ELECTRON MICROSCOPY

Transmission electron microscopy (TEM) and scanning electron microscopy (SEM) have been widely used to study polymer blends [58]. TEM has often been used to study phase separation, to determine the size of domains in polymer blends and to define the scale of mixing. SEM has been use to analyze surface textures which in the case of a blend will correspond to the blend texture.TEM is quite similar to visible light microscopy; the main difference between them is that the lenses in TEM are electromagnetic instead of glass and it uses an electron beam instead of a light beam. As the λ in TEM is shorter ($\lambda \sim 12 / v^{1/2}$, where v is the voltage. For a v = 100 kv, λ = 0.04 Å) it has better resolving power (Rp) than light microscopy because the lens has greater angle of acceptance θ)

$$Rp = \lambda / 2\eta \sin(\theta / 2) \qquad 2.165$$

In order to avoid scattering of the electrons TEM has to work at very low pressures (10^{-5} torr).The contrast in this microscopy is a result of electron scattering and is an inverse function of the accelerating voltage. TEM has some limitations: (a) it has to work at low pressures, (b) the preparation of the specimens is bothersome, (c) the electron beam can easily damage the specimen and (d) particularly in the case of polymer blends the contrast tends to be poor or non existent because the elemental compositions of many polymers are not very different. To enhance the contrast, electron scattering substances, such as bromine or osmium tetroxide, may be used; unfortunately this method may cause artifacts, specially in blends, where it may promote phase separation [3, 58]. In some cases annealing the sample under the electron beam can also help to improve the contrast [68].

SEM is easier to use than TEM. The contrast may be obtained by breaking the specimen or polishing the surface. If the contrast is not sufficient it may be improved by solvent or chemical etching, this again, in the case of polymer blends, may affect their miscibility [3, 58].

2.5.4 SCATTERING METHODS

Scattering methods are very commonly used to determine the miscibility and phase boundary of polymer blends. These techniques may also provide an idea of the size of the domains when the blend is phase separated. The principle of these methods is the following; the sample under study is subjected to a certain type of radiation which could be light, X-rays or neutrons. If the radiation in question does not find any obstacle

(inhomogeneities) in its path it will simply be transmitted, but if there are inhomogeneities in the medium they will scatter the radiation [3]. The resulting scattering pattern may contain information on the shape and dimension of the inhomogeneities and their average spacing (d). The presence of inhomogeneities in the sample causes variation in a physical property called the contrast factor K*, which is a function of the type of radiation used. In light, K* is the polarizability or refractive index difference, for x-rays it is the electron density difference and for neutrons it is the difference in scattering length of the nuclei [65, 69]. The choice of radiation depends on: (1) the dimensions of the inhomogeneities (path length), which should be of the same order of magnitude as λ of the radiation, (i.e. light 4000-8000 Å, neutrons 5-15 Å, X-rays ~ 1.5 Å). (2) The value of the contrast factor arising from inhomogeneities which should be reasonable for the type of radiation choosen. (3) Experimental convenience and availability of radiation sources etc [69]. Clearly the source of radiation used determines the scale of phase separation observed [69, 70].

In light scattering if K* is favourable enough (there is sufficient difference between the refractive indices of the components of the blend) the blend will develop cloudiness when phase separating.This phenomenon which is used as an indicator of the miscibility limits of a polymer mixture, is the basis of the cloud point method. The transition between the transparent and turbid state is considered as the point of incipient phase separation and is called the cloud point (CP). The determination of the CP for a series of compositions of a blend generates what is known as the phase boundary [3] and as mentioned earlier on (p. 22) it may coincide with the binodal curve. The phase separated state may be produced by variations of temperature, pressure or composition of the mixture. It is most common to use the temperature as the variable.

In light scattering the following equation [3] is very important as it suggests a method for the determination of the spinodal. As mentioned in expression 2.87 (p. 22), the spinodal corresponds to the loci of points where $\partial^2 G/\partial\phi_1\partial\phi_2 = \partial\mu_1/\partial c = 0$. Inspection of 2.166 shows that this corresponds to the points where R^o_θ will tend to infinity [69]:

$$R^o_\theta = [K^* (1+\cos^2\theta)RTV_1c] / (-\delta\mu_1 / \delta c)_{T,P} \qquad 2.166$$

where R^o_θ and K* are

$$R^o_\theta = r^2 I_s / I_o \qquad 2.167$$

$$K^* = (2\pi^2\eta_o^2 / \lambda^4 r^2 N_{AV})(d\eta / dc)^2 \qquad 2.168$$

and I_s is the scattered light, I_o is the incident light, θ is the scattering angle, λ is the wavelength of light, r is the radiation distance, N_{AV} is the Avogadro number, η_o and η are the refractive indices of the solvent and the solution respectively, c is the concentration of the solution.

In some systems the domains are too small to be determined by light scattering so neutron or X-ray scattering may be used instead. Neutron scattering is very powerful and can be used to study the conformation of molecules in liquid solution or in blends. The K* in neutron scattering is:

$$K^* = [(\rho b^p - \rho b^s) / \rho]^2 \qquad 2.169$$

where

$$\rho b = \Sigma b / M\rho \qquad 2.170$$

and ρb^p and ρb^s are scattering length densities and ρ is the density

K* can be increased by labelling with deuterium although this may sometimes peturb the original state of miscibility of the blend. One disadvantage of neutron scattering is the relative inaccessibility of neutron sources.

X-rays may also be used for the same measurements as those performed with light or neutron scattering. K* in this case is:

$$K^* = [I_e^2(\rho e^p - \rho e^s) / \rho^2]N_{AV} \qquad 2.171$$

where $I_e = e^2/mc^2$, the Thompson factor (effective cross-section of an electron for scattering and X-ray), ρe^p is the mean electron density of the particles and ρe^s is that of the solvent [69].

The angular dependance of scattering may provide information about the type of phase separation mechanism followed by the blend and it may give an idea of the size of the domains. If the blend phase separates by spinodal decomposition a diffraction ring pattern is formed by the scattered radiations. This is a consequence of the increase in amplitude of the particular wavelength which becomes favoured during the decomposition. The ring pattern moves to smaller wave vectors (Q) as the size of the domain (d) increases. Q is the absolute value of the difference between the incident q and the scattered q" wave vectors and is given by:

$$Q = (4\pi / \lambda)\eta \sin \theta / 2 \qquad 2.172$$

where η is the refractive index of the medium (for X-rays and neutrons $\eta = 1$)

In binodal decomposition there is no formation of a diffraction ring as there is no a regular structure formation during nucleation and growth. If I_s is plotted as a function of angle, traces similar to those presented in figure 2.4 may be obtained. Diagram A corresponds to the typical exponential scattering pattern shown by a blend undergoing phase separation by nucleation and growth. (The exponential behaviour denotes a distribution of sizes rather than a preferred size of domains). Diagram B shows a peak with a maximum at a particular value of θ. This pattern is usually presented by systems undergoing spinodal decomposition. Although it is not very common, nucleation and growth may also show this type of pattern. This behaviour corresponds to the case

where the size of domains is quite similar. One way of verifying if spinodal decomposition or nucleation and growth are taking place is through the determination of the diffusion coefficient D from isothermal scattering experiments. A positive D is indicative of nucleation and growth, a negative D corresponds to spinodal decomposition.

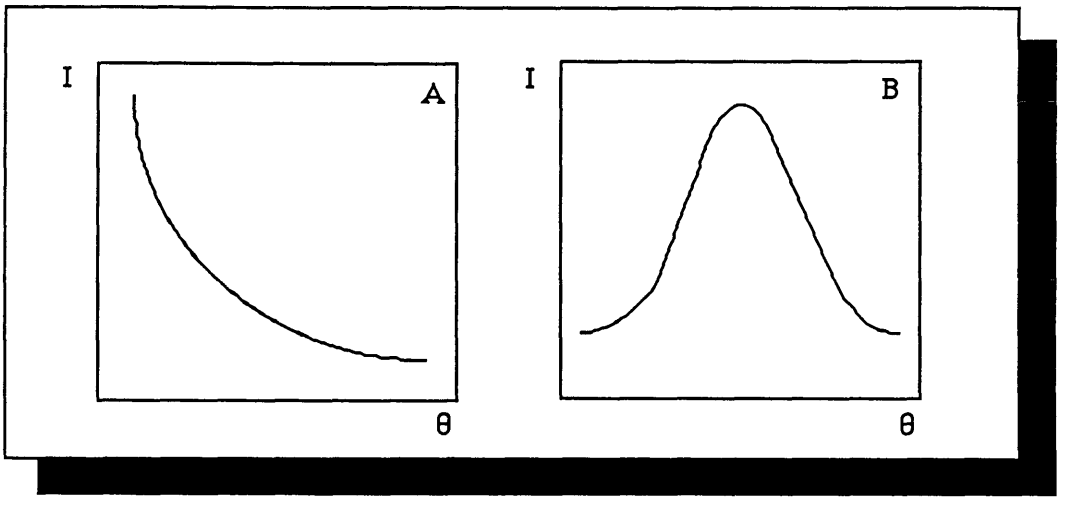

Figure 2.4 Scattering behaviour of a blend undergoing phase separation by: (a) nucleation and growth and (b) by spinodal decomposition.

When a blend is phase separating by nucleation and growth, it is possible to use the Guinier law:

$$I = \exp[(-Q^2R_g{}^2)/3] \qquad 2.173$$

to work out the size of domains by plotting lnI vs Q^2. As shown in A in figure 2.5 a straight line of slope $-R_g{}^2/3$ (R_g is the radius of gyration) may be the result. If instead of a straight line a curve is obtained, as shown in B, R_g may be calculated from the slopes of the curve at high and low values of lnI. These resultant values of R_g will provide the limiting value of the domain size range

In the case of a blend undergoing spinodal decomposition it is possible to work out the correlation length by determining the θ corresponding to the peak maximum; using this value and equation 2.179 it is possible to obtaine the value of Q. The correlation length (d) may be determined using the following expression:

$$d = 2\pi / Q \qquad 2.174$$

This expression is simply obtained by substituting into expression 2.172 Bragg's law:

$$2d\sin(\theta/2) = \lambda \qquad 2.175$$

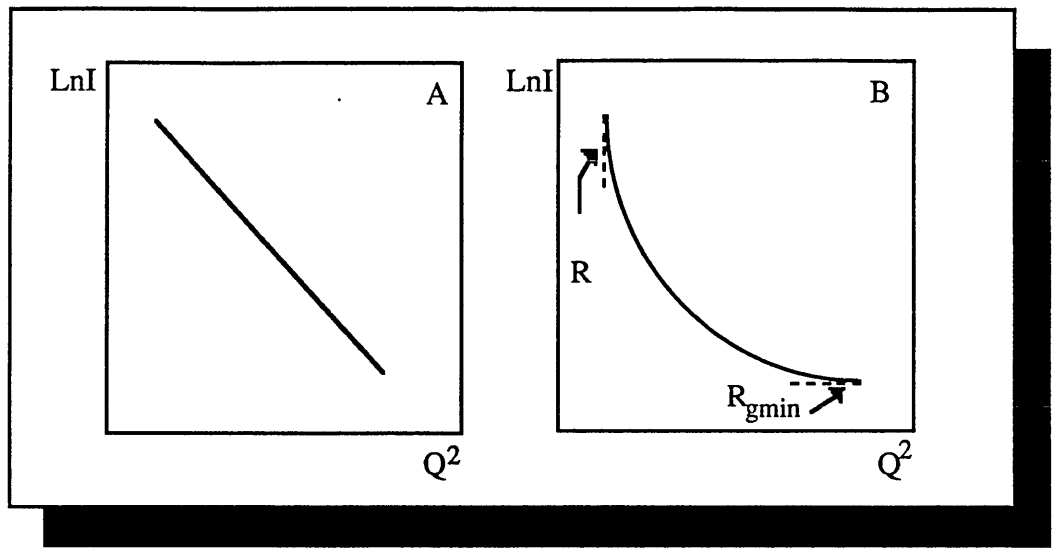

Figure 2.5 Plots of lnI vs Q^2. Diagram (a) represents a linear behaviour. The slope gives R_g. Diagram (b) represents a non linear behaviour. The slope at high and low values of lnI provide the limiting values of the domain sizes.

SUMMARY

This chapter summarizes the theoretical background which will be needed to analyze the experimental work presented in the next chapter. The techniques and methods introduced in this chapter were used throughout the experimental work. Further details of practical methods are presented when the results are introduced and discussed.

CHAPTER 3
EXPERIMENTAL

This chapter outlines the experimental work involved in the study of the effect of crosslinking one of the components of a blend on its miscibility and phase separation behaviour. The chapter includes the preparative techniques (materials and purification, blending, crosslinking, etc.) and the characterization methods used to study the miscibility and phase separation behaviour (dynamic mechanical analysis, light scattering, etc.)

3.1 MATERIALS AND PURIFICATION

The polymers and blends selected for this work are shown in table 3.1. The polymers listed under component I were crosslinked after being blended with a second polymer which appears on the line corresponding to component II.

3.1.1 SULPHOCHLORINATED POLYETHYLENES

3.1.1.1 SULPHOCHLORINATED POLYETHYLENE WITH 43% Cl CONTENT AND 1% S AS SO_2Cl GROUPS.

A sulphochlorinated polyethylene with 43% Cl content and 1% S as SO_2Cl groups, was provided under the name of Hypalon 48 by Du Pont U.K. Ltd. and will henceforth be called $SCPE_{43}$. Before using it, it was necessary to remove the talc added to it by the manufacturers. This was performed by preparing a 5% solution of $SCPE_{43}$ in methyl ethyl ketone (MEK) analar grade (BDH Chemicals Ltd). The MEK was previously dried over a molecular sieve. The resultant solution was centrifuged at 14,000 rpm for 30 min at 17°C (the ultracentrifuge used was an MSE high speed 25). The supernatant liquid was poured into a petri dish. The MEK was then allowed to evaporate slowly by partially covering the petri dish until a film was obtained. Last traces of MEK were eliminated by leaving the film a minimum of 7 days in a vacuum oven at 50°C. Du Pont specifies that this material is sulphochlorinated by a solution process which should yield

in principle an amorphous material. However, when viewed between cross polars in a microscope (Nikon Optiphot Universal), characteristic spherulitic structures were still present (see figure 3.1). Du Pont technical personnel commented that this was to be expected due to the characteristics of the solution process followed industrially.

Component I	Component II				
	PVC	EVA_{45}	PBA_{LMW}	PBA_{HMW}	$PMMA_{1.4}$
$SCPE_{43}$	X	X			
$SCPE_{54}$			X	X	X

$SCPE_{43}$ = sulphochlorinated polyethylene containing 43% Cl and 1% S as SO_2Cl groups.

$SCPE_{54}$ = sulphochlorinated polyethylene containing 54% Cl and 1% S as SO_2Cl groups.

EVA_{45} = copolymer of ethylene-vinyl acetate containing 45% vinyl acetate

PBA_{LMW} = poly(butyl acrylate) with a $\bar{M}_n$= 27,000

PBA_{HMW} = poly(butyl acrylate) with a $\bar{M}_n$=183,000

$PMMA_{1.4}$ = poly(methyl methacrylate) with intrinsic viscosity of 1.4

Table 3.1 Polymers and blends studied in the present work.

3.1.1.2 SULPHOCHLORINATED POLYETHYLENE WITH 54% Cl CONTENT AND 0.94% S AS SO_2Cl GROUPS

As indicated in chapter 1 (p. 6), SCPE samples with Cl contents higher than 50% are required to prepare miscible blends with PMMA or PBA. As SCPEs of Cl contents higher than 43% are not commercially available, it was necessary to prepare them. The chlorosulphonation method followed was based on Mc.Queen's [111] method. This procedure, is an extension of the chlorosulphonation reaction of small molecules known as the Reed reaction [76, 112].

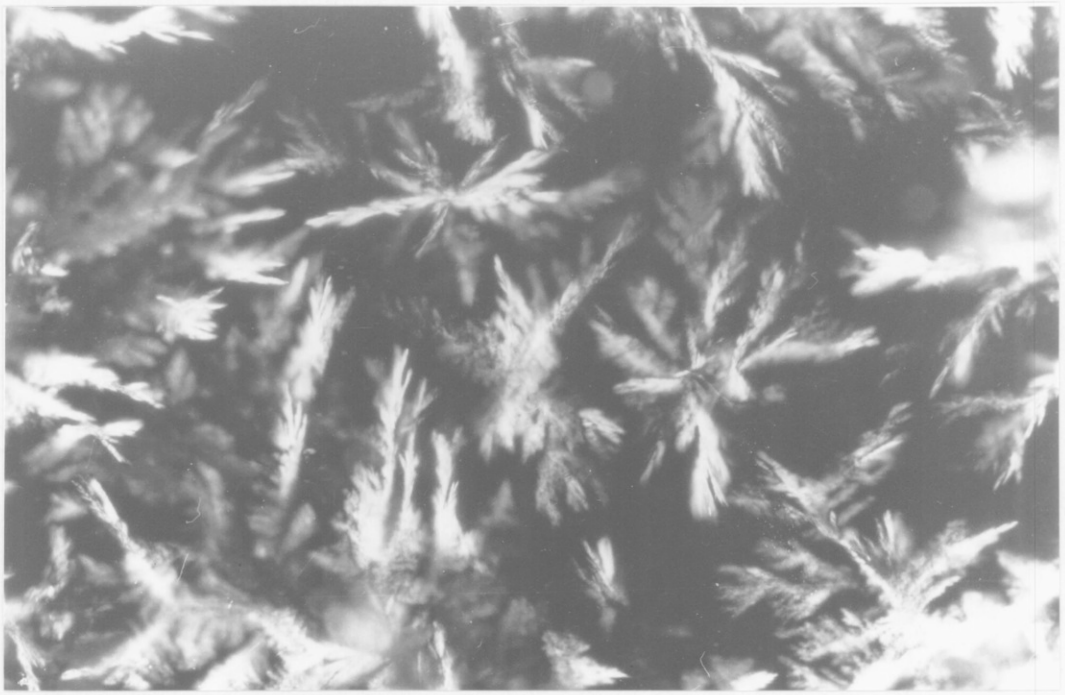

Figure 3.1 Micrograph of the spherulitic structures observed in $SCPE_{43}$

$$RH + Cl_2 + SO_2 \xrightarrow{h\nu} RSO_2Cl \qquad 3.1$$

This reaction follows a free radical substitution mechanism and needs visible or u.v. light to catalyse the homolysis of Cl_2 [112].

In the present work, 60 g of high density polyethylene (HDPE) (BDH Chemicals Ltd.) were placed with 1.2 litres of chlorobenzene analar grade (BDH Chemicals Ltd.) in a 2 litre round bottom flask fitted with a glass stirrer, a reflux condenser and inlets for N_2, Cl_2 and SO_2. Lecture bottles containing Cl_2 and SO_2, were connected to wash bottles with concentrated H_2SO_4 which in turn were connected to flowmeters and then to gas inlets. A soda lime trap was used to collect unreacted Cl_2 and SO_2. N_2 was bubbled slowly into the chlorobenzene which was warmed up to 130°C to dissolve the HDPE. Stirring was provided continuously during the whole reaction. When the HDPE was completely dissolved, two tungsten lamps (60 watts each) were turned on and Cl_2 was passed into the flask with a flow of 40 ml / min for 110 min. The temperature was then allowed to drop to 56°C and, while keeping Cl_2 constantly flowing, the SO_2 was passed into the flask for 53 min. (McAlevy [77] points out that the final SO_2Cl content may be controlled by employing the appropiate quantity of reactant which must be introduced at temperatures around 56°C to favour the formation of RSO_2Cl). Then the introduction of SO_2 was stopped and the temperature was increased again, letting the Cl_2 flow for

another 6.25 h (see table 3.2). To determine the content of Cl and S already introduced to the HDPE, elemental analysis was carried on. For this purpose, a few ml of the product were precipitated and washed with an excess of methanol. This was left drying at 50°C for a week. The sample was analyzed in an elemental anlyzer (Carlo Erba, model 1102) which provided facilities for the determination of C, H, O, and N. Cyclohexanone-2,4-dinitro-phenylhydrazone and benzoic acid were used as standards for the CHN and O analysis respectively. The S content was calculated by assuming that all the S and O were present in SO_2Cl groups; the Cl content was then obtained by difference. At this stage the sample contained 45.55% of Cl_2 and 0.63% of S.

As the Cl and S contents were still below the required level, the rest of the product kept in solution was chlorosulphonated again. On this occasion, the Cl_2 was introduced for 3.20 h (see table 3.2) and the SO_2 for 55 min. The final product, whose Cl and S content were determined as before, had 54% Cl and 0.94% S, which was a suitable composition for the purposes of this work. In table 3.2 the efficiency of conversion (E) is shown for each of the chlorosulphonation stages. The E may be defined as:

$$E = [\, WR / (\, WS \times T \,) \,]100 \qquad 3.2$$

where WR is the total weight of Cl_2 reacted, WS is the total weight of Cl_2 supplied in unit time and T is the reaction time.

As can be seen in table 3.2 the introduction of the first 45.55% of Cl and 0.63% S in the HDPE have a degree of conversion of 32.6% and 12.48% respectively (see $SCPE_{54}$ (a)). A further introduction of 8.45% of Cl and 0.31% of S to the molecule is more difficult due to steric hindrance of the atoms of Cl and S already introduced. At this stage, E decreased to 20.74% for Cl and to 5.92% for S (see SCPE54 (b)). This effect was also clearly observed for the chlorination reactions of HDPE previously performed by Chai [26, 113] and Rostami [114]. As shown in table 3.2, the E values for the Cl introduction in CPE_3, which contained almost the same percentage of Cl_2 as that in $SCPE_{54}$, are quite similar (29.96% and 28.39% respectively) and that of the CPE_{20}, which was chlorinated exhaustively, is very low.

3.1.2 POLY(VINYL CHLORIDE) (PVC).

A bulk polymerized PVC known as Breon M 110/50 (BP Chemicals Ltd.), was purified by centrifuging a 5% solution in dried MEK at 14,000 rpm for 30 min. The supernatant liquid was cast on a petri dish, allowing the solvent to evaporate slowly. Traces of MEK in the resultant film were eliminated by leaving the sample for one week at 48°C in a vacuum oven.

			Cl introduction				SO_2 introduction			
Sample	Reference	HDPE weight (g)	%Cl	Flow cm^3/min	Time min	E* %	$\%SO_2$	Flow cm^3/min	Time min	E* %
$SCPE_{54}$ (a)	This work	60	45.55	40	660	32.60	0.63	20	53	12.48
$SCPE_{54}$ (b)	This work	60	54	40	193	20.74	0.94	20	55	5.92
$SCPE_{54}$	This work	60	54	40	853	29.96	0.94	20	108	9.14
CPE_3	114	20	52.65	30	390	28.39	—	—	—	—
CPE_{20}	26,113	10	62.1	28	600	11.60	—	—	—	—

* % Efficiency of conversion = E = (WR/ (WS x T) 100
WR is the total weight of chlorine reacted, WS is the total weight of chlorine introduced, T is the reaction time

Table 3.2 Efficiency of conversion of the Cl_2 and SO_2 introduction during chlorosulphonation.

3.1.3 VINYL CHLORIDE (VCM).

225 g of VCM monomer were supplied in a lecture bottle by Matheson (UK agent Cambrian gases). The monomer was used as provided.

3.1.4 ETHYLENE-VINYL ACETATE COPOLYMER (EVA_{45}).

An ethylene-vinyl acetate copolymer containing 45% of vinyl acetate (EVA_{45}) was provided by Bayer. The material was used as supplied.

3.1.5 POLY(BUTYL ACRYLATE)

3.1.5.1 POLY(BUTYL ACRYLATE) OF LOW MOLECULAR WEIGHT (PBA_{LMW})

A poly(butyl acrylate) of $\bar{M}_n$ = 27,000 was supplied as a 20% solution in toluene (Polysciences Inc.). The solution was evaporated to dryness in a petri dish. The last traces of toluene were eliminated by leaving the petridish in a vacuum oven at 50°C for a minimum of two weeks.

3.1.5.2 POLY(BUTYL ACRYLATE) OF HIGH MOLECULAR WEIGHT (PBA_{HMW})

A poly(butyl acrylate) of $\bar{M}_n$ = 183000, (PBA_{HMW}) was kindly provided by Dr C. K. Sham.The polymer was obtained by polymerizing N-butyl acrylate in emulsion. Potassium persulphate was used as initiator, sodium lauryl sulphate as micelle generator, and dodecane-1-thiol as chain transfer agent. The resultant polymer was precipitated into a 5% sodium chloride solution and then washed with water and dried. It was purified by dissolving in MEK and reprecipitating with water. In this work (PBA_{HMW}) was redissolved in MEK, reprecipitated with methanol and left drying at 50°C for a minimum of two weeks.

3.1.6 POLY(METHYL METHACRYLATE) (PMMA 1.4).

A poly(methyl methacrylate) with an intrinsic viscosity of 1.4 (Polysciences, Inc.) was purified by dissolving in MEK (analar) (BDH Chemicals) and precipitating in methanol (GPR, BDH Chemicals). The polymer was left at 80°C in a vacuum oven for

one week.

3.2 POLYMER CHARACTERIZATION

Before blending, the polymers were characterized in terms of their molecular weights, glass transition temperatures, and densities.

3.2.1 MOLECULAR WEIGHT DETERMINATION

Gel permeation chromatography (GPC) is a powerful separation technique in which a polymer is fractionated in solution according to the size of its molecules. Basically this takes place when a dilute polymer solution passes through the separation media. Here a gradient in concentration between the mobile and stationary phase forces the polymer to diffuse into the pore structure of the media. The diffusion of the polymer is a function of its hydrodynamic volume ([η]M) which, according to Grubisic [119] and Benoit [118], determines the retention in the chromatographic column (volume of elution (Vr)). GPC data is correlated with the determination of molecular weights by constructing a calibration curve of the log (M) of homologous polymer standards vs Vr . However, due to the lack of standards, it is customary to relate the molecular weight of the polymer under study to a polystyrene curve. If one is dealing with linear polymers, it is possible, if the Mark-Houwink-Sakurada parameters are known, to calculate their molecular weight from a universal calibration curve (plot of [η]M vs Vr). For branched polymers, this calibration is not valid since a branched polymer may have the same hydrodynamic volume as a linear one of lower molecular weight.

In the present work the GPC was performed in a high pressure GPC from Applied Chromatography Systems Ltd model LC 750. The measurements were performed at room temperature by injecting 100 ml of a 0.2 g/cm^3 solution of polymer in THF (analar grade, BDH Chemicals Ltd.), the flow rate was 1cm^3/min. The data were correlated to a polystyrene calibration curve using the following relationships:

$$M_n = \Sigma N_i M_i / \Sigma N_i \qquad 3.3$$

$$M_w = \Sigma N_i M_i^2 / \Sigma N_i M_i \qquad 3.4$$

$$Z = M_w / M_n \qquad 3.5$$

where M_n is the number average molecular weight, M_w is the weight average molecular weight, Z is the polydispersity, M_i is the molecular weight of the polymer relative to the polystyrene standard and $N_i M_i$ is proportional to the concentration of polymer at Vr_i. The results are collected in table 3.3.

Polymer	$\bar{M}_n$	$\bar{M}_w$	Z
$SCPE_{43}$	23,000	237,000	10
$SCPE_{54}$	33,000	652,000	20
PVC^{1}	31,000	164,000	5
EVA_{45}	51,000	370,000	7
PBA_{LMW}	27,000	165,000	6
PBA_{HMW}	183,000	2,000,000	11
$PMMA^{1}_{1.4}$	73,000	199,000	3

[1] These results were corrected using the relationship: $k_1 M_1^{\alpha_1 + 1} = k_2 M_2^{\alpha_2 + 1}$. The k, α values for PVC and PMMA in THF at 20°C were obtained from refs. 134 and 135 respectively.

Table 3.3 Molecular weights of polymers determined by GPC. The values are related to polystyrene standards

3.2.2 GLASS TRANSITION DETERMINATION

Of the many methods that may be used for the measurement of T_g [73], Differential Thermal Analysis (DTA) and Dynamic Mechanical Analysis (DMA) were selected for this work because the measurements are relatively rapid, easy and have high sensitivity (see section 2.5.1.1, p. 47).

3.2.2.1 DIFFERENTIAL THERMAL ANALYSIS

The DTA was performed with a Du Pont modular thermal analyser model 990. The instrumentation and procedure is fully described by the manufacturers [120]. Basically the equipment measures the thermal effects accompanying physical or chemical changes in

the sample as its temperature is varied through a region of transition or reaction. In the present work the DTA was used in the DSC mode (Boersma DSC cell). This implies that with the proper calibration and operating conditions the output may be used to calculate the ΔH involved during the transformation [73, 120]. The samples, weighing a few mg, (3-5) were placed in aluminium pans (provided by the manufacturer) which were sealed to prevent corrosion of the equipment by evolving gases. The heating rate was 10°C/min. Figure 3.2 shows a typical DSC curve. The T_g is obtained at the first point at which the ΔT vs T curve changes in slope (the extrapolated onset). This is also shown in figure 3.2 The results are collected in table 3.4. The accuracy of the temperature measurements is ± 1°C; T_gs are usually reproducible within ±2°C.

3.2.2.2 DYNAMIC MECHANICAL ANALYSIS (DMA)

As the DTA may present artifactual phenomena (see section 2.5.1.1, p. 47) which may cause problems in the interpretation of the thermal behaviour of the blends studied, the T_g was also determined using DMA which was carried out with two types of

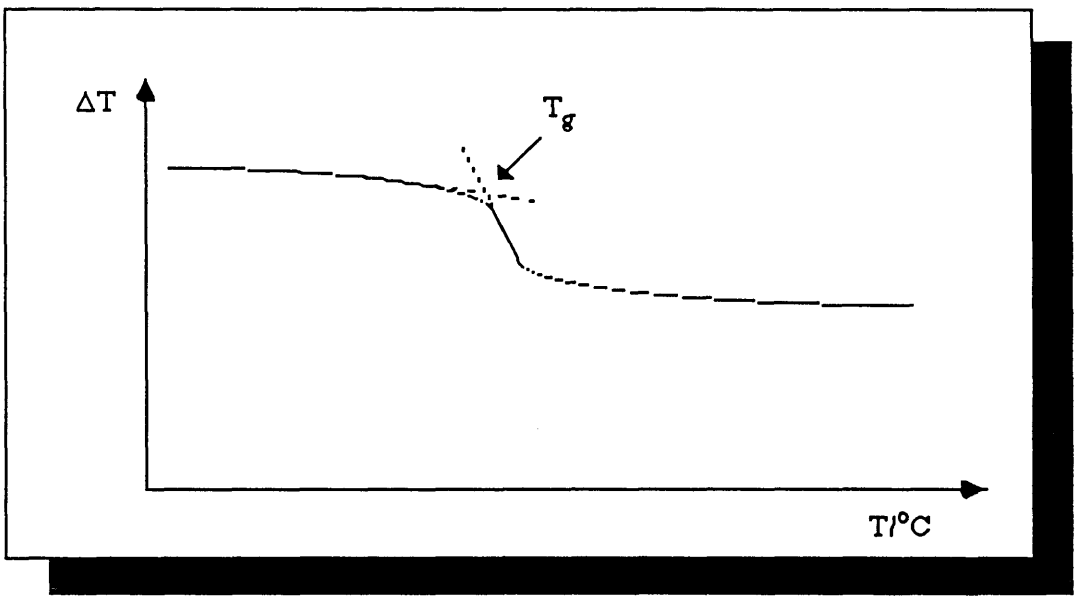

Figure 3.2 Typical DSC curve

equipment: the Rheovibron, model DDV IIC direct - reading dynamic viscoelastometer (Toyo Baldwin Co. Ltd.) and the Dynamic Mechanical Thermal Analyser (DMTA) (Polymer Laboratories). In the Rheovibron a sinusoidal strain of fixed frequency (monitored by a transducer) is applied to a small sample (held under slight tension) and

the response (stress) is measured by another transducer. The two signals are processed to provide a direct reading of tanδ and the data required to calculate E' and E". In this work the Rheovibron was operated at 11 Hz, the heating rate was approximately 2.5° C/min, and the samples, which were always presented as films, measured 20x0.5x0.3 mm approximately.

The DMTA was used when it became available in preference to the Rheovibron. The advantages of the DMTA are (1) greater accuracy in measuring the maximum of tanδ, (2) very superior performance for measurements between 0-30°C because of the improved design, and (3) accurate and straightforward measurements of E' and E". Modulus measurements with the Rheovibron involved very complex end corrections to allow for the finite length of the sample. Even when corrections are made the overall accuracy is not very good. All measurements of E' were made using the DMTA to avoid problems. Basically the principal difference between the Rheovibron and the DMTA is the sample clamping and the degree of automation. In the DMTA both ends of the sample are clamped rigidly and its central point vibrated sinusoidally. The strain is proportional to the displacement and the stress is proportional to the current supplied to the vibrator. Appropriate electronics provide direct measurements of tanδ, E' and E".

Measurements were performed at 10 Hz, the heating rate was 3°C/min. Usually strips of 20x5x0.3 mm were tested. The T_gs of rubbery samples such as polybutadienes were measured using an alternative clamping based on a shear sandwich geometry. A typical plot of tanδ and E' vs temperature is shown in fig 3.3. The T_g values obtained with the Rheovibron and the DMTA are shown in table 3.4. The maximum in tanδ was taken as the T_g. Some workers have used other definitions for T_g, such as the maximum in E"; the values obtained are slightly different.The accuracy of the Rheovibron is about ±2°C, the DMTA is nominally accurate to ±1°C.

As may be seen in table 3.4 , the mechanical tests show a T_g around 30°C above the transition recorded by DSC. The two techniques are in fact sensitive to different aspects of the molecular processes which occur at the T_g. The mechanical techniques record a maximum tanδ or alternatively a maximum in E" which is interpreted as the T_g. This occurs when the maximum number of molecular motions have a correlation time that matches the test frequency (this is discussed more fully in section 2.5.1, p. 45). In contrast, calorimetric technniques such as DSC are sensitive to all the thermal processes independent of their molecular frequency and therefore detects the onset of the T_g as soon as molecular motion increases significantly; DSC will therefore always record a lower transition temperature than any frequency dependent method. All T_g measurements are very dependent on the exact technique used and great caution must be taken in

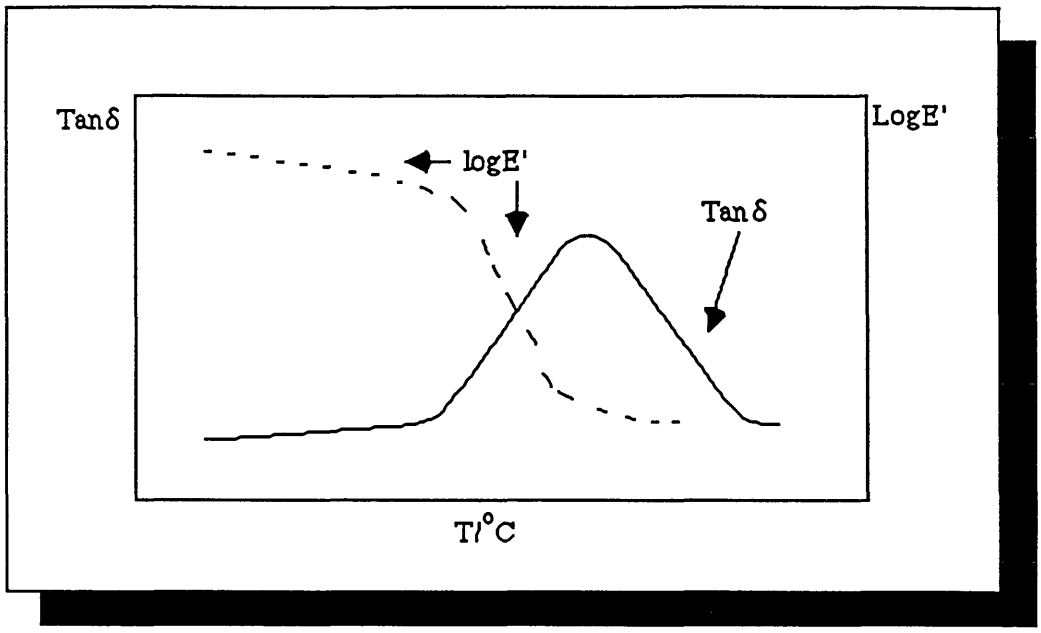

Figure 3.3 Typical tanδ and Log G' vs temperature plots.

interpreting results obtained with different techniques.

All T_g techniques for investigating blend miscibility share a common disadvantage. At temperatures above the T_g the system may be unstable and undergo phase changes during the experiment before the required information can be recorded. The usefulness of these techniques will be a function of various factors such as the kinetics of the transformation processes and the difference between the lowest T_g and the temperatures of interest.

3.2.3 DENSITY DETERMINATION

The densities of the polymers were measured with a density bottle of 10 ml capacity at 25±1°C. The procedure was as follows: a piece of polymer, previously, weighed, was placed in the density bottle which was then filled up with distilled water approximately at 25°C. The bottle with its contents, was placed in a thermostated bath at 25°C and was left to equilibrate for a minimum of 10 min. After this the bottle was removed from the bath, the excess water on the stopper and bottle quickly wiped off, and then the bottle with its contents quickly weighed. The procedure was repeated at least 10 times for each sample. The density was calculated with he following :

$$\rho_p = \rho_{H2O\ 25^oC}\ W_p / (W_w'-W_w) \qquad 3.6$$

where $\rho_{H2O\ 25^oC}$ is the density of the water at 25 °C (0.99707 g/ml), W_p is the weight of polymer, W_w' is the weight of the density bottle containing the polymer sample, W_s is

the weight of the density bottle filled up with distilled water. The results shown in table 3.5 have an accuracy of only ±2% because the technique involves subtraction of two very similar weights.

	Temperature /°C		
Polymer	DSC	Rheovibron	DMTA
$SCPE_{43}$	-7	19	20
$SCPE_{54}$	20	53	61
PVC	50	82	—
EVA_{45}	—	-16	-17
$PMMA_{1.4}$	73	103	100
PBA_{LMW}	—	—	-21
PBA_{HMW}	—	—	-26

Table 3.4 Values of T_g determined by DSC, Rheovibron and DMTA.

Polymer	Density (g/ml)
$SCPE_{43}$	1.245
EVA_{45}	1.374
$SCPE_{54}$	0.890
PBA_{LMW}	1.022
PBA_{HMW}	1.000
$PMMA_{1.4}$	1.129

Table 3.5 Density values of homopolymers at 25 ±1°C

3.3 BLEND PREPARATION METHODS

Table 3.6 shows the sample codes used for the blends studied in this work. Blend *B* is not included in the above table as insufficient time was available to complete all the required measurements. (Blend *B* was a mixture of PMMA/$SCPE_{54}$ in which PMMA was the crosslinked polymer).

In order to identify the specific composition of a blend, a number, corresponding to the percent by weight of the first indicated component, will be written in the right hand side of the code, so for example A_{70} is the blend $SCPE_{43}/EVA_{45}$ with 70% w/w of $SCPE_{43}$.

All the blends analyzed in this work were prepared by solvent casting. Besides this method blend *E* was also prepared by *insitu* polymerization. In the following two sections the methods followed will be explained.

Polymer	Code
$SCPE_{43}/EVA_{45}$	*A*
$SCPE_{54}/PMMA_{1.4}$	*C*
$SCPE_{54}/EVA_{45}$	*D*
$SCPE_{43}$/PVC	*E*
$SCPE_{43}/PBA_{LMW}$	*F*
$SCPE_{43}/PBA_{HMW}$	*G*

Table 3.6 Codes used for the blends in this work.

3.3.1 SOLVENT CASTING

An approximate total of two grams of both polymers (weighed in the required proportions) were mixed for 24 hours in a common solvent to yield a 5% W/V solution.The resultant solution was poured into a petri dish. The solvent was allowed to evaporate slowly by covering the petri dish until a film was obtained. Depending on the volume of the solvent used, the total evaporation took about 4 days. To remove traces of solvent left in the film, the petri dish was left at 50°C for one week (if the blend was rubbery) or two weeks (if the blend was glassy). In order to control the thickness of the film (0.3 mm for films used in the DMA, Light Scattering, etc, or 0.5 mm for samples

used in tensile tests and degree of crosslinking measurements) the initial weighing of the polymers was based on the approximate density of the blend (average of the densities of both components, see table 3.5) and the diameter of the petri dish used. The solvents used for casting were MEK (BDH, analar) dried previously over molecular sieve, and tetrahydrofuran (THF) (BDH, analar). MEK was used to cast blends *B*, *C*, *F* and *G*. THF was used for systems *A* and *D*. Traces of MEK or THF and the possible presence of water, as impurities were determined by Gas Chromatogrphy (GC). A 2% solution of the polymer or blend was dissolved in dichloromethane (DCM) (BDH, special for liquid chromatography) which was previously dried over calcium hydride. MEK or THF were detected using a Flame chromatograph (PYE Unicam). Samples of 0.5ml were injected in a column of Poropak Q, heated to 120°C, the sensitivity range was 16. Traces of water were determined in a thermal conductivity chromatograph (PYE Unicam). Samples of 0.5 ml were injected in a column of Poropak N at 150°C. Helium was used as a carrier. The percent by weight of MEK, THF and water found in the samples is reported in table 3.7. The water content of the polymers is significantly greater than the solvents used. It is presumed that this excess water was absorbed from the atmosphere in normal laboratory operations; such effects are commonly observed in polar polymers.

3.3.2 *INSITU* POLYMERIZATION

As mentioned before, only the system *E* was prepared by solvent casting and by *insitu* polymerization. The method used was as follows. In order to handle the vinyl chloride monomer (VCM) a vacuum line was constructed[19] within a fume cupboard and VCM was never allowed outside the fume cupboard. A diagram of the vaccum line is shown in figure 3.4 (p. 71).

To enable the addition of the exact amount of VCM required for the preparation of the blend, the arm on the vacuum line was calibrated [20, 23]. Such calibration was performed by measuring the pressure exerted by a known weight of dichloromethane. Specially made glass containers, fitted with PTFE seals were used as reactor vessels. A typical sample preparation was as follows: 1 ml of 0.2% w/v solution of t-butyl cyclohexyl peroxidicarbonate (Laporte) (used as initiator) in methanol was introduced to the reaction vessel. The methanol was then removed by vacuum. $SCPE_{43}$ (1.5 g) was loaded into the vessel which was attached to the arm of the vacuum line and degassed until the pressure reached 10^{-3} torr. The arm was then isolated from the rest of the

Sample	THF % w/w	MEK % w/w	H_2O % w/w
$SCPE_{43}$	0.3	—	0.4
$SCPE_{54}$	—	0.3	1.0
EVA_{45}	0.02	—	0.7
PBA_{LMW}	—	0.1	0.7
PBA_{HMW}	—	0.04	2.0
$PMMA_{1.4}$	—	0.6	1.0
A_{20}	0.4	—	3.0
A_{70}	0.1	—	3.0
C_{20}	—	1.0	2.0
C_{70}	—	0.7	0.5
D_{20}	0.05	—	3.0
D_{70}	0.2	—	2.0
F_{20}	—	0.2	2.0
F_{70}	—	0.1	0.7
G_{20}	—	0.2	1.0
G_{70}	—	0.4	1.4

Table 3.7 Determination of traces of THF, MEK and water in the polymers and polymer blends studied.

system and the required amount of VCM was then introduced and condensed into the reaction vessel. The reaction vessel was then sealed and removed from the vacuum line. The VCM dissolved the $SCPE_{43}$ and the resultant solution was left to equilibrate for 5 days at 30°C. After this period the VCM was polymerized by heating it at 60°C for 60 hours. The difference in weights between the unopened and opened vessel gave the amount of VCM reacted and so it was possible to work out the final composition of the blend. Only samples of 50/50 ± 5% composition were prepared. The blends obtained from the reactor were small cylinders, which were transparent and had a light pink colour. Sections of 0.3 mm thick, which were later characterized by various techniques, were prepared by microtoming.

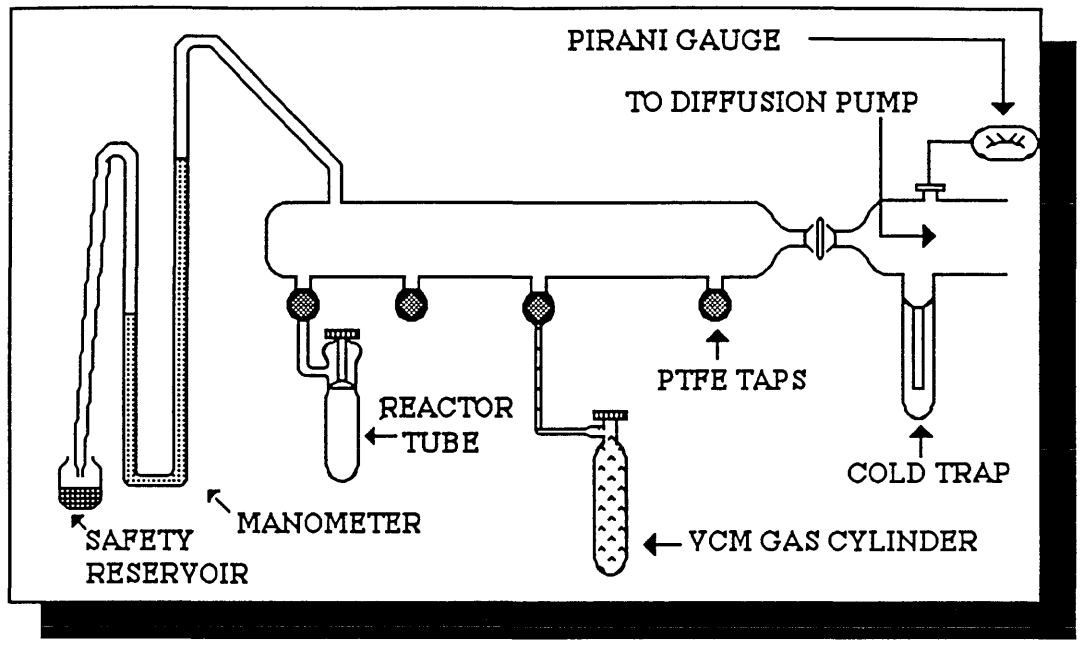

Figure 3.4 Vacuum line used for preparing the *insitu* blend $SCPE_{43}$ / PVC 50/50 (E_{50}).

3.4 CROSSLINKING REACTIONS OF $SCPE_{43}$, $SCPE_{54}$ AND THEIR BLENDS

As specified in section 2.4.1.1(p. 31-2) the great reactivity of the SO_2Cl groups allows a diversity of crosslinking agents such as metal oxides, glycol, aziridines, quinoxalines, diamines, etc. The first four crosslinking agents were not used in the present work because they required high temperatures which may cause phase separation and / or degradation of the blends studied. Besides this, metal oxides may also interfere with characterization methods such as microscopy, glycols required a complex system in order to crosslink [35, 79] and 2, 3 - dimethylquinoxaline develops grey discoloration after crosslinking [83]. Contrary to the characteristics of these curing agents, diamines, ammonia and hexamethylenetetramine may crosslink SCPE efficiently at room temperature [75, 76, 83]. Although these curing agents may also present some disadvantages (by-products may cause water sensitivity and the vulcanizates may not present good colour [75]) they constitute the best choice to crosslink the SCPEs before and after blending.

To indicate the particular curing agent used, its abbreviation in italics will be written as a subscript to the polymer or blend which it modified. The following abbreviations will be used for the curing agents employed in this work:

Curing agent	Abbreviation
Ammonia solution	*NH 4OH*
Hexamethylenetetramine	*HMTA*
Diethylenetriamine	*DETA*

Table 3.8 Abbreviations for the curing agents used in the present work.

3.4.1 CROSSLINKING REACTION WITH AMMONIA

It is believed that NH_3 crosslinks the SCPE by the formation of polysulphonamide crosslinks [76]. The probable mechanism of crosslinking may consist of firstly an S_N2 reaction of the SO_2Cl groups with the NH_3, to yield a sulphonamide:

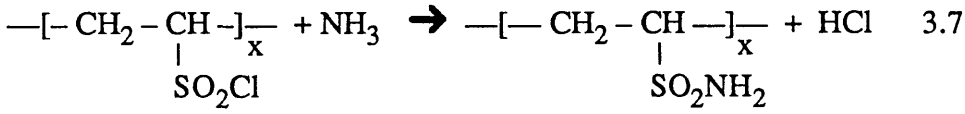

3.7

and secondly an S_N2 reaction between the sulphonamide and a SO_2Cl in another chain forming the crosslink:

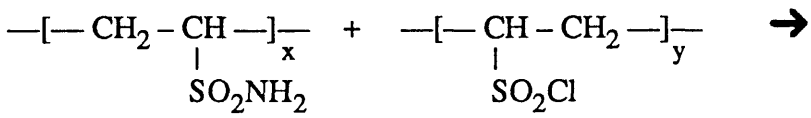

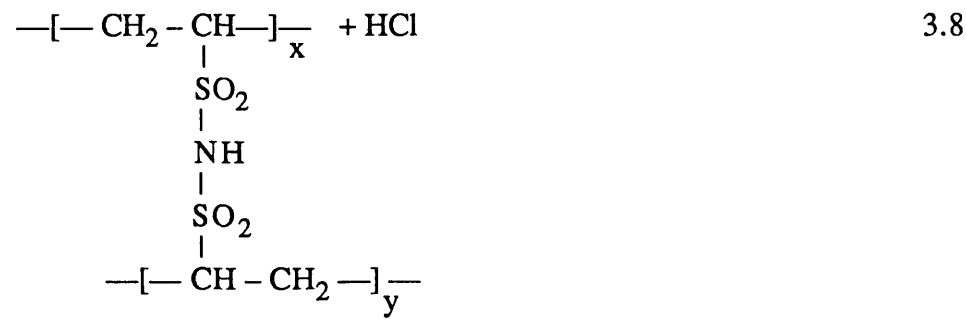

3.8

was obtained by measuring the weight percentage remaining undissolved after solvent extraction with MEK (technical grade, BDH Chemicals Ltd.). It was found that although the percentage of undissolved material increased proportionally to the concentration of NH_3, the values were low (~20%) even with the most concentrated solution. By increasing the temperature better results were obtained. Samples were crosslinked at 50°C for a total period of 144 hours. The progress of reaction was followed by measuring the weight percentage of insoluble polymer as before. A 17.5% ammonia solution gave 60% of insoluble polymer after 96 hours. Further crosslinking occured on postcuring the already crosslinked samples at 100°C for 1 hour. It was found that the maximum conversion was 72% after 72 hours of reaction plus 1 hour postcure. The experiments were repeated with fractionated $SCPE_{43}$ using the fraction of highest molecular weight (the fractionation was performed at room temperature by precipitating the $SCPE_{43}$ with methanol from a 1% w/v solution of the polymer in benzene) giving a conversion of 82% under the same previous crosslinking conditions. Longer reaction times gave significantly less overall crosslinking, further details of the variation of crosslinking with time, temperature and fractionation are given subsequently in section 4.1.1 (p. 92-4). These optimum conditions were used for crosslinking $SCPE_{43}$ when blended with PVC. Only the *insitu* polymerized 50/50 blend (B_{50}) was used as the solvent cast blend was found to be two phases (see section 4.1.2, p. 94-7). The *insitu* blend was prepared as described in section 3.3.2 (p. 69-71)with the difference that the highest molecular weight fraction of $SCPE_{43}$ was used. Sections of the resultant blend were obtained by microtoming.The resultant sections were immesrsed in a 17.5 % ammonia solution at 50°C for 96 hours and then postcured 1 hour at 75°C. Higher postcuring temperatures were not employed as the blend may have phase separated. The weight percentage of undissolved material was 35%.

3.4.2 CROSSLINKING WITH HEXAMETHYLENE - TETRAMINE

Hexamethylenetetramine (HMTA), which has the structure shown below, was first reported to be used as curing agent for SCPE by Switzer [82]. It has the advantage of acting as a curing agent and acid acceptor although the mechanisms by which such functions are performed are not yet fully understood. It is usually incorporated by the use of solvents, dispersants and by milling. As HMTA is only soluble in halogenated solvents, it was incorporated in the $SCPE_{43}$ and $SCPE_{54}$ by mixing the polymer and the HMTA in $CHCl_3$. The resulting solutions were solvent cast in a petri dish to obtain film

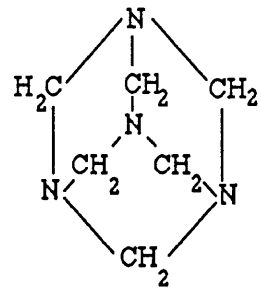

which were left to crosslink at 50°C in a vacuum oven for 72 hours. The crosslinking of the $SCPE_{43}$ and $SCPE_{54}$ when blended was not pursued further since none of their blends studied here were miscible when solvent cast from $CHCl_3$ and other co-solvents were not found.

3.4.3 CROSSLINKING WITH DIAMINES

SCPE is readily crosslinked by diamines due to the facility of reaction of the SO_2Cl groups with the NH_2-R-NH_2 yielding sulphonamide links. Diamines were first reported to be used as crosslinking agents by McAlevy [81]. Later on, Busse and Billmeyer [76] studied the gelation reactions of SCPEs with diamines (alkyl and aromatic) and other types of nitrogen compounds. They observed that the rate of crosslinking increases with the basicity of the diamine (aliphatic diamines are more basic than aromatic diamines) allowing, in some cases, the production of strong gels in less than a minute.They also reported that the diamines perform as curing agents and acid acceptors simultaneously and that the resulting cured products exhibit values of tensile strength greater than those achieved by organic curing agents and comparable to those of metal oxides [81].

In this work diethylenetriamine (*DETA*) with the formula $(NH_2\text{-}CH_2\text{-}CH_2)_2NH$ (95%, Aldrich Co Ltd.) was evaluated as curing agent because the small size of its molecules offers the facility of curing the SCPEs and their blends by diffusion. The method used was as follows: 200 ml of *DETA* were placed in a 1 litre flat bottom glass container which was tightly closed and then placed in a water bath at 45°C for an hour. After this period of time, a sample, which was previously weighed, was quickly placed in contact with the *DETA* vapours at 45°C. To ensure an even diffussion of the crosslinking agent, the sample was placed vertically in the middle of the chamber on a stainless steel support. The amount of *DETA* taken up by the sample was monitored every 5 minutes, by quickly weighing the sample in a tared glass container fitted with a stopper. The reaction was terminated when the amount of *DETA* diffused into the sample was sufficient to cure the SCPE and neutralize the HCl obtained as by-product. Then the

sample was placed in a small glass bottle which was closed tightly and left inside an oven at 45°C for 24 hours to ensure the completion of the crosslinking reaction.

To determine the amount of *DETA* to be introduced into the sample, the stoichiometric balance of the possible mechanism followed during crosslinking plus the excess of *DETA* necessary to neutralize HCl, were calculated beforehand. Due to the steric hindrance of the macromolecules it is quite likely that mainly the amine groups at the ends of the *DETA* molecule react with the SO_2Cl groups:

$$2RSO_2Cl+NH_2(CH_2)_2NH(CH_2)_2NH_2 \rightarrow RSO_2NH(CH_2)_2NH(CH_2)_2NHSO_2R+ 2HCl \qquad 3.9$$

With respect to the neutralization of HCl, it is very likely that due to the high basicity of the three amine groups in the *DETA*, one mole of this is sufficient to neutralize three moles of HCl:

$$NH_2\text{-}(CH_2)_2\text{-}NH\text{-}(CH_2)_2\text{-}NH_2 + 3HCl \rightarrow \overset{-\ +}{ClNH_3}\text{-}(CH_2)_2\text{-}\overset{Cl}{NH_2}\text{-}(CH_2)_2\overset{+\ -}{NH_3Cl} \qquad 3.10$$

Examples of the curing conditions used in this work are shown in table 3.9 (p. 77). Only the 40/60 and 60/40 compositions for each system are shown. It is important to point out that *DETA* sorption is diffusion controlled and therefore strongly dependent on T_g and the thickness of the sample (when solvent casting the SCPEs and their blends precautions were taken to prepare samples with thickness around 0.3 mm). The experimental weight of the sample plus the *DETA* incorporated may differ by ±2.5% from that quoted in the table.

After crosslinking, samples were transparent but showed a brownish discoloration, an effect which is commonly observed when SCPEs are cured with diamines [78]. This effect may be caused by the unsaturation along the chain produced by the loss of hydrogen protons in α positions with respect to the sulphonamide group (equation 3.11)

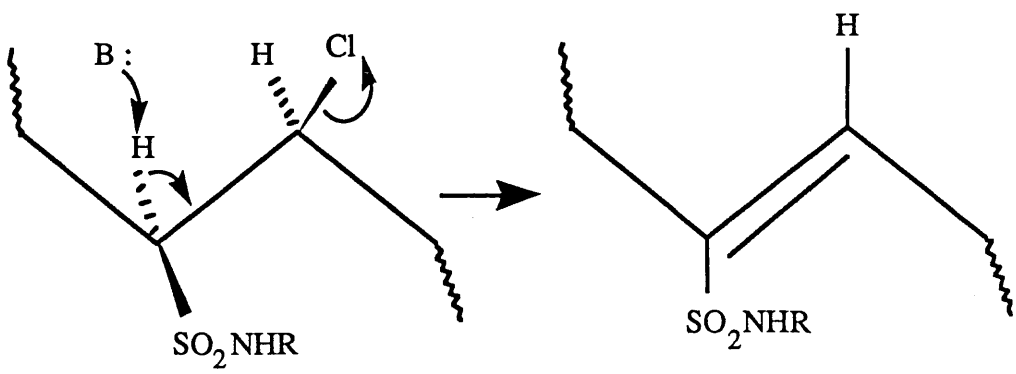

3.11

This loss is catalysed by the attack of basic entities (in this case *DETA*) present in the media.Unsaturations due to the loss of SO_2 and small amounts of HCl are unlikely as these reactions usually proceed at temperatures above 150°C [76].

3.5 DETERMINATION OF DEGREE OF CROSSLINKING

The degree of crosslinking of the cured polymers before and after blending were determined using two different methods; swelling and tensile measurements. The theory on which both are based (outlined briefly in section 2.4.2, pp 32-7) and the experimental conditions for the measurement of the degree of crosslinking have been fully described by many authors [87- 91]. As pointed out in sections 2.4. 2.1 and 2.4.2.2 due to the limitations of both theories, the interpretation of the values of the molecular weight between crosslinks ($\bar{M}_c$) must be made in a qualitative way. In this work the interpretation of $\bar{M}_c$ is further complicated by the presence of a second component in the case of the blends. However as will be explained in the next two sections it is possible to get around this problem in both methods.

3.5.1 SWELLING MEASUREMENTS

The procedure used to calculate the degree of crosslinking by swelling measurements ($\bar{M}_{cSWELL}$) is based on the method of Ellis and Welding [89]. The specimen, a rectangular section obtained from the cured polymer or blend, was firstly accurately weighed (average weights 0.2 g) and then placed in a stoppered bottle containing 50 ml of the swelling liquid, which was a good solvent for the polymer or polymer components of the blend (MEK was used for blends C_{DETA} , F_{DETA} and G_{DETA} , THF for A_{DETA} and D_{DETA}). The weight of the immersed sample was then checked periodically during seven days. To avoid drifts in weight in the swollen sample, caused by solvent evaporation, the following weighing procedure was used: after removing the sample from the solvent, the excess was removed by quickly shaking the sample which was then immediately dropped into a stoppered tared bottle. This was then weighed and the sample returned immediately to the swelling solvent.

Blend *	Weight sample (g)	SCPE content % w/w	SO_2Cl content (moles)	*DETA* (calculated) (moles)	weight sample+*DETA* (calculated) (g)	*DETA* sorption Time (min)
A_{40}	0.6524	40	8.13×10^{-5}	6.77×10^{-5}	0.6593	30
A_{60}	0.5520	60	1.03×10^{-4}	8.60×10^{-5}	0.5608	30
D_{40}	0.7098	40	8.33×10^{-5}	6.94×10^{-5}	0.7169	45
D_{60}	0.5439	60	9.58×10^{-5}	7.98×10^{-5}	0.5521	45
C_{40}	0.3926	40	4.61×10^{-5}	3.84×10^{-5}	0.3965	40
C_{60}	0.6443	60	1.11×10^{-4}	9.45×10^{-5}	0.6540	90
F_{40}	0.7148	40	8.39×10^{-5}	6.99×10^{-5}	0.7220	15
F_{60}	0.6520	60	1.11×10^{-4}	9.57×10^{-5}	0.6618	20
G_{40}	0.9272	40	1.09×10^{-4}	9.07×10^{-5}	0.9365	25
G_{60}	0.8101	60	1.43×10^{-4}	1.19×10^{-4}	0.8223	25

* For explanation of nomenclature see table 3.6, p. 70.

Table 3.9
Examples of curing conditions when *DETA* was used as curing agent

3.5.1.1 CALCUALTION OF $\bar{M}_{cSWELL}$.

The value of $\bar{M}_{cSWELL}$ was calculated using three different expressions: theFlory-Rehner equation, the Hermans equation and the James and Guth equation (see relationships 2.126, 2.127and 2.128 respectively p. 36). These equations are:

$$-\ln(1-\phi_2) - \phi_2 - \chi\phi_2^2 = V_1\rho_2\bar{M}_c^{-1}[\, q_o^{2/3}\phi_2^{1/3} - \phi_2/2\,]$$

$$-\ln(1-\phi_2) - \phi_2 - \chi\phi_2^2 = V_1\rho_2\bar{M}_c^{-1}[\, q_o^{2/3}\phi_2^{1/3} - \phi_2\,]$$

$$-\ln(1-\phi_2) - \phi_2 - \chi\phi_2^2 = V_1\rho_2\bar{M}_c^{-1}[\, q_o^{2/3}\phi_2^{1/3}\,]$$

where χ is the Flory-Huggins interaction parameter for a specific polymer-solvent pair ($SCPE_{43DETA}$ or $SCPE_{54DETA}$ as cured polymers and MEK or THF as swelling liquids), ρ_2 is the density of the polymer, V_1 is the partial molar volume of the solvent, q_o is unity, and ϕ_2 is the volume fraction of the crosslinked polymer in the swollen state. In chapter 4 the experimental data is analyzed using each of these equations and the results compared.

In order to estimate ϕ_2 for the cured polymers when blended, allowance was made for the second component (which is extracted during the period of immersion), by basing the calculation of ϕ_2 on the weight of the unswollen sample (D), instead of its original weight. The relationship used was:

$$\phi_2 = V_p/(V_p+V_s) = (D - FT)\rho^{-1} / [(D - FT)\rho^{-1} + A_o\rho_s^{-1}] \qquad 3.12$$

where V_p and V_s are the volumes in the swollen state of the cured polymer and of the solvent imbibed in the sample respectively, F is the weight fraction of insoluble material (if present in the cured polymer or blend), T is the weight of the sample before swelling, A_o is the equilibrium weight of the solvent imbibed in the sample, ρ_s is the density of the solvent.

The estimate of A_o was made from a plot of swelling (w'_t) vs the square root of the time of immersion ($t^{1/2}$) (see fig 3.5), w'_t was calculated from the crude weight ratio

$$w't = (s_t - T)/T \qquad 3.13$$

where s_t is the weight of the swollen test piece.

A_o is considered to lie at the intercept of lines plotted through the initial and later data points. In theory, at this point, the weight of imbibed solvent should reach a plateau, but as seen in figure 3.5 it is quite common to find that it increases slightly if the network

suffers some oxidative degradation or hydrolysis. To correct this, an extrapolation of the weight was done to t = 0. This gave the crude weight ratio in the absence of the increment w'_0 which was estimated from:

$$d't = 100 (w'_t - w'_0) / w'_0 \qquad 3.14$$

A_0 was then finally calculated from:

$$A_0 = A_t (1 - d'_t / 100) \qquad 3.15$$

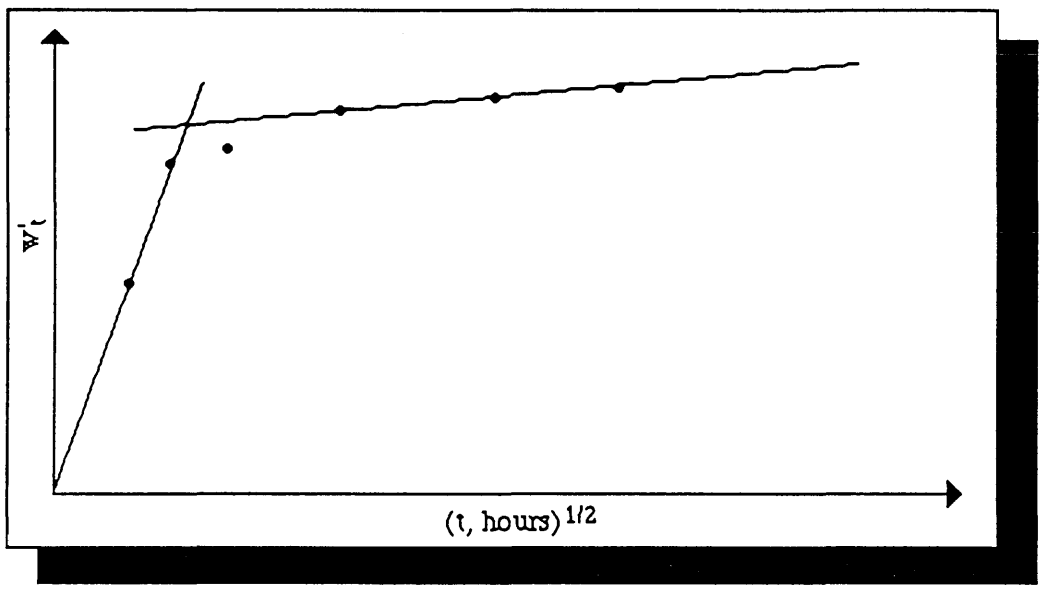

Figure 3.5 Degreee of swelling (w'_t) vs square root of time ($t^{1/2}$).

3.5.2 STRESS-STRAIN MEASUREMENTS

As shown in section 2.4.2.1 (see p. 32-5) the determination of $\bar{M}_c$ from stress strain measurements ($\bar{M}_{cMECH}$) is based on the measurement of the shear modulus G. As the tensile modulus (E) is easier to measure than G only the values of E were measured and were related to G with the following relationship:

$$G = E / 3 \qquad 3.16$$

The determination of E, was performed in a similar way to the ASTM method D882-75b [128], which applies to thin plastic sheeting, and to the method described by Gumbrell *et al* [87].

The samples were rectangular sections of approximately 40x5x0.3 mm cut directly from the films of the cured polymer and blends (due to sample quantity limitation, the length of the samples was smaller than 250 mm, which was the recommended length in the ASTM method). The widths and thicknesses of the specimens were measured at

several points on the samples. The widths were measured with a travelling microscope and the thicknesses with a micrometer screw gauge. The apparatus used was an Instron 1185. This instrument is essentially a machine in which a sample is clamped between two grips which are pulled apart at a constant strain rate. In this experiment the strain rate was kept to the value of 0.05 mm/min to allow equilibrium to be reached during the measurements. The samples were conditioned for 40 hours prior the test at 20°C and 40% relative humidity. Due to sample quantity limitations, the number of test specimens was two instead of the recommended five. Small clamps, specially designed for the size of samples used, were fixed 20 mm apart which permitted clamping the specimens on the area beyond two reference lines (20 mm apart) previously marked on them. The exposed section of the sample between the reference lines was the tested area. The load range for each sample was selected after a few trial runs. Values could vary from 2 to 50 N. The experiment was performed in the region of small deformations which later on will permit the calculation of the shear modulus G with equation 2.119 (see p. 35) [87] which was:

$$G = 1 / 2fA_0^{-1}(\lambda - \lambda^{-2})^{-1}$$

Due to the small size of the specimens it was not possible to use an extensometer to measure the deformation on the sample. However as the crosshead separation rate was known, it was possible to work out the deformation from the curve load vs grip separation recorded during the experiment. A typical curve is shown in figure 3.6.

E was determined by plotting $(1/2)fA_0^{-1}$ vs $\lambda - \lambda^{-2}$ which yields a straight line of slope equal to E. f in Newtons (N), is the load required to extend the sample to a certain value L. A_0 (m^2) is the crossectional area of the sample. The ratio f/A_0 corresponds to the engineering stress (σ) ($\sigma = f / A_0$). λ is the ratio of the final length (L) to the initial length L_0 ($l = L / L_0$).

The data were also used to determine the value of the Young's modulus (Y) which was obtained by drawing a tangent to the initial linear portion of the load-extension curve, selecting any point on this tangent and dividing the tensile stress by the corresponding strain. When no proportionality was evident on the load-extension curve, a secant modulus was calculated, which simply consists of dividing the corresponding stress by the specified strain.

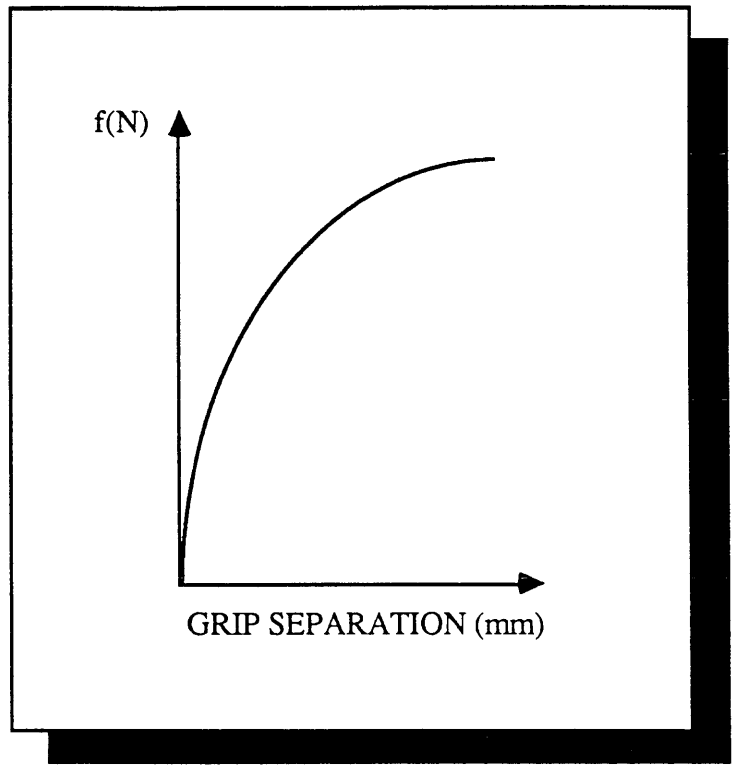

Figure 3.6 Typical trace of a load curve vs grip separation

3.5.2.1 DETERMINATION OF $\bar{M}_{cMECH}$.

For crosslinked homopolymers the $\bar{M}_{cMECH}$ was obtained from equation 2.117 (p.35):

$$G = \rho RT\bar{M}_c^{-1}(1 - 2\bar{M}_c\bar{M}^{-1})$$

an expression which, as mentioned in section 2.4.2.1 (p.35), considers the effect of free ends, where G is the shear modulus obtained from the values of E obtained from the plot of $(1/2)fA_o^{-1}$ vs $\lambda - \lambda^{-2}$, ρ is the density of the crosslinked polymer (see section 3.2.3 p. 66).

To calculate $\bar{M}_{cMECH}$ of the crosslinked polymer when blended, it was necessary to disregard the contribution of the second component to the measured modulus, and thus obtain the shear modulus of the network (G_N). G_N was therefore estimated in four different ways:

(1) G_N was considered to be equal to the experimental value of the shear moduli of the crosslinked blend (G_{XB})

(2) G_N was considered to be the difference between the moduli of the blend before (G_B) and after crosslinking

$$(G_N = G_{XB} - G_B) \qquad 3.17$$

(3) Assuming a rule of mixtures G_{XB} may be considered to be a function of the moduli and the content of the crosslinked polymer and of the unmodified component:

$$G_{XB}=G_N\phi_N+G_U\phi_U \qquad 3.18$$

where G_U is the shear modulus of the unmodified polymer, ϕ_U and ϕ_N are the volume fraction of the unmodified polymer and the network respectively.

From expression 3.17 G_N is:

$$G_N = (G_{XB} - G_U\phi_U) \phi_N \qquad 3.19$$

(4) As will be seen in chapter 4, in general, the blends studied in this work were one phase up to a certain content of SCPE and two phases for those compositions rich in SCPE. Taking this into account, G_N was calculated as in (3) for the compositions behaving as one phase. For the compositions behaving as two phases G_N was calculated using the Budiansky equation[106]:

$$\phi_2 = [(G_1-G_N) / G_N (G_1 - G_2)][3 / 5 G_N + 2 / 5 G_2] \qquad 3.20$$

which applies to two phase systems with domain-domain interactions.

3.5.2.2 DEGREE OF CROSSLINKING FROM DYNAMIC-MECHANICAL MEASUREMENTS ($\bar{M}_{cDYN}$)

As will be shown in chapter 4 in many cases, though not for A_{DETA} , it was only possible to make swelling and stress-strain measurements below the T_g or T_gs of the blend composition under study. In such cases, where the samples were not behaving as rubbers, the use of the relationships developed for both methods is quite debatable and in the particular case of the stress-strain measurements is inappropriate. In spite of this, many researchers use swelling measurements at room temperature for crosslinked polymers with high T_gs, such is the case of Bell [143], who studied amine-cured epoxy resins which exhibited T_gs above 100°C. In the case of the mechanical measurements, Hermans[145] derived an equation for networks of stiff chains. Unfortunately the use of such relationships is difficult as it requires the knowledge of some inaccessible parameters. Determinations of swelling or static modulus at higher temperatures were not carried out because they involve a great deal of experimental difficulties. At this point the use of the DMTA technique provided an attractive alternative, as the method provides the storage modulus (E') as a function of temperature, and thus indirectly the dynamic shear modulus (G'). It was therefore possible to obtain modulus values 20°C above T_g where the sample is definitely rubbery (rubbery plateau)(see figure 3.7). As in the stress-strain measurements, the same four calculation methods were used to obtain the G' of the network (G'_N).

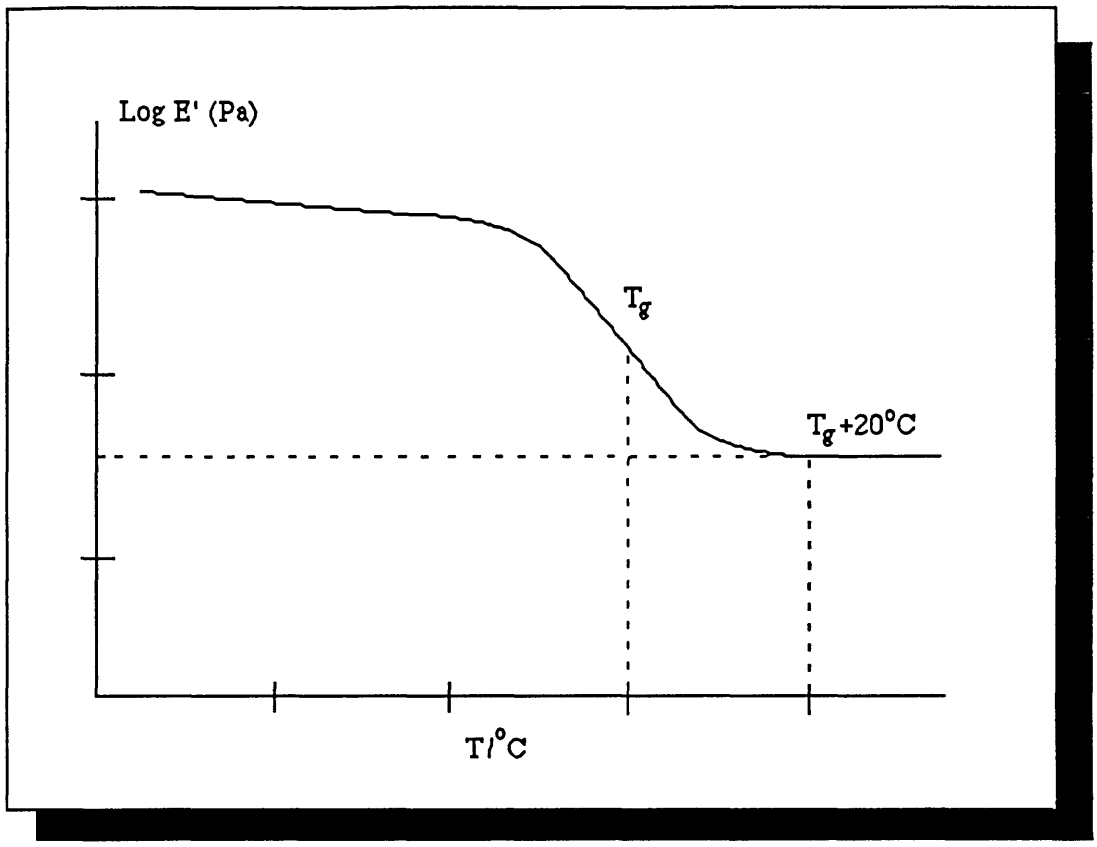

Figure 3.7 This figure shows the temperature at which E' was measured for the degree of crosslinking determination in a plot of logE' vs T.

3.6 MISCIBILITY DETERMINATION

As there is no absolute criterion to determine miscibility in blends, it is always desirable to assess miscibility with as many methods as possible. In the present work optical clarity, microscopy and glass transition were selected as criteria to determine miscibility. In the following sections brief descriptions of the experimental techniques involved are given.

3.6.1 OPTICAL CLARITY

The visual confirmation of the transparency of the samples was used as a preliminary indication of miscibility. The criterion was applied to uncrosslinked and crosslinked blends.

3.6.2 LIGHT MICROSCOPY

Microscopic methods were used when possible as they may show directly the presence or absence of domains in the samples. As basically transparent specimens were studied, it was found that phase contrast microscopy was very convenient as the contrast relies on the refractive index and thickness of the phase objects present in the samples (see section 2.5.3.1 p. 50).

Two types of microscopes were used: the Pereval Interphako interference microscope from Carl Zeiss-Jena and the Nikon Optiphot Universal Microscope set in the differential contrast mode. As the operation of both microscopes is clearly explained in their operation manuals [66,67], only a brief description of the basic principles and experimental details of both techniques will be given in the following paragraphs.

In the Pereval Interphako, a wave front, which results from the interference between diffraction maxima of the light passing through a phase object, is split into two parts which contain the full object information. These two parts are recombined in the Micro Mach Zehnder interferometer which shears one beam vertically against the other producing interference. When white light is used for illumination a system of interfering colours is produced.

The experimental procedure basically consisted of: (a) adjusting the coarse motion mechanism of the microscope and the illumination, which in this case was white light, (b) centring of the objectives and (c) setting the microscope on the shearing mode. Immiscible blends produced an image in which colours were interfering, for miscible blends no interference was produced and so only a uniform background colour was observed. Micrographs were obtained with a photographic camera mounted on top of the microscope; as it did not have an automatic exposure timer, various exposure times were used, those between 3 to 7 seconds gave the best results. The film used was a Kodak vericolor II, Professional 50255.

In the Nikon Optiphot Universal microscope (which was fitted with a differential interference attachment "NT" for the transmitted Normarsky technique) a bundle of plane polarized light is differentially split with the Normarsky prism to produce a separation of adjacent beams of a few microns which pass through the specimen and are influenced by it. The two beams are recombined by a second prism and then passed through an analyser which produces the image [129]. The image of immiscible blends showed different regions which stood out in apparent relief. In miscible blends a uniform background was produced. Photomicrographs were obtained with a camera attached at the top of the microscope, a monochromatic film FP4-125 ASA was used.

3.6.3 TRANSMISSION ELECTRON MICROSCOPY (TEM).

Despite of the experimental complications which transmission electron microscopy implies (TEM) (see section 2.5.3.2 p. 51) it was chosen due to its great resolving power. Specimens were prepared by microtoming with an ultramicrotome (L.K.B. - Produckter AB Sweden) which required freshly prepared glass knives for trimming and sectioning the sample. The ultramicrotome only provided facilities for microtoming samples with T_gs above room temperature. The resulting sections of 700-1000Å diameter in thickness were collected with copper grids of 400 mesh and 3 mm diameter (Emscope Laboratories Ltd.). Blends containing one chlorinated compound showed natural contrast and did not required any further treatment.

It was possible to have access to two different TEMs: one was a Jeol JEM 100B of 100 KV and the other was an AEI 1000 KV which was fitted with a variable hot stage having a thermocouple to indicate the sample temperature. The process consisted of three steps: (a) the alignment of the TEM (b) obtaining the image of the specimen by selecting an appropiate magnification value, beam intensity and focus (c) production of the micrographs. The image of miscible blends consisted of a uniform background; those of immiscible systems consisted of random dark spots (component containing heavy atoms) on a uniform background.

3.6.4 GLASS TRANSITION DETERMINATION

As mentioned in section 2.5.1 (p. 46), the determination of T_g as a criterion for assessing the miscibility of blends is frequently used due to the relative simplicity of the measurements and the availability of standarized equipment. In this work it was possible to apply this technique due to the components having a difference in T_g of greater than 20°C (see table 3.4). The determinations of the T_gs and the equipment used are the same as described in secion 3.2.2 (p. 63) The technique was applied to blends before and after crosslinking one of their components.

3.7 PHASE BOUNDARY DETERMINATION

The temperature at which a certain blend composition phase separates, may be determined by monitoring any property which undergoes a measurable change when phase separation takes place. A common way to determine the temperature of phase separation is by heating the blend composition under study to various temperatures,

quenching it and then determining the presence of one or two phases by microscopy, T_g measurements, etc. Other popular methods are scattering techniques, which basically consist of detecting the point at which the intensity of the radiation scattered by the sample increases (cloud point). In the present work the great majority of the phase boundaries were determined with light scattering methods due to the reasonable refractive index difference between the components in the blends studied, availability of radiation sources and experimental convenience.

3.7.1 LIGHT SCATTERING

Light scattering measurements were performed with two Small Angle Light Scattering (SALS) instruments which differed in design and in the type of radiation source employed. One instrument used polychromatic light generated by a tungsten lamp and the other the monochromatic light from a He/Ne laser. The design characteristics of both sets of equipment have been fully described elsewhere [70, 131] and so only a brief description will be given.

3.7.1.1 POLYCHROMATIC LIGHT SALS OR TURBIDIMETER

The turbidimeter, which employed polychromatic light, consisted of 4 parts: (a) heating block, (b) light source, (c) temperature controller and (d) a microprocessor. The heating block housed four cylindrical sample slots, a platinum resistance thermometer, the hot junction of a thermocouple which in turn was connected to the programmable temperature controller and wire wound resistors employed for heating the block. The light sources were four 50 watt tungsten lamps run from a stabilized supply. The intensity of the light scattered at 45°from each cell, was measured by photodiodes. This signal together with the temperature of the cell, were fed, at a specific time, into an analog multiplexer which sent a signal to a digital voltmeter and then to a computer. The data were then assembled, processed and formatted by programmed software control and finally sent to a cassette recorder which filed the intensity of the scattered light vs temperature.

The samples were films measuring 20x5x0.3 mm and were supported by cylindrical brass sample holders placed in the sample slots. The heating rate used was 0.1°C/min and the experiments were run from room temperature to temperatures (when possible) 30-50 degrees above the CP. A typical trace of the intensity of the scattered light (arbitrary units) vs temperature is shown in figure 3.8.

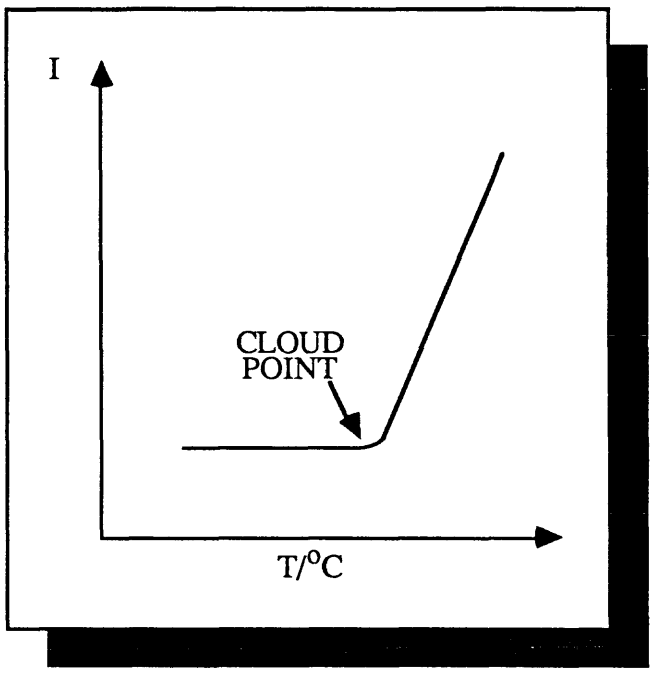

Figure 3.8 Intensity vs temperature plot of a blend composition going through its CP temperature.

The temperature at which the first point of deviation from linearity was observed was taken as the CP. This procedure was repeated for various blend compositions, enabling the construction of the CP curves. Unfortunately, this instrument was not very stable. Although the power supply to the lamps was stable, the light intensities varied significantly during a run. A crude check on performance was made by having a standard sample in one position, but there was no particular reason for the lamp efficiencies to vary simultaneously. The instrument would be greatly improved by adding some system to monitor each light source continuously. In practice, the reproducibility of the data was rather variable and some data had to be discarded.

3.7.1.2 LASER SMALL ANGLE LIGHT SCATTERING (LASER-SALS)

When available the cloud point temperatures were determined with a SALS which used a 5 mW He/Ne laser (Aerotech model 1105) (λ = 6328Å). In this apparatus a light beam from a laser, which was horizontally supported, was deflected through 90° by a prism mounted on an adjustable base. The beam was then passed through the sample which was contained within a temperature controlled brass heating block. The scattered radiation was detected by an array of 16 diodes mounted on a curved aluminium plate which could be moved as required. This array simultaneously recorded the scattered light

on an arc of 32° and was manually positioned to detect the scattered light in the range 0-90°. The signals from the diodes were fed to a multiplexer A/D convertor and stored in a BBC microcomputer.

Before any measurement, the dark signal from each photodiode was measured and then subtracted from the signal produced by a standarized scatterer (a drop of milk diluted in water); these data were used to normalize subsequent measurements. Measurements were performed on samples which were solvent cast on cover slips. It was possible to prepare the crosslinked blends by curing them when already cast on the cover slips, the procedure followed was similar to that in section 3.4 (p. 74-6). A typical cloud point measurement consisted of: (a) checking the alignment of the laser, (b) normalizing the readings of the photodiodes (as described above), (c) selecting the range of temperatures to scan and the rate of heating during the experiment, (d) positioning the array of diodes at a convenient angle and (e) running a computer program to store the intensity of scattered light as a function of temperature and the angle of scattering. The traces obtained from these data were similar to those shown in figure 3.9. In this figure the intensity of the light scattered is shown at two different angles: θ_1 and θ_2, the CP was taken at the angle at which the increase in scattered light was observed at the lowest temperature, being in this case θ_1.

3.7.2 SMALL ANGLE X- RAY SCATTERING (SAXS)

In the case of the blend *C* (see section 4.6.4, p 182-5) it was not possible to determine its cloud point curve by light scattering as the domain sizes were smaller than the wavelength of light used (for tungsten light $\lambda \sim 6500$ Å and for the laser 6328 Å) and so X-rays were used instead. The chlorine present in the SCPE provided the contrast needed by the method.

SAXS was carried out at Unilever, Colworth House, Bedford. The instrument consisted of a monochromatic source of X-rays (a copper target X-ray tube, filter system and collimator) a sample holder, beam stopper and a counter system which measures the intensity of the scattered X-rays as a function of angle. A computer system recorded and displayed the scattered intensity as a function of angle. Single phase systems gave a smooth variation of scattered intensity with θ while a phase separated one gave a sharp maximum. For two phase systems the angle of maximum scattering was recorded for subsequent analysis (see section 3.8, p.89-90).

To determine the temperature of phase separation, the samples were previously quenched from temperatures at 10 degree intervals between 70 and 170°C. The samples

were left for 10 minutes in the heating block of the SALS, which was preheated to the required temperature. After this period, the samples were cooled down rapidly to room temperature (since the blend T_gs are higher than room temperature, the resultant structure will be permanently frozen in this way). All samples measured 0.1x10x10 mm.

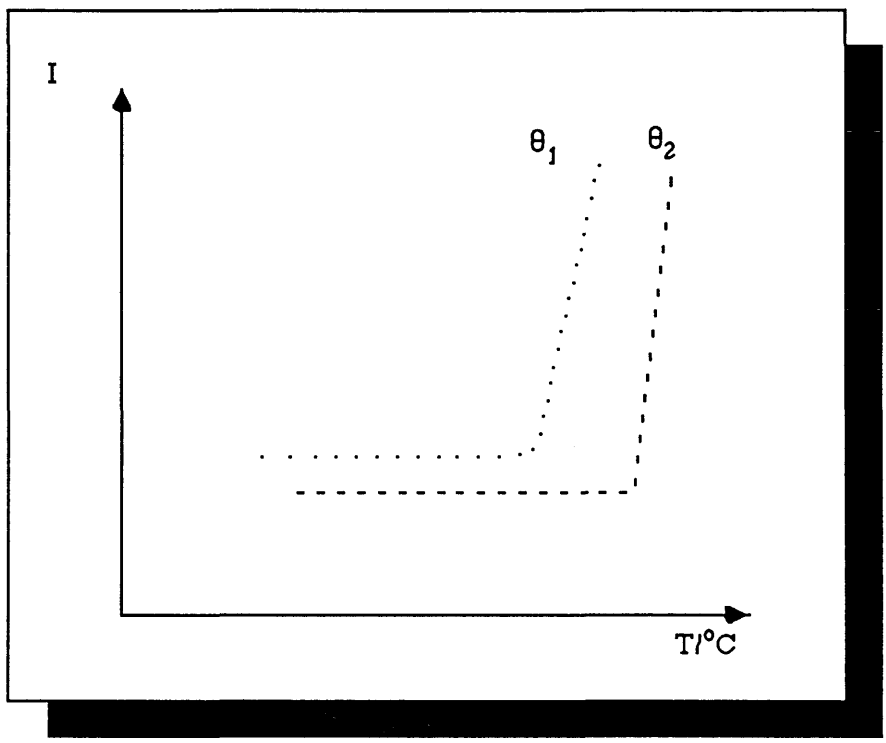

Figure 3.9 Typical traces of the intensity of the scattered light vs temperature measured at two different angles θ_1 and θ_2 with the laser-sals.

3.8 DOMAIN SIZE MEASUREMENT

As mentioned in section 2.5.4 (p. 51-2) the scattering methods are very commonly used in order to measure the domain sizes in phase separated blends. In order to do such measurements, no additional experiments were required: the laser-SALS and SAXS scattering data obtained in determining the phase separation temperatures contained the required information.

The procedure followed to measure the domain sizes was the following: from the laser-SALS and SAXS the intensity of the scattered light (I) was plotted as a function of the angle at a particular temperature. Traces similar to those shown in figure 3.10A and 3.9B were obtained. If the behaviour observed was that shown in figure A, the sample, quite likely, phase separated by nucleation and growth. Figure 3.10B corresponds to a blend undergoing spinodal decompositon.

In the case of a blend undergoing spinodal decomposition it is possible to work out the correlation length by determining the θ corresponding to the peak maximum; using this and equation 2.172 (p. 53) will give the value of Q. The correlation length (d) may be determined using the following expression:

$$d = 2\pi / Q \qquad 3.20$$

This expression is simply obtained by substituting into expression 2.172 Bragg's law:

$$2d\sin(\theta/2) = \lambda \qquad 3.21$$

If a blend compositon phase separates by nucleation and growth, it is possible using the Guinier law:

$$I = \exp(- Q^2 R_g{}^2) / 3 \qquad 3.22$$

to work out the size of domains by plotting lnI vs Q^2. As shown in figure 3.10C a straight line of slope $- (R_g^2) / 3$ (R_g is the radius of gyration) may be the result. If instead of a straight line a curve is obtained, as shown in 3.10D, the R_g may be calculated from the slopes of the curve at high and low values of lnI. These resultant values of R_g will provide the limiting value of the domain size range.

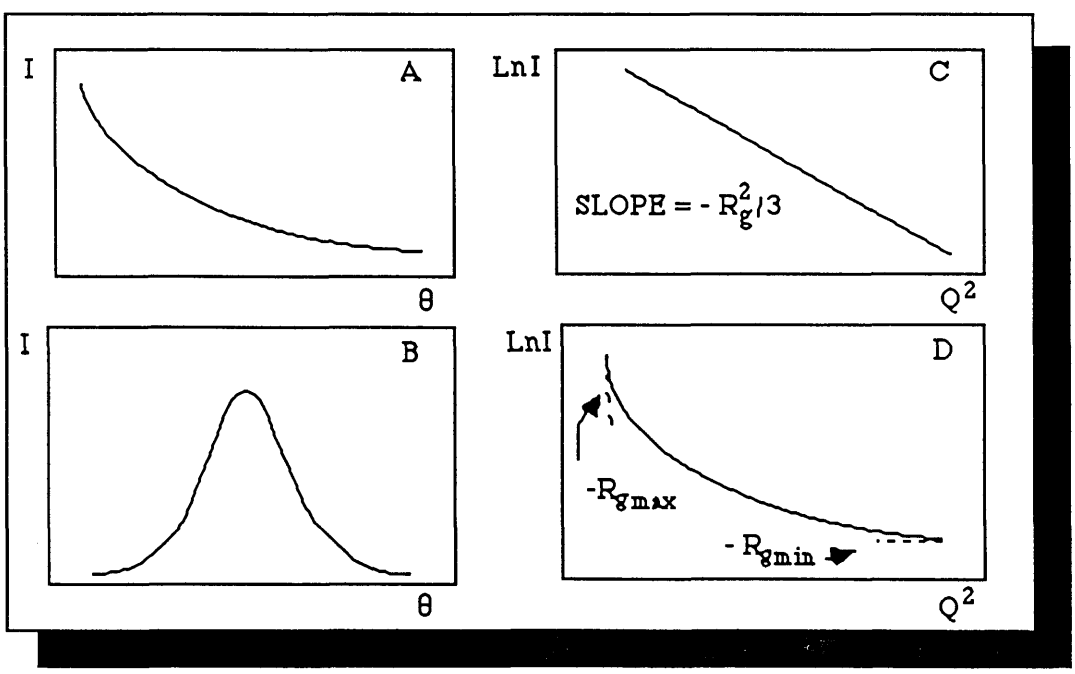

Figure 3.10 Diagram A corresponds to the typical exponential scattering of a blend phase separating by nucleation and growth. Diagram B shows the scattering pattern of a blend compositon undergoing spinodal decomposition. Diagrams C and D are plots of lnI vs Q^2 for a blend compositon phase separating by nucleation and growth. Diagram C represents a linear behaviour. The slope gives $-R_g{}^2/3$. The diagram in D represents a non linear behaviour. The slope at high and low values of lnI provide the limiting values of the domain sizes observed in this experiment.

SUMMARY

This chapter contains all the experimental procedures involved in the present work. The characterization methods for miscibility and phase separation behaviour are generally applicable to the study of polymer blends. The method of crosslinking the blends and evaluating the products are more specific to this project. The results of applying these techniques to the systems studied in this work are given in the next chapter.

CHAPTER 4
RESULTS AND INTERPRETATION

This chapter presents the results of the experimental work and its interpretation. To preserve clarity the material will be divided according to the type of system studied. The discussion will be presented in the next chapter.

4.1 $SCPE_{43}$/PVC 50/50 (E_{50})

The complex morphology of PVC makes it a difficult choice for miscibility studies (see chapter 1, p. 5). In spite of this, its blend with $SCPE_{43}$ was studied here due to the great interest shown in this blend recently [24, 25]. $SCPE_{43}$ is the commercial sulphochlorinated polyethylene known as Hypalon 48 ($\bar{M}_n$ = 23000). In the solvent cast blend a commercial PVC (Breon M 110/50, $\bar{M}_n$ = 31000) was mixed in MEKwith the $SCPE_{43}$ (sect 3.3.1 p. 68-9). In the *insitu* blend, the vinyl chloride monomer (VCM) was polymerized in the presence of $SCPE_{43}$ (section 3.3.2, pp 69-71). In both cases only the composition containing 50% $SCPE_{43}$ was studied.

4.1.1 DEGREE OF CROSSLINKING

As mentioned in section 3.4.1 (pp 72-3), E_{50} was crosslinked with ammonia solution. A crude estimate of the degree of crosslinking was obtained by measuring the weight percent of residue remaining undissolved after solvent extracting the cured polymer or blend. Figures 4.1 and 4.2 show the results of such experiments.

Figure 4.1 shows the weight percentage of undissolved cured polymer when E_{50} was crosslinked with different concentrations of aqueous ammonia solutions. As may be seen the higher the concentration of NH_3 used, the higher the percentage of undissolved $SCPE_{43}$ in the sample. Figure 4.2 shows a comparison of the weight percent of undissolved $SCPE_{43}$ when cured in a 17.5% NH_3 solution in water.This figure

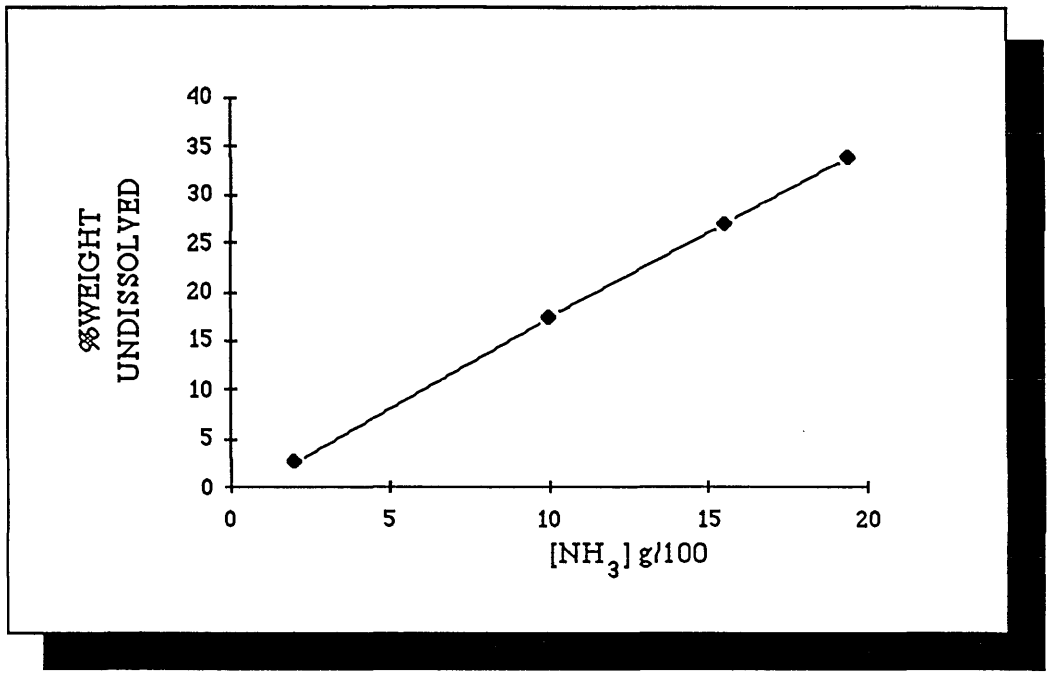

Figure 4.1 Percentage weight of undissolved $SCPE_{43}$ cured with ammonia solution vs ammonia concentration. The values reported are after 120h of immersing the polymer in the crosslinking agent.

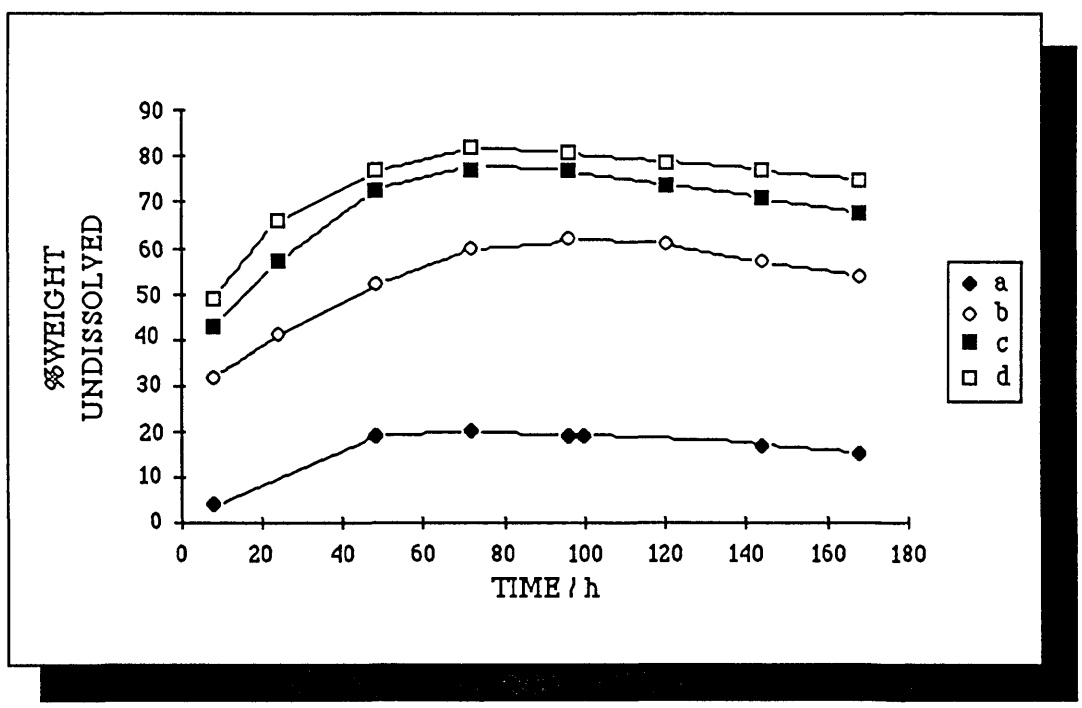

Figure 4.2 Percentage weight of undissolved $SCPE_{43}$ crosslinked with a 17.5% of NH_3 in solution at the following conditions: (a) room temperature, (b) 50°C, (c) crosslinked at 50°C and postcured at 100°C, (d) fractionated $SCPE_{43}$ crosslinked at 50°C and postcured at 100°C.

shows that the highest degree of crosslinking was achieved when fractionated $SCPE_{43}$ was crosslinked at 50°C and postcured at 100°C. When blended with PVC, $SCPE_{43}$ (E_{50}) was crosslinked under the same conditions yielding 35% of undissolved weight.

4.1.2 MISCIBILITY BEHAVIOUR.

While solvent cast E_{50} was hazy, the *insitu* polymerized E_{50} was transparent with a light pink colour. In the Pereval Interphako phase contrast microscope the solvent cast blend showed the presence of spherical domains of size between 10-24 μm (figure 4.3). In the *insitu* blend a uniform background was obtained (figure 4.4). These visual and microscopic observations suggested that the solvent cast blend was not homogeneous whilst the *insitu* was.

These observations were confirmed by the T_g determinations of both blends obtained with the Rheovibron and DSC. Figure 4.5 and table 4.1 show the Rheovibron results for the solvent cast blend and the *insitu* blend before and after crosslinking.

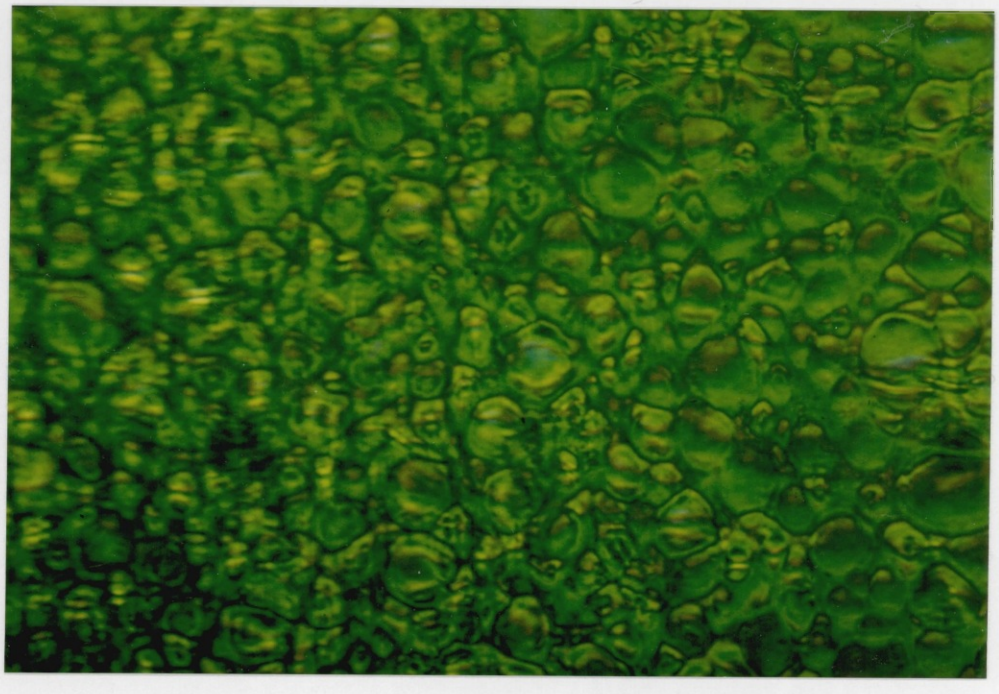

Figure 4.3 Micrograph taken with the Pereval Interphako of E_{50} at room temperature.

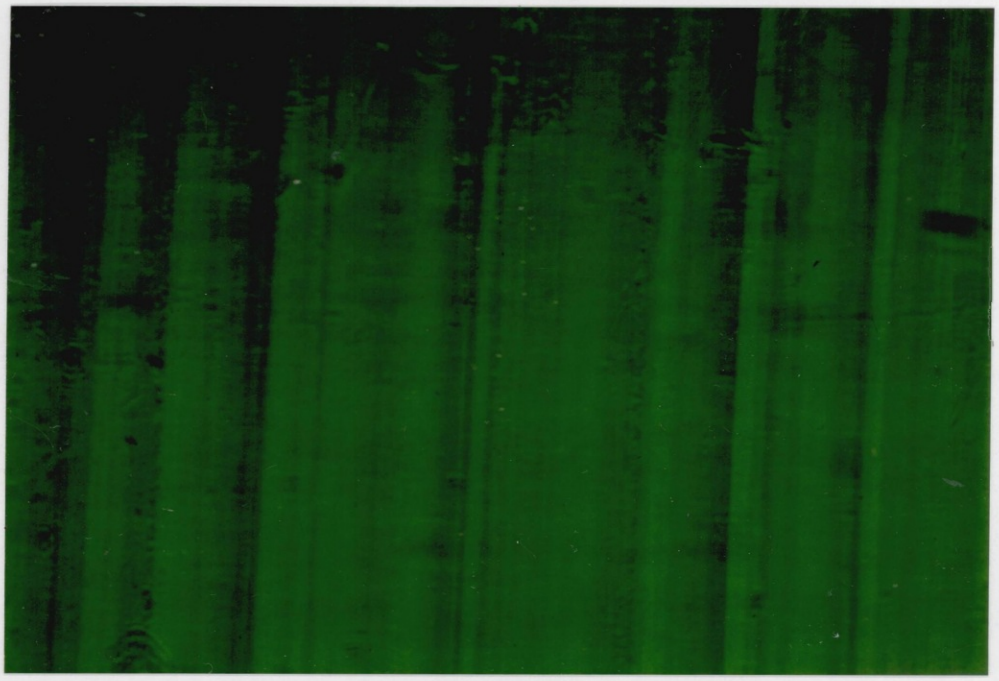

Figure 4.4 Micrograph taken with the Pereval Interphako of E_{50} at room temperature

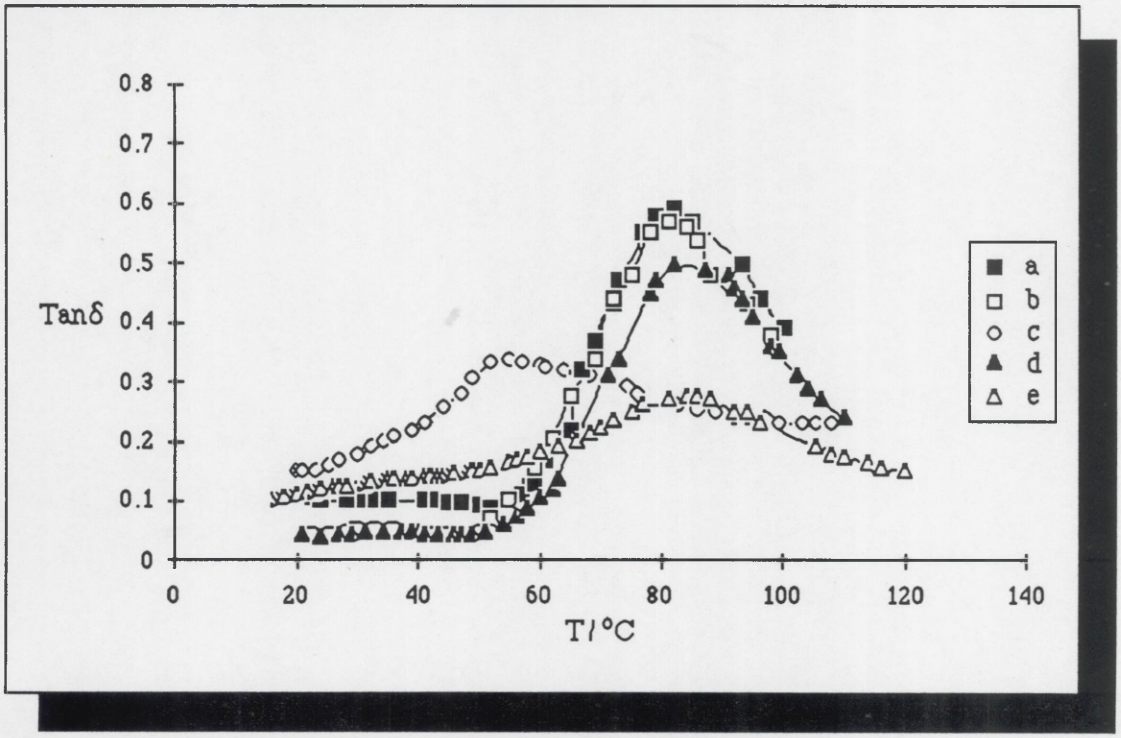

Figure 4.5 T_gs obtained with the Rheovibron for (a) PVC, (b) E_{50}, (c) $E_{50insitu}$, (d) $E_{50NH4OH}$ and (e) $E_{50insituNH4OH}$.

Figure 4.6 shows the DSC curves for the components, the solvent cast blend and the *insitu* blend before and after curing. As may be seen in figure 4.5 the solvent cast blend has two peaks (curve b) while the *insitu* blend (curve c) shows only one broad peak with a maximum at 57°C. The DSC results for both samples (curves c and e, figure 4.6) confirm the Rheovibron observations. After crosslinking, the solvent cast sample remained two phases (curve b in figure 4.5 and curve c in figure 4.6) and the *insitu* blend became phase separated (curve e in figure 4.5 and curve g in figure 4.6).

By using the Fox equation and the T_g values for the transitions observed with the Rheovibron (see figure 4.5 and table 4.1), the composition and the mass balance in each of the phases in the immiscible samples were calculated as shown in table 4.2 (the T_g of pressed PVC was used in the calculations).

Sample	T_gs observed °C	Max value tan δ	Comments
PVC	82	0.60	sharp peak
PVC pressed	107	0.42	sharp peak
* $SCPE_{43}$	18	1.55	sharp peak
E_{50}	23, 81	0.05, 0.57	small hump overlapping sharp peak
E_{50NH_4OH}	36, 82	0.04, 0.50	small hump overlapping sharp peak
$E_{50insitu}$	56	0.33	broad peak
$E_{50insituNH_4OH}$	30, 84	0.14, 0.27	small hump overlapping sharp peak
* Not shown in figure 4.5			

Table 4.1. T_gs for E_{50} when solvent cast and *insitu* polymerized.

Sample	T_gs °C	Max value tanδ	Composition % w/w	Mass balance g/g initial mixture
E_{50}	33 81	0.05 0.57	74 / 26 1 / 99	0.48 / 0.17 0.003 / 0.33
E_{50NH_4OH}	36 82	0.04 0.50	69 / 31 0 / 100	0.5 / 0.22 0 / 0.28
[1] $E_{50insituNH_4OH}$	30 84	0.14 0.27	84 / 16 21 / 79	0.39 / 0.07 0.11 / 0.43
[1] The T_g value used in this calculation for the PVC was that of PVC pressed (see Table 4.1)				

Table 4.2 Composition and mass balance of the two phases present in E_{50}, $E_{50NH4OH}$ and $E_{50insituNH4OH}$.

4.1.3 PHASE SEPARATION BEHAVIOUR

As it was not possible to reach the CP temperature of $E_{50insitu}$ using the turbidimeter, the temperature of phase separation was determined using samples quenched at different temperatures which then were observed with the Pereval Interphako microscope, TEM and Rheovibron. The Pereval Interphako microscope showed that the *insitu* blend was one phase at room temperature (see figure 4.7) and two phases at 90°C (figure 4.8). At higher temperatures, it was possible to observe that the size of such domains kept increasing (see figure 4.9). Figure 4.10 shows that the crosslinked *insitu* blend was phase separated at room temperature. Figure 4.11 and 4.12 show that the size of domains present in the crosslinked *insitu* blend keep increasing with temperature.

Using the Jeol Jem 100B 100K electron microscope, it was possible to see the presence of domains in $E_{50insitu}$ at room temperature (figure 4.13), which increased to the sizes shown in figure 4.14 at 90°C.

The results obtained with the Rheovibron for $E_{50insitu}$ and $E_{50insituNH4OH}$ at different temperatures are shown in figs 4.15 and 4.16 respectively. As may be seen, the Rheovibron results confirm what was observed previously using phase contrast and transmission electron microscopy; curve a in figure 4.15 shows that $E_{50insitu}$ is one phase at room temperature, the presence of two peaks in curve b shows clearly that $E_{50insitu}$ begins to phase separate at 90°C, phase separation increasing at higher temperatures. Figure 4.15 shows that $E_{50insituNH4OH}$ is phase separated at room temperature and is increasingly phase separated at higher temperatures. It was possible to

see how phase separation proceeded with temperature for the two phase solvent cast blend, before and after being crosslinked. Table 4.3 shows the values of the T_g and tanδ for E_{50} and $E_{50NH4OH}$ after treatment at temperatures from room temperature to 150°C to increase phase separation.

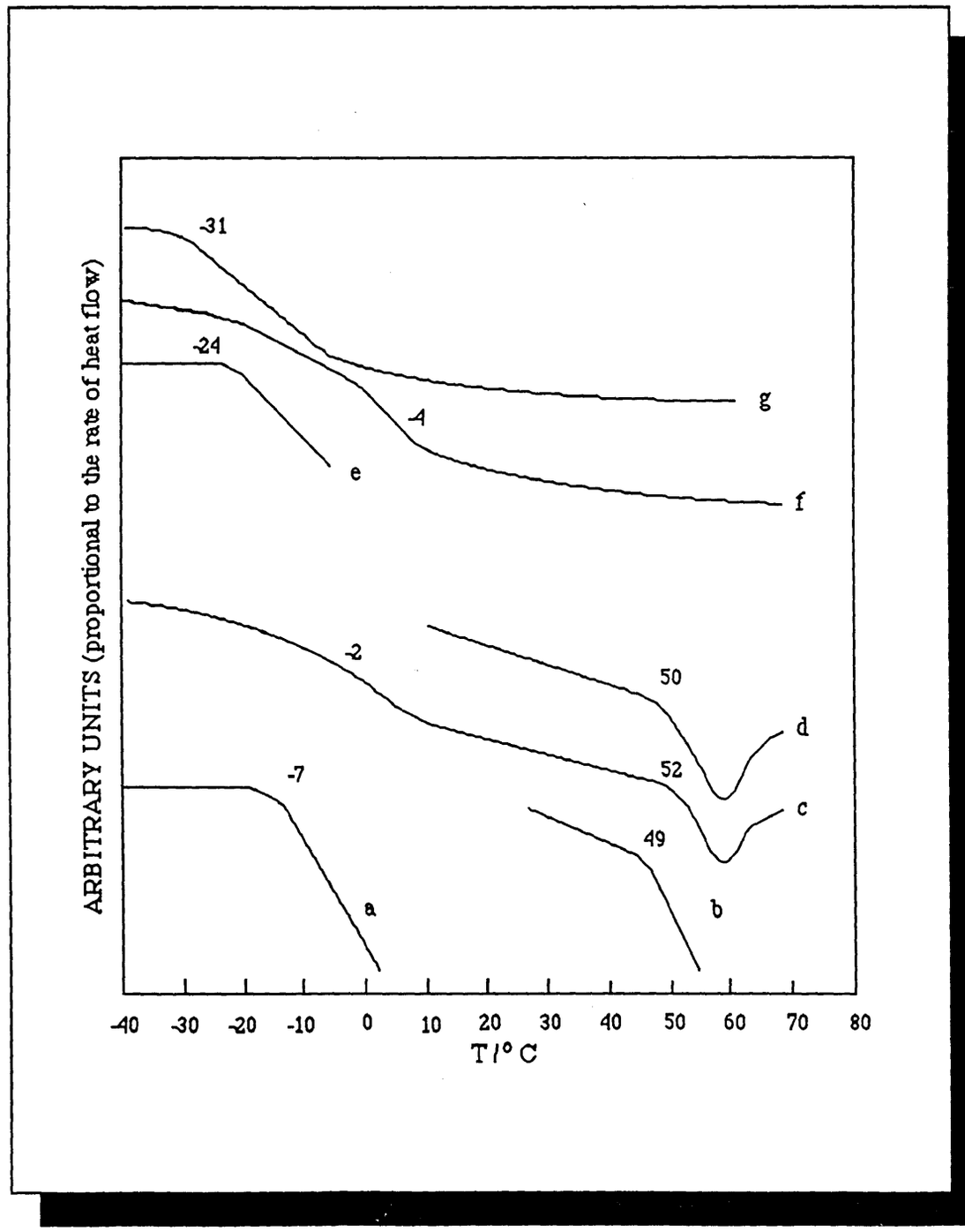

Figure 4.6 DSC curves of (a) $SCPE_{43}$, (b) PVC solvent cast, (c) E_{50}, (d) $E_{50NH4OH}$, (e) $E_{50insitu}$ (f)$E_{50insitu}$ dried at 90°C, (g) $E_{50insituNH4OH}$.

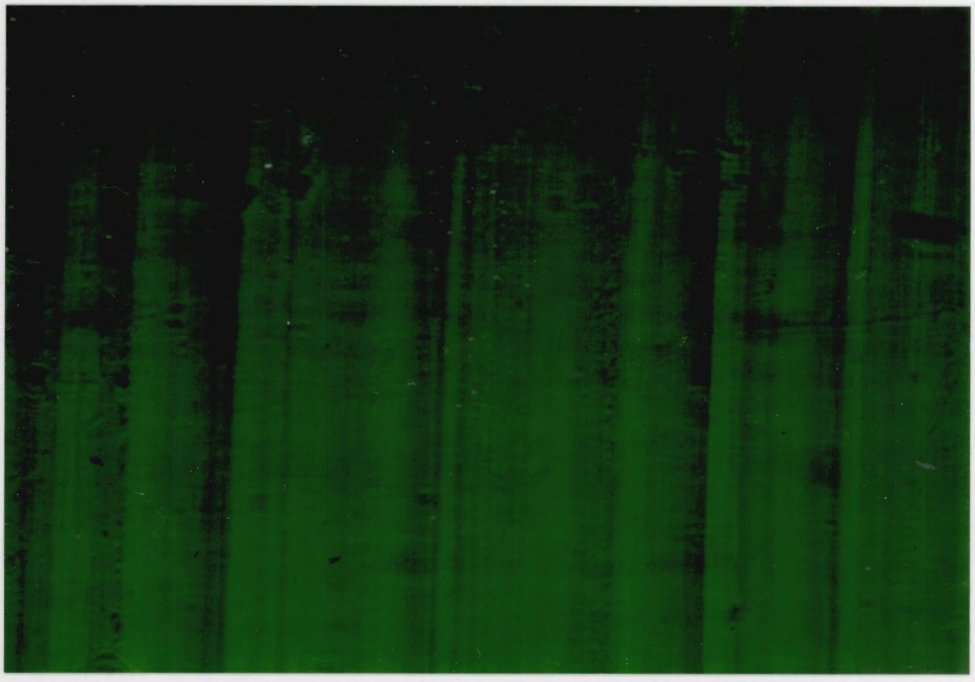

Figure 4.7 Micrograph taken with the Pereval Interphako of $E_{50insitu}$ at room temperature.

Figure 4.8 Micrograph taken with the Pereval Interphako of $E_{50insitu}$ at 90^{o}C.

Figure 4.9 Micrograph taken with the Pereval Interphako of $E_{50insitu}$ at 120°C.

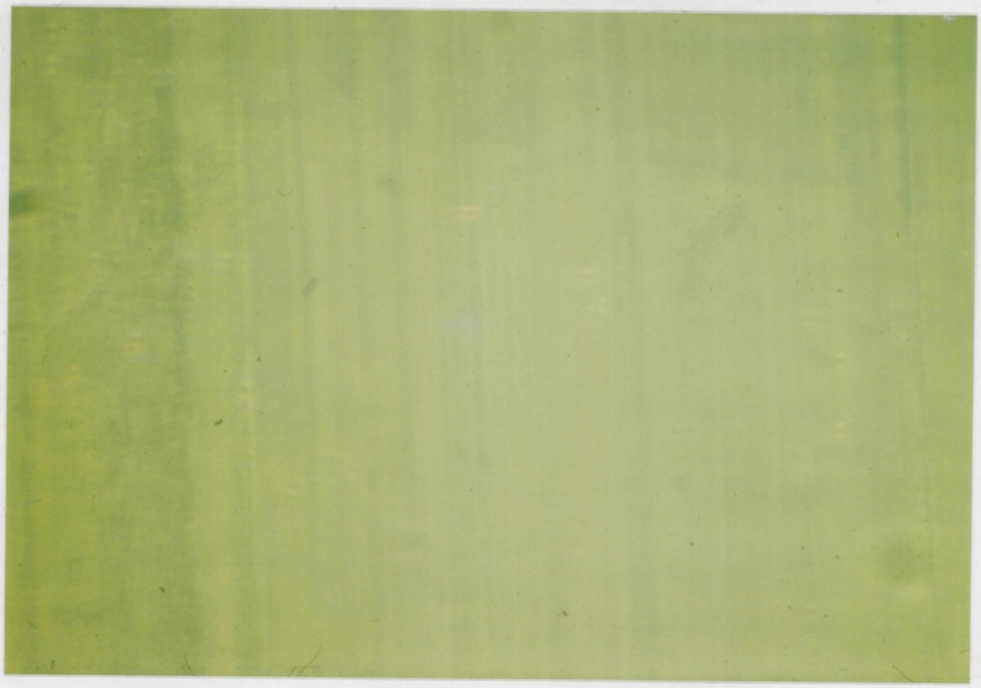

Figure 4.10 Micrograph taken with the Pereval Interphako of $E_{50insituNH4OH}$ at room temperature

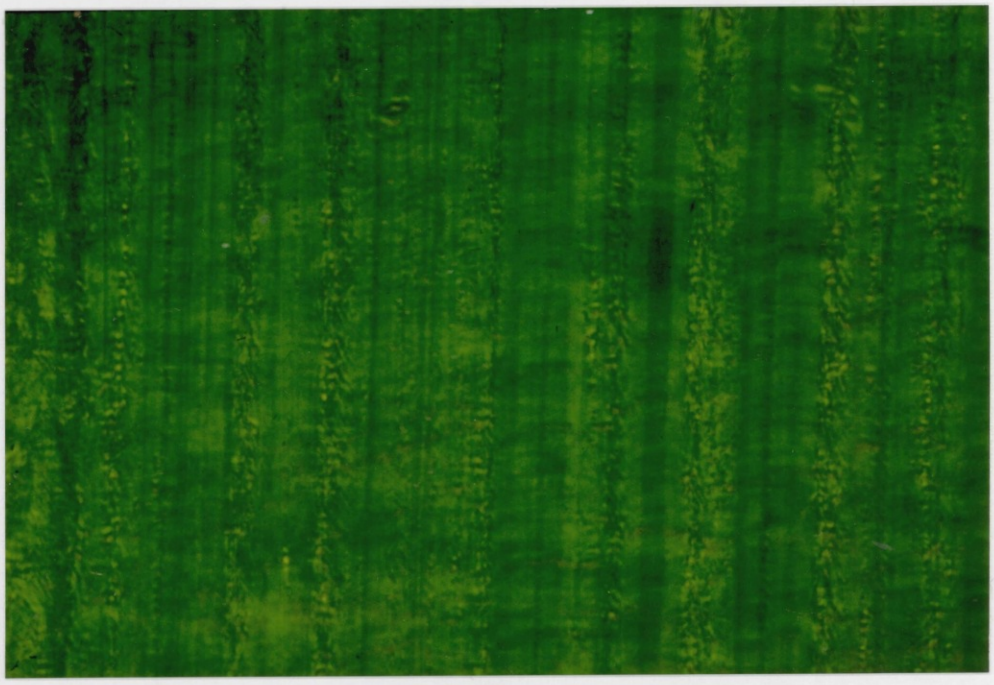

Figure 4.11 Micrograph taken with the Pereval Interphako of $E_{50insituNH4OH}$ at 90°C.

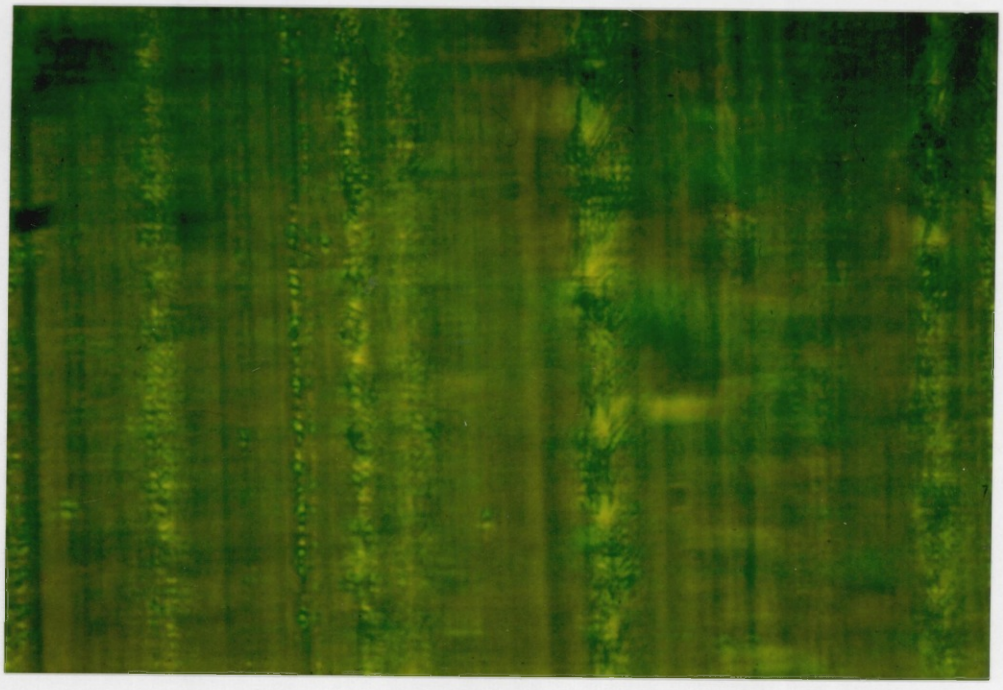

Figure 4.12 Micrograph taken with the Pereval Interphako of $E_{50insituNH4OH}$ at 120°C.

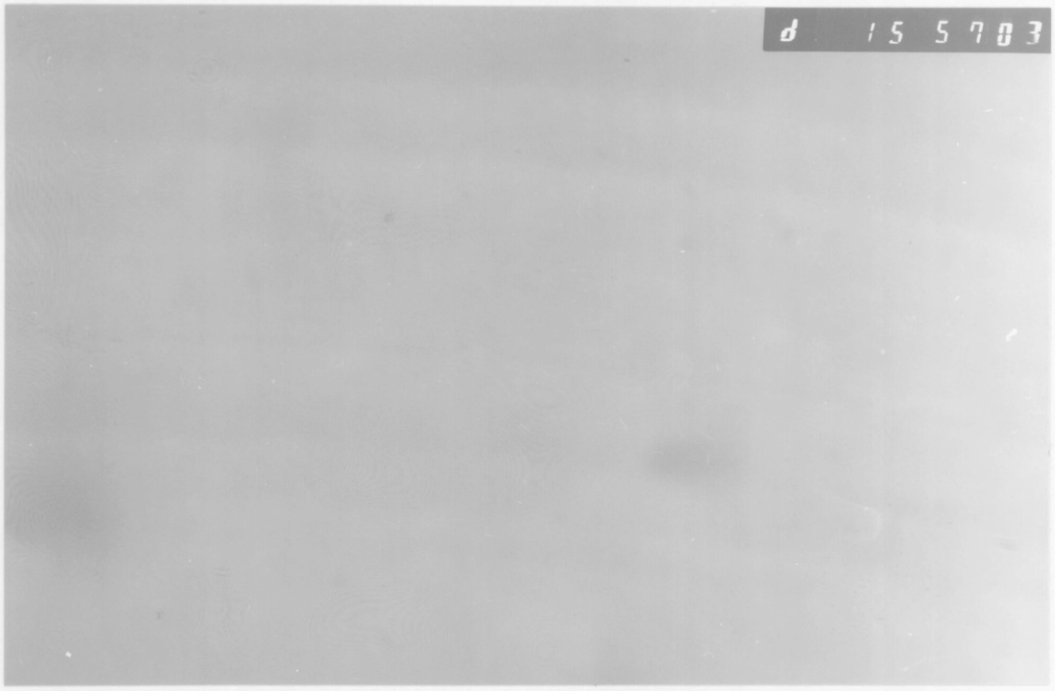

Figure 4.13 Micrograph taken with the Jeol Jem100B 100K TEM of $E_{50insitu}$ at room temperature.

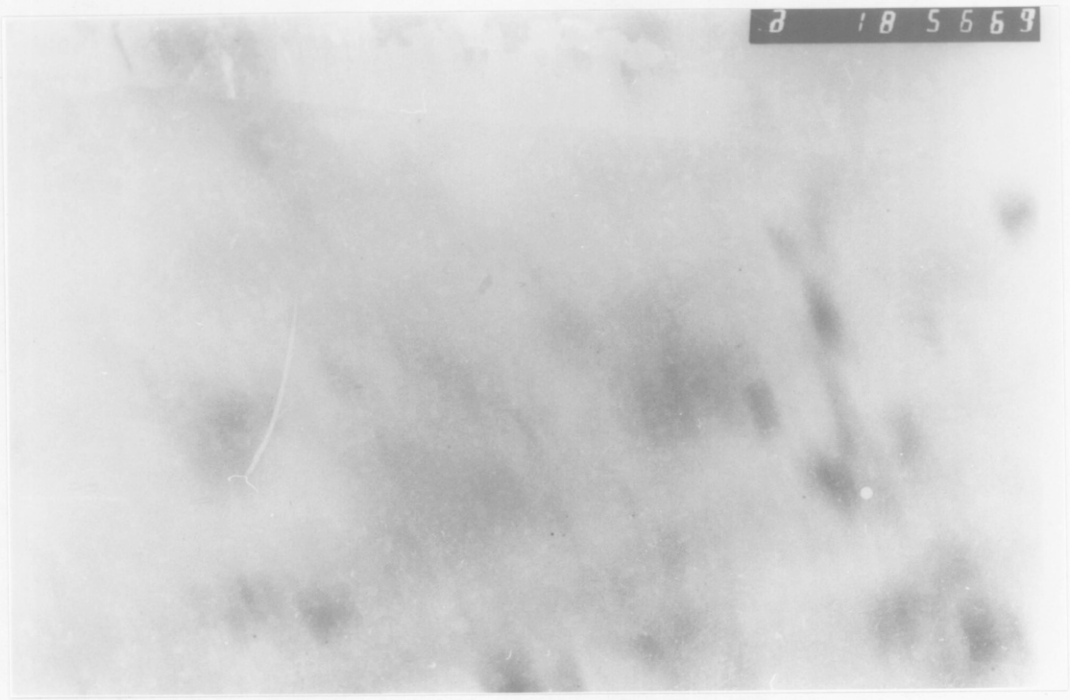

Figure 4.14 Micrograph taken with the Jeol Jem100B 100K TEM of $E_{50insitu}$ at 90°C.

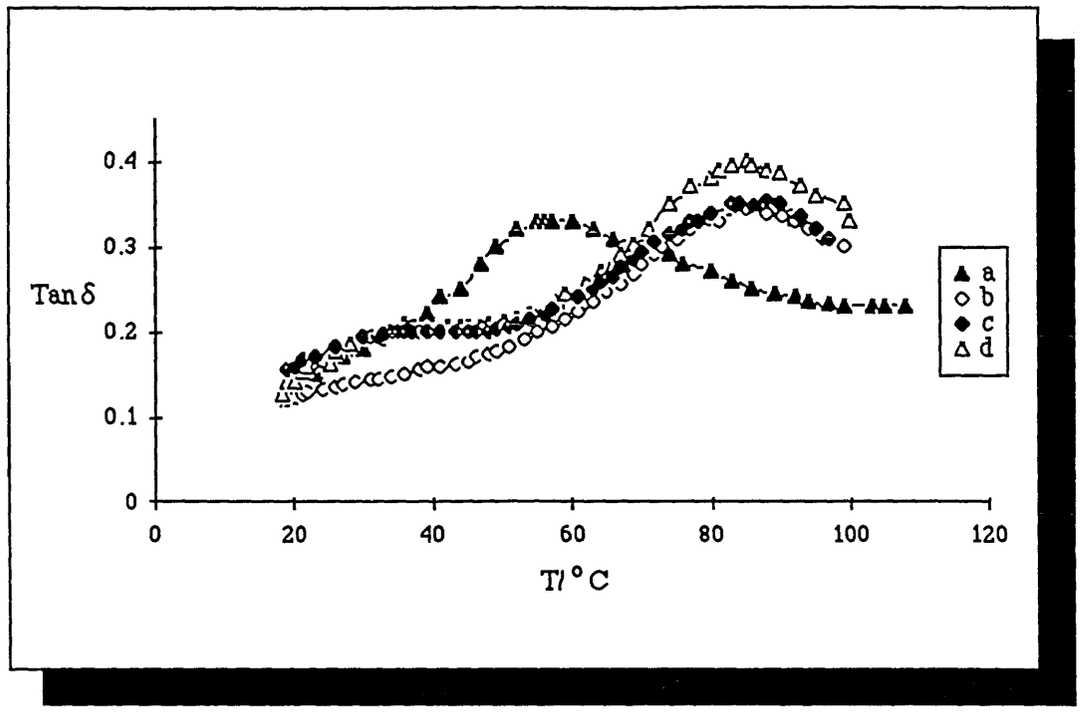

Figure 4.15 T_gs of $E_{50insitu}$ at (a) room temperature (T_g at 56°C), (b) 90°C (T_gs at 35? and 85°C), (c) 120°C (T_gs at 30, 85°C) and (d) 150°C (T_gs at 28 and 84°C).

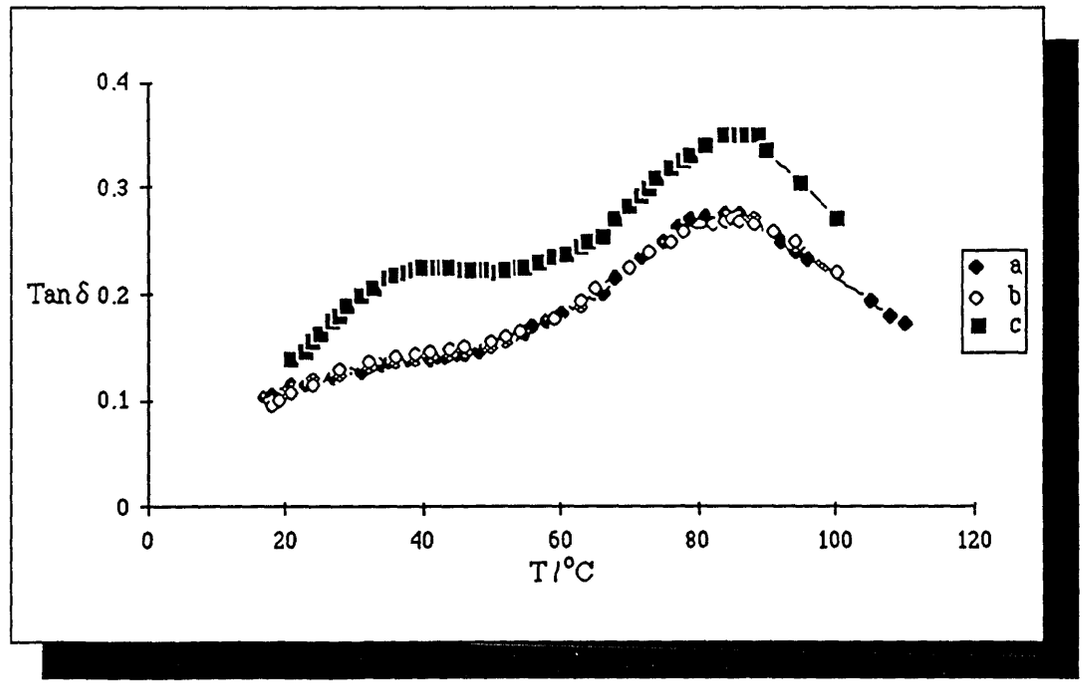

Figure 4.16 T_gs of $E_{50insituNH4OH}$ (a) room temperature (T_gs at 40 and 85 °C), (b) 90°C (T_gs at 40 and 85°C) and (c) t 130°C (T_gs 42 and 86°C).

Sample	T/°C	Heating period (min)	T_{g1}	tan δ_1	T_{g2}	tanδ_2
E_{50}	* RT	——	33	0.055	81	0.57
"	110	10	31	0.060	80	0.69
"	120	"	25	0.078	80	0.67
"	130	"	33	0.056	87	0.81
"	140	"	28	0.055	87	0.86
"	150	20	25	0.071	88	0.83
"	150	20	27	0.070	94	0.95
E_{50NH_4OH}	RT	——	36	0.048	82	0.50
"	110	10	32	0.067	86	0.67
"	120	"	35	0.062	87	0.72
"	130	"	33	0.061	88	0.77
"	140	"	32	0.068	87	0.83
"	130	20	37	0.054	93	0.85
"	150	20	24	0.077	96	0.92
*RT= room temperature						

Table 4.3 Values of the T_g and tanδ for the two transitions present in solvent cast E_{50} before and after being crosslinked with NH_4OH, after treatment at several temperatures

4.2 SCPE$_{43}$/EVA (SYSTEM *A*)

This blend was previously studied by Walsh *et al* [28, 29]. The $SCPE_{43}$ used contains 43% Cl and 0.1% S as SO_2Cl groups (see section 3.1.1.1 p. 56-7).The EVA_{45} is an ethylene-vinyl acetate copolymer containing 45% of vinyl acetate (see section 3.1.4 p 61). Of all the blends studied in this work, *A* is the only one behaving as a rubbery system for the whole composition range because the T_gs of both components are below room temperature (EVA_{45} $\bar{M}_n$= 51000, T_g = -19°C ; $SCPE_{43}$ $\bar{M}_n$ = 23000, T_g = 19°C); this is advantageous when measuring the degree of crosslinking as the theories on which the measurements are based will be more applicable. The blend was solvent cast in THF and, when dried, was crosslinked with *DETA* (see sections 3.3.1 pp 68-9 and 3.4.2 pp 73-4).

4.2.1 DEGREE OF CROSSLINKING OF A_{DETA}

For *A* and the great majority of the systems in this work, the degree of crosslinking was determined by measurements of swelling ($\bar{M}_{cSWELL}$), stress - strain curves ($\bar{M}_{cMECH}$) and DMTA measurements ($\bar{M}_{cDYN}$). Swelling was performed at 25°C, stress-strain measurements at room temperature and, for the DMTA, the data were obtained 20°C above the T_g of the blend. The results obtained by these techniques are collected in tables 4.4, 4.5 and 4.6 respectively. For the swelling measurements in 4.4, three different equations were used: (1) a modified version of the Flory-Rehner [71] equation (considers free end chains and interlooping), (2) James and Guth equation [74,146] and (3) Herman equation [71, 143, 144] (see section 2.4.2.2 pp 35-7) (these last two equations differ from that of Flory in the method of computing ΔS_{el}). These three equations required the calculation of ϕ_2, which was obtained using standard data. (The value of the interaction parameter between $SCPE_{43}$-THF at 25 °C (χ_{12}= 0.4095) was calculated from the value χ_{12} reported at 120 °C by Doubé and Walsh [25], assuming that χ_{12} is a linear function of temperature). The results obtained by any of these three equations are quite similar. A comparison of these values with the $\bar{M}_n$ of $SCPE_{43}$ (23000) suggests that the $SCPE_{43}$ both when pure and when blended with EVA is lightly crosslinked.

Table 4.5 shows the values of $\bar{M}_{cMECH}$ obtained using values of G_N (shear modulus of the network) calculated in 4 different ways: (1) G_N was considered to be equal to the experimental value of G_{XB} (shear moduli of the crosslinked blend), (2) G_N was considered to be the difference between the moduli of the blend before and after crosslinking ($G_N = G_{XB}-G_B$), (3) assuming the rule of mixtures ($G_{XB}= G_N\phi_N + G_U\phi_U$) $G_N =(G_{XB}- G_U\phi_U) / \phi_N$ where G_U = shear modulus of the unmodified polymer, ϕ_U and ϕ_N are the volume fraction of the unmodified polymer and the network respectively, (4) as will be seen in next section the blend compositions A_{10} to A_{50} behave as one phase systems while A_{60} to A_{90} as two phase. For the one phase systems G_N was calculated as in (3). For A_{60} to A_{90} G_N was obtained using the Budiansky equation which applies to two phase systems with domain-domain interactions [106]. Table 4.6 shows the values of $\bar{M}_{cDYN}$ obtained using the DMTA data 20°C above the T_g of each blend composition. The final value of G'_N (dynamic shear loss modulus for the network) was calculated using the same 4 methods described for table 4.5. As may be seen in tables 4.5 and 4.6, the values obtained by stress-strain or dynamic measurements (using any of the four calculation methods above mentioned) are smaller than the results obtained by swelling measurements.

The experimental errors in all these measurements of $\bar{M}_c$ are significant, but the major reason for the discrepancies between the techniques used is the fact that the system is not ideally rubbery, and therefore the theories used are not strictly applicable. This problem is more acute with all the other systems studied here; the values of $\bar{M}_c$ obtained from static and dynamic modulus measurements on these other systems are clearly unsatisfactory, although the dynamic modulus values were determined at 20 degrees above the T_g of each blend (the higher T_g for two phase systems) in an attempt to obtain data for the system in a rubbery state. $\bar{M}_c$ values obtained from modulus measurements have, therefore, not been reported for the other systems studied.This topic will be discussed further at the appropriate point in chapter 5, and some of the unsatisfactory results are shown there.

SWELLING MEASUREMENTS $\bar{M}_{cSWELL}$ g/mole*			
Sample	(1)	(2)	(3)
A_{10DETA}	11500	11500	11500
A_{20DETA}	11490	11460	11460
A_{30DETA}	11470	11410	11480
A_{40DETA}	11490	11470	11470
A_{50DETA}	11490	11480	11480
A_{60DETA}	11490	11460	11460
A_{70DETA}	11500	11470	11470
A_{80DETA}	——	——	——
A_{90DETA}	11400	11200	11170
$SCPE_{43DETA}$	11500	11500	11500
* $\bar{M}_{cSWELL}$ calculated with (1) a modified version of Flory-Rehner [71] eq. (2) James and Guth eq.[71, 143] and (3) Herman eq.[71, 143, 144]. All these equations include the correction for free ends.			

Table 4.4 Values of $\bar{M}_{cSWELL}$ for A_{DETA}.

Mechanical measurements $\bar{M}_{cMECH}$ g/mole				
Sample	Method*			
	(1)	(2)	(3)	(4)
A_{10DETA}	7540	——	8630	8630
A_{20DETA}	6420	9840	3580	3570
A_{30DETA}	5910	8350	3640	3640
A_{40DETA}	5654	8240	3900	3890
A_{50DETA}	6212	8732	3000	2980
A_{60DETA}	5525	9153	4420	3920
A_{70DETA}	4538	6260	3670	3220
A_{80DETA}	5449	7974	3730	3760
A_{90DETA}	3884	5650	3580	3470
$SCPE_{43DETA}$	760	6760	760	760

* $\bar{M}_{cMECH}$ obtained from G_N which was calculated from the following methods: (1) $G_N = G_{XB}$ (2) $G_N = G_{XB} - G_B$ (3) $G_N = (G_{XB} - G_U \phi_U)/\phi_N$ (4) From A_{10DETA} to A_{50DETA} inclusive, method (3) was used; from A_{60DETA} onwards the Budianski[106] equation was used.

Table 4.5 Values of $\bar{M}_{cMECH}$ for A_{DETA} obtained from stress-strain measurements using four different calculation methods.

Dynamic mechanical measurements $\bar{M}_{cDYN}$ g/mole				
Sample	Method *			
	(1)	(2)	(3)	(4)
A_{10DETA}	1480	6160	——	——
A_{20DETA}	1450	——	1350	1350
A_{30DETA}	1510	2580	1210	1210
A_{40DETA}	850	1110	2170	2170
A_{50DETA}	1960	3600	1580	1580
A_{60DETA}	——	——	——	——
A_{70DETA}	1760	2080	1360	1150
A_{80DETA}	1560	1641	1240	1160
A_{90DETA}	1140	1210	1050	1000
$SCPE_{43DETA}$	280	320	278	278

* $\bar{M}_{cDYN}$ was obtained from G'_N. G'_N was calculated from: (1) $G'_N = G'_{XB}$ (2) $G'_N = G'_{XB} - G'_B$ (3) $G'_N = (G'_{XB} - G'_U \phi_U)/\phi_N$ (4) From A_{10DETA} to A_{50DETA} inclusive method (3) was used. From A_{60DETA} onwards the Budianski[106] equation was used.

Table 4.6 Values of $\bar{M}c_{DYN}$ for A_{DETA} obtained from the DMTA experiments using four different calculation methods.

4.2.2 MISCIBILITY OF *A* AND A_{DETA}

Blend *A* looked transparent up to 40% w/w $SCPE_{43}$. From A_{50} onwards a slight haziness began to develop. The transparency of the samples did not change with crosslinking but they develop a typical brown discoloration characteristic of diamine crosslinking.

The appearance of haziness from A_{50} upwards suggests that these compositions are no longer one phase systems, behaviour which was later confirmed with the determination of the T_g using the Rheovibron and DMTA. These results are shown in figures 4.18, 4.19, tables 4.7 and 4.8.The T_gs for the pure polymers are shown in figure 4.17.

As may be seen A_{10} to A_{40} have one T_g (see figure 4.18). A_{50} shows a broad peak, which is a typical behaviour for a blend composition at the edge of being compatible [12] (see section 2.5.1 p. 46). From A_{60} to A_{90}, two peaks were observed. These peaks were inward shifted with respect to the T_gs of the pure polymers, which is typical of partially miscible systems [3,4].

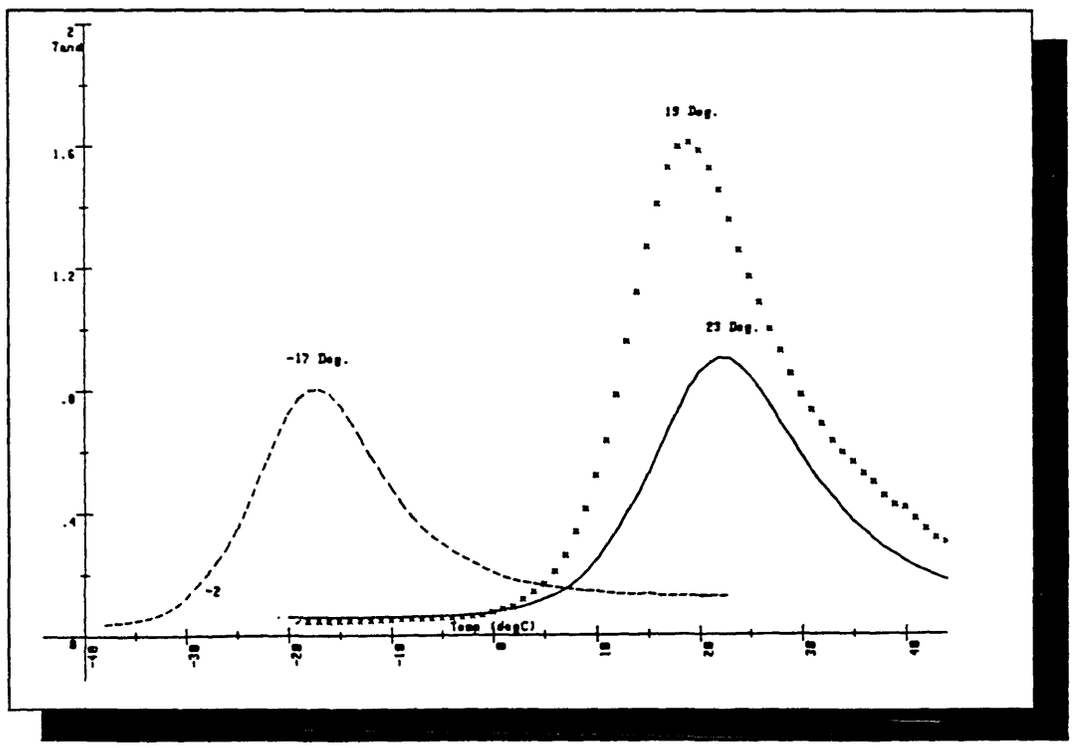

Figure 4.17 T_gs of EVA_{45} (-17°C(- -)), $SCPE_{43}$ (19°C(x) and $SCPE_{43DETA}$ (23°C(–)).

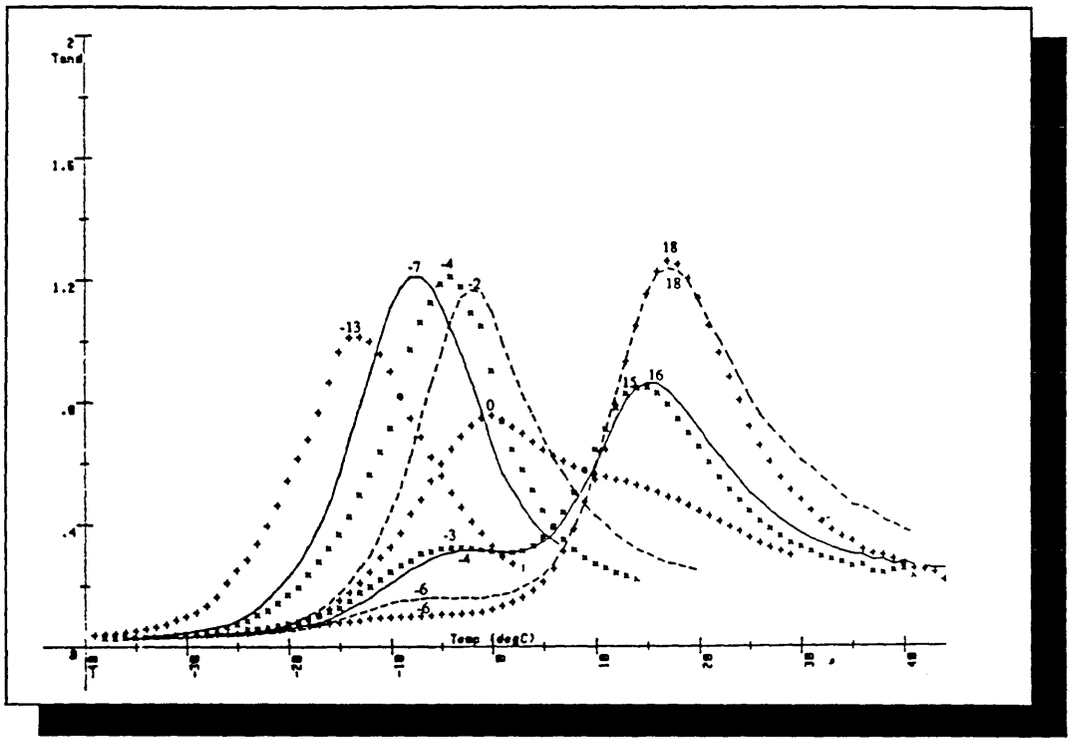

Figure 4.18 T_gs for the whole composition range of system *A* ($SCPE_{43}/EVA_{45}$). A_{10} (-13°C(+)), A_{20} (-7°C(—)), A_{30} (-4°C(x)), A_{40} (-2°C(- -)), A_{50} (0°C(+)), A_{60} (-4, 16 °C(—)), A_{70} (-3, 15°C(x)), A_{80} (-6, 18°C(- -)), A_{90} (-6, 18°C(+)).

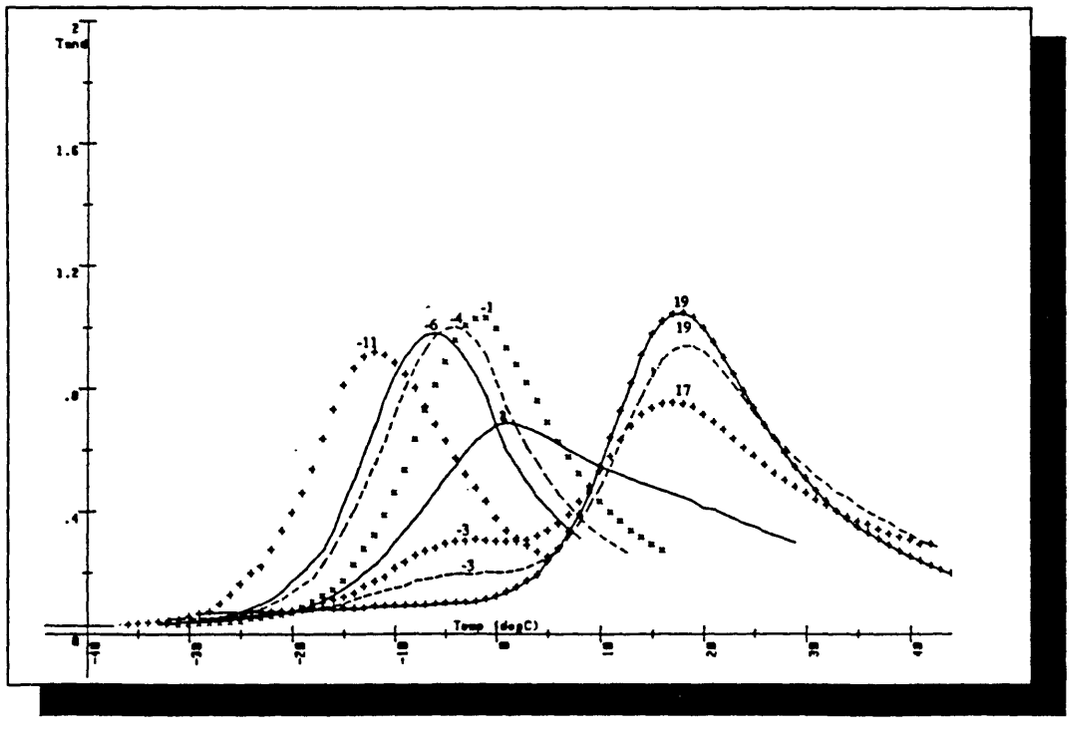

Figure 4.19 T_gs for the whole composition range of system A_{DETA} ($SCPE_{43DETA}/EVA_{45}$). A_{10DETA} (-11°C(+)), A_{20DETA} (-6°C(—)), A_{30DETA} (-4°C(- -)), A_{40DETA} (-1°C(x)), A_{50DETA} (2°C(–)), A_{70DETA} (-3, 17°C(+)), A_{80DETA} (-3, 19°C(- -)), $A_{90\ DETA}$ (?, 19°C(+)).

	Rheovibron			DMTA		
Sample *	Tgs observed (o C)	Max. value tanδ	Comments	Tgs observed (o C)	Max. value tanδ	Comments
EVA45	-16	0.93	sharp peak	-17	0.80	sharp peak
A_{10}	-11	1.05	sharp peak	-13	1.00	sharp peak
A_{20}	-8	1.15	sharp peak	-7	1.14	sharp peak
A_{30}	-7	1.25	sharp peak	-4	1.20	sharp peak
A_{40}	-2	1.30	sharp peak	-2	1.16	sharp peak
A_{50}	-2	1.10	broad peak	0	0.75	broad peak
A_{60}	0, 14	0.63, 0.65	peaks overlap	-4, 6	0.31, 0.86	peaks overlap
A_{70}	-5, 15	0.17, 1.50	peaks overlap	-3, 16	0.32, 0.85	peaks overlap
A_{80}	-8, 17	0.08, 1.45	small hump overlapping with sharp peak	-6, 18	0.16, 1.15	small hump overlapping with sharp peak
A_{90}	-12, 16	0.03, 1.52	v. small hump overlapping with sharp peak	-6, 18	0.10, 1.25	v. small hump overlapping with sharp peak
$SCPE_{43}$	18	1.55	sharp peak	20	1.68	sharp peak

* For explanation of the nomenclature see tables 3.1 and 3.6 pp 57 and 68.

Table 4.7 Comparison of the T_gs of system *A* obtained with the Rheovibron and the DMTA.

	Rheovibron			DMTA		
Sample *	T_gs observed (° C)	Max. value tanδ	Comments	T_gs observed (° C)	Max. value tanδ	Comments
EVA_{45}	-16	0.93	sharp peak	-17	0.80	sharp peak
A_{10DETA}	-13	0.86	sharp peak	-11	0.91	sharp peak
A_{20DETA}	-8	1.15	sharp peak	-6	0.94	sharp peak
A_{30DETA}	-7	0.86	sharp peak	-4	1.00	sharp peak
A_{40DETA}	-2	0.72	sharp peak	-1	1.02	sharp peak
A_{50DETA}	-2	0.57	broad peak	2	0.69	broad peak
A_{60DETA}	-3, 22	0.33, 0.60	peaks overlap	—	—	—
A_{70DETA}	-10, 22	0.12, 0.91	peaks overlap	-3, 17	0.31, 0.75	peaks overlap
A_{80DETA}	-8, 17	0.08, 1.45	small hump overlapping with sharp peak	-3, 19	0.21, 0.94	peaks overlap
A_{90DETA}	-15, 16	0.03, 1.52	very small hump overlapping with sharp peak	19	1.04	only one sharp peak was apparent
$SCPE_{43}$	17	1.4	sharp peak	25	0.92	sharp peak

* For explanation of the nomenclature see tables 3.1 and 3.6 in pp 58 and 69 and section 3.4, pp 71-2.

Table 4.8 Comparison between the T_gs of A_{DETA} obtained with the Rheovibron and the DMTA.

In similar way to Scarito and Sperling[100], the compositions of each of the phases present in A_{60} to A_{90} were determined using the Fox equation. These calculations were performed using the DMTA results and are shown in table 4.9.

As may be observed in this table the composition of each of the two phases present in A_{60} to A_{90} is similar: the phase with the lower T_g contains around 60 % of EVA_{45} while the phase with higher T_g is richer in $SCPE_{43}$. The mass balance analysis shows that as the amount of $SCPE_{43}$ increases in the sample a corresponding larger quantity of the SCPE-rich phase is formed while the composition of the two phases remains relatively constant.

Sample	T_gs °C	Max value Tanδ	$SCPE_{43}/EVA_{45}$	
			* Composition	** Mass balance g/g
A_{60}	-4 16	0.31 0.86	38 / 62 90 / 10	0.22 / 0.30 0.38 / 0.05
A_{70}	-3 16	0.32 0.85	41 / 59 90 / 10	0.17 / 0.24 0.53 / 0.06
A_{80}	-6 18	0.16 1.15	33 / 67 95 / 5	0.08 / 0.16 0.72 / 0.04
A_{90}	-6 18	0.10 1.25	33 / 67 95 / 5	0.03 / 0.05 0.87 / 0.05

*The number at the left hand side of the slash gives the composition of $SCPE_{43}$ and the number at the right gives the composition of EVA_{45}

**Calculation based on 1 g of the original mixture of both polymers.

Table 4.9 Composition and mass balance of the two phases present in the samples A_{60} to A_{90}.

Similar results to those obtained with the Rheovibron were previously obtained by Rostami [136] (see fig 4.20 and table 4.10). The blend in his work was named H48/EVA45 (H48=$SCPE_{43}$, EVA45 is the same copolymer used in this work). As may be observed in figure 4.20, the samples containing 20, 40, 50 and 80% w/w of H48, behaved in the same way as their counterparts in this work: A_{20}, A_{40}, A_{50} and A_{80}. It is important to point out, as mentioned in table 4.10, that the presence of a small hump

overlapping with a sharp peak at higher temperatures in the sample containing 80% H48 was also evident in Rostami's work.

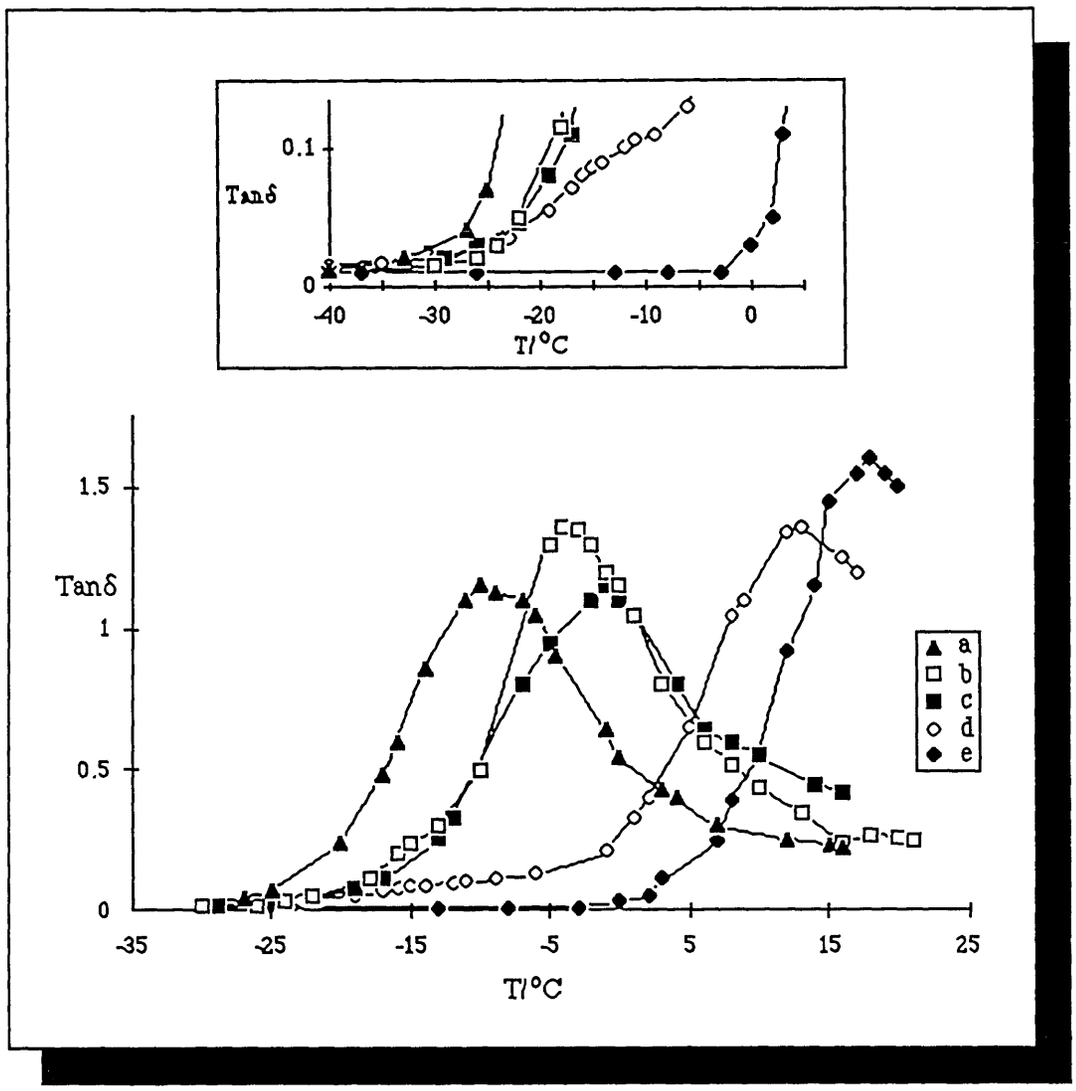

Figure 4.20 T_g results obtained for the system studied by S. Rostami: H48/EVA45 [136]. (H48 = $SCPE_{43}$. Curves (a), (b), (c), (d) and (e) are samples containing 20%, 40%, 50%, 80% and 100% w/w H48 which are equivalent to A_{20}, A_{40}, A_{50}, A_{80} and $SCPE_{43}$.

As may be seen in fig. 4.19 and table 4.8, very similar results to those obtained for the unmodified samples were also obtained for the whole range of compositions of A_{DETA}. For example, samples A_{10DETA}- A_{40DETA} showed one T_g, A_{50DETA} had a broad peak and A_{60DETA} to A_{90DETA} showed two T_gs inward shifted with respect to $SCPE_{43DETA}$ and EVA_{45} peaks. As previously reported for the two phase compositions

* This work code	T_gs observed (° C)	Max value of tanδ	Comments	Rostami's code	T_gs observed (° C)	Max value of tanδ	Comments
A_{20}	-8	0.93	sharp peak	H48:EVA45 20:80	-10	1.15	sharp peak
A_{40}	-2	1.30	sharp peak	H48:EVA45 40:60	-4	1.36	sharp peak
A_{50}	-2	1.10	broad peak	H48:EVA45 50:50	-1	1.15	less broad peak than observed in present work
A_{80}	-8, 17	0.08, 1.45	small hump overlapping sharp peak	H48:EVA45 80:20	-10, 13	0.10, 1.36	small hump overlapping sharp peak
$SCPE_{43}$	18	1.55	sharp peak	H48	18	1.60	sharp peak
* For explanation of the nomenclature see tables 3.1 and 3.6 pp 57 and 68							

136

Table 4.10 Comparison between the T_gs and tanδ of system *A* observed in this work and in H48: EVA45

in A, the Fox equation (see section 2.5.1 p. 46) was again used to calculate the composition of the two phases present in A_{60DETA} to A_{90DETA} (see table 4.11).

As indicated in table 4.11, phases rich in EVA_{45} and $SCPE_{43}$ are also observable in the phase separated compositions of A_{DETA}. A comparison between tables 4.9 and 4.11 shows that the mass balance of the two components in each phase is changed by crosslinking.

Sample	T_gs °C	Max value Tan δ	$SCPE_{43}/EVA_{45}$	
			* Composition	** Mass balance g/g
A_{60DETA}	—	—	—	—
A_{70DETA}	-3 17	0.31 0.75	37 / 63 83 /17	0.10 / 0.18 0.60 / 0.12
A_{80DETA}	-3 19	0.20 0.94	37 / 63 88 / 12	0.06 / 0.10 0.73 / 0.10
A_{90DETA}	—	—	—	—

* The number at the left hand side of the slash gives the composition of $SCPE_{43}$ and the number at the right gives the compositon of EVA_{45}.
** Calculation based on 1 g of the original mixture of both polymers.

Table 4.11 Composition and mass balance of the two phases present in the A_{60DETA} to A_{90DETA}.

4.2.3 STATIC AND DYNAMIC MECHANICAL PROPERTIES

The static tensile Young's moduli Y (Nm^{-2}) were obtained from the stress-strain measurements performed on the Instron (deformation rate 0.05 mm-min^{-1}). These data were also used to obtain the degree of crosslinking (see section 4.2.1, pp 105-107). A comparison of Y for A and A_{DETA} as a function of composition is shown in figure 4.21. Inspection of this figure shows that before and after crosslinking the values of Y show a clear dependence on blend composition. After crosslinking, Y increases for the whole composition range.

Figures 4.22 to 4.25 plot the log of the dynamic storage modulus (E') for different

blend compositions as a function of temperature. Figure 4.22 shows logE' for the pure blends. As curves b and c show clearly, E' increases in $SCPE_{43}$ after being crosslinked. Figures 4.23 and 4.24 show logE' for the whole composition of A and A_{DETA}. As may be seen in both figures, the log E' curves shift upwards as the content of $SCPE_{43}$ (component with higher E') increases. Also, depending on the state of miscibility of the sample under study, the number of inflection points and the steepness in the modulus will vary. For example, if the specimen under study is one phase, the logE' curve shows only one inflection point and the curve is steep (curves a to c in both figures). When the sample is close to being one phase the transition is broadened and the slope of the curve is not so steep (curve d in fig 4.23). If the sample is two phase, then two inflection points are clearly seen (curves e to h in figure 4.23 and curves e to g in figure 4.24). Figure 4.25 compares logE' curves for some of the blend compositions before and after crosslinking. As may be observed crosslinking increases the logE' values.

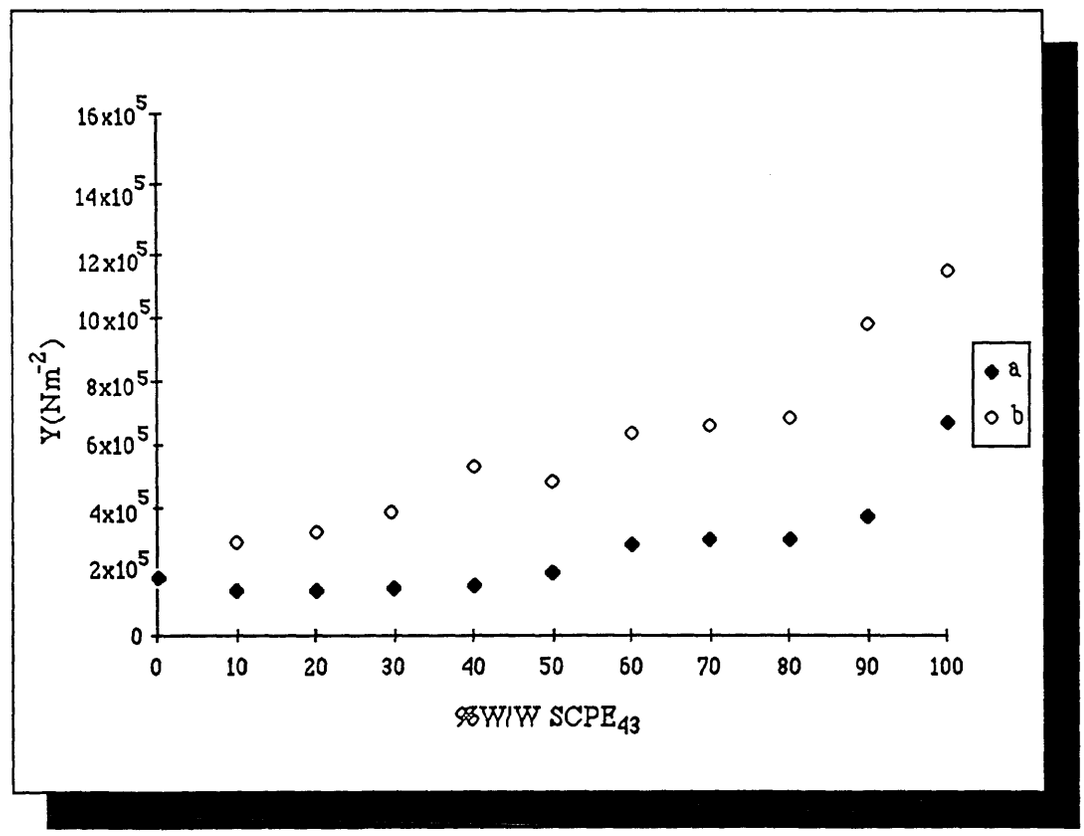

Figure 4.21 The tensile Young moduli (Y) (Nm^{-2}) of (a) A and (b) A_{DETA} as a function of composition at a crosshead rate of 0.05 $mm\text{-}min^{-1}$.

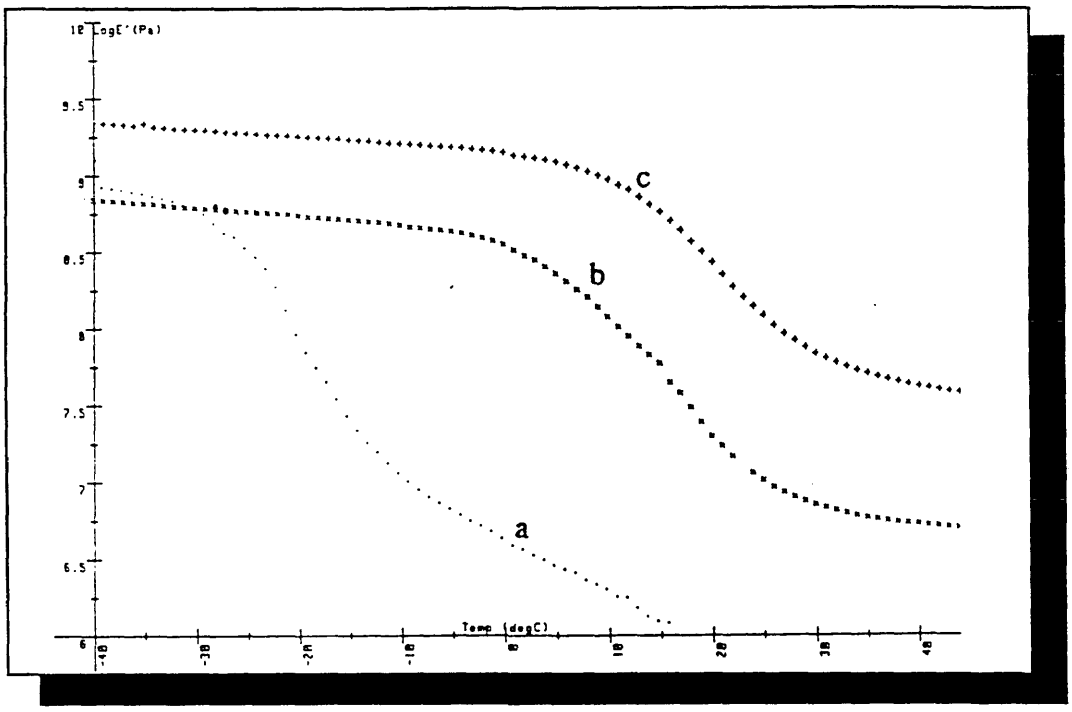

Figure 4.22 Values of logE' vs temperature for: EVA_{45} (a·), $SCPE_{43}$(bx) and $SCPE_{43DETA}$ (c+).

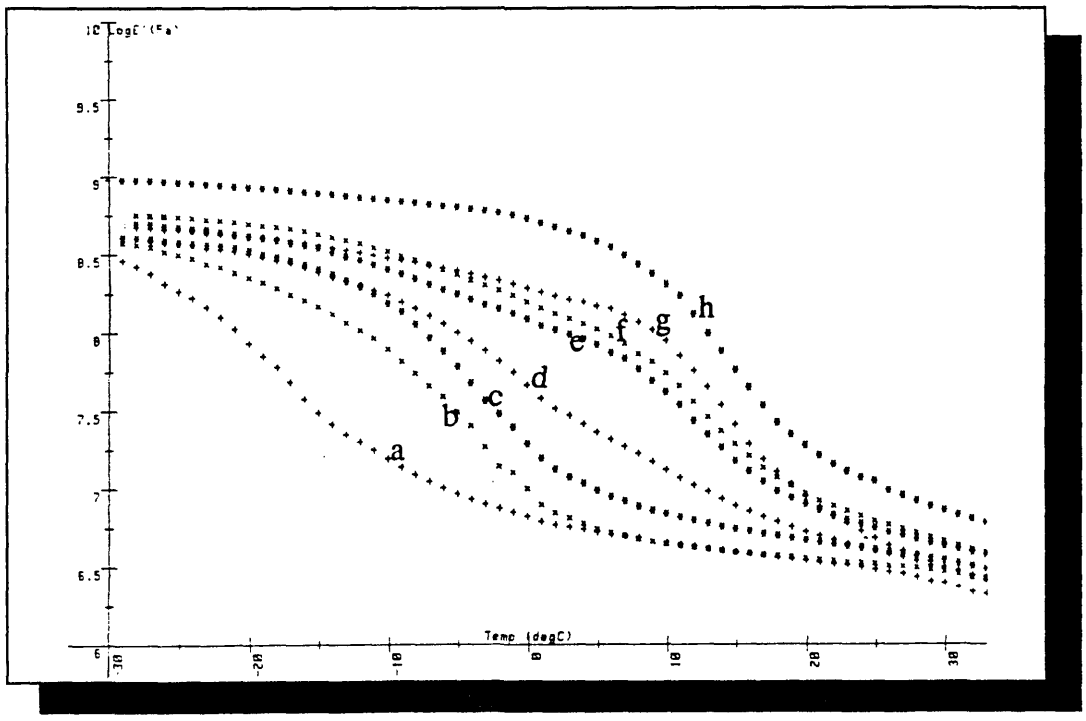

Figure 4.23 Values of logE' vs temperature for the whole composition range of system *A* ($SCPE_{43}/EVA_{45}$). A_{10} (a+),A_{30} (bx), A_{40} (c*), A_{50} (d+), A_{60} (e*), A_{70} (fx),) A_{80} (g+), A_{90} (h*).

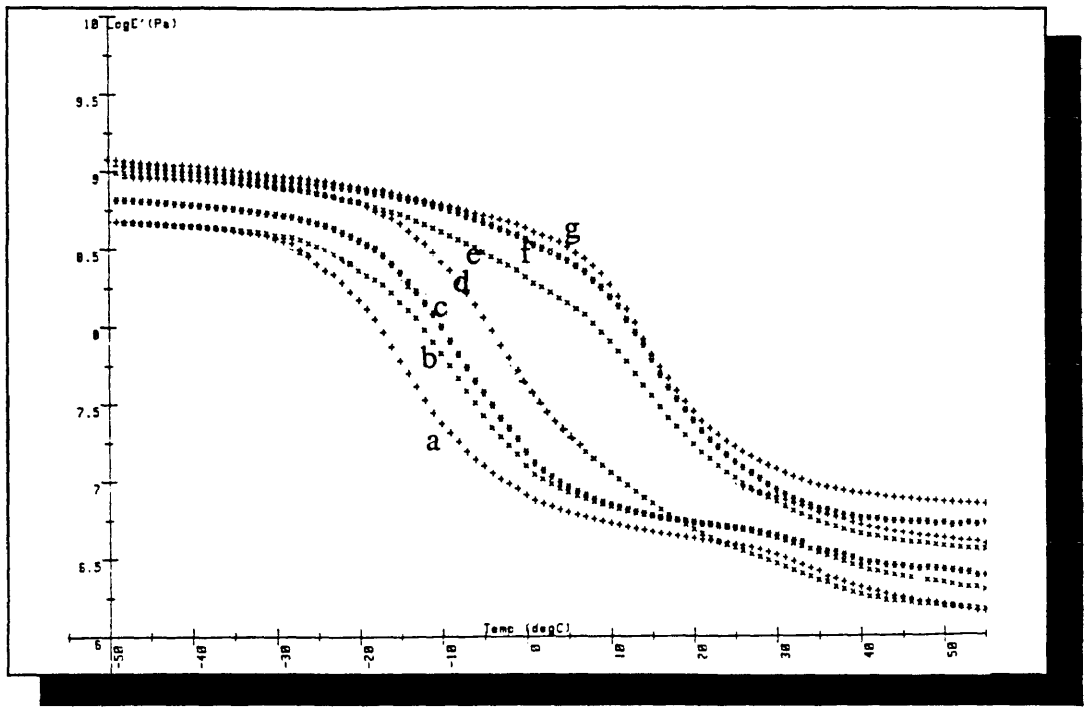

Figure 4.24 Values of logE' vs temperature for the whole composition range of system A_{DETA} ($SCPE_{43DETA}$/EVA_{45}). A_{10DETA} (a+), A_{20DETA} (bx), A_{30DETA} (c*), $A_{40\ DETA}$ (d+), A_{70DETA} (ex), A_{80DETA} (f*), $A_{90\ DETA}$ (g+).

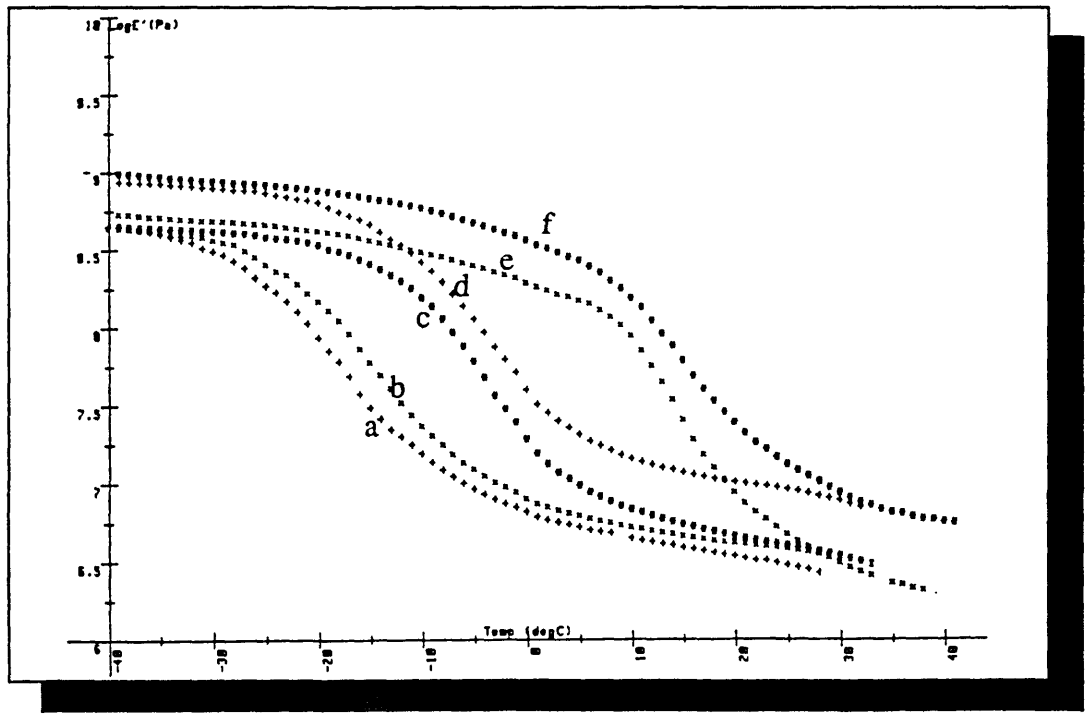

Figure 4.25 Comparison of logE' for some compositions of A and A_{DETA}. A_{10} (a+), A_{10DETA} (bx), A_{40} (c*), $A_{40\ DETA}$ (d+), A_{80} (ex), A_{80DETA} (f*).

4.2.4 CLOUD POINT MEASUREMENTS

Figure 4.26 shows the intensity versus temperature plots for some compositions of A and A_{DETA}. As expected, the slope of the curves decreases for the crosslinked samples. Figures 4.27 and 4.28 show the turbidimeter CP temperatures as a function of composition for A and A_{DETA} respectively. The heating rate used was 0.1°C/min. The error bars in both figures represent the range of values obtained in repeated experiments. Figure 4.29 shows the CP temperatures for A obtained with the laser-SALS at a heating rate of 1°C/min.The rectangular bars shown in the figure correspond to the only two crosslinked compositions studied by this technique. The CP curves obtained from the turbidimeter for A and A_{DETA} show that from 50%W/W $SCPE_{43}$ content upwards, the CP temperatures are more or less constant. A comparison of the CP curves of A and A_{DETA} shows that after crosslinking there is an increase of 5 to 10 degrees in the temperature at which the CP appears. Essentially the same conclusions can be drawn from the laser-SALS experiments, except that the CP temperatures for the crosslinked samples are 10 to 20 degrees higher than those of the unmodified samples.

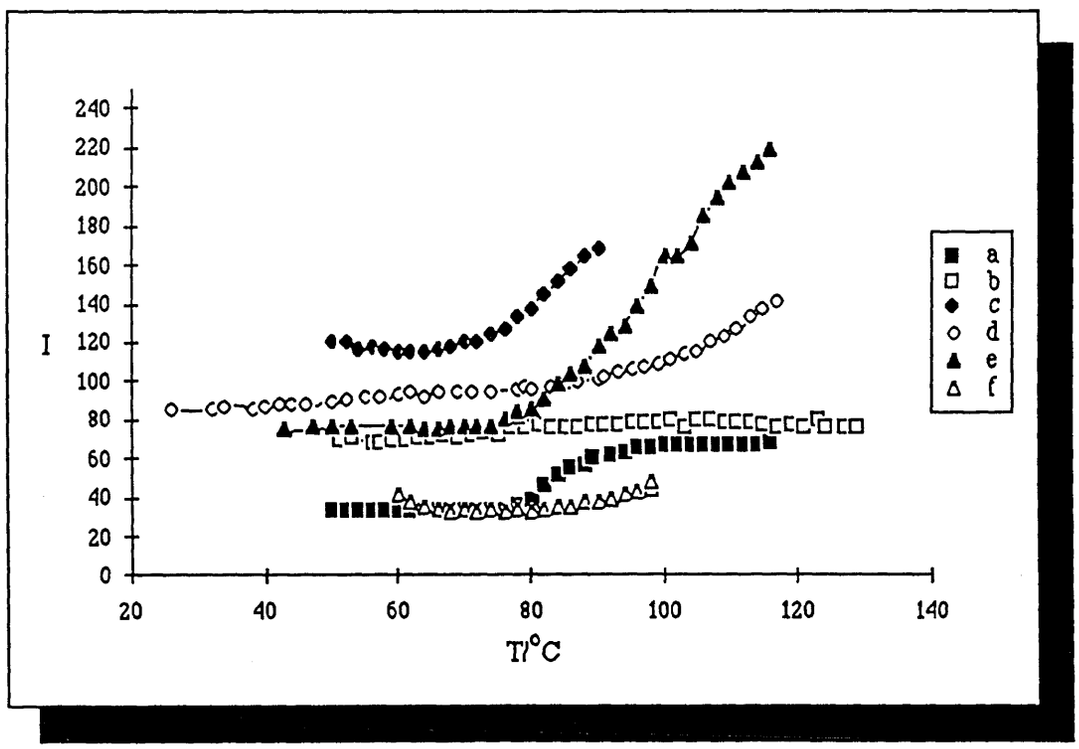

Figure 4.26 Cloud point temperatures obtained with the turbidimeter (heating rate 0.1°C) for some compositions of A and A_{DETA}. (a) A_{20} (CP = 76°C), (b) A_{20DETA} (CP = 73°C), (c) A_{60} (CP = 69°C), (d) A_{60DETA} (CP = 88°C), (e) A_{80} (CP = 73°C), (f) A_{80DETA} (CP = 88°C).

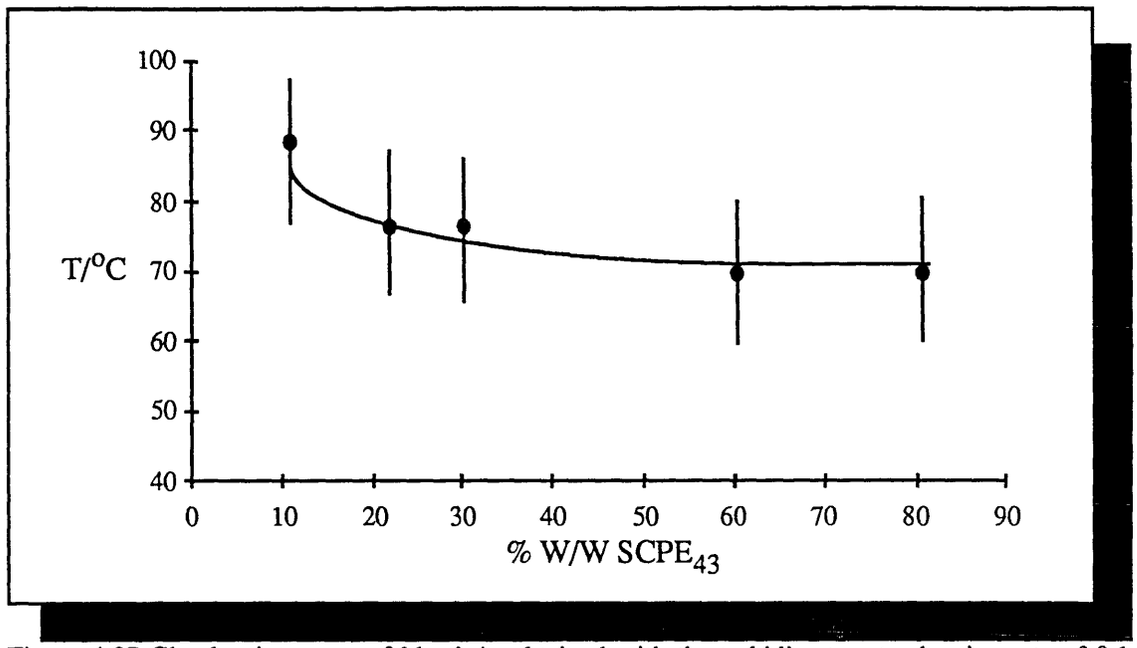

Figure 4.27 Cloud point curve of blend *A* obtained with the turbidimeter at a heating rate of 0.1 °C/min.

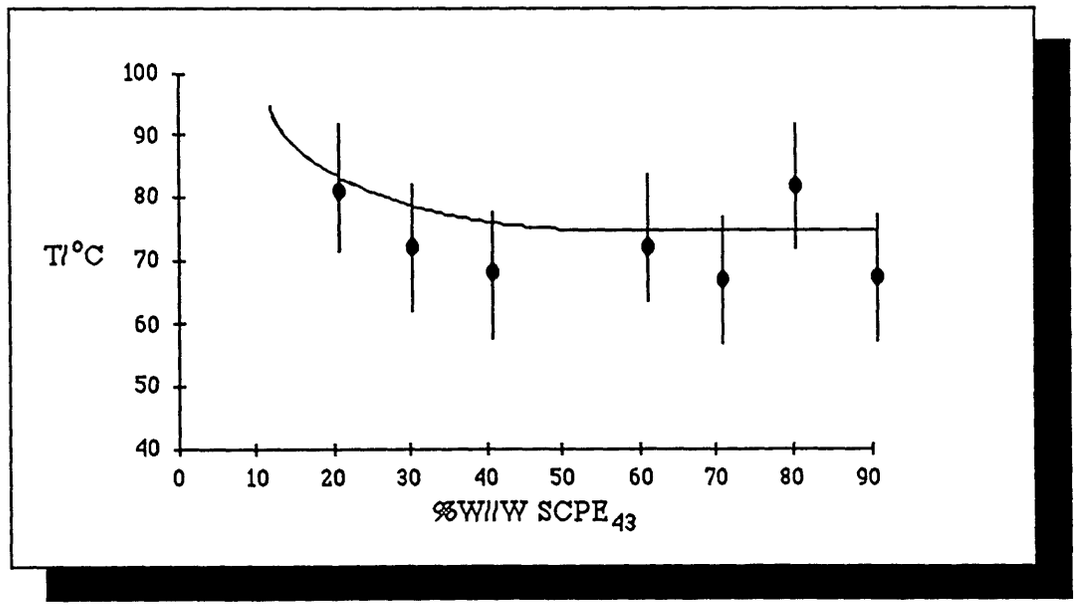

Figure 4.28 Cloud point curve of blend A_{DETA} obtained with the turbidimeter at a heating rate of 0.1 °C/min.

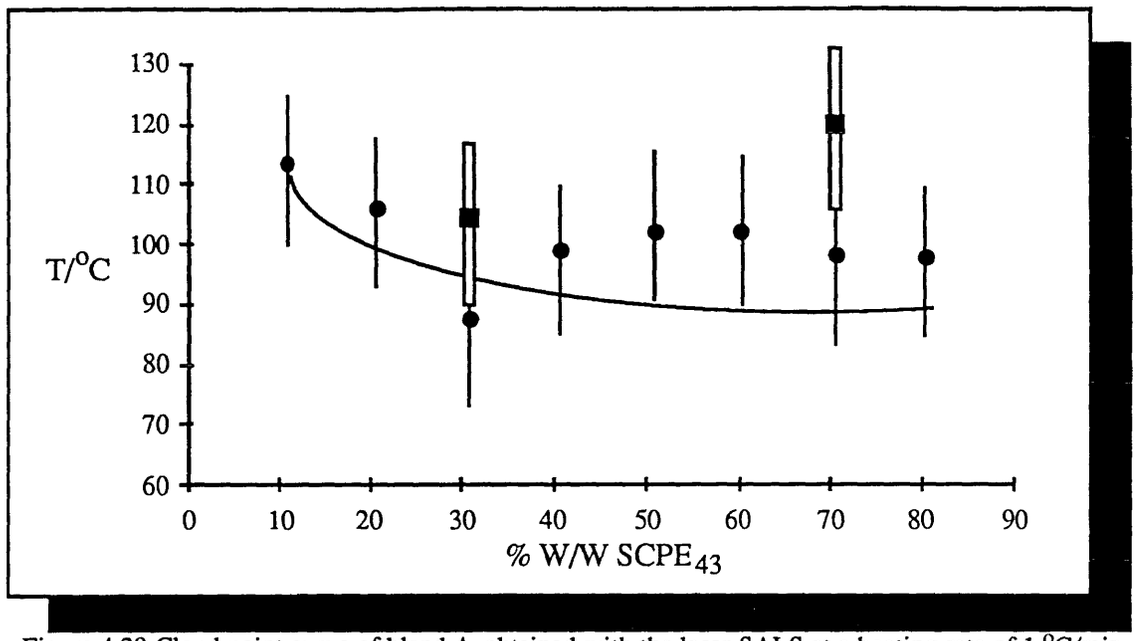

Figure 4.29 Cloud point curve of blend *A* obtained with the laser-SALS at a heating rate of 1 °C/min. The rectangles represent the only two data obtained for the crosslinked blend.

4.2.5 DETERMINATION OF DOMAIN SIZES

The domain sizes for various blend compositions before and after crosslinking were measured 30°C and 50°C above their respective CP temperatures (CP temperatures obtained with the laser-SALS). These data were determined by reprocessing the data obtained form the laser-SALS experiments. The angular range scanned in these studies was from 5° to 35° (see section 3.8, p. 89-90). Figure 4.30 shows the intensity of the scattered light (I) vs the angle of scattering (θ) for A_{30} and A_{30DETA} (A_{30} CP = 81°C and A_{30DETA} CP = 104°C). As shown both samples have an exponential decay pattern in the angular range studied. This behaviour was also observed for the rest of the blend compositions before and after crosslinking. The domain sizes were obtained from the slope at high and low values of I of the plot lnI vs Q^2 (see sect.3.8, p. 90). Figure 4.31 shows these curves for A_{30} and A_{30DETA} at the CP temperature and 30°C above it.

Tables 4.12 and 4.13 show the range of the sizes obtained for some of the blend compositions studied. Table 4.12 shows the values 30°C above the CP determined with the laser-SALS. Table 4.13 contains the values measured 30°C above the CP determined with the turbidimeter. Comparing the values of the domain sizes of A_{30}, A_{70}, A_{30DETA} and A_{70DETA} shown in each table it may be seen that after crosslinking the range of domain sizes is reduced. A comparison of the results in tables 4.12 and 4.13 shows that the values of the domain sizes measured 30°C above the CP determined with the turbidimeter and the laser-SALS are quite similar. Although the CP temperature for

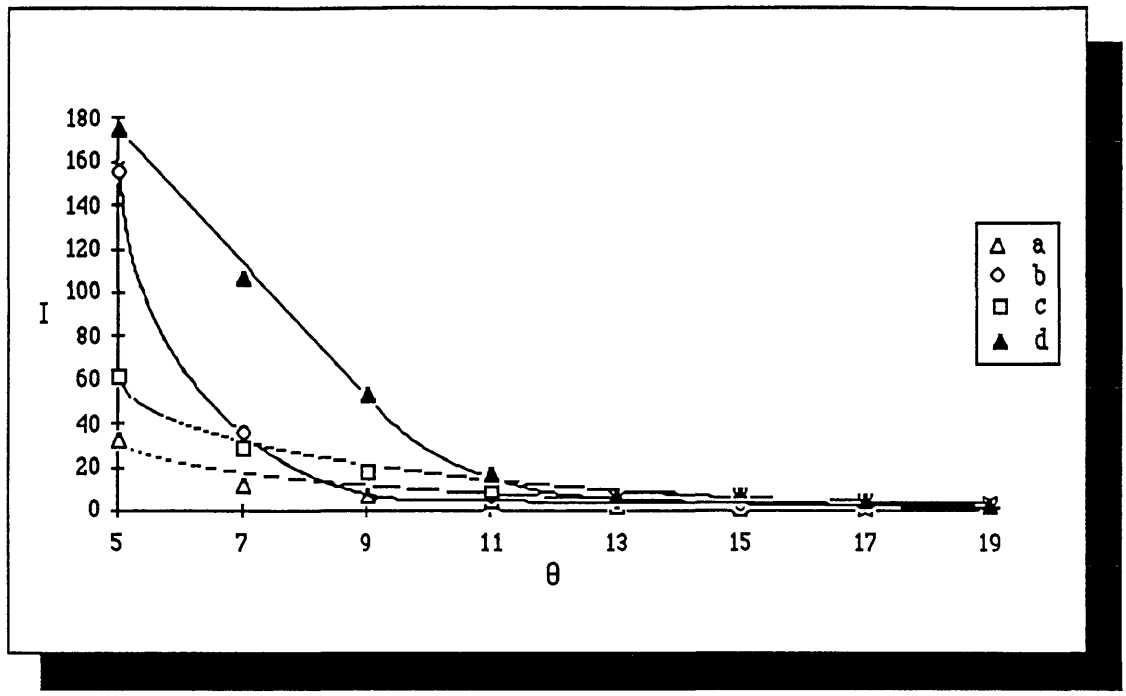

Figure 4.30 Plots of the intensity of the scattered light (I) as a function of angle (θ) for A_{30} and A_{30DETA}. (a) A_{30} at 81°C, (b) A_{30} at 112°C, (c) A_{30DETA} at 104°C and (d) A_{30DETA} at 134°C.

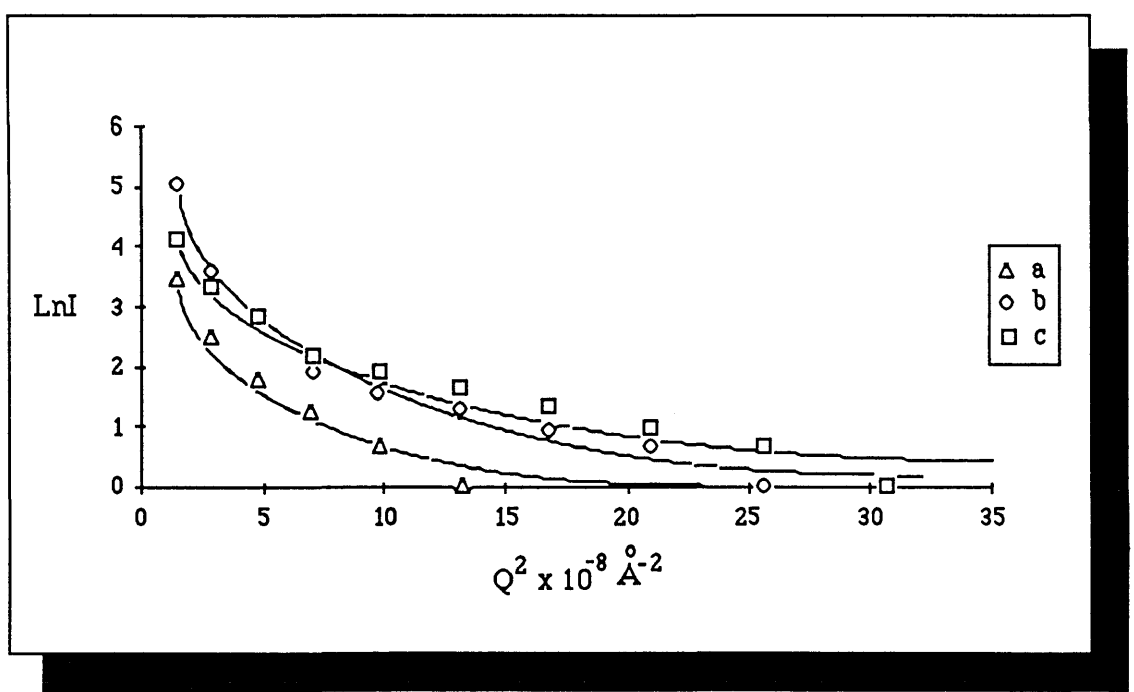

Figure 4.31 Plots of LnI as a function of the square of the wave vector (Q^2) for A_{30} and A_{30DETA}. (a) A_{30} at 81°C, (b) A_{30} at 112°C and (c) A_{30DETA} at 104°C

Sample	CP temperature (°C)	Domain sizes Range observed (Å)	At temperature (°C)
Uncrosslinked blend			
A_{10}	112	$5x10^3$ - $9x10^3$	142
A_{20}	83	$4x10^3$ - $1x10^4$	113
A_{30}	81	$5x10^3$ - $1x10^4$	111
A_{70}	76	$2x10^3$ - $1x10^4$	103
Crosslinked blend			
A_{30DETA}	104	$6x10^3$ - $9x10^3$	134
A_{70DETA}	126	$3x10^3$ - $9x10^3$	156

Table 4.12 Range of domain sizes obtained with the laser - SALS. The data were obtained 30°C above the CP temperature of each sample. (The values of CP used are those obtained with the laser-SALS).

Sample	* CP temperature (°C)	Domain sizes Range observed (Å)	At temperature (°C)
Uncrosslinked blend			
A_{10}	88	$3x10^3$ - $9x10^3$	118
A_{20}	77	$4x10^3$ - $9x10^3$	107
A_{30}	76	$5x10^3$ - $1x10^4$	106
A_{70}	71	$4x10^3$ - $1x10^4$	101
Crosslinked blend			
A_{30DETA}	71	$3x10^3$ - $7x10^3$	101
A_{70DETA}	82	$3x10^3$ - $8x10^3$	112
* CP temperature obtained with the turbidimeter.			

Table 4.13 Range of domain sizes obtained with the laser-SALS The data were measured 30°C above the CP temperature of each sample. (The values of CP used in this table were obtained with the turbidimeter).

each blend measured by the two techniques differ by 5 to 30 degrees, the domain sizes observed do not vary significantly. This suggests that the domains are not growing rapidly as temperatures increases and therefore only the data in which the CP values used are those which were obtained with the laser-SALS will be included.

The sizes of the domains can be related to the interfacial energy γ_{ie} by the Donatelli equation (see equation 2.151, p. 42). Using the measured domain sizes estimates for γ_{ie} were obtained and are shown in table 4.14. A consideration of model systems would suggest that the domain sizes should be of the same order of magnitude as the rms

distance between network crosslinks $\langle s^2 \rangle^{1/2}$ ($\langle s^2 \rangle^{1/2} = N^{1/2} L$, where N is the number of monomeric units and L is the length of the monomer unit). This distance can be estimated from $\bar{M}_c$ and standard bond lengths and angles; values are given in table 4.14. Clearly, there is no correlation with the measured domain sizes, but these are a function of the techniques used. This topic will be discussed further in section 5.2.5 (p. 202).

Sample	Experimental Domain size ($x10^3$ Å)	$\langle s \rangle^{1/2}$ between crosslinks (x10 Å)	γ_{ie} from Donatelli equation (x 10^2dn/cm)
A_{30DETA}	6 - 9	3	7
A_{70DETA}	3 - 9	3	10

Table 4.14 Comparison of the experimental domain sizes and the values of domains obtained with $\langle s^2 \rangle^{1/2}$ for some compositions of A_{DETA}. The values of γ_{ie} were calculated with the Donatelli equation .

4.3 BLEND SCPE $_{54}$/EVA (SYSTEM *D*)

It was found in previous work [28, 29] that by increasing the chlorine content in SCPE the miscibility between this polymer and EVA increased substantially. In this section the results obtained for a blend containing a SCPE with 54% Cl and 0.94% S as SO_2Cl are presented ($SCPE_{54}$, $\bar{M}_n$=33000, T_g=61°C (DMTA), EVA_{45}, $\bar{M}_n$=51000, T_g=-17°C (DMTA)).The main difference between blends *A* and *D* is that *A* contains a SCPE with 43% chlorine content and 1% SO_2Cl (see section 4.2, p. 104). A similar system to *D* was studied previously by Walsh et al [28, 29] the blend, known as CPE3/EVA45, contained the same EVA used in this work and a chlorinated polyethylene with 53.65% Cl. The present blend was prepared by solvent casting $SCPE_{54}$ and EVA_{45} in THF and was crosslinked with *DETA* (see section 3.3.1, pp 68-9 and 3.4.3 p. 74-6).

4.3.1 DEGREE OF CROSSLINKING

Table 4.15 shows the degree of crosslinking results measured by swelling. The experimental conditions followed for these measurements and the calculation methods used are the same as those described in sect. 4.2.1, p. 105. Taking in consideration that the $\bar{M}_n$ of $SCPE_{54}$ is 33000, the values of $\bar{M}_c$ obtained are relatively large. This

suggests that the whole composition range of D_{DETA} is lightly crosslinked.

SWELLING MEASUREMENTS $\bar{M}_{cSWELL}$ g/mole*			
Sample	(1)	(2)	(3)
D_{10DETA}	——	——	——
D_{20DETA}	16370	16370	16370
D_{30DETA}	16370	16380	16380
D_{40DETA}	16770	16420	16755
D_{50DETA}	16440	16570	16580
D_{60DETA}	16480	16690	16041
D_{70DETA}	16580	16940	17000
D_{80DETA}	16400	16470	16470
D_{90DETA}	16500	16780	16800
$SCPE_{54DETA}$	22120	28820	18164

* $\bar{M}_{cSWELL}$ calculated with (1) a modified version of Flory - Rehner [71] eq. (2) James and Guth eq. [71, 143] and (3) Herman eq. [71, 143, 144]. All these equations include the correction for free ends.

Table 4.15 Values of $\bar{M}_{cswell}$ for D_{DETA}.

4.3.2 MISCIBILITY BEHAVIOUR

A visual inspection of blend *D* showed that the whole range of compositions were transparent. As in system *A* (section 4.2.2, p. 108), after crosslinking all samples remained transparent although a brownish discoloration developed. In contrast with this visual inspection the Rheovibron and DMTA results in table 4.16 and figure 4.33 revealed that system *D* was miscible up to D_{50}. At D_{60} one peak, much smaller and broader than that in D_{50}, was observed. From D_{70} onwards two peaks shifted towards each other with respect to the T_gs of the pure polymers were clearly observed. A comparison of these results with those of CPE3/EVA45, a system studied previously by Rostami and Walsh[28,114], are shown in table 4.17. As may be seen, except for the samples containing 80% of the chlorinated polymer the results for both systems are quite similar. Table 4.18 and figure 4.34 show that after crosslinking, the blend behaved in a similar way to that observed before modifying the blend. As in section 4.2.2 (p. 112) the composition of the two phases present in the samples containing 60 to 90 % SCPE in *D* and D_{DETA}, were obtained by substituting the T_gs obtained with the DMTA into the Fox relationship. The results are collected in tables 4.19 and 4.20. Inspection of these

data shows that as in the blend A and A_{DETA}, two phases are present in D_{60} to D_{90} and D_{60DETA} to D_{90DETA}, one rich in EVA and the other rich in $SCPE_{54}$. Examination of the mass balance analysis data shows that as the amount of $SCPE_{54}$ increases in the sample, a larger quantity of the SCPE-rich phase is formed although the composition of the two phases is relatively constant.

4.3.3 STATIC AND DYNAMIC MECHANICAL PROPERTIES

Figures 4.35 and 4.36 (p. 132) show the static Young's moduli Y (Nm^{-2}) (deformation rate of 0.05 mm-min^{-1}) and the storage modulus E' (measured at 20°C with the DMTA) for D and D_{DETA}. Inspection of figure 4.35 shows that, within the scatter, Y increases smoothly up to 70% content $SCPE_{54}$ and crosslinking increased Y for these compositions. Above this composition, the data appear very scattered, which might be due to experimental error. In order to confirm the behaviour of this system above 70% $SCPE_{54}$ content, a plot of E' versus composition was extracted from the DMTA data shown in figures 4.37 to 4.40 (133-5) and is given as figure 4.36. The sample geometry and end corrections are less well defined in the dynamic

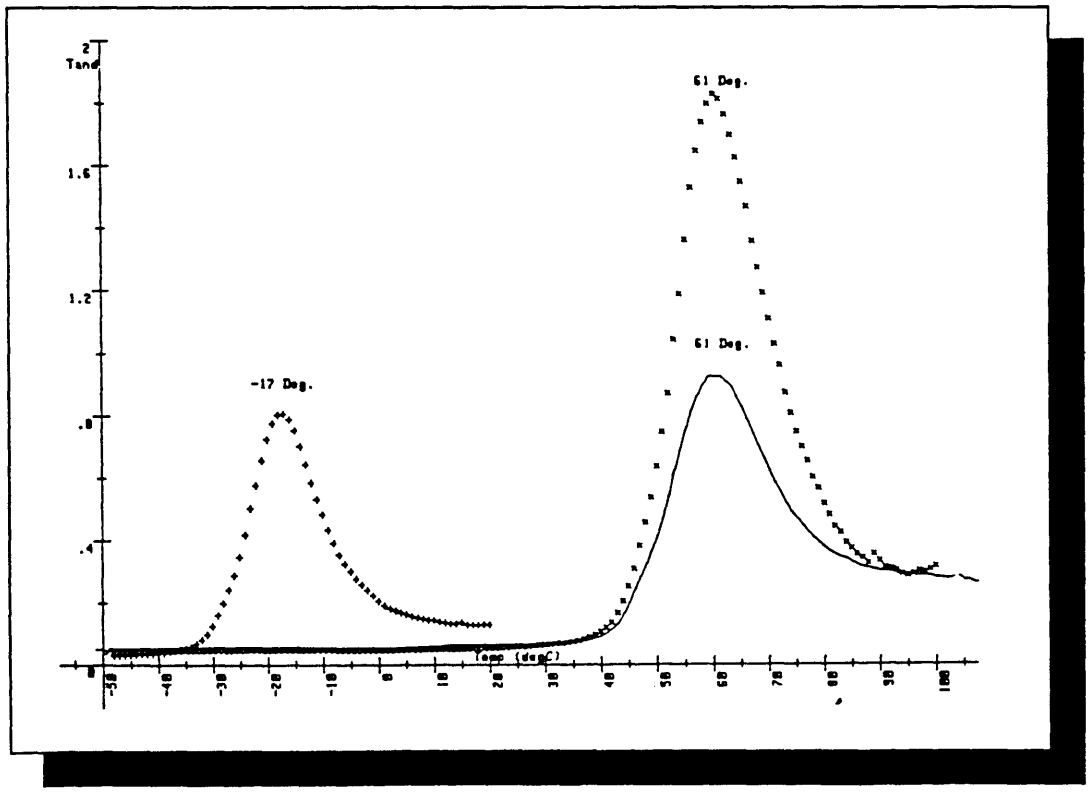

Figure 4.32 T_gs of EVA_{45} (-17°C(+)), $SCPE_{54}$ (61°C(x) and $SCPE_{54DETA}$ (61°C(–)).

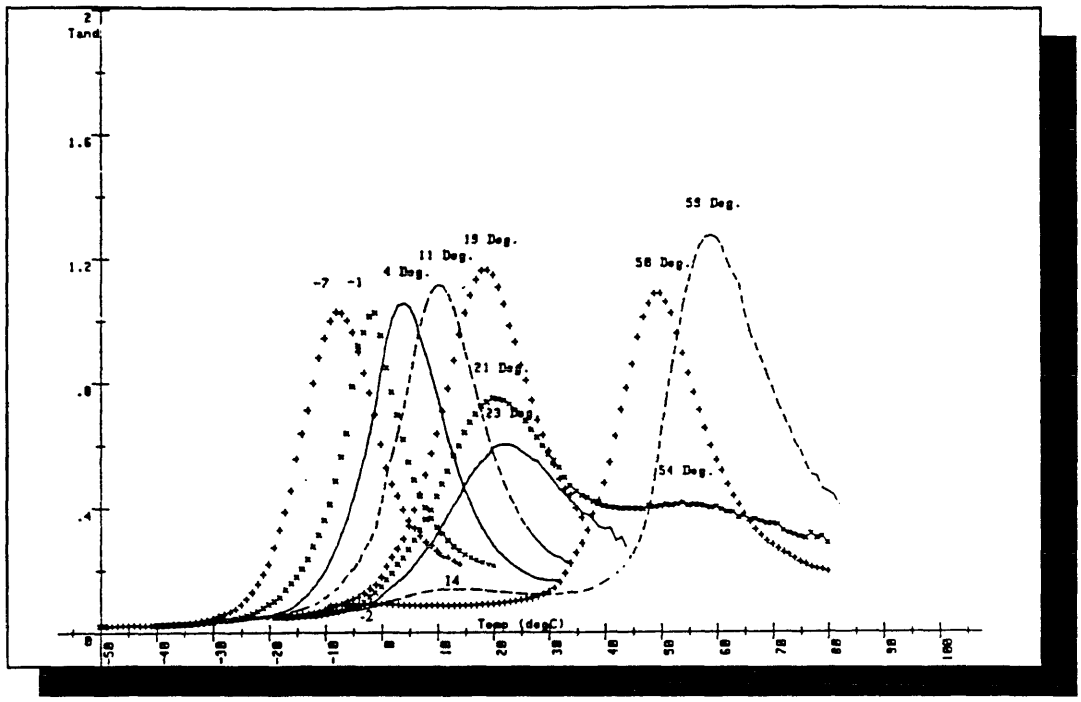

Figure 4.33 T_gs for the whole composition range of system *D* ($SCPE_{54}/EVA_{45}$). D_{10} (-7°C(+)), D_{20} (-1°C(x)), D_{30} (4°C(–)), D_{40} (11°C(- -)), D_{50} (19°C(+)), D_{60} (23°C(—)), D_{70} (21, 54°C(x)), D_{80} (14, 59°C(- -)), D_{90} (-2, 50°C(+)).

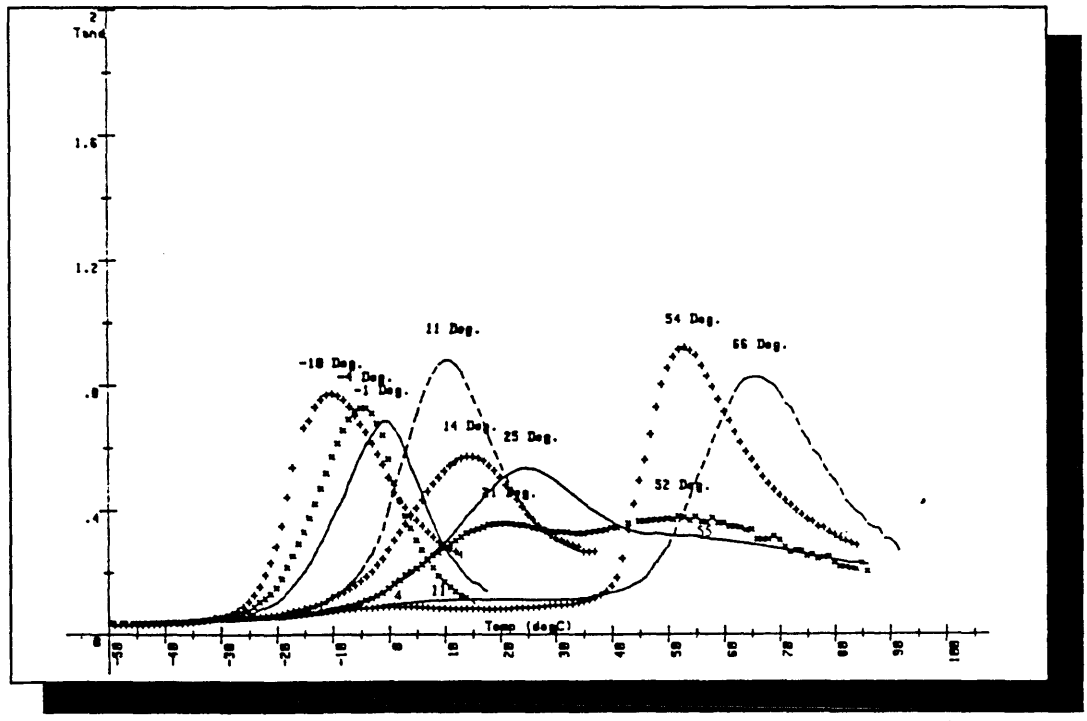

Figure 4.34 T_gs for the whole composition range of system D_{DETA} ($SCPE_{54DETA}/EVA_{45}$). D_{10DETA} (-10°C(+)), D_{20DETA} (-4°C(x)), D_{30DETA} (-1°C(—)), $D_{40\ DETA}$ (11°C(- -), D_{50DETA} (14°C(+)), D_{60DETA} (21, 52°C(x)) D_{70DETA} (25, 55°C(–)), D_{80DETA} (11, 66°C(- -)), $D_{90\ DETA}$ (4, 54°C(+)).

	Rheovibron			DMTA		
* Sample	T_gs observed (° C)	Max. value tanδ	Comments	T_gs observed (° C)	Max. value tanδ	Comments
EVA_{45}	-16	0.93	sharp peak	-17	0.80	sharp peak
D_{10}	-7	0.96	sharp peak	-7	1.04	sharp peak
D_{20}	-1	1.10	sharp peak	-1	1.06	sharp peak
D_{30}	3	1.30	sharp peak	4	1.09	sharp peak
D_{40}	7	1.21	sharp peak	11	1.11	sharp peak
D_{50}	16	1.22	sharp peak	19	1.19	sharp peak
D_{60}	21	0.80	broad peak	23	0.62	broad peak
D_{70}	23	0.91	broad peak	21, 54	0.75, 0.42	two small peaks overlapping
D_{80}	8, 59	0.14, 1.4	small hump overlapping sharp peak	14, 59	0.14, 1.28	small hump overlapping sharp peak
D_{90}	51	1.12	only one sharp peak visible	-2, 50	0.11, 1.10	very small hump overlapping sharp peak
$SCPE_{54}$	53	1.45	sharp peak	61	1.86	sharp peak

*For explanation of the nomenclature see tables 3.1 and 3.6 in pp 57 and 68 respectively.

Table 4.16 Comparison of the T_gs of *D* obtained with the Rheovibron and the DMTA.

* This work code	T_gs observed (°C)	Max value of tanδ	Comments	[28, 114] CPE3 / EVA45	T_gs observed (°C)	Max value of tanδ	Comments
EVA_{45}	-16	0.93	sharp peak	EVA45	-18	0.90	sharp peak
D_{20}	-1	1.10	sharp peak	CPE3 / EVA45 20 : 80	-5	1.20	sharp peak
D_{50}	16	1.22	sharp peak	CPE3 / EVA45 50 : 50	5	1.20	sharp peak
D_{80}	8, 59	0.14, 1.40	small hump overlapping sharp peak	CPE3 / EVA45 80 : 20	36	1.40	broader peak than 50:50, weak signal between -10 to 10 °C
$SCPE_{54}$	61	1.45	sharp peak	CPE3	44	1.60	sharp peak

* For explanation of the nomenclature see tables 3.1 and 3.6 pp 57 and 68 respectively.

Table 4.17 Comparison of the Tgs and tanδ values of system *D* with those of system CPE3/EVA45 studied by Rostami[28] and Walsh[114]

	Rheovibron			DMTA		
* Sample	T_gs observed (o C)	Max. value tan δ	Comments	T_gs observed (o C)	Max. value tanδ	Comments
EVA_{45}	-16	0.93	sharp peak	-17	0.80	sharp peak
D_{10DETA}	-8	0.86	sharp peak	-10	0.78	sharp peak
D_{20DETA}	-1	0.86	sharp peak	-4	0.74	sharp peak
D_{30DETA}	3	0.86	sharp peak	-1	0.69	sharp peak
D_{40DETA}	8	0.73	sharp peak	11	0.89	sharp peak
D_{50DETA}	18	0.85	broad peak	14	0.58	broad peak
D_{60DETA}	30, 50	0.51, 0.50	two small peaks overlapping	21, 52	0.37, 0.37	two small peaks overlapping
D_{70DETA}	21, 69	0.47, 0.46	two small peaks overlapping	25, 55	0.54, 0.31	small peak overlapping another one not well defined
D_{80DETA}	15, 61	0.08, 1.10	small hump overlapping sharp peak	11, 66	0.12, 0.85	small hump overlapping sharp peak
D_{90DETA}	50	1.02	broad peak	4, 54	0.10, 0.93	small hump overlapping sharp peak
$SCPE_{54DETA}$	56	1.07	sharp peak	61	0.92	sharp peak

* For explanation of the nomenclature see tables 3.1 and 3.6 in pp 57 and 68 respectively and section 3.4 in p 71-2.

Table 4.18 Comparison of the T_gs of D_{DETA} obtained with the Rheovibron and the DMTA.

Sample*	T_gs °C	Max. value Tanδ	$SCPE_{54}/EVA_{45}$	
			** Composition	*** Mass balance g/g
D_{60}	—	—	—	—
D_{70}	21 54	0.75 0.42	55 / 45 93 / 7	0.33 / 0.27 0.36 / 0.03
D_{80}	14 59	0.14 1.28	45 / 55 98 / 2	0.15 / 0.19 0.65 / 0.01
D_{90}	-2 50	0.11 1.11	33 / 67 89 / 11	0.01 / 0.02 0.87 / 0.08

* For explanation of the nomenclature see tables 3.1 and 3.6 pp 57 and 68 and section 3.4, pp 71-2.
**The number at the left hand side of the slash gives the composition of $SCPE_{54}$ and the number at the right gives the composition of EVA_{45}
*** Calculation based on 1 g of the original mixture of both polymers.

Table 4.19 Composition and mass balance of the two phases present in systems D_{60} to D_{90}.

Sample*	T_gs °C	Max value Tanδ	$SCPE_{54}/EVA_{45}$	
			** Composition	*** Mass balance g/g
D_{60DETA}	21 52	0.37 0.37	55 / 45 91/ 9	0.49 / 0.39 0.13 / 0.01
D_{70DETA}	25 55	0.54 0.31	60 /40 94 / 6	0.42 / 0.28 0.28 / 0.02
D_{80DETA}	—	—	—	—
D_{90DETA}	4 54	0.10 0.93	33 / 67 93 / 7	0.02 / 0.03 0.88 / 0.07

* For explanation of the nomenclature see tables 3.1 and 3.6 pp 57 and 68 and section 3.4, pp 71-2.
**The number at the left hand side of the slash gives the composition of $SCPE_{54}$ and the number at the right gives the composition of EVA_{45}.
*** Calculation based on 1 g of the original mixture of both polymers.

Table 4.20 Compositon and mass balance of the two phases present in samples D_{60DETA} to D_{90DETA}.

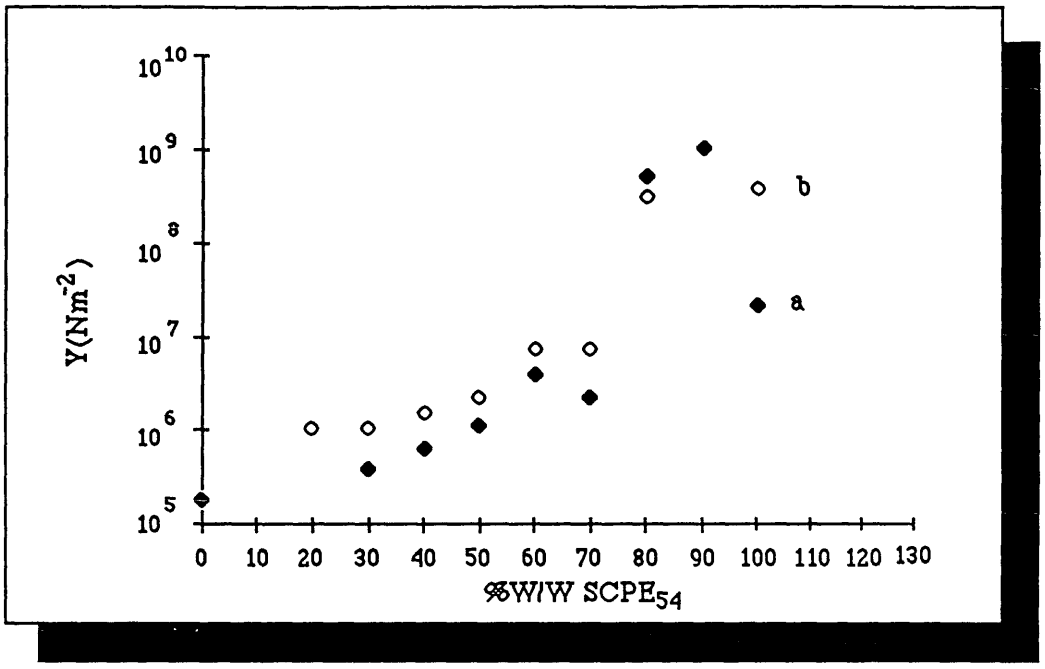

Figure 4.35 The tensile Young moduli (Y) (Nm^{-2}) for (a) *D* and (b) D_{DETA} as a function of composition at a crosshead rate of 0.05 mm-min^{-1}.

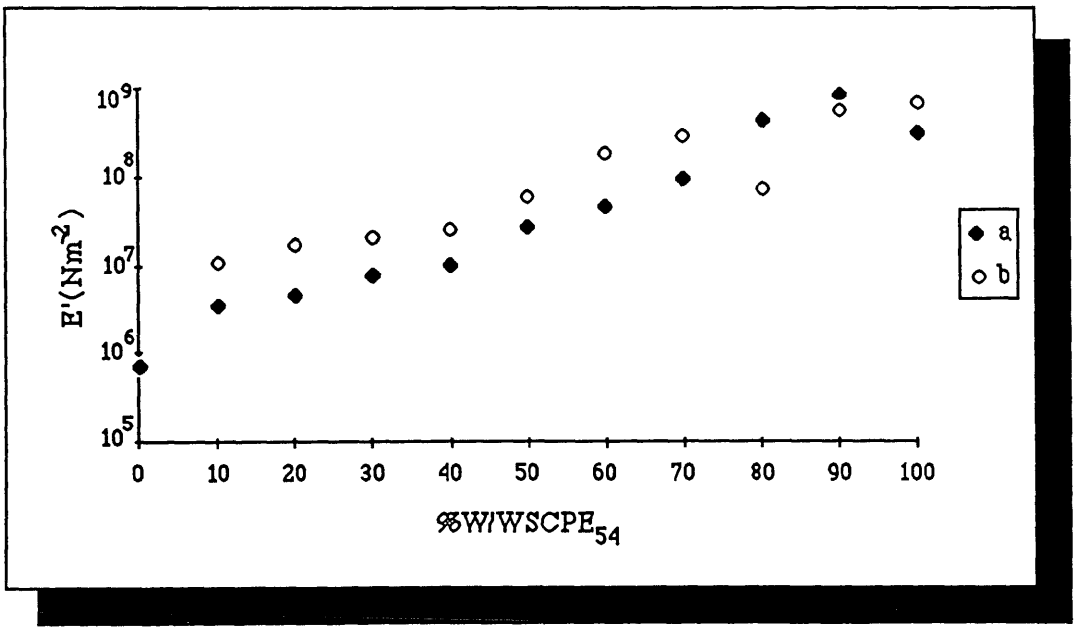

Figure 4.36 The storage dynamic moduli E' (Nm^{-2}) for (a) *D* and (b) D_{DETA} as a function of composition. The data was obtained at 20°C from the logE' results obtained with the DMTA.

modulus measurements, so the accuracy is probably not as great as in the static measurements; the rate of testing is also very different. Inspection of figure 4.36 shows that the data above D_{70} are less scattered than in figure 4.35; however the modulus-composition curve in both figures is similar. E' plots are not given for other systems where Young's moduli are satisfactory.

Figs. 4.37 to 4.39 show respectively log E' as a function of temperature for the pure components, blend D and blend D_{DETA}. Examination of figures 4.38 and 4.39 show that generally the logE' curves shift upwards as the content of $SCPE_{54}$ (component with higher E') increases. For the one phase samples (curves a to e) the curves are steep and only one inflection point is observable. For the two phases samples, two inflection points are clear and the slope in the curves is not so steep (curves g, h and i). For D_{60}, which is very close to complete miscibility, (see curve f), only one inflection point in the logE' curve is observed. The same behaviour is observed in figure 4.39 for the crosslinked samples. Comparison of the logE' between the samples before and after crosslinking (see figure 4.40) shows clearly that crosslinking increases the values of E', especially at the rubbery plateau.

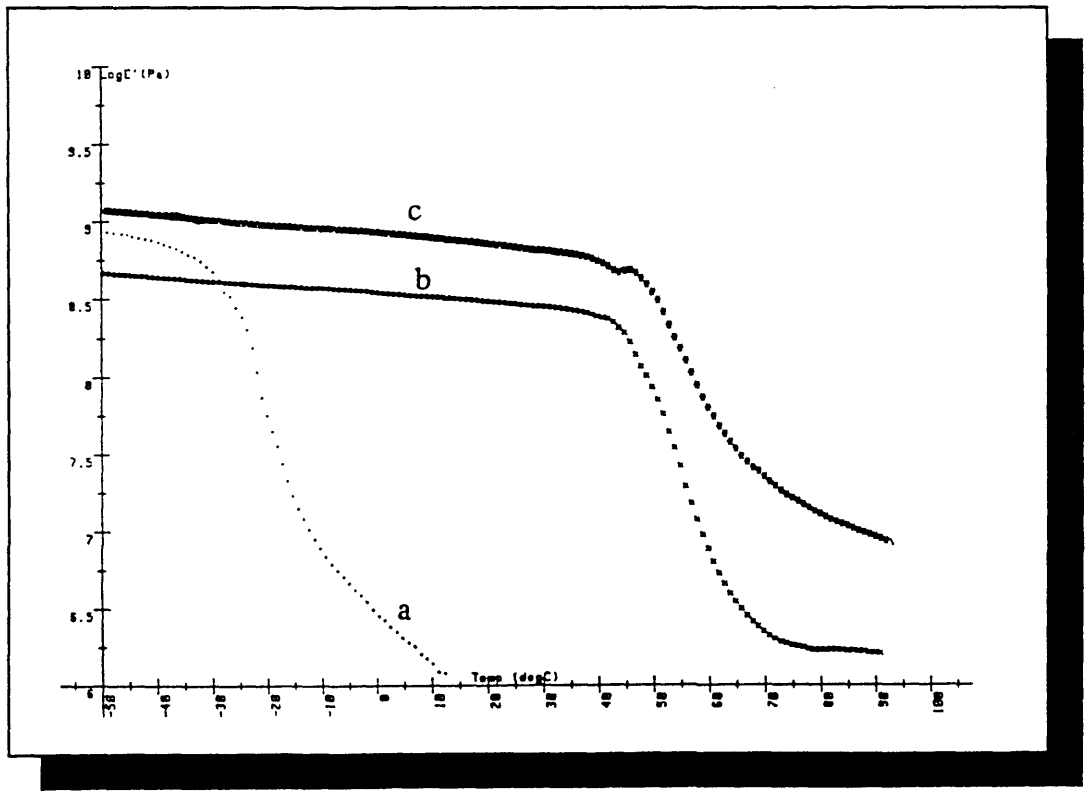

Figure 4.37 Values of logE' vs temperature for: EVA_{45} (a.), $SCPE_{54}$ (bx) and $SCPE_{54DETA}$ (c*).

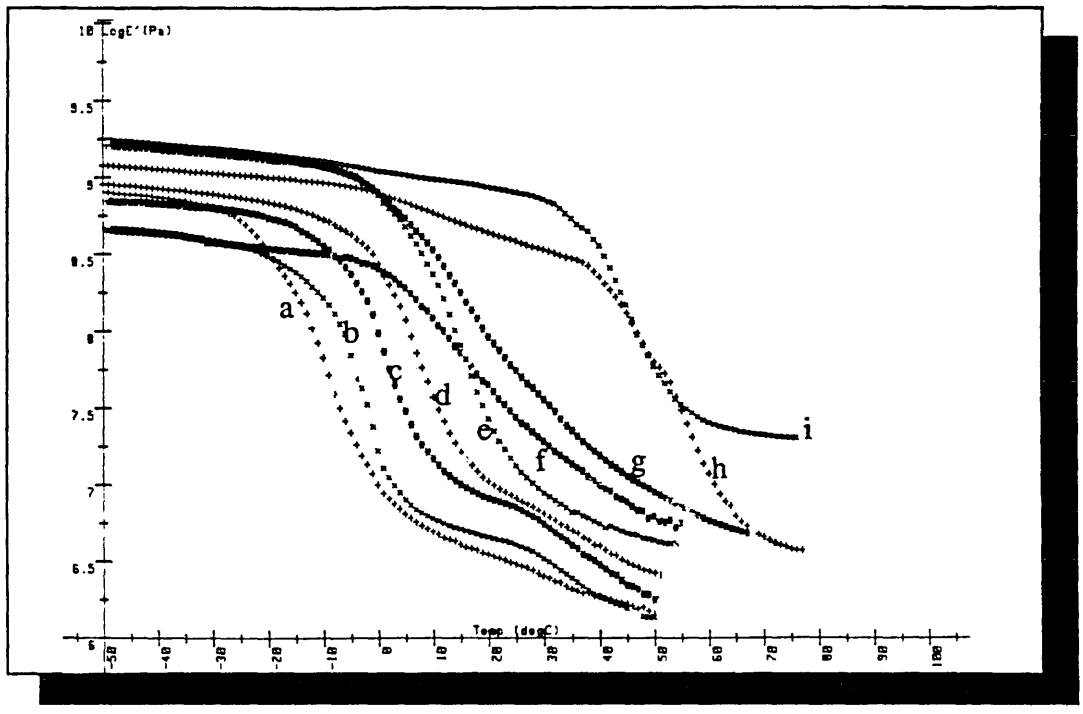

Figure 4.38 Values of logE' vs temperature for the whole composition range of system D ($SCPE_{54}/EVA_{45}$). D_{10} (a+), D_{20} (bx) D_{30} (c*), D_{40} (d+), D_{50} (ex), D_{60} (f*), D_{70} (g*), D_{80} (h+), D_{90} (ix).

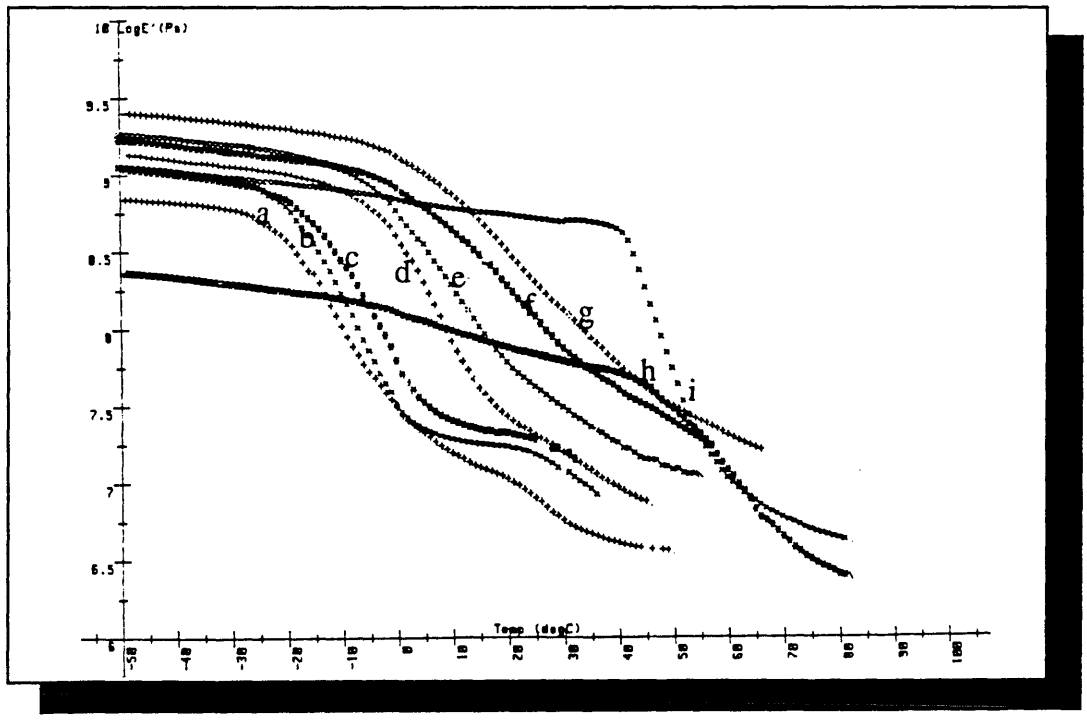

Figure 4.39 Values of logE' vs temperature for the whole composition range of system D_{DETA} ($SCPE_{54DETA}/EVA_{45}$). D_{10DETA}(a+), D_{20DETA} (bx), D_{30DETA} (c*), D_{40DETA} (d+), D_{50DETA} (ex), D_{60DETA} (f*), D_{70DETA} (g+), D_{80DETA}(h*), $D_{90\ DETA}$ (ix).

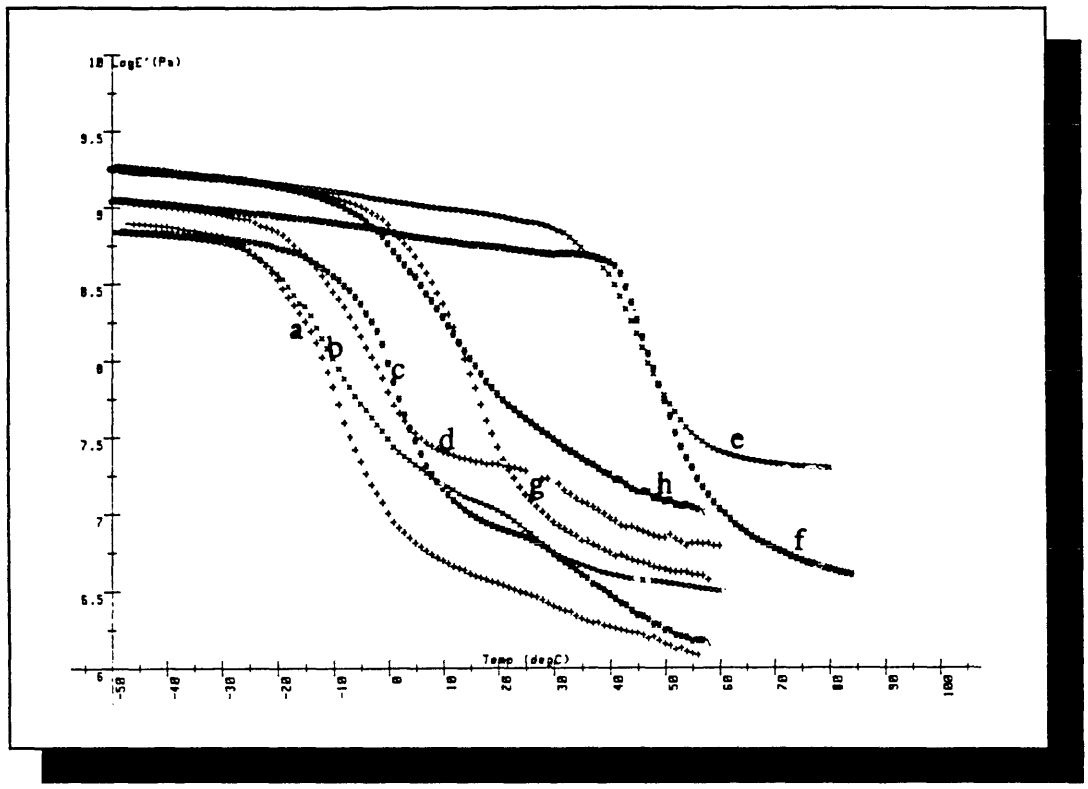

Figure 4.40 Comparison of logE' for some compositions of D and D_{DETA}. D_{10} (a+), D_{10DETA} (bx), D_{30} (c*), D_{30DETA} (d+), D_{50} (g+), D_{50DETA} (h*), D_{90} (ex), D_{90DETA} (f*).

4.3.4 CLOUD POINT MEASUREMENTS

Figure 4.41 shows the CP curve obtained for D with the laser-SALS. The error bars represent the scatter in data obtained in repeated experiments. This figure also shows the range of CP temperatures observed for some D_{DETA} compositions (see rectangular bars).Examination of figure 4.41 shows that from D_{30} onwards the CP temperatures measured were more or less constant. After crosslinking the CPs appeared 7 to 15 degrees higher than the values observed in the unmodified samples.

4.3.5 SIZE OF DOMAINS

Figure 4.42 shows the plot of I vs θ for D_{20} at various temperatures. The data clearly correspond to an exponential decay. This plot is representative of the behaviour of the rest of the compositions of D and D_{DETA} studied. The sizes of the domains were therefore determined as described in section 4.2.5, p. 121. The results are shown in table 4.21. Comparing the data for the uncrosslinked and crosslinked samples in this

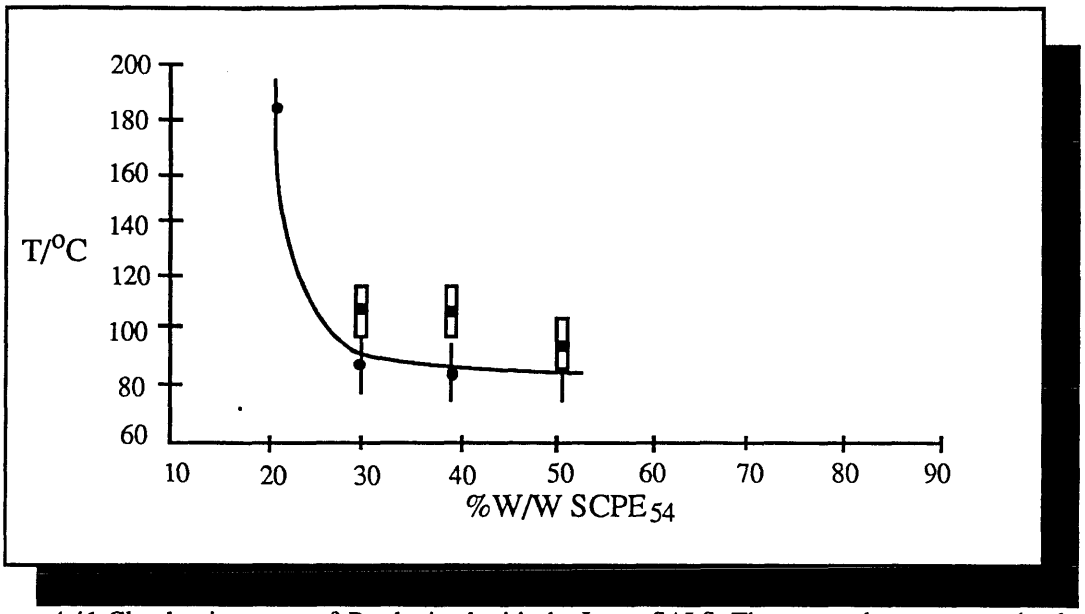

Figure 4.41 Cloud point curve of D obtained with the Laser SALS. The rectangles represent the data obtained for D_{DETA}.

table shows that after crosslinking, the range of domains sizes is narrower. Table 4.22 compares the experimental domain sizes and estimates of $\langle s^2 \rangle^{1/2}$ for some D_{DETA} compositions. Clearly, there is no correlation between these two quantities.The values of γ_{ie} were calculated with the Donatelli equation (eq. 2.151, p. 42).

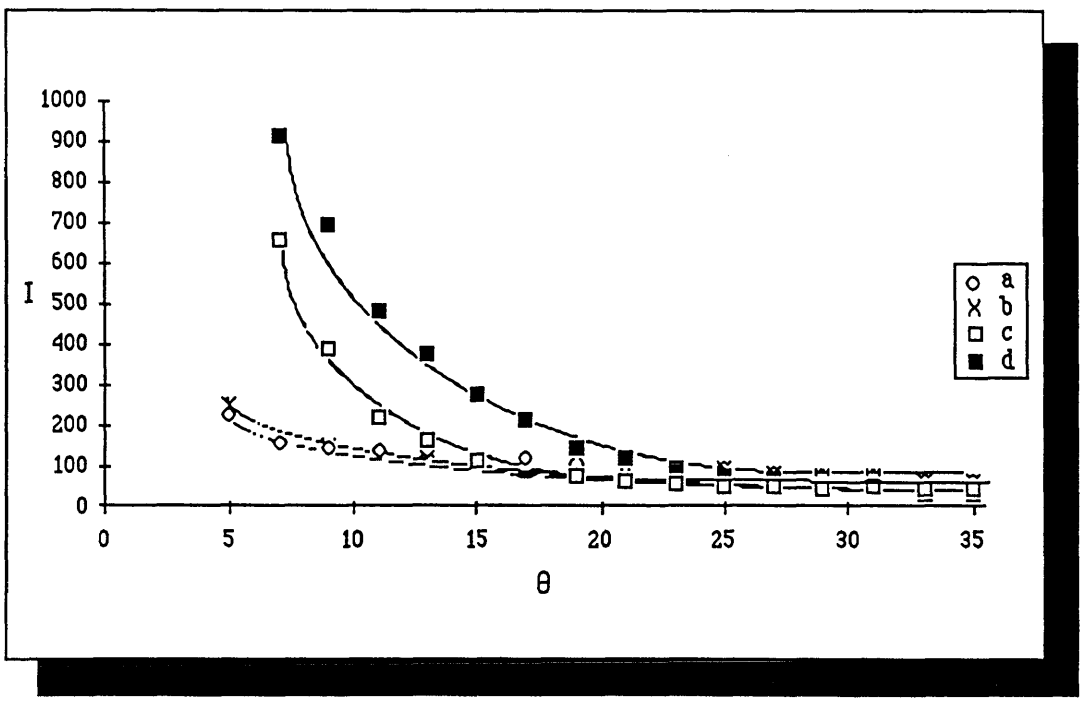

Figure 4.42 Intensity of the scattered light (I) as a function of angle for D_{20} at (a) 30°C, (b) 88°C (CP temperature), (c) 118°C and (d) at 138°C.

Sample	CP temperature (°C)	Domain sizes Range observed (Å)	At temperature (°C)
Uncrosslinked blend			
D_{20}	88	$1x10^2$ - $3x10^3$	118
D_{30}	88	$1x10^2$ - $1x10^3$	118
D_{50}	88	$3x10^3$ - $8x10^3$	118
Crosslinked blend			
D_{20DETA}	105	$1x10^4$ - $2x10^4$	135
D_{30DETA}	110	$3x10^3$ - $6x10^3$	140

Table 4.21 Range of domain sizes obtained for some compositions of D and D_{DETA} with the laser-SALS. The data were measured 30°C above the CP temperature of each sample. (The values of CP used are those obtained with the laser-SALS).

Sample	Experimental Domain size ($x10^4$ Å)	$< s^2 >^{1/2}$ between crosslinks (x10 Å)	γ_{ie} from Donatelli equation (x 10 dn/cm)
D_{20DETA}	1 - 2	3	5
D_{30DETA}	0.3-0.6	3	9

Table 4.22 Comparison of the experimental domain sizes and the values of domains obtained with $<s^2>^{1/2}$. The values of γ_{ie} were calculated with the Donatelli equation.

4.4 $SCPE_{54}/PBA_{LMW}$ (SYSTEM *F*).

Chai [27,137] and Walsh [27] previously studied similar blends to *F* . They blended the same PBA used in this work with CPEs of different chlorine content (48, 49.8 and 62.1 %W/W chlorine). In the present work, $SCPE_{54}$ (54% chlorine content and 0.94% S as SO_2Cl groups) was solvent cast in MEK with commercial low molecular weight PBA (PBA_{LMW}, T_g= -21°C (DMTA), $\bar{M}_n$= 27000). When dried the resulting blend was crosslinked with *DETA* (sections 3.3.1, pp 68-9 and 3.4.3, pp 74-6).

4.4.1 DEGREE OF CROSSLINKING

As in the previous systems, the degree of crosslinking was determined using swelling measurements. Table 4.23 shows these results. The experimental conditions and methods of calculation are the same as those described in section 4.2.1, p. 105. As in system D_{DETA} , taking into consideration the $\bar{M}_n$ of $SCPE_{54}$ (33000), (see section 4.3.1, pp 124-5) the results obtained by swelling suggest that the the whole composition range is lightly crosslinked.

4.4.2 MISCIBILITY BEHAVIOUR

The unmodified blends containing up to 60% w/w of $SCPE_{54}$ were transparent; above 70% loading they were slightly hazy. As in the previous blends, after crosslinking all samples developed a brownish discoloration. The Rheovibron and DMTA results (tables 4.24 and 4.26, figures 4.43 to 4.45) show that F and F_{DETA} were miscible up to a 50% $SCPE_{54}$ content (only one peak was visible). The

SWELLING MEASUREMENTS $\bar{M}_{cSWELL}$ g/mole *			
Sample	(1)	(2)	(3)
F_{10DETA}	——	——	——
F_{20DETA}	——	——	——
F_{30DETA}	——	——	——
F_{40DETA}	16600	16900	16900
F_{50DETA}	16500	17500	16900
F_{60DETA}	17600	20300	21300
F_{70DETA}	17300	19300	19800
F_{80DETA}	17700	20800	21800
F_{90DETA}	——	——	——
$SCPE_{54DETA}$	22118	23800	18200

* $\bar{M}_{cSWELL}$ calculated with (1) a modified version of Flory - Rehner [71] eq. (2) James and Guth eq.[71, 143] and (3) Herman eq.[71, 143, 144] . All these equations include the correction for free ends.

Table 4.23 Values of $\bar{M}_{cSWELL}$ for F_{DETA} .

sample containing 60% W/W $SCPE_{54}$ showed quite a small peak in comparison with the peaks of the previous compatible compositions. This suggests that this sample is no longer behaving as a one phase system. From F_{70} onwards, the blend was phase separated (two peaks were observed). A comparison of the T_gs for *F* and PBA/CPE20[28, 140] is shown in table 4.25 (CPE20 = chlorinated polyethylene with a 62.1 %W/W Cl content). Despite of the 25° difference between the T_gs of the chlorinated polyethylenes used in the two systems, which increases the T_gs for the whole composition range, the behaviour in both systems is similar. They only differed in the composition containing 90% W/W of the chlorinated polyethylene: F_{90} showed a small hump overlapping a sharp peak while the corresponding sample in PBA/CPE20 showed only a sharp peak.

The composition and mass balance of the two phases present in these samples were calculated using the Fox equation and DMTA results (see tables 4.27 and 4.28). These data show that the two phases present in each sample are richer in $SCPE_{54}$. The mass balance analysis in both tables indicates that as the amount of $SCPE_{54}$ increases in the sample, a larger quantity of this polymer is present in the phase with higher T_g.

4.4.3 STATIC AND DYNAMIC MECHANICAL PROPERTIES

Figures 4.46 and 4.47 show the static Young's moduli $Y(Nm^{-2})$ (measured with an Instron with a deformation rate of 0.05 $mm\text{-}min^{-1}$) and the storage modulus E' (measured at 20°C with the DMTA) for *F* and F_{DETA}. Although the data for *F* and F_{DETA} are rather incomplete an examintation of the curve for F_{DETA} shows that within the scatter Y increases smoothly up to 60% content $SCPE_{54}$, above this composition Y increases rapidly. In order to confirm the behaviour of *F* and F_{DETA} a plot of E' versus composition was extracted from the DMTA data shown in figures 4.48 to 4.50 and is shown in figure 4.47. As mentioned in section 4.3.3 (p. 126-33), although the rate of testing in the dynamic experiments is very different from that used in the static measurements and the accuracy of the dynamic modulus measurements is not as great as that in the static measurements the shapes of Y and E' should be similar. Examination of figure 4.47 shows a smooth increment of E' with higher contents of $SCPE_{54}$ in the blend. The plot also shows a small increase in E' in the crosslinked samples.

	Rheovibron			DMTA		
Sample*	T_gs observed (°C)	Max. value tanδ	Comments	T_gs observed (°C)	Max. value tanδ	Comments
PBA_{LMW}	——	——	very soft to be measured	-21	1.33	shear mode may distort peak shape
F_{10}	——	——	very soft to be measured	-10	1.12	shear mode may distort peak shape
F_{20}	——	——	very soft to be measured	1	1.32	shear mode may distort peak shape
F_{30}	——	——	very soft to be measured	10	1.38	shear mode may distort peak shape
F_{40}	11	1.70	sharp peak	14	1.47	sharp peak
F_{50}	25	1.66	sharp peak	25	1.62	sharp peak
F_{60}	35	1.63	sharp peak	32	0.80	small and broad peak
F_{70}	25, 62	0.47, 0.97	small hump overlaps sharp peak	27, 57	0.36, 0.22	two small peaks overlapping
F_{80}	23, 67	0.15, 1.35	small hump overlaps sharp peak	25, 61	0.21, 0.64	two small peaks overlapping
F_{90}	11, 61	0.05, 1.70	very small hump overlaps sharp peak	18, 60	0.10, 1.51	small hump overlapping sharp peak
$SCPE_{54}$	53	1.45	sharp peak	61	1.86	sharp peak

* For explanation of the nomenclature see tables 3.1 and 3.6 in pages 57 and 68 respectively.

Table 4.24 Comparison of the T_gs of *F* obtained with the Rheovibron and the DMTA.

This work code*	T_gs observed (° C)	Max value of tanδ	Comments	PBA/CPE20[27, 137]	T_gs observed (° C)	Max value of tanδ	Comments**
F_{50}	25	1.66	sharp peak	0.4612	32	1.76	sharp peak
F_{60}	35	1.63	sharp peak	0.6409	54	1.76	sharp peak
F_{90}	11, 61	0.05, 1.70	small hump overlapping sharp peak	0.8473	80	1.45	sharp peak
$SCPE_{54}$	53	1.45	sharp peak	1.0000	78	1.77	sharp peak

* For explanation of the nomenclature see tables 3.2 and 3.6 pp 57 and 68 respectively.
**Data only reported approximately 20 degrees below and above T_g.

Table 4.25 Comparison of the T_gs and values of tanδ observed in this work and for the blend PBA/CPE20[27, 137]

	Rheovibron			DMTA		
Sample *	T_gs observed (° C)	Max. value tanδ	Comments	T_gs observed (° C)	Max. value tanδ	Comments
PBA_{LMW}	——	——	very soft to be measured	-21	1.33	shear mode may distort peak shape
F_{10DETA}	——	——	very soft to be measured	——	——	——
F_{20DETA}	——	——	very soft to be measured	1	1.11	shear mode may distort peak shape
F_{30DETA}	——	——	very soft to be measured	13	1.00	shear mode may distort peak shape
F_{40DETA}	12	1.38	sharp peak	13	1.19	sharp peak
F_{50DETA}	25	1.41	sharp peak	24	1.17	sharp peak
F_{60DETA}	28, 60	0.27, 0.50	small and broad peak overlaps hump	26	0.49	small and broad peak
F_{70DETA}	23, 69	0.29, 0.81	small hump overlaps sharp peak	24, 58	0.25, 0.19	two small peaks overlapping
F_{80DETA}	20, 72	0.17, 0.97	small hump overlaps sharp peak	23, 61	0.18, 0.45	two small peaks overlapping
F_{90DETA}	13, 72	0.06, 1.19	very small hump overlaps sharp peak	18, 62	0.10, 1.03	small hump overlapping sharp peak
$SCPE_{54DETA}$	56	1.07	sharp peak	61	0.92	sharp peak

* For explanation of the nomenclature see tables 3.1 and 3.6 in pp 57 and 68 respectively and section 3.4, pp 71-2.

Table 4.26 Comparison of the T_gs of F_{DETA} obtained with the Rheovibron and the DMTA.

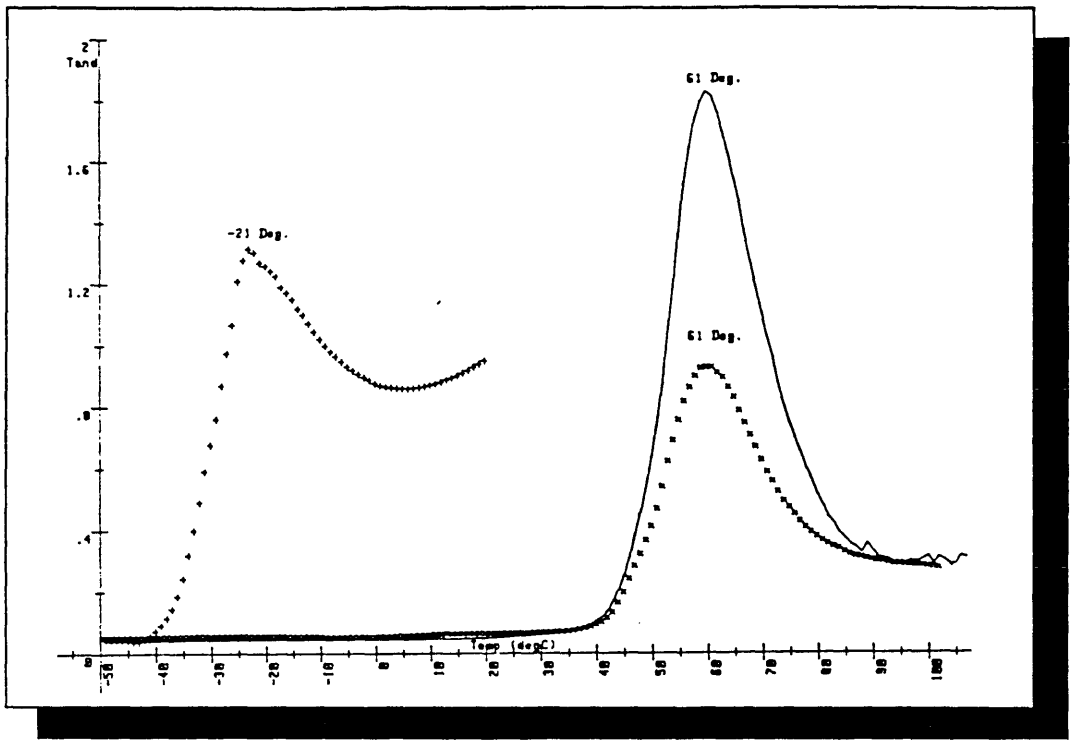

Figure 4.43 T_gs of PBA_{LMW} (-21°C(+)), $SCPE_{54}$ (61°C(—)) and $SCPE_{54DETA}$ (61°C(x)).

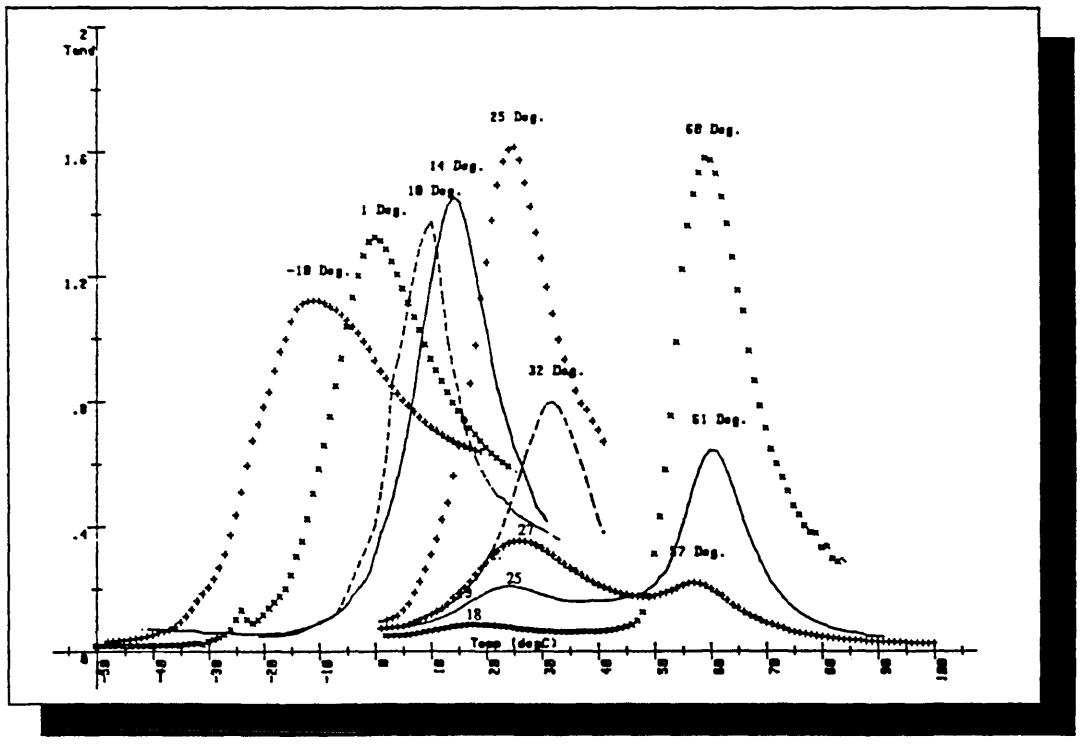

Figure 4.44 T_gs for the whole composition range of system *F* ($SCPE_{54}$/ PBA_{LMW}). F_{10} (-10°C(+)), F_{20} (1°C(x)), F_{30} (10°C(- -)), F_{40} (14°C(–)), F_{50} (25°C(+)), F_{60} (32°C(- -)), F_{70} (27, 57°C(+)), F_{80} (25, 61°C(–)), F_{90} (18, 60°C(x)).

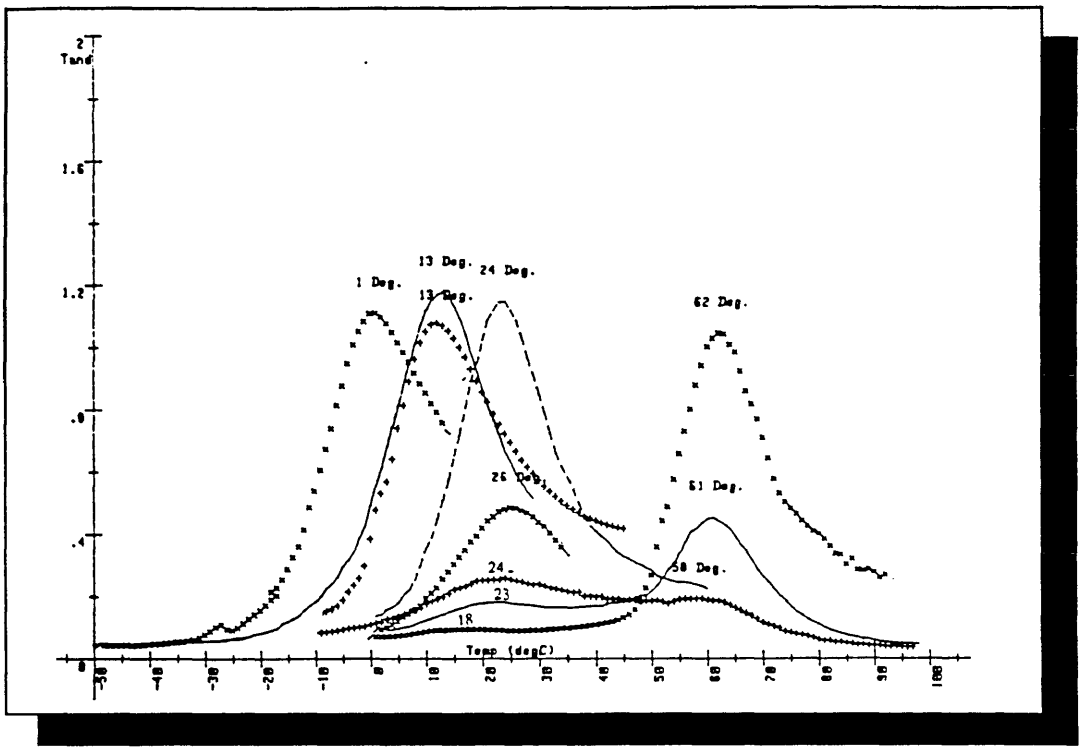

Figure 4.45 T_gs for the whole composition range of system F_{DETA} ($SCPE_{54DETA}$/PBA_{LMW}). F_{20DETA} (1°C(x)), F_{30DETA} (13°C(+)), $F_{40\,DETA}$ (13°C(–)), F_{50DETA} (24°C(- -)), F_{60DETA} (26°C(x)) F_{70DETA} (24, 58°C(+)), F_{80DETA} (23, 61°C(—)), $F_{90\,DETA}$ (18, 62°C(x)).

Sample*	T_gs °C	Max value Tanδ	$SCPE_{54}$ / PBA_{LMW}	
			** Composition	*** Mass balance g/g
F_{70}	27 57	0.36 0.22	65 / 55 96 / 4	0.54 / 0.29 0.15 / 0.01
F_{80}	25 61	0.21 0.64	58 / 42 100 / 0	0.28 / 0.20 0.52 / 0
F_{90}	18 60	0.10 1.51	55 / 45 99 / 1	0.11 / 0.09 0.79 / 0.08

* For explanation of the nomenclature see tables 3.1 and 3.6 pp 57 and 68 and section 3.4, pp 71-2.

** The number at the left hand side of the slash gives the composition of $SCPE_{54}$ and the number at the right gives the composition of PBA_{LMW}.

*** Calculation based on 1 g of the original mixture of both polymers.

Table 4.27 Composition and mass balance of the two phases present in samples F_{70} to F_{90}.

Sample*	T_gs °C	Max value Tanδ	$SCPE_{54DETA}$ / PBA_{LMW}	
			** Composition	*** Mass balance g/g
F_{70DETA}	24 58	0.25 0.19	62 / 38 97 / 3	0.40 / 0.29 0.22 / 0.01
F_{80DETA}	23 61	0.18 0.45	61 / 39 100 / 0	0.31 / 0.20 0.49 / 0
F_{90DETA}	18 62	0.10 1.03	55 / 45 100 / 0	0.12 / 0.10 0.78 / 0

*For explanation of the nomenclature see tables 3.1 and 3.6 p 57 and 68 and section 3.4 pp 71-2.

**The number at the left hand side of the slash gives the composition of $SCPE_{54DETA}$ and the number at the right gives the composition of PBA_{LMW}.

***Calculation based on 1 g of the original mixture of both polymers.

Table 4.28 Composition and mass balance of the two phases present in samples F_{70DETA} to F_{90DETA}

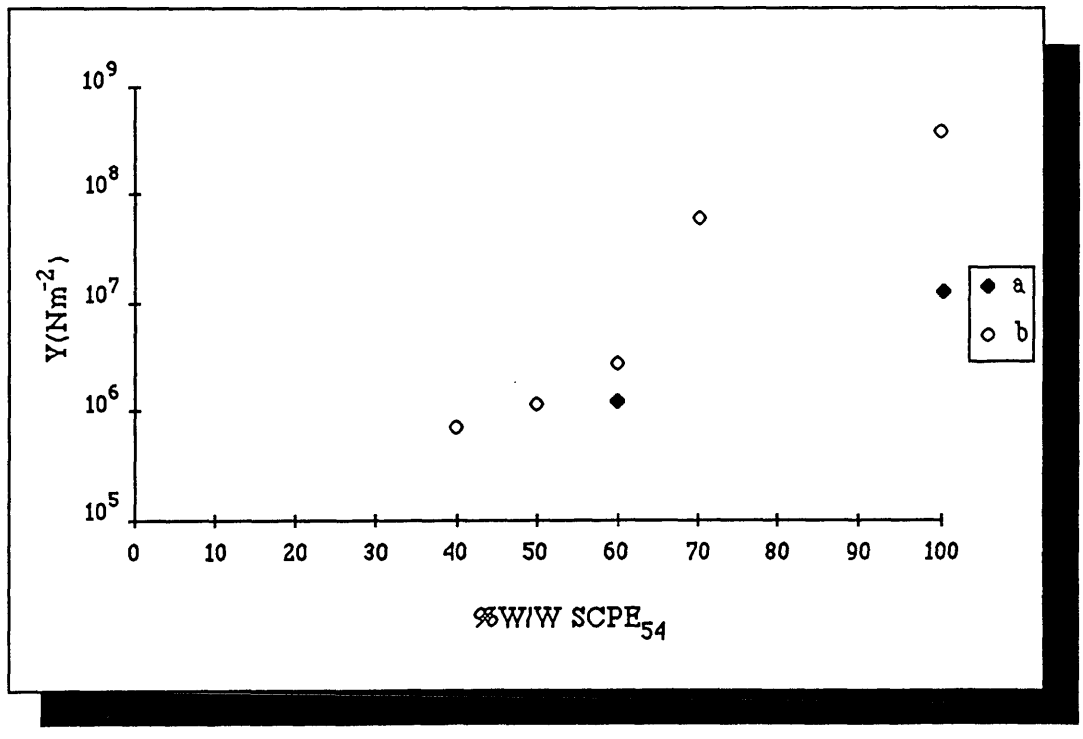

Figure 4.46 The tensile Young moduli (Y) (Nm^{-2}) of (a) blend F and (b) blend F_{DETA} as a function of composition at a crosshead rate of 0.05mm-min^{-1}.

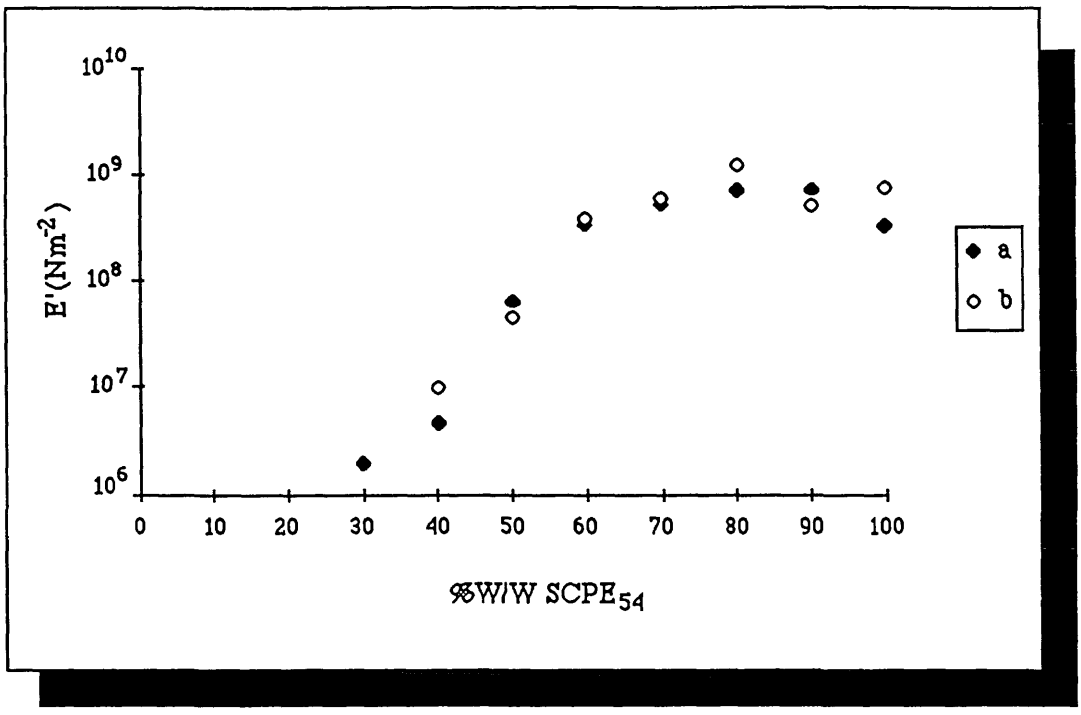

Figure 4.47 The storage dynamic moduli (E) (Nm^{-2}) of (a) blend *F* and (b) blend F_{DETA} as a function of composition. The data was obtained at 20°C from the logE' results obtained with the DMTA.

Figures 4.48 to 4.51 show logE' as a function of temperature. Figure 4.48 shows the values for the pure polymers, figures 4.49 and 4.50 show the results for *F* and F_{DETA} respectively. Figure 4.51 compares logE' as a function of temperature for some compositions of *F* and F_{DETA}. Inspection of figures 4.49 and 4.50 show that generally the logE' curves shift upwards as the content of $SCPE_{54}$ (component of higher E') increases. Depending on the state of miscibility the shapes of the logE' curves vary considerably; from steep curves showing only one inflection point (one phase samples, see curve a in figure 4.49 and figure 4.50) to less steep curves where two inflection points were observable (two phase samples, see curve c, d in fig 4.49 and curve c in figure 4.50).The comparison of the logE' between the samples before and after being crosslinked in figure 4.51 shows clearly that crosslinking increases the values of E', specially in the rubbery plateau.

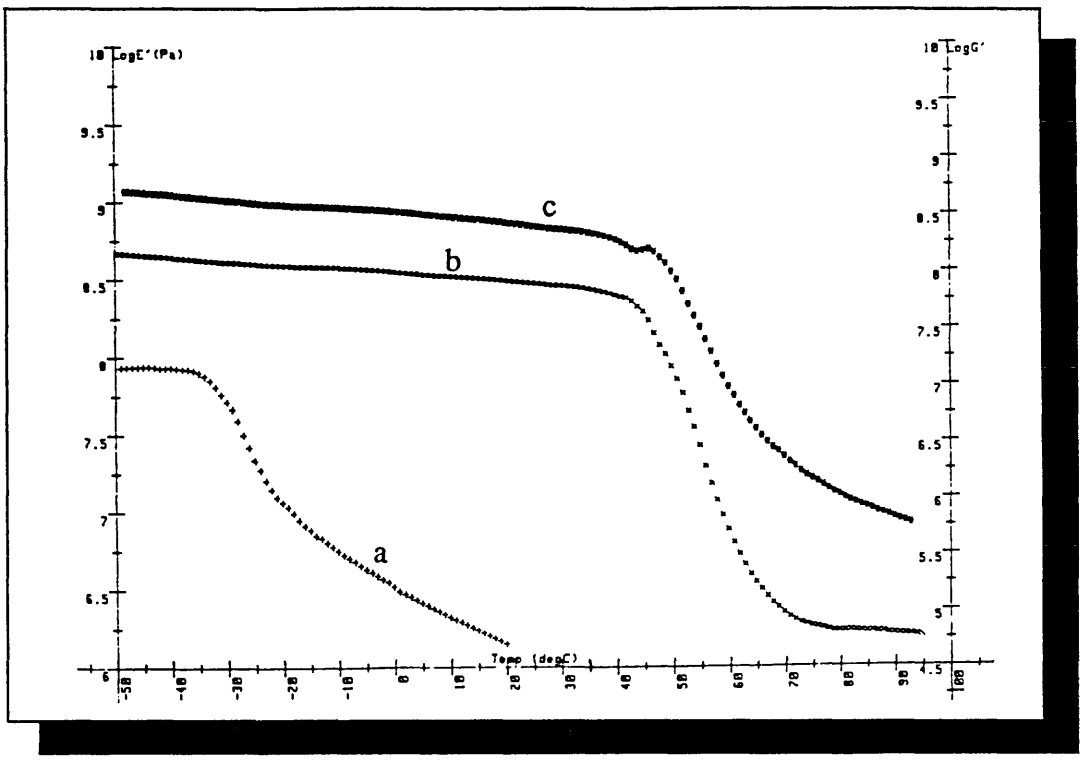

Figure 4.48 Values of logE' vs temperature for: PBA_{LMW} (a+), $SCPE_{54}$ (bx) and $SCPE_{54DETA}$ (c*).

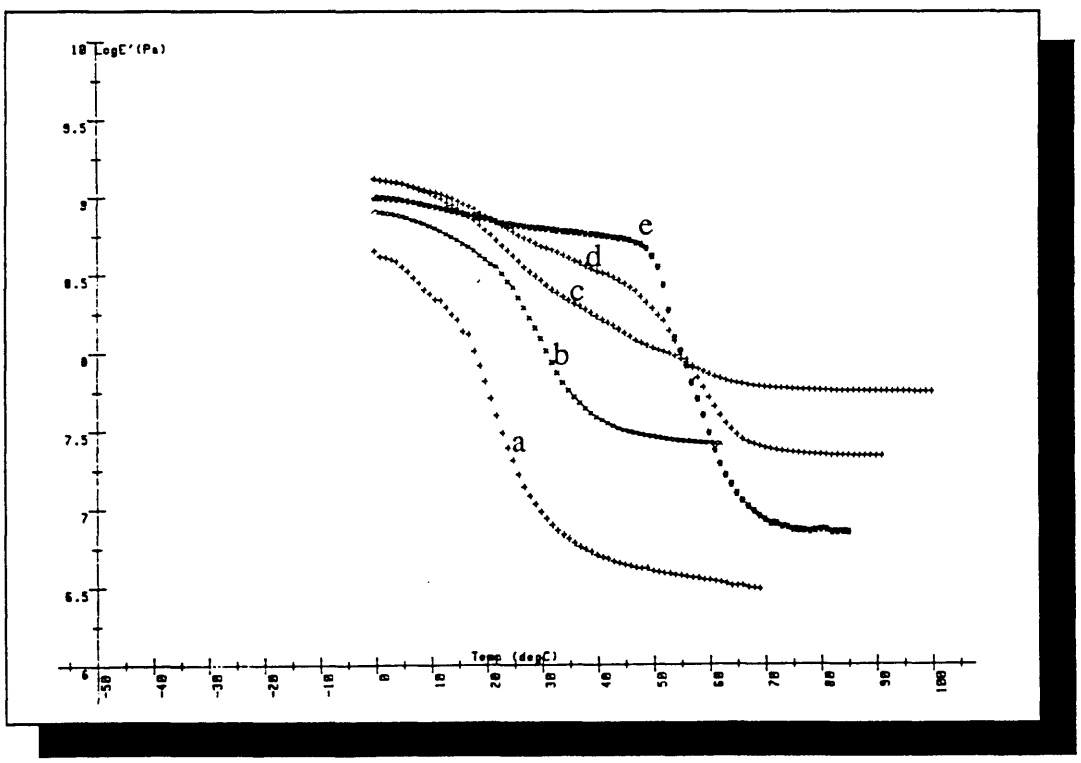

Figure 4.49 Values of logE' vs temperature for the whole composition range of system *F* ($SCPE_{54}/PBA_{LMW}$). F_{50} (a+), F_{60} (bx), F_{70} (c+), F_{80} (d+) and F_{90} (e*).

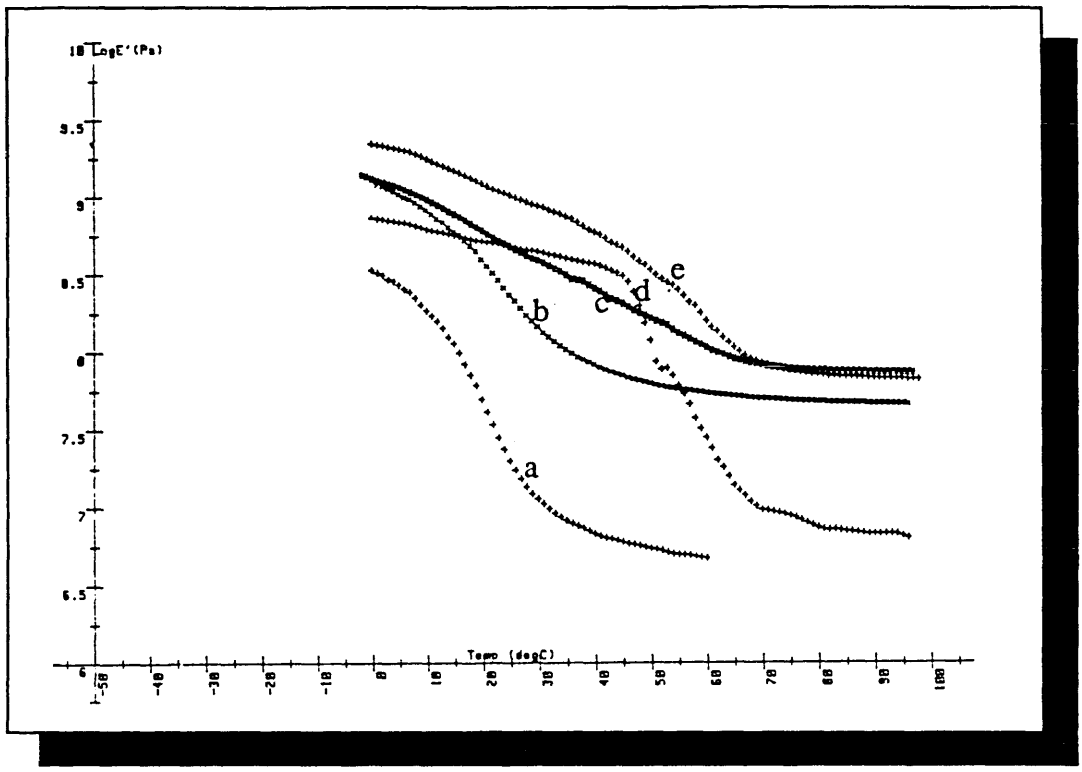

Figure 4.50 Values of logE' vs temperature for the whole composition range of system F_{DETA} ($SCPE_{54DETA}/PBA_{LMW}$). F_{50DETA} (a+), F_{60DETA} (bx), F_{70DETA} (c*), $F_{80\,DETA}$ (d+), F_{90DETA} (e+).

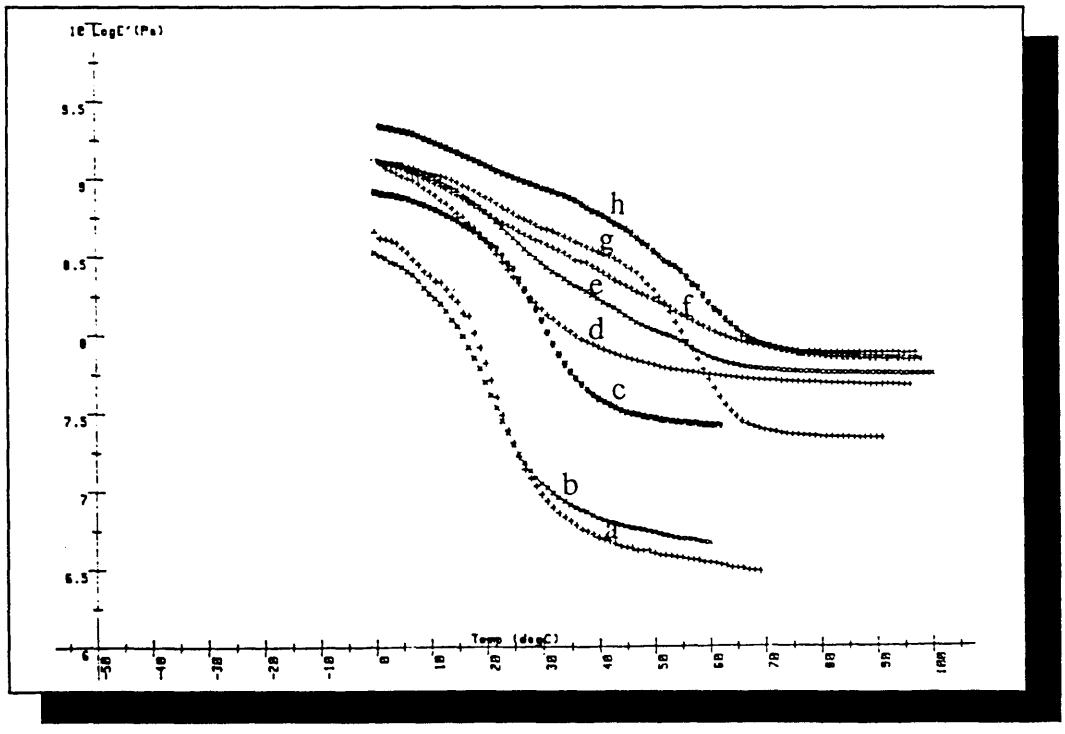

Figure 4.51 Comparison of logE' for some compositions of F and F_{DETA}. F_{50} (a+), F_{50DETA} (bx), F_{60} (c*), $F_{60\,DETA}$ (d+), F_{70} (ex), F_{70DETA} (f+), F_{80} (g+), D_{80DETA} (h*).

4.4.4 CLOUD POINT MEASUREMENTS

Figure 4.52 compares the plots of the intensity of the scattered light (I) vs temperature obtained with the turbidimeter for some compositions of F and F_{DETA}. This figure clearly illustrates a decrease in the slope of the curves corresponding to the crosslinked samples.

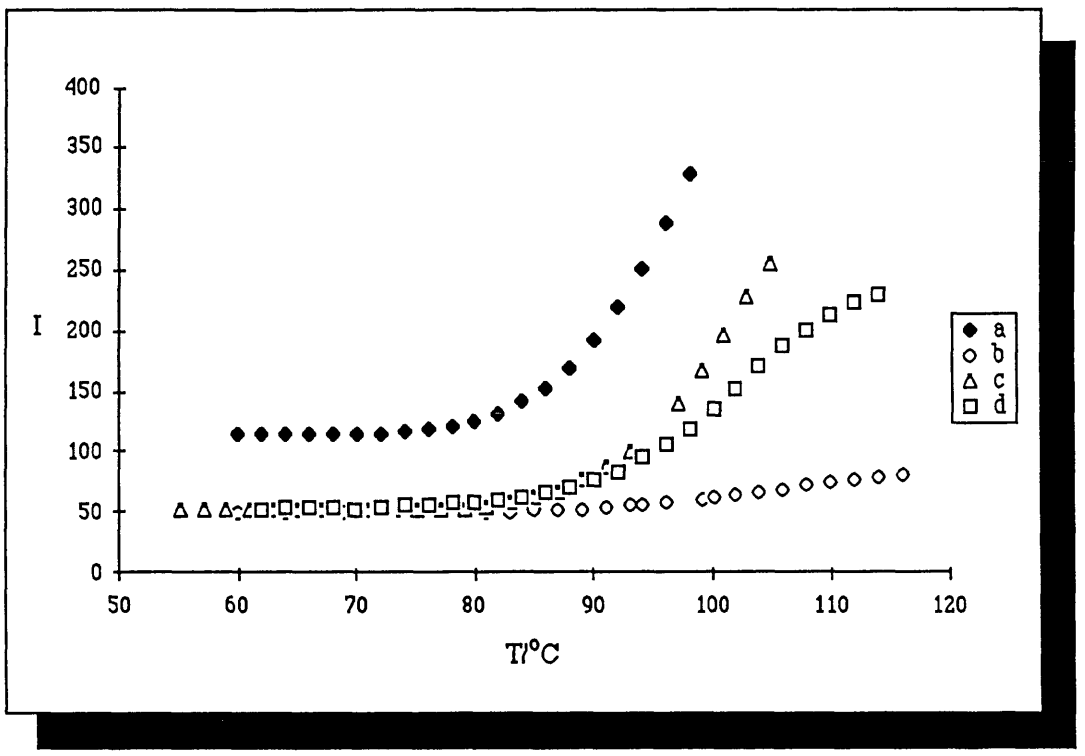

Figure 4.52 Cloud point temperatures obtained for some compositions of F and F_{DETA} with the turbidimeter (heating rate 0.1°C). (a) F_{70} (CP= 74°C), (b) F_{70DETA} (CP= 83°C), (c) F_{80} (CP= 76°C) and (d) F_{80DETA} (CP= 80°C).

The CP curves obtained as a function of composition for F and F_{DETA} are shown in figures 4.53 to 4.56. The first two plots illustrate the results obtained with the turbidimeter, the other two show the laser-SALS data. As may be observed, the scatter in the data for F and F_{DETA} is smaller than that previously obtained for the other systems (sections 4.2.4 (pp 119-121) and 4.3.4 (pp 135-6). Comparison of the curves for F and F_{DETA}, obtained by any of the two scattering techniques used, show that after crosslinking the CP curve increases between 5 to 10 degrees.

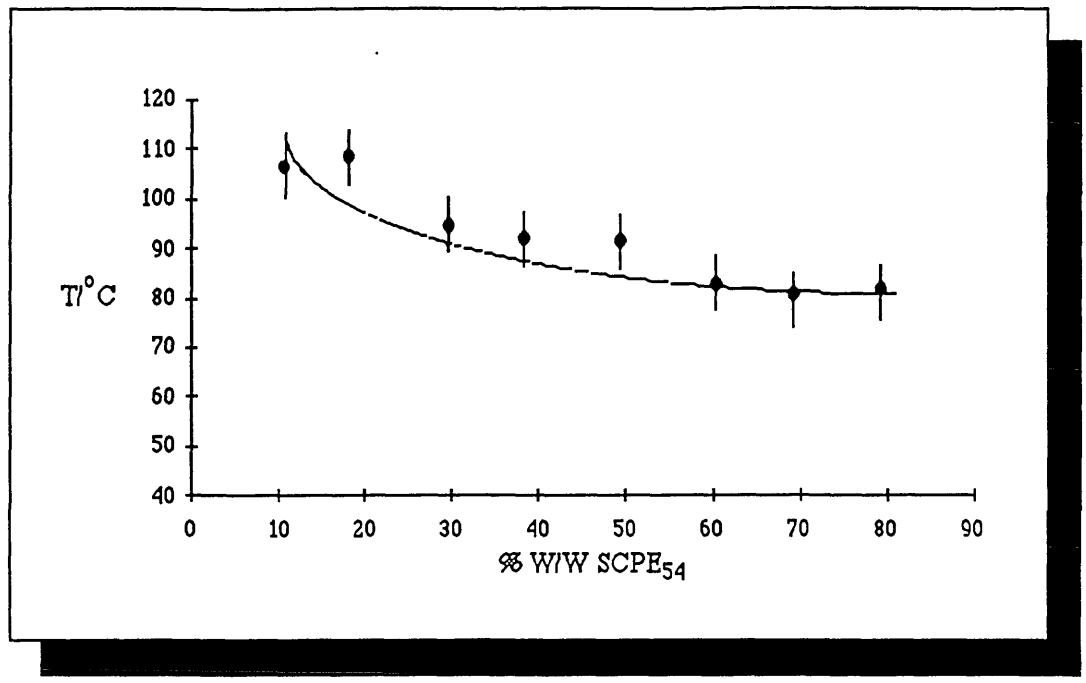

Figure 4.53 Cloud point curve of blend *F* obtained with the turbidimeter at a heating rate of 0.1°C/min.

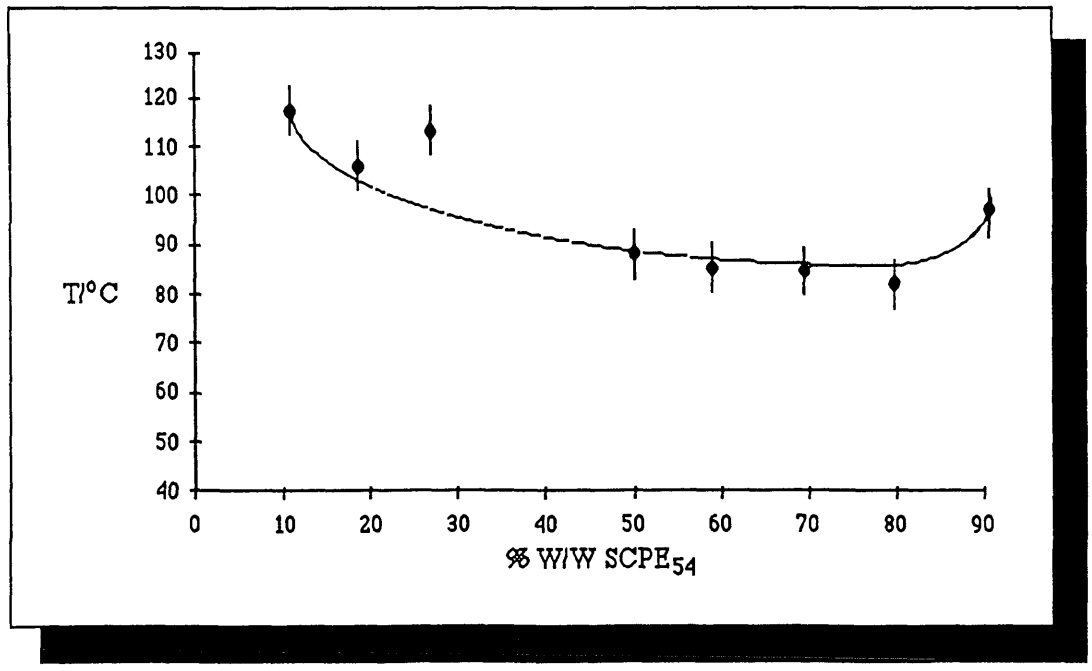

Figure 4.54 Cloud point curve of blend F_{DETA} obtained with the turbidimeter at a heating rate of 0.1°C/min.

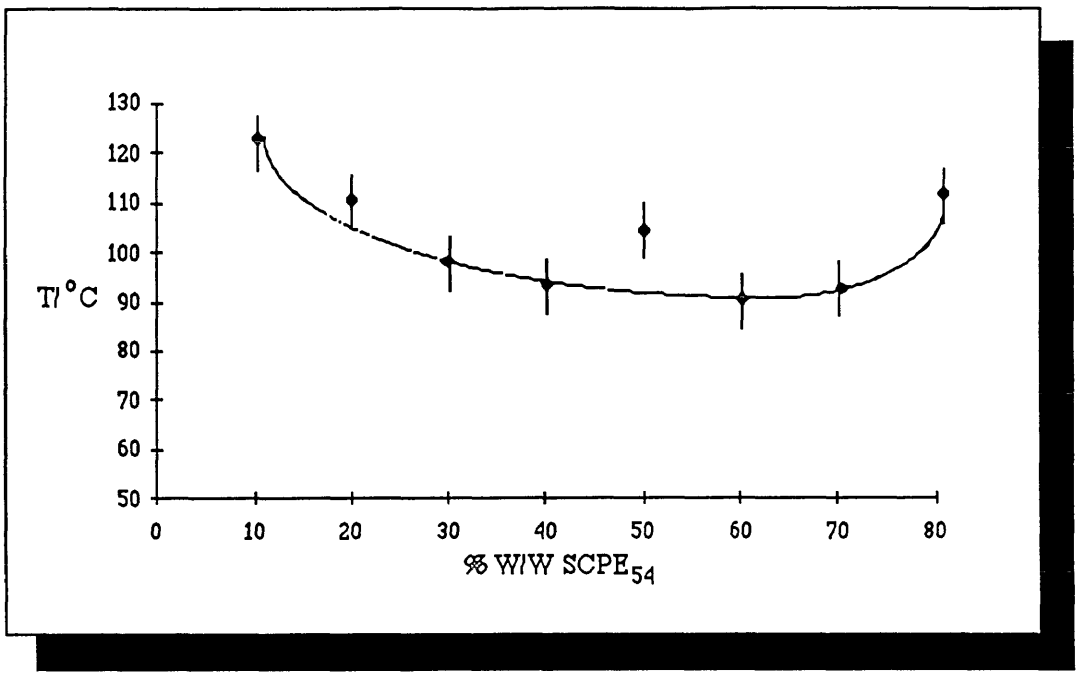

Figure 4.55 Cloud point curve of blend *F* obtained with the laser- SALS at a heating rate of 1°C/min.

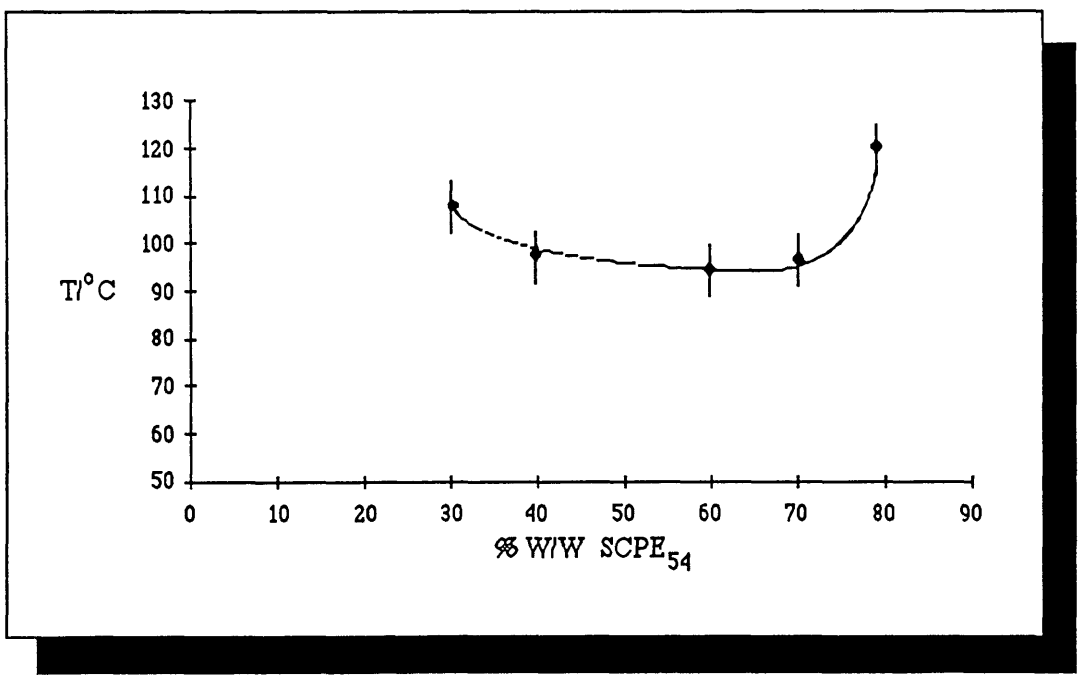

Figure 4.56 Cloud point curve of blend F_{DETA} obtained with the laser-SALS at a heating rate of 1°C/min.

4.4.5 DOMAIN SIZE MEASUREMENTS

Figures 4.57, 4.58,4.59 and 4.60 show examples of the intensity vs θ obtained for the following F and F_{DETA} compositions: F_{30}, F_{30DETA}, F_{60} and F_{60DETA} respectively. The data were obtained by reprocessing the results from the laser-SALS experiments. In contrast with previous systems (see sections 4.2.5, (p.121-4) and 4.3.5, (pp 135-7), this blend (before and after being crosslinked) shows the appearance of peaks during phase separation. Inspection of figure 4.57, which corresponds to F_{30}, shows the appearance of a peak at 122°C with a maximum at an angle of 25° (curve c). As may be seen in curve d, as the temperature increases the maximum of the peak shifts to smaller angles (T= 102°C, peak maximum at 21°). Curve e shows that at 152°C the peak has already shifted to angles smaller than 5°. Figure 4.58 shows a similar behaviour for F_{30DETA}, the difference being that the peak starts to appear at higher temperatures. Figures 4.59 and 4.60 illustrate a similar behaviour for F_{60} and F_{60DETA} respectively.

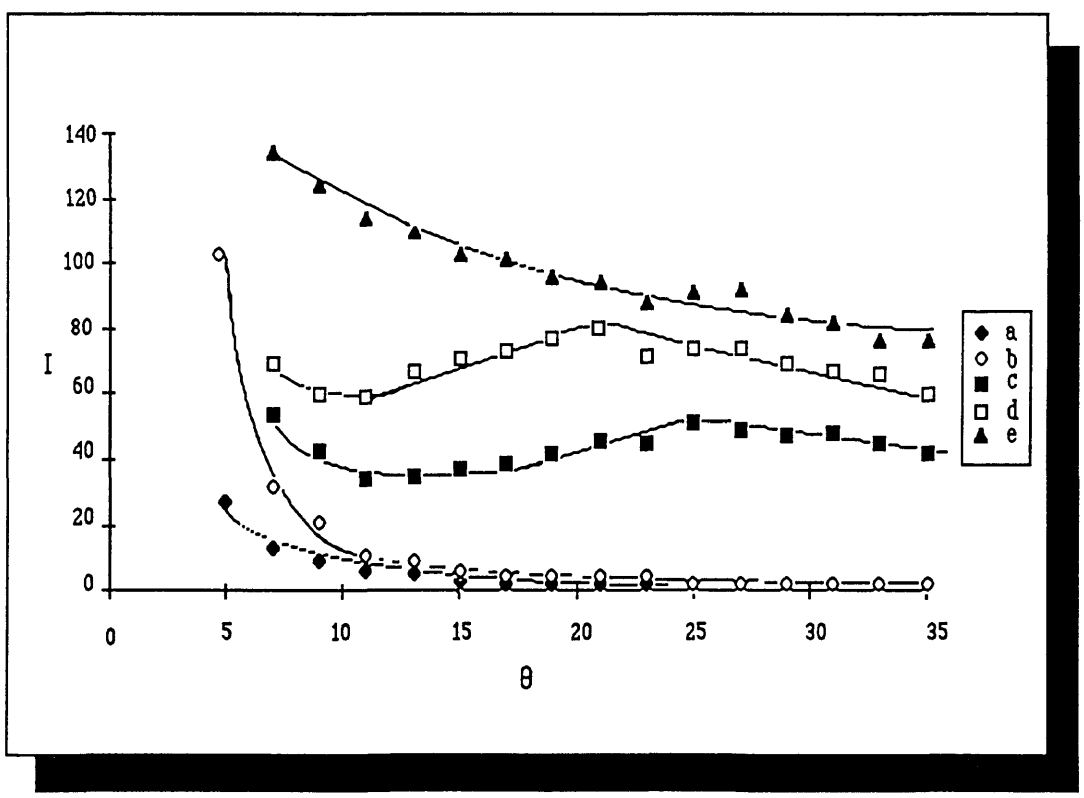

Figure 4.57 Intensity of the scattered light (I) as a function of angle (θ) for F_{30} at (a) 37°C, (b) 102°C, (c)122°C, (d) 132°C and (e) 152°C.

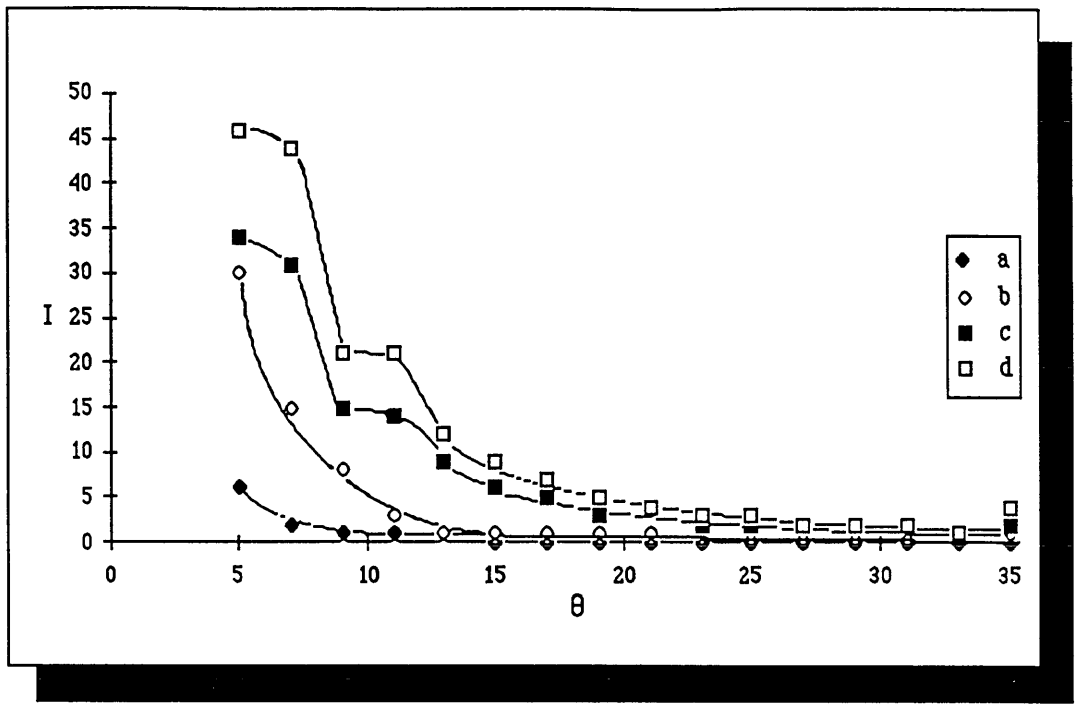

Figure 4.58 Intensity of the scattered light (I) as a function of angle (θ) for $F_{30\ DETA}$ at (a) 38°C, (b) 108°C, (c) 138°C and (d) 158°C.

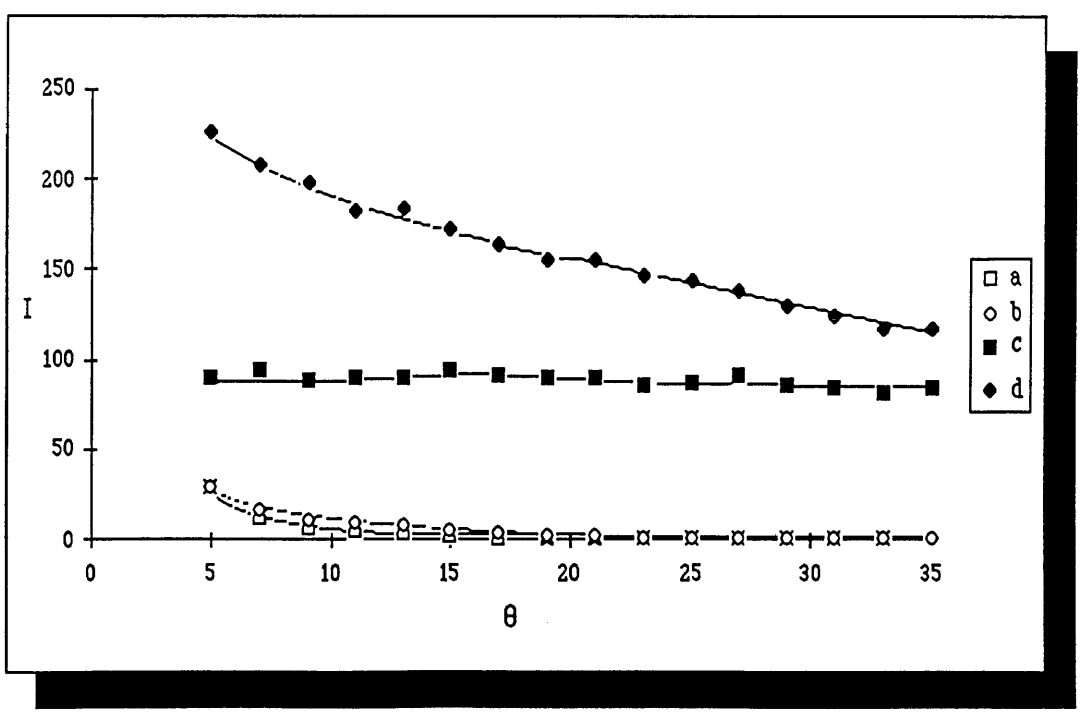

Figure 4.59 Intensity of the scattered light (I) as a function of angle (θ) for F_{60} at (a) 30°C, (b) 90°C, (c)120°C and (d) 140°C.

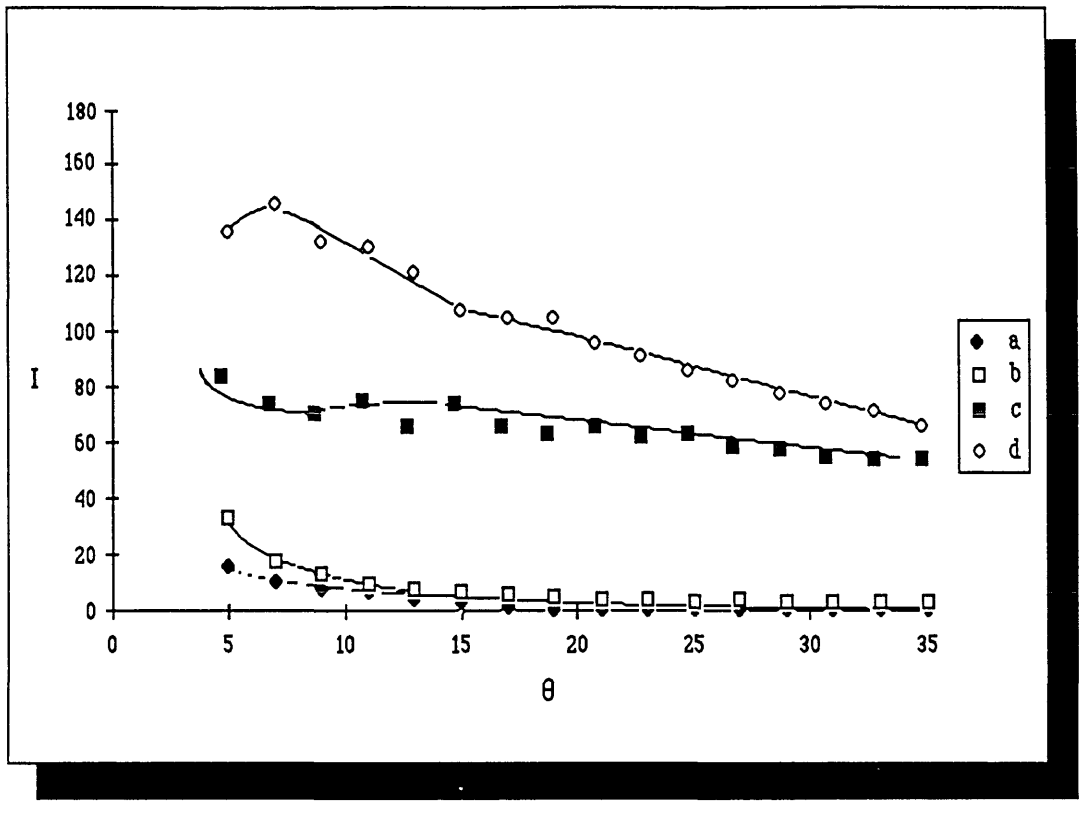

Figure 4.60 Intensity of the scattered light (I) as a function of angle (θ) for $F_{60\ DETA}$ at (a) 33°C, (b) 94°C, (c)124°C and (d) 144°C.

Following the procedure in section 3.9, the domain sizes for the different compositions of F and F_{DETA} were obtained 30°C above the CP of each sample. Examination of the data in table 4.29 shows that in the majority of cases, the size of the domains decreases after crosslinking. The effect of crosslinking on domain sizes is not as marked as in other systems (A_{DETA} and D_{DETA}) but does not contradict the general conclusion. In the case of F_{10DETA} and F_{20DETA} the presence of a peak was not evident in the scanned angular range of 5 to 35°. It was then assumed that such peaks may have been observed at larger angles, which means an effective decrease in the size of domains with crosslinking. Table 4.30 shows a comparison between the experimental results for the size of domains and the predictions obtained with the $\langle s^2 \rangle^{1/2}$ calculated between crosslinks.The values of γ_{ie} shown in the same table were calculated using the experimental results and the Donatelli equation. As in previous blends (see sections 4.2.5 (pp 123-4), 4.3.5 (pp 135-7)) inspection of the data in this table shows no correlation between the experimental domain sizes and the $\langle s^2 \rangle^{1/2}$.

Sample	CP temperature (°C)	Domain sizes Size observed Å	At temperature °C
Uncrosslinked blend			
F_{10}	123	5.19×10^4	153
F_{20}	111	2.88×10^4	141
F_{30}	102	1.24×10^4	132
F_{40}	92	1.53×10^4	122
F_{50}	104	2.88×10^4	134
F_{60}	90	1.73×10^4	120
F_{70}	90	2.00×10^4	120
F_{80}	111	3.70×10^4	141
F_{90}	—	—	—
Crosslinked blend			
F_{10DETA}	123	$< 0.752 \times 10^4$	153
F_{20DETA}	111	$< 0.752 \times 10^4$	141
F_{30DETA}	108	2.36×10^4	138
F_{40DETA}	96	7.88×10^3	126
F_{50DETA}	—	—	—
F_{60DETA}	94	2.36×10^4	124
F_{70DETA}	97	2.36×10^4	127
F_{80DETA}	119	2.36×10^4	149
F_{90DETA}	—	—	—

Table 4.29 Range of domain sizes obtained with the laser-SALS. The data was measured 30° above the CP temperature of each sample. (The values of CP used are those obtained with the laser-SALS).

Sample	Experimental Domain size ($\times 10^4$ Å)	$\langle s^2 \rangle^{1/2}$ between crosslinks ($\times 10$ Å)	γ_{ie} from Donatelli equation ($\times 10^2$ dn/cm)
F_{40DETA}	3.14	3.1	2.47
F_{60DETA}	2.36	3.1	2.5
F_{70DETA}	2.88	3.0	4.0
F_{80DETA}	3.70	3.1	7.6

Table 4.30 Comparison of the experimental domain sizes and the values of domains obtained with $\langle s^2 \rangle^{1/2}$. The values of γ_{ie} were calculated with the Donatelli equation.

4.5 $SCPE_{54}/PBA_{HMW}$ (SYSTEM *G*).

G has the same polymeric components as system *F* (section 4.4, p. 137) the only difference being that the PBA used in *G* has higher molecular weight than that used in *F* (PBA_{HMW}, T_g=-26°C, $\bar{M}_n$=183000). This difference in molecular weight is expected to modify some aspects of the behaviour of the blend especially in its phase separation behaviour. Just as before PBA_{HMW} was solvent cast with $SCPE_{54}$ in MEK and crosslinked with *DETA* (sections 3.3.1, pp 68-9 and 3.4.3 pp 74-6).

4.5.1 DEGREE OF CROSSLINKING

Table 4.31 shows the degree of crosslinking measured by swelling for the whole composition range of G_{DETA}. The experimental conditions and the calculation methods used are those shown in section 4.2.1 (p. 105).

SWELLING MEASUREMENTS $\bar{M}_{cSWELL}$ g/mole*			
Sample	(1)	(2)	(3)
G_{10DETA}	——	——	——
G_{20DETA}	——	——	——
G_{30DETA}	16800	16500	16500
G_{40DETA}	16900	16900	16900
G_{50DETA}	16900	16800	16400
G_{60DETA}	16500	16800	16900
G_{70DETA}	17400	16600	18600
G_{80DETA}	17400	18500	18800
G_{90DETA}	——	——	——
$SCPE_{54DETA}$	22100	23800	18200
* $\bar{M}_{cSWELL}$ calculated with (1) a modified version of Flory-Rehner eq. [71] (2) James and Guth eq. [71, 143] and (3) Herman eq. [71, 143, 144]. All these equations include the correction for free ends.			

Table 4.31 Values of $\bar{M}_{cSWELL}$ for G_{DETA}.

The results show that the crosslinking behaviour of this system is very similar to the previous systems reported in this chapter (A_{DETA}, D_{DETA} and F_{DETA} sections 4.2.1 (p.105-6), 4.3.1 (p. 124-5), 4.4.1 (p. 138)). The relatively large values of $\bar{M}_{cSWELL}$ indicate that only a small number of crosslinks per chain were formed. Table 4.31 also shows that there is no strong dependence of crosslinking upon blend composition. Similar behaviour was also observed in the previous systems. Systems A_{DETA}, D_{DETA},

F_{DETA} and G_{DETA} all show rather similar values of $\bar{M}_{cSWELL}$; the second component does not strongly affect the crosslinking behaviour of the SCPE used.

4.5.2 MISCIBILITY BEHAVIOUR

After visual inspection the unmodified blend was transparent up to a 60% content of $SCPE_{54}$, above this composition the blend was slightly hazy. As in the previous blends (sect 4.2.2 (p. 108), 4.3.2 (p. 125) and 4.4.2 (p. 138)) all compositions developed a brownish discolouration after crosslinking.

The number of T_gs present in the blend before and after crosslinking were determined with the DMTA and the Rheovibron, the results are shown in tables 4.32 and 4.34 and figures 4.61 to 4.63. As PBA_{HMW} is very soft, the blend compositions containing 70 to 90% PBA_{HMW} were not analysed with the Rheovibron (G_{10}-G_{30} or G_{10DETA}-G_{30DETA}) however it was possible to study them using DMTA in shearing mode. Table 4.32 and figure 4.62 show that, as in the case of system *F*, only one T_g was present up to 60% $SCPE_{54}$ content, above this composition two peaks which were moved towards each other in comparison to the T_gs of the components were always observed. Due to the similarity of *G* to *F*, the Rheovibron results were also compared with Chai and Walsh's[27,137] PBA/CPE20. The comparison is shown in table 4.33. Once again despite the 25° difference between the T_gs of the chlorinated polyethylenes used in Chai's blend and in *G*, which increases the T_gs for the whole composition range in the PBA/CPE20 blend, the behaviour observed in both systems is quite similar. The only difference observed was again for the composition containing 90% W/W of the chlorinated polyethylene. In G_{90} it was possible to observe a very small hump overlapping a sharp peak while the corresponding sample in Chai's work showed only a sharp peak. Table 4.34 and figure 4.63 show the results for the crosslinked blend. From the composition containing 70% W/W $SCPE_{54}$ onwards, two peaks inwardly shifted with respect to the peaks of the pure components were observed. This behaviour suggests that these blend compositions are semicompatible. As before, the composition and mass balance of the phases present in *G* and G_{DETA} were calculated using the Fox equation and the DMTA data. These results are shown in tables 4.35 and 4.36 respectively. Examination of these data shows that the two phases present in each sample are richer in $SCPE_{54}$. The mass balance analysis, shown in these tables, indicates that as the amount of $SCPE_{54}$ increases in the sample, a larger quantity of this polymer is present in the phase with higher T_g.

	Rheovibron			DMTA		
Sample *	T_gs observed (° C)	Max. value tanδ	Comments	T_gs observed (° C)	Max. value tanδ	Comments
PBA_{HMW}	—	—	too soft to be measured	-26	1.88	sharp peak
G_{10}	—	—	too soft to be measured	-12	1.26	sharp peak
G_{20}	—	—	too soft to be measured	-1	1.23	sharp peak
G_{30}	—	—	too soft to be measured	1	1.32	sharp peak
G_{40}	12	1.55	sharp peak	10	1.32	sharp peak
G_{50}	25	1.73	sharp peak	22	1.71	sharp peak
G_{60}	27	1.62	sharp peak	26	1.58	sharp peak
G_{70}	31, 59	0.47, 0.90	peaks overlap	29, 57	0.48, 0.74	peaks overlap
G_{80}	26, 63	0.15, 1.25	small hump overlapping with sharp peak	25, 62	0.21, 1.22	small hump overlapping with sharp peak
G_{90}	25, 67	0.08, 1.45	v. small hump overlapping with sharp peak	12, 56	0.10, 1.40	v. small hump overlapping with sharp peak
$SCPE_{54}$	53	1.45	sharp peak	61	1.86	sharp peak

* For explanation of the nomenclature see tables 3.1 and 3.6 pp 57 and 68 respectively.

Table 4.32 Comparison of the T_gs of system *G* obtained with the Rheovibron and the DMTA.

* This work code	T_gs observed (°C)	Max. value tanδ	Comments	[27, 137] PBA/CPE20 %W/WCPE20	T_gs observed (°C)	Max. value tanδ	** Comments
G_{50}	25	1.73	sharp peak	0.4612	32	1.76	sharp peak
G_{60}	35	1.62	sharp peak	0.6409	54	1.76	sharp peak
G_{90}	25, 67	0.08, 1.42	v. small hump overlapping sharp peak	0.8473	80	1.45	sharp peak
$SCPE_{54}$	53	1.45	sharp peak	1.0000	78	1.77	sharp peak

* For explanation of the nomenclature see tables 3.1 and 3.6 pp 57 and 68 respectively.
**Data only reported approximately 20 degrees below and above T_g.

Table 4.33 Comparison between the T_gs and tanδ values of blend *G* and those obtained in PBA/CPE20 [27, 137]

	Rheovibron			DMTA		
Sample *	T_gs observed (° C)	Max. value tanδ	Comments	T_gs observed (° C)	Max. value tanδ	Comments
PBA_{LMW}	—	—	too soft to be measured	-26	1.88	sharp peak
G_{10DETA}	—	—	too soft to be measured	-11	1.15	sharp peak
G_{20DETA}	—	—	too soft to be measured	0	1.14	sharp peak
G_{30DETA}	—	—	too soft to be measured	0	1.40	sharp peak
G_{40DETA}	13	1.36	sharp peak	10	1.59	sharp peak
G_{50DETA}	25	1.36	sharp peak	23	1.40	sharp peak
G_{60DETA}	24	0.98	sharp peak	21	0.75	sharp peak
G_{70DETA}	27, 70	0.30, 0.73	peaks overlap	19, 63	0.21, 0.60	peaks overlap small hump
G_{80DETA}	68	0.95	only one small peak was apparent	22, 67	0.20, 0.96	overlapping with sharp peak
G_{90DETA}	14, 70	0.06, 1.07	very small hump overlapping with sharp peak	20, 69	0.11, 1.08	very small hump overlapping with sharp peak
$SCPE_{54DETA}$	56	1.07	sharp peak	61	0.92	sharp peak

* For explanation of the nomenclature see tables 3.1 and 3.6 pp 57 and 68 and section 3.4 p 71-2.

Table 4.34 Comparison of the T_gs of G_{DETA} obtained with the Rheovibron and the DMTA.

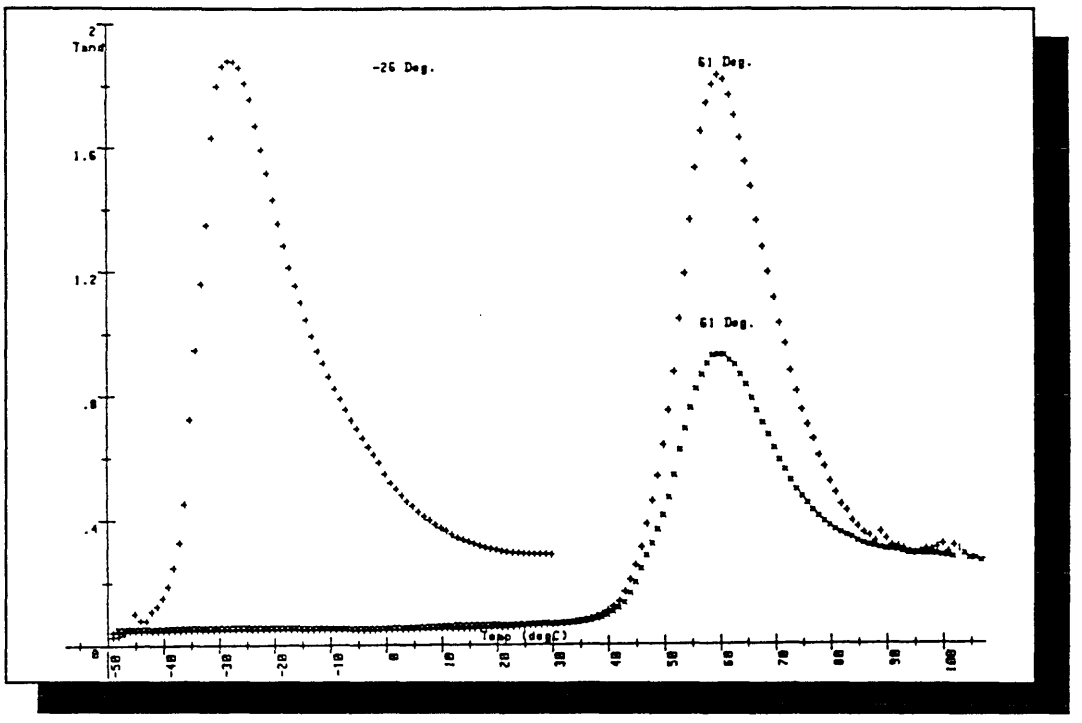

Figure 4.61 T_gs of PBA_{HMW} (-26°C(+)), $SCPE_{54}$ (61°C(+)) and $SCPE_{54DETA}$ (61°C(x)).

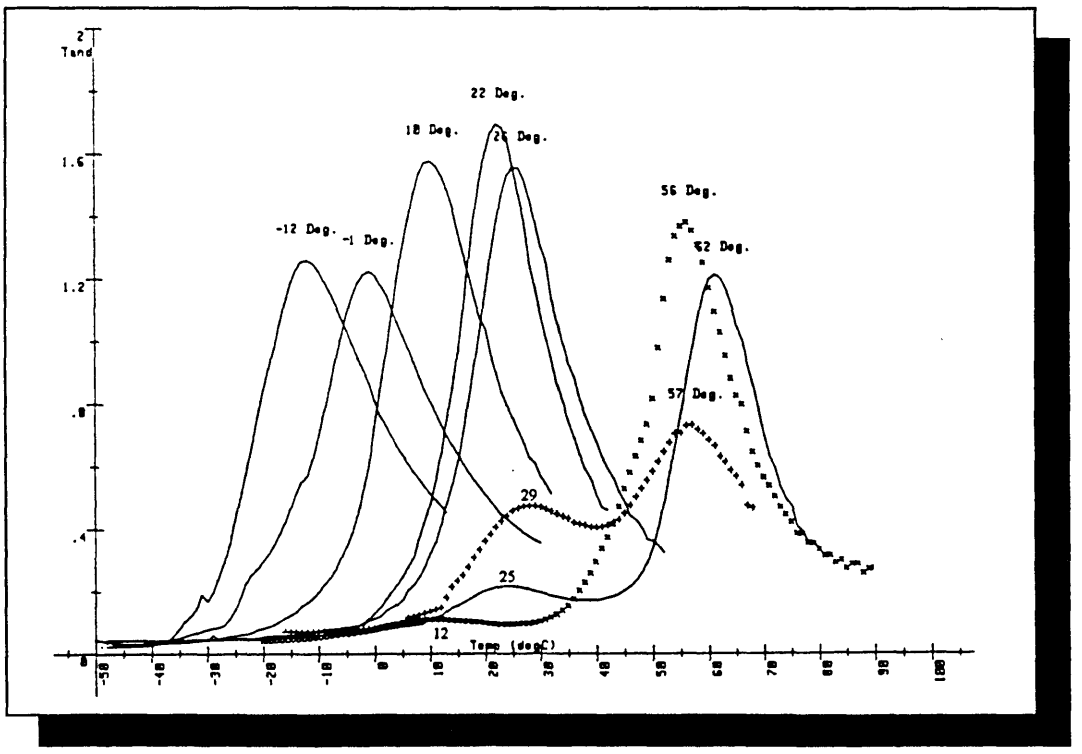

Figure 4.62 T_gs for the whole composition range of system G ($SCPE_{54}/PBA_{HMW}$). G_{10} (-12°C(-)), G_{20} (-1°C(-)), G_{30} (1°C(not shown)), G_{40} (10°C(-)), G_{50} (22°C(-)), G_{60} (26°C(-)), G_{70} (29, 57°C(+)), G_{80} (25, 62°C(-)), G_{90} (12, 56°C(x)).

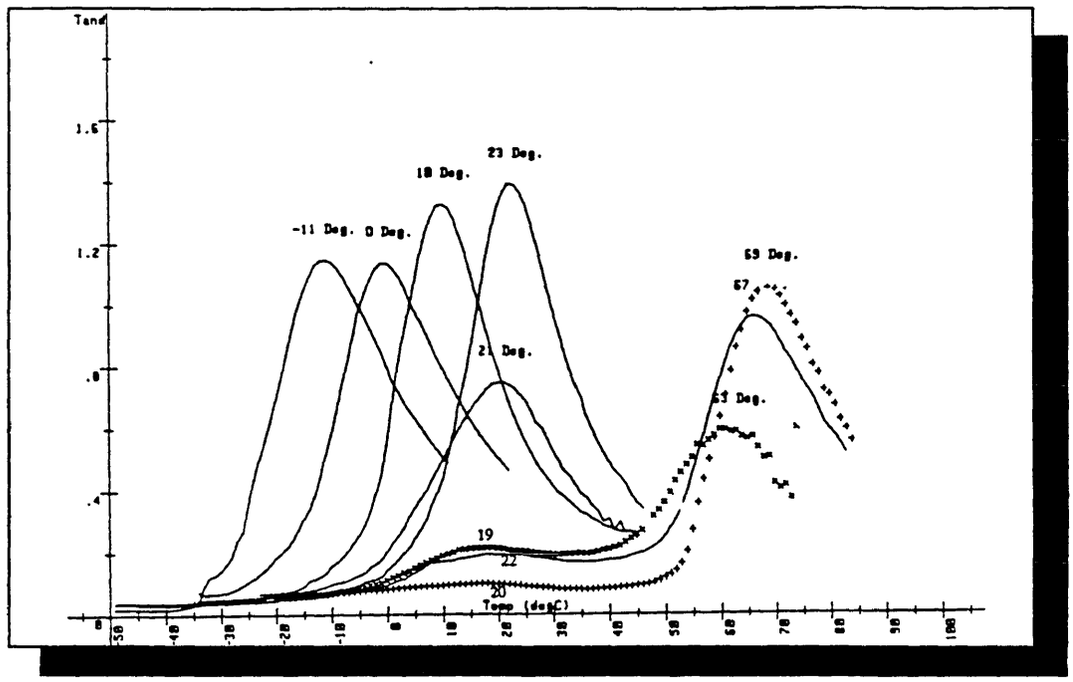

Figure 4.63 T_gs for the whole composition range of system G_{DETA} ($SCPE_{54DETA}$/PBA_{HMW}).G_{10DETA} (-11°C(–)), G_{20DETA} (0°C(–)), G_{30DETA} (0°C(not shown) G_{40DETA} (10°C(–)), G_{50DETA} (23°C(–)), G_{60DETA} (21°C(–)), G_{70DETA} (19, 63°C(x)), G_{80DETA} (22, 67°C(–)), G_{90DETA} (20, 69°C(+)).

Sample*	T_gs °C	Max value Tanδ	$SCPE_{54}$/PBA_{HMW}	
			** Composition	*** Mass balance g/g
G_{70}	29 57	0.48 0.74	69 / 31 97 / 3	0.66 / 0.29 0.04 /0.001
G_{80}	25 62	0.21 1.22	66 / 34 100 / 0	0.39 / 0.20 0.41/ 0
G_{90}	12 56	0.10 1.40	51 / 49 96 / 4	0.07 / 0.06 0.83 / 0.03

*For explanation of the nomenclature see tables 3.1 and 3.6 pp 57 and 68 and section 3.4, p. 71-2.

**The number at the left hand side of the slash gives the composition of $SCPE_{54}$ and the number at the right gives the composition of PBA_{HMW}.

***Calculation based on 1 g of the original mixture of both polymers.

Table 4.35 Composition and mass balance of the two phases present in samples G_{70} to G_{90}.

Sample*	Tgs °C	Max value Tanδ	$SCPE_{54DETA}$ /PBA_{HMW}	
			** Composition	*** Mass balance g/g
G_{70DETA}	19 63	0.21 0.60	59 / 41 100 / 0	0.43 / 0.30 0.27 / 0
G_{80DETA}	22 67	0.20 0.96	62 / 38 100 / 0	0.33 / 0.20 0.47 / 0
G_{90DETA}	20 69	0.11 1.08	60 / 40 100 / 0	0.15 / 0.10 0.75 / 0

* For explanation of the nomenclature see tables 3.1 and 3.6 pp 57 and 68 and section 3.4 pp 71-2.

** The number at the left hand side of the slash gives the composition of $SCPE_{54DETA}$ and the number at the right gives the composition of PBA_{HMW}.

***Calculation based on 1 g of the original mixture of both polymers.

Table 4.36 Composition and mass balance of the two phases present in samples G_{70DETA} to G_{90DETA}

4.5.3 STATIC AND DYNAMIC MECHANICAL PROPERTIES

Figure 4.64 shows the Young's moduli Y (Nm^{-2}) as a function of composition for G and G_{DETA}. The measurements were performed on the Instron at 0.05 mm-min^{-1}. Due to the softness of PBA_{HMW} it was only possible to measure Y in the unmodified samples from 60% W/W $SCPE_{54}$ content onwards. After crosslinking it was possible to measure Y from 50% W/W $SCPE_{54}$ content onwards. Although the data obtained are limited, it may be seen that Y increases rapidly above 60% W/W $SCPE_{54}$. Despite the scatter in these results, figure 4.64 also shows an increase in Y with crosslinking. Figures 4.65 to 4.68 show logE' as a function of temperature. Figure 4.65 shows the logE' curves for $SCPE_{54}$ and $SCPE_{54DETA}$. As PBA_{HMW} is very soft the shear modulus G' was determined and logG' is shown in the figure 4.65. Figures 4.66 and 4.67 show the results for G and G_{DETA} respectively. Figure 4.68 compares the logE' curves for some compositions of G and G_{DETA}. Figures 4.66 and 4.67 show the expected increase in modulus with increasing $SCPE_{54}$ content confirming the behaviour observed for the previous systems discussed here. The number and abruptness of the inflections of the logE' traces reflect the miscibility behaviour for each blend in the same way as in previous systems.

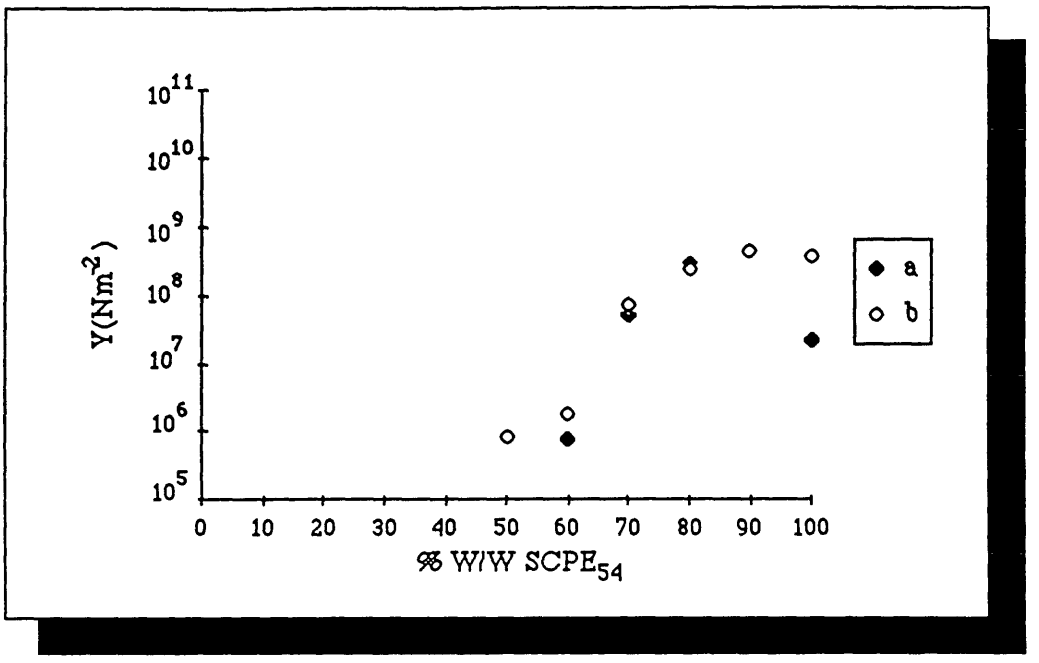

Figure 4.64 The tensile Young's moduli (Y) (Nm^{-2}) of blends (a) *G* and (b) G_{DETA} as a function of composition at a crosshead rate of 0.05 mm-min^{-1}.

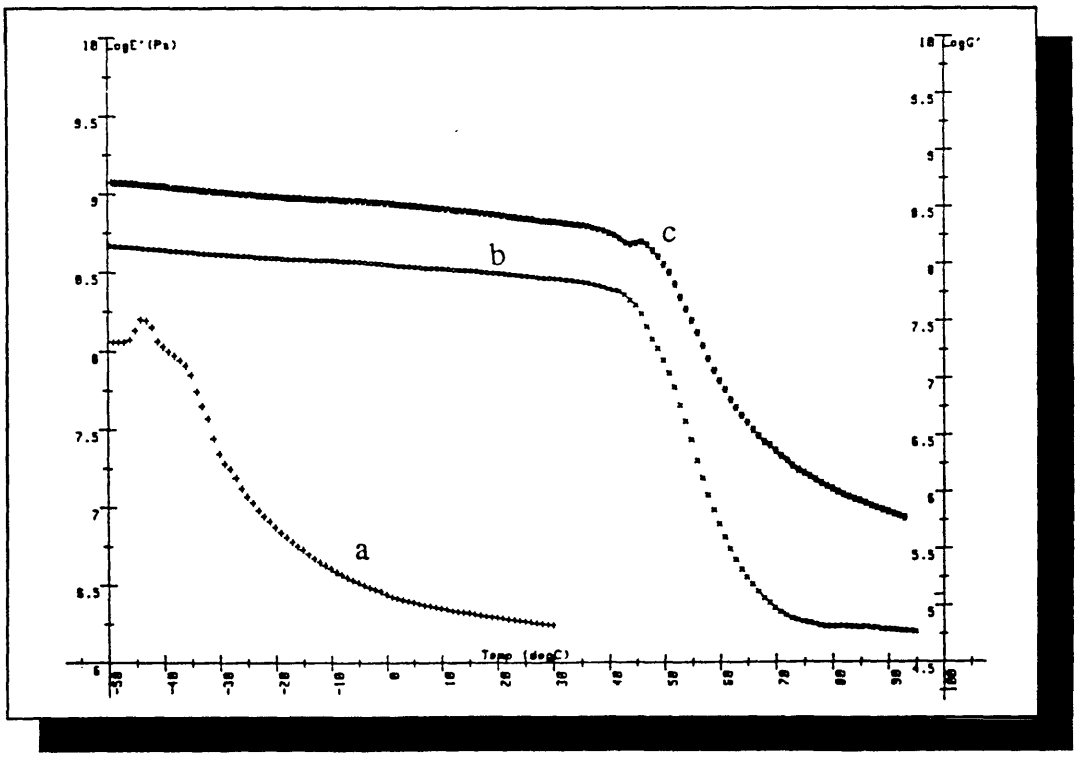

Figure 4.65 Values of logE' vs temperature for: PBA$_{HMW}$ (a+), SCPE$_{54}$ (bx) and SCPE$_{54DETA}$ (c*).

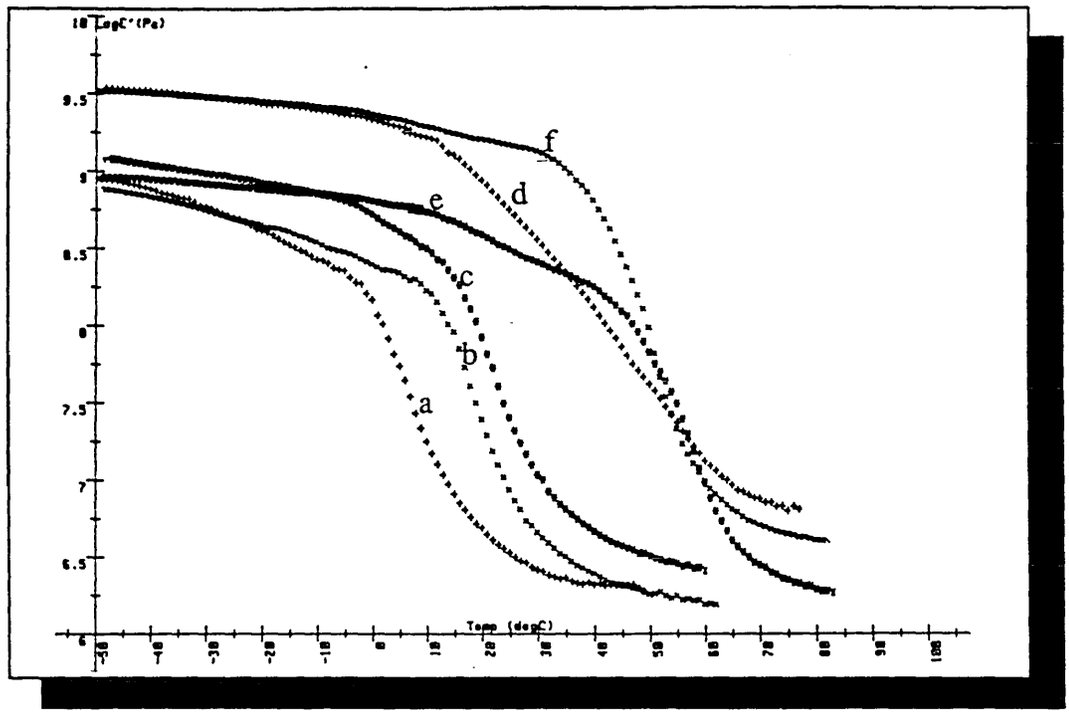

Figure 4.66 Values of logE' vs temperature for some compositions of system G ($SCPE_{54}$/ PBA_{HMW}). G_{40} (a+), G_{50} (bx), G_{60} (c*), G_{70} (d+),G_{80} (e*) and G_{90}(fx).

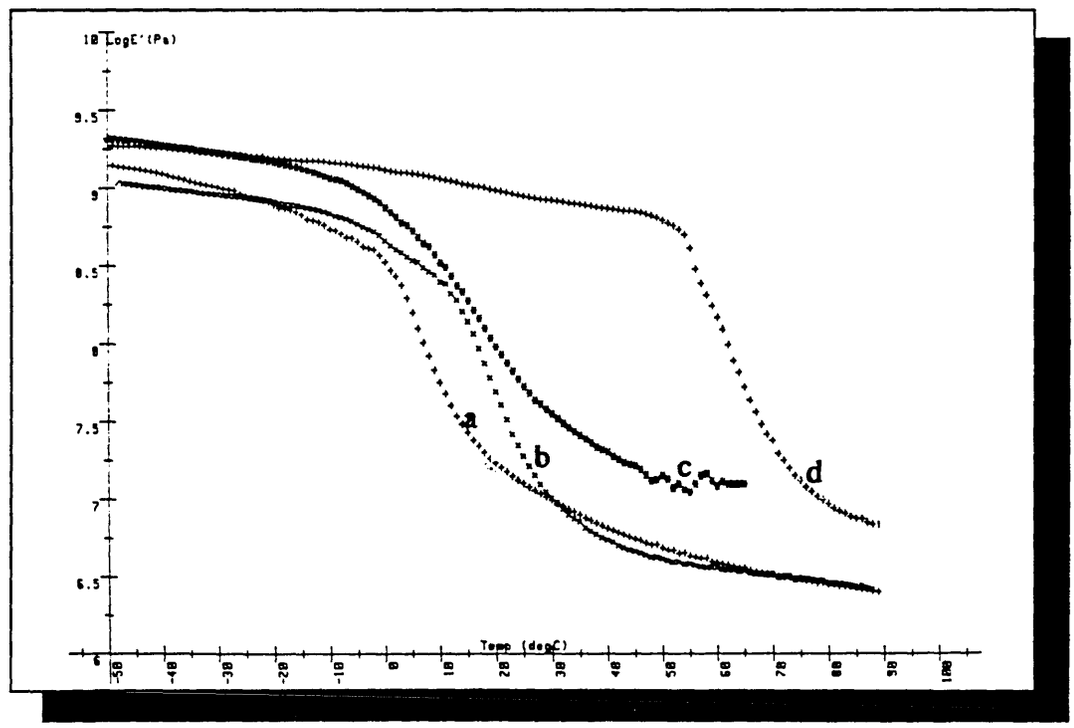

Figure 4.67 Values of logE' vs temperature for some compositions of system G_{DETA} ($SCPE_{54DETA}$/PBA_{HMW}). G_{50DETA} (a+), G_{60DETA} (bx), G_{70DETA} (c*) and G_{90DETA} (d+).

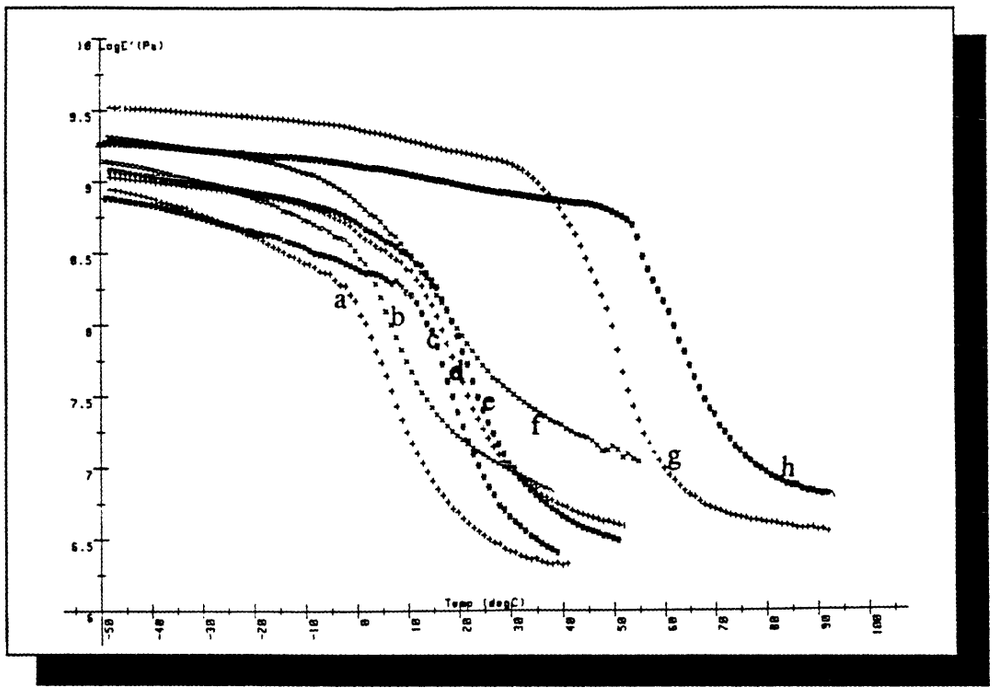

Figure 4.68 Comparison of logE' for some compositions of G and G_{DETA}. G_{40} (a+), G_{40DETA} (bx), G_{50} (c*), G_{50DETA} (d+), G_{60} (e*), G_{60DETA} (fx), G_{90} (g+), G_{90DETA} (h*).

4.5.4 CLOUD POINT MEASUREMENTS

The intensity vs temperature plots obtained for some compositions before and after crosslinking are shown in figure 4.69. This figure shows clearly a decrease in the slope of the intensity of the scattered light and a slight increase in the CP temperatures of the samples after crosslinking. Figures 4.70 and 4.71 show the CP data obtained with the turbidimeter for G and G_{DETA} respectively. The laser-SALS results for G and G_{DETA} are those shown in figure 4.72. The bars represent the data for G, the rectangles show the CP for some G_{DETA} compositions. The data in all these curves cannot be represented by a single smooth curve. This is apparently a consequence of phase separation from 60% $SCPE_{54}$ content onwards. As shown in tables 4.35 and 4.36 (p. 162-3), at higher $SCPE_{54}$ contents the two phases have approximately constant composition and the CP observed in this composition region corresponds to the phase of lower T_g. This will be discussed further in section 5.5.4 (p. 220). Comparison of the data for the samples before and after being crosslinked, show an increase in the CP temperatures with crosslinking. An increase of 2 to 9^o was observed with the turbidimeter. A more substantial increase was observed with the laser-SALS (10 to 30^o).

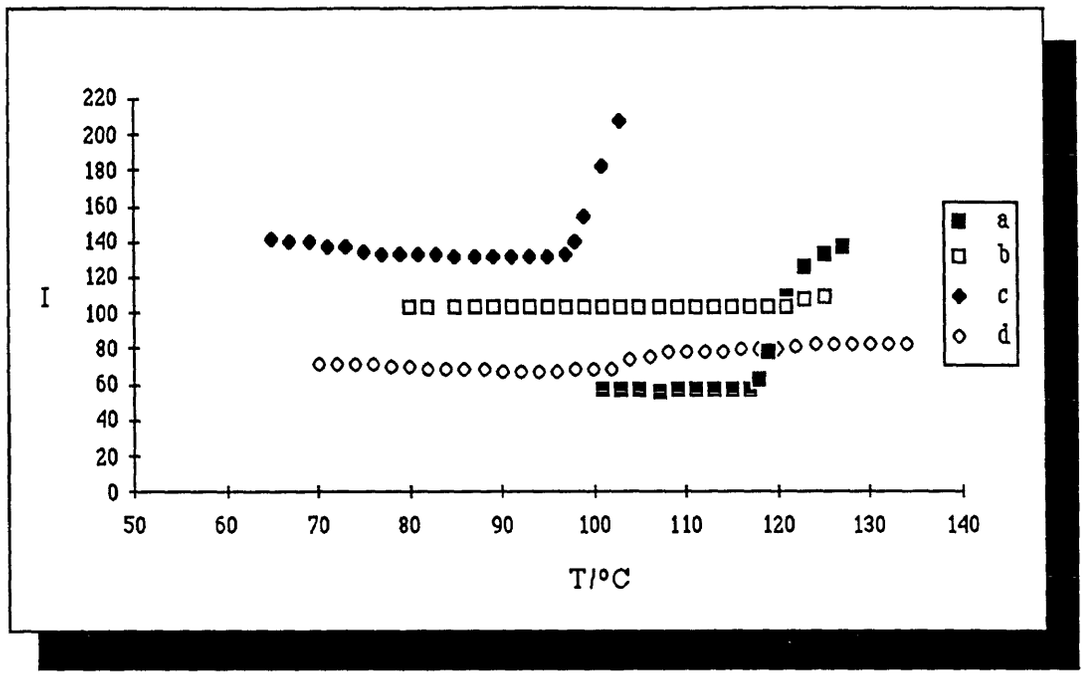

Figure 4.69 Cloud point curves obtained with the turbidimeter (heating rate=0.1°C/min) for: (a) G_{10} (CP=118°C), (b) G_{10DETA} (CP=122°C), (c) G_{30} (CP=97°C), (d) G_{30DETA} (CP=102°C).

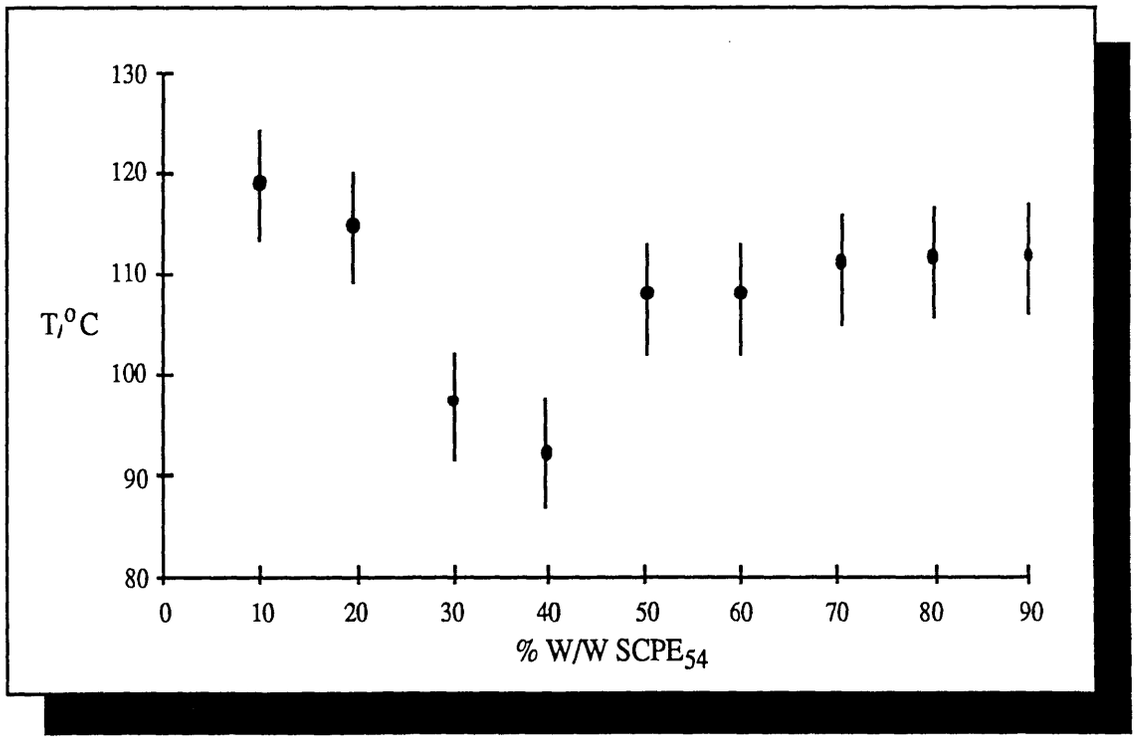

Figure 4.70 Cloud point temperatures as a function of composition for blend *G*. The data were obtained with the turbidimeter at a heating rate of 0.1 °C/min.

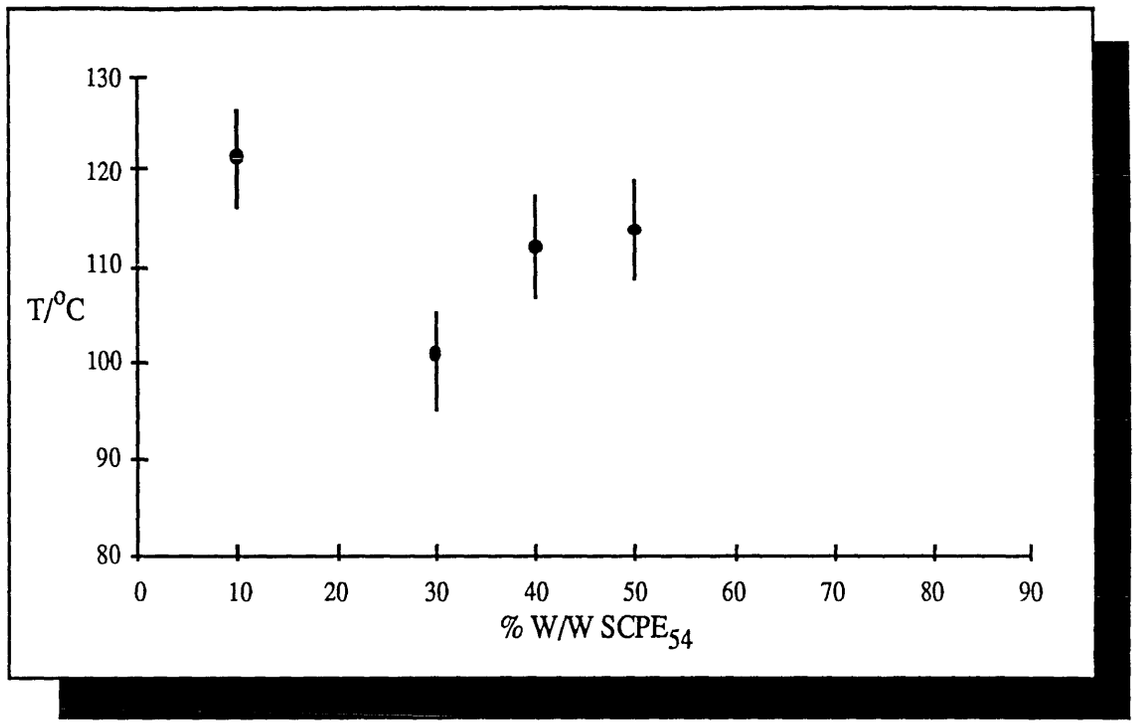

Figure 4.71 Cloud point temperatures as a function of composition for blend G_{DETA}. The data were obtained with the turbidimeter at a heating rate of 0.1 °C/min.

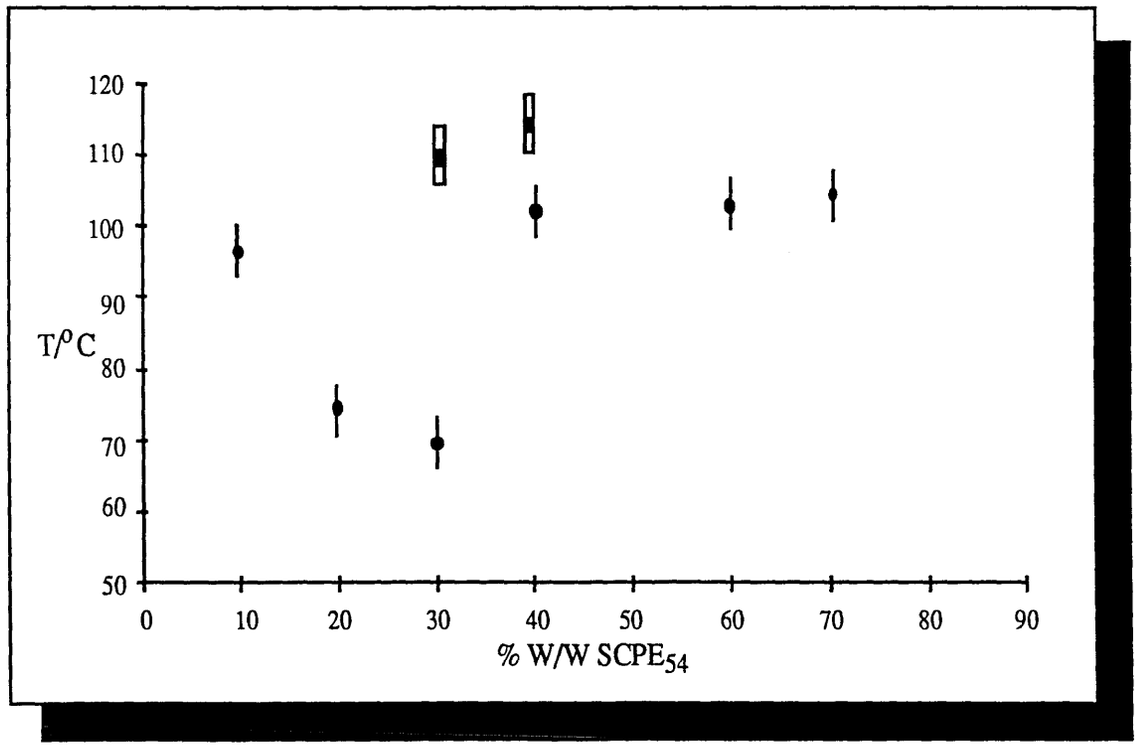

Figure 4.72 Cloud point temperatures as a function of composition for blend G (bars) and for some compositions of G_{DETA} (rectangles). The data were obtained with the laser-SALS at a heating rate of 1°C/min.

4.5.5 DOMAIN SIZE MEASUREMENTS

The intensity vs θ plots for G_{40} and G_{40DETA} at various temperatures are shown in figures 4.73 and 4.74. These data were obtained by reprocessing the results from the laser-SALS experiments. Inspection of the data for G_{40} in figure 4.73 shows that during phase separation the presence of a peak was evident at 132°C. With the exception of G_{10} to G_{30}, which did not show a peak in the range between 5 to 35°, similar behaviour was observed for the rest of the blend. After crosslinking, only two compositions were studied: G_{30DETA} and G_{40DETA}. Figure 4.74 shows that in the case of G_{40DETA} the appearence of peaks during phase separation was not evident. Similar behaviour was observed in G_{30DETA}.

Table 4.37 shows the correlation length (d) for the blend before and after crosslinking. The data were measured at 30°C above the CP temperature for each composition. For the samples showing a peak during phase separation, d was obtained according to the procedure in section 3.8, p. 90. For the samples which did not show a peak in the angular range studied, it was assumed that such peaks may have been present at angles larger than 35°. This will correspond to d smaller than 0.72×10^4 Å.

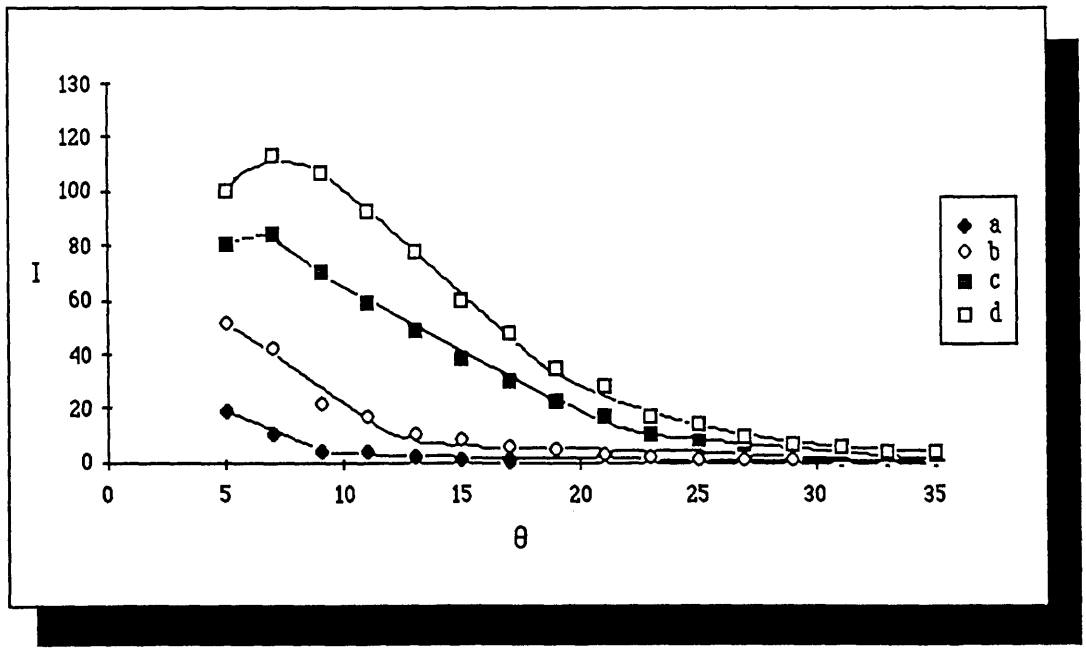

Figure 4.73 Intensity of the scattered light (I) as a function of angle (θ) for G_{40} at (a) 25°C, (b) 113°C, (c)132°C and (d) 143°C.

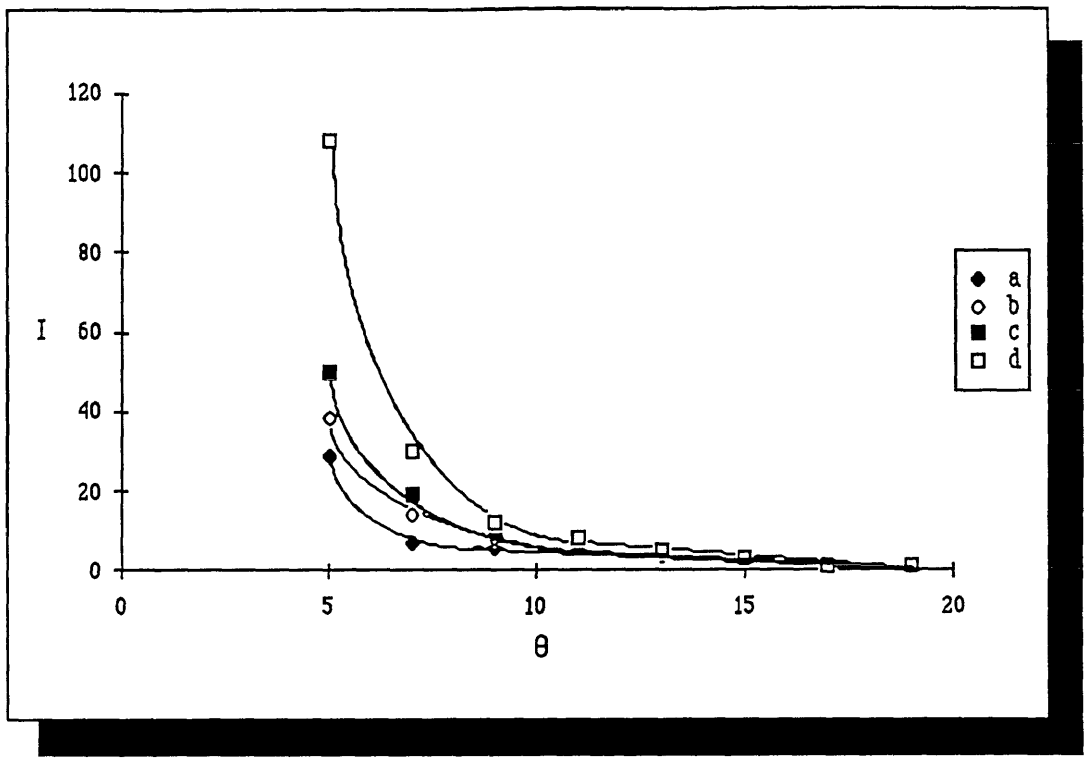

Figure 4.74 Intensity of the scattered light (I) as a function of angle (θ) for G_{40DETA} at (a) 28°C, (b) 106°C, (c) 112°C and (d) 142°C.

Sample	CP temperature (°C)	Correlation length (Å)	At temperature (°C)
Uncrosslinked blend			
G_{10}	118	$< 0.752 \times 10^4$	148
G_{20}	120	$< 0.752 \times 10^4$	150
G_{30}	71	$< 0.752 \times 10^4$	101
G_{40}	113	3.70×10^4	143
G_{50}	—	—	—
G_{60}	112	0.796×10^4	142
G_{70}	113	0.752×10^4	143
G_{80}	111	1.13×10^4	141
G_{90}	—	—	—
Crosslinked blend			
G_{30DETA}	112	$< 0.752 \times 10^4$	142
G_{40DETA}	90	$< 0.752 \times 10^4$	120

Table 4.37 Correlation lengths (d) obtained with the laser-SALS for G and G_{DETA}. The data were measured 30°C above the CP temperature of each sample. (The values of CP used are those obtained with the laser-SALS).

4.6 $SCPE_{54}/PMMA_{1.4}$ (SYSTEM *C*)

Of the systems studied so far *C* is the only one in which both components have T_gs above room temperature (SCPE $_{54}$ T_g=61°C, $\bar{M}_n$=33,000; $PMMA_{1.4}$ T_g=100°C, $\bar{M}_n$=73,000). This fact introduces certain restrictions not only experimentally, but also in the interpretation of results. A similar system to *C*, PMMA1.4/CPE16, was previously studied by Chai and Walsh [26,137] and was found to be miscible. (CPE16= chlorinated polyethylene containing 51.6% w/w of Cl). In the present work *C* was solvent cast in MEK and was crosslinked with *DETA* (sections 3.3.1, pp 68-9 and 3.4.3 p. 74-6).

4.6.1 DEGREE OF CROSSLINKING

Stress- strain and swelling measurements were undertaken in an attempt to determine the degree of crosslinking in the blend; however these experiments were not successful because the whole range of blend compositions are glassy at the temperatures of the measurements and the theories on which both techniques are based are not strictly applicable. A crude estimate of the degree of crosslinking was obtained in a similar way to that used in system *E* in sec 4.1.1 (pp 92-4), i.e. measuring the weight percentage of remaining undissolved residue after solvent extracting the crosslinked blend. The results in figure 4.75 show that the percentage of undissolved residue increases more or less proportionally with the content of $SCPE_{54}$ present in each composition.

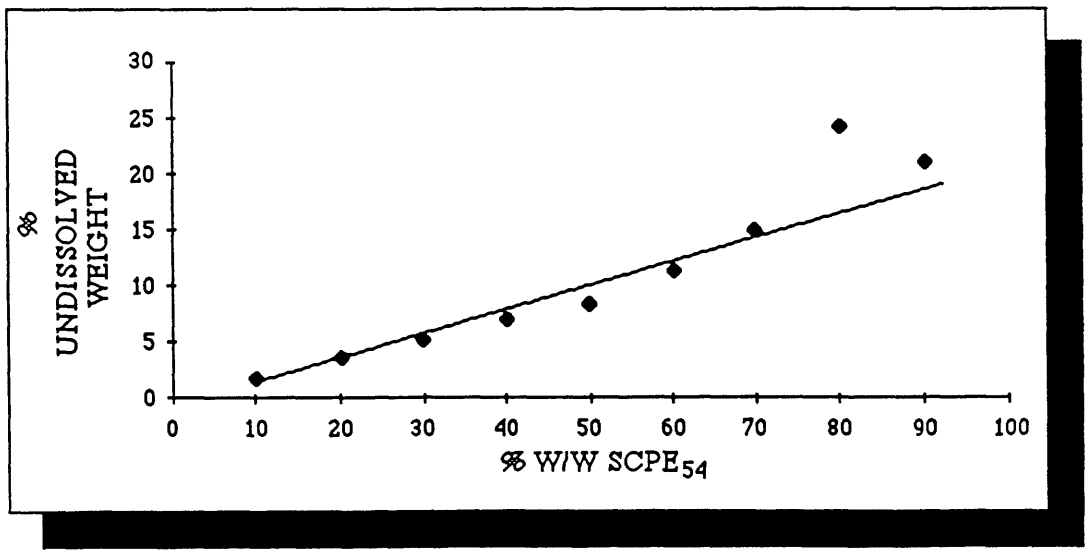

Figure 4.75 Percentage of undissolved residue as a function of $SCPE_{54}$ content for system C_{DETA}

4.6.2 MISCIBILITY BEHAVIOUR

All compositions of *C* were transparent and, as in all previous blends, developed a brownish colour after crosslinking. Phase contrast microscopy confirmed the absence of domains for *C* and C_{DETA}. The data obtained for *C* and C_{DETA} with the Rheovibron and DMTA (see tables 4.38 and 4.40 respectively) show the presence of only one T_g for the whole composition range of the blend before and after being crosslinked. This suggests that *C* is miscible for the whole composition range and that crosslinking does not affect its state of miscibility. Figure 4.76 illustrates the DSC results for *C*, once again they show the presence of only one T_g. Figures 4.77 to 4.79 show the DMTA results for some compositions of *C* and C_{DETA} respectively. A comparison between the results obtained for *C* and those of a similar system studied by Chai and Walsh, PMMA1.4/CPE16 [26,137], is shown in table 4.39. Although the values of the T_gs in PMMA1.4 /CPE16 are lower than in system *C* (the T_gs of CPE16 and $SCPE_{54}$ are 39 and 53°C respectively) inspection of these data show that the behaviour in both systems is quite similar as only one T_g was observed for all compositions.

4.6.3 STATIC AND DYNAMIC MECHANICAL PROPERTIES

Figure 4.80 (p. 178) shows the Young's moduli (Y (Nm^{-2})) for *C* and C_{DETA} (crosshead rate of 0.05 mm min^{-1}). Inspection of these data show, despite the scatter, that Y decreases linearly as the content of $SCPE_{54}$ (component of lower Y) increases in the mixture. This figure also shows that the moduli of the samples studied increases with crosslinking. The plots of logE' as a function of temperature are shown in figures 4.81 to 4.84 (pp 180-1). Figure 4.81 shows the logE' curves for the pure components. Figures 4.82 and 4.83 show the curves for C_{40}, C_{60} and C_{70} before and after crosslinking respectively. Examination of these figures shows that the logE' curves shift upwards as the content of $PMMA_{1.4}$ increases in the sample. All the curves, in both figures, are steep and show only one inflection point which corresponds to the sole T_g present in these samples. Figure 4.84 compares the logE' curves for the compositions containing 60 and 70% $SCPE_{54}$ before and after crosslinking. As in all the systems previously studied (see sections 4.2.3 (pp 115-8), 4.3.3 (pp 126-35), 4.4.3 (pp 139-48) and 4.5.3 (pp 163-6)) the increment of E' with crosslinking was clearly observed especially at the rubbery plateau.

	Rheovibron			DMTA		
Sample*	T_gs observed (° C)	Max. value tanδ	Comments	T_gs observed (° C)	Max. value tanδ	Comments
$PMMA_{1.4}$	103	1.26	broad peak	100	1.11	broad peak
C_{10}	97	1.32	broad peak	—	—	—
C_{20}	91	1.30	broad peak	99	1.01	broad peak
C_{30}	86	1.30	broad peak	88	1.20	broad peak
C_{40}	80	1.25	broad peak	75	0.90	broad peak
C_{50}	78	1.22	broad peak	—	—	—
C_{60}	70	1.20	broad peak	72	0.90	broad peak
C_{70}	67	1.19	broad peak	64	0.90	broad peak
C_{80}	50	1.17	broad peak	—	—	—
C_{90}	52	1.02	broad peak	—	—	—
$SCPE_{54}$	53	1.45	sharp peak	61	1.86	sharp peak

* For explanation of the nomenclature see tables 3.1 and 3.6 pp 57 and 68 respectively.

Table 4.38 Comparison of the T_gs of system *C* obtained with the Rheovibron and the DMTA.

* This work code	T_gs observed (° C)	Max value of tanδ	Comments	[27, 137] PMMA1.4/CPE16 %W/WCPE16	T_gs observed (° C)	Max value of tanδ	Comments
$PMMA_{1.4}$	103	1.26	broad peak	0	100	1.14	broad peak
C_{20}	91	1.30	broad peak	0.2474	88	1.14	broad peak
C_{50}	78	1.22	broad peak	0.5224	79	1.17	broad peak
C_{70}	67	1.19	broad peak	0.7417	56	1.24	sharper peak
C_{90}	52	1.02	broad peak	0.8999	37	1.41	sharper peak
$SCPE_{54}$	53	1.45	sharp peak	CPE16	39	—	not shown

* For explanation of nomenclature see tables 3.1 and 3.6 pp 57 and 68 respectively.

Table 4.39 Comparison of the T_gs and tanδ values observed in blends *C* [26, 137] and PMMA1.4/CPE16

	Rheovibron			DMTA		
Sample*	T_gs observed (° C)	Max. value tanδ	Comments	T_gs observed (° C)	Max. value tanδ	Comments
$PMMA_{1.4}$	103	1.26	broad peak	100	1.11	broad peak
C_{10DETA}	99	1.21	broad peak	—	—	—
C_{20DETA}	96	1.41	broad peak	90	0.93	broad peak
C_{30DETA}	94	1.18	broad peak	86	0.91	broad peak
C_{40DETA}	86	1.40	broad peak	83	0.98	sharp peak
C_{50DETA}	85	1.30	broad peak	—	—	—
C_{60DETA}	82	1.02	broad peak	80	0.86	broad peak
C_{70DETA}	80	1.32	broad peak	78	0.70	broad peak
C_{80DETA}	50	1.17	broad peak	—	—	—
C_{90DETA}	—	—	—	63	0.58	broad peak
$SCPE_{54DETA}$	56	1.07	sharp peak	61	0.92	sharp peak

* For explanation of the nomenclature see tables 3.1 and 3.6 pp 57 and 68 and section 3.4 pp 71-2.

Table 4.40 Comparison of the Tgs of C_{DETA} obtained with the Rheovibron and the DMTA.

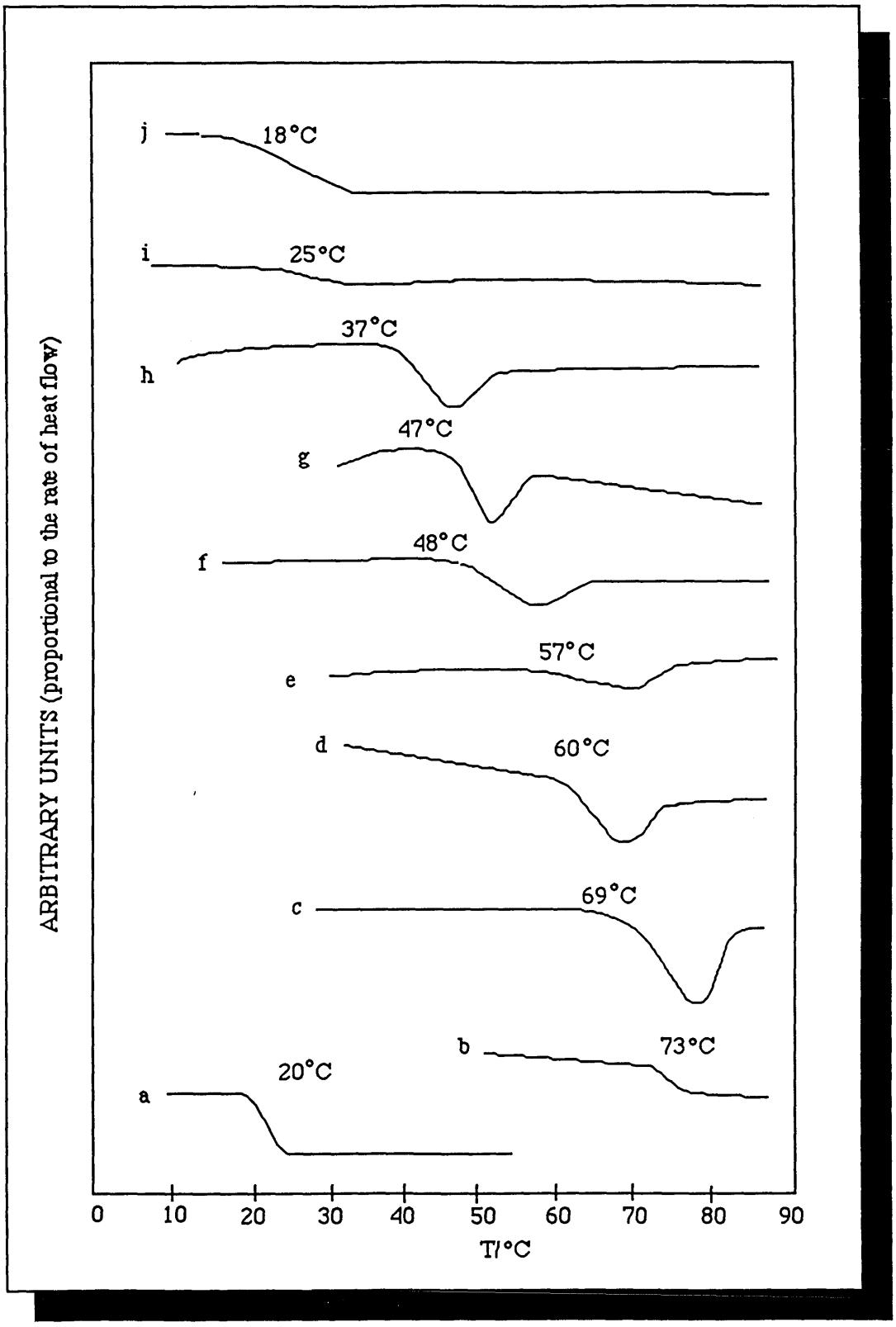

Figure 4.76 DSC curves for the system C . (a) $SCPE_{54}$, (b) $PMMA_{1.4}$, (c) C_{10} , (d) C_{20} , (e) C_{30} , (f) C_{40} , (g) C_{50} , (h) C_{70} , (i) C_{80} and (j) C_{90} .

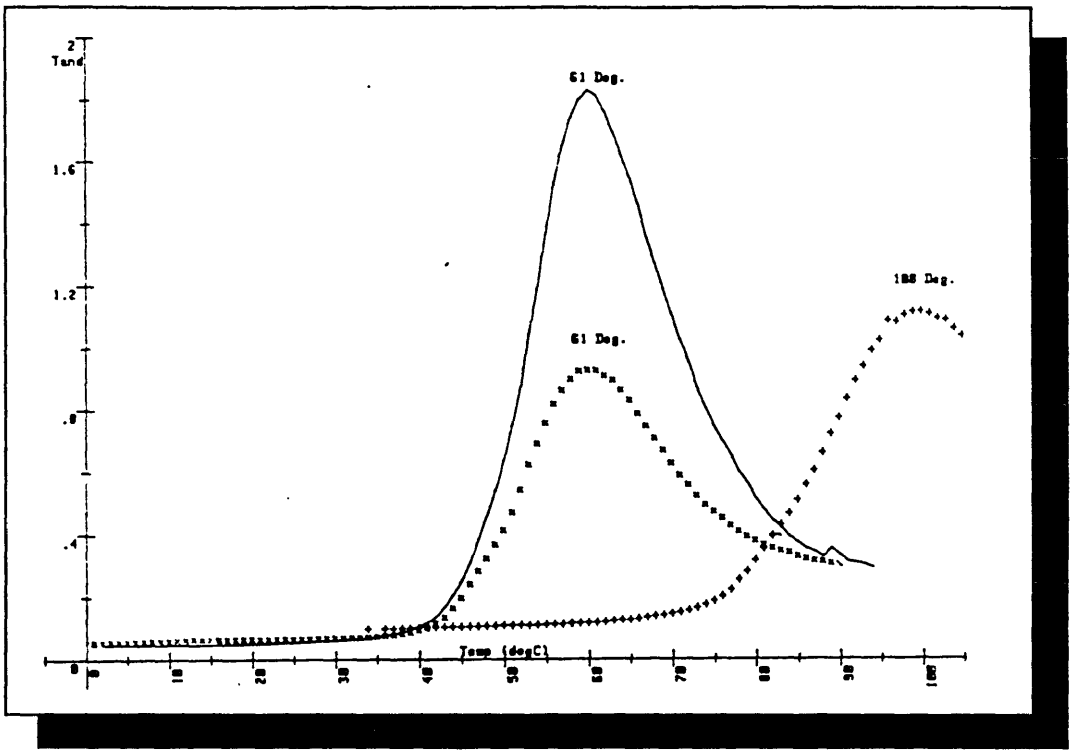

Figure 4.77 T_gs of $SCPE_{54}$ (61°C(–)), $SCPE_{54DETA}$ (61°C(x)) and $PMMA_{1.4}$ (100°C(+)).

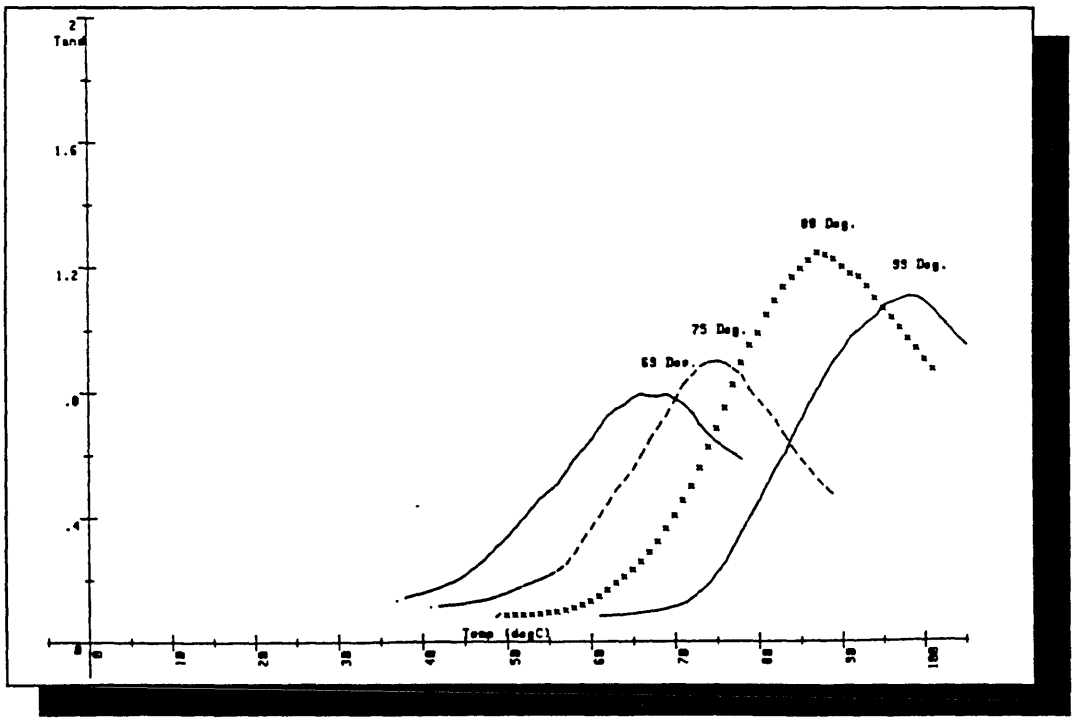

Figure 4.78 T_gs for the some compositions of system *C* ($SCPE_{54}$/$PMMA_{1.4}$). C_{20} (99°C(–)), C_{30} (88°C(x)), C_{40} (75°C(- -)) and C_{60} (69°C(–))).

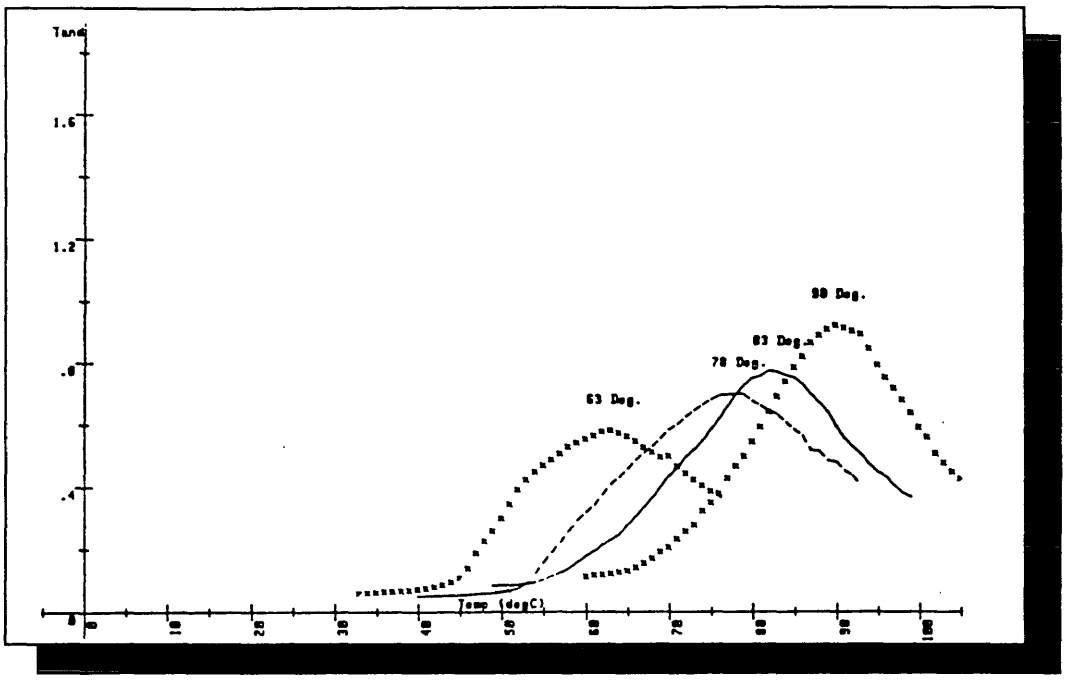

Figure 4.79 T_gs for some compositions of system C_{DETA} ($SCPE_{54DETA}/PMMA_{1.4}$). C_{20DETA} (90°C(x)), C_{40DETA} (83°C(–)), C_{70DETA} (78°C(- -)) and G_{90DETA} (63°C(x)).

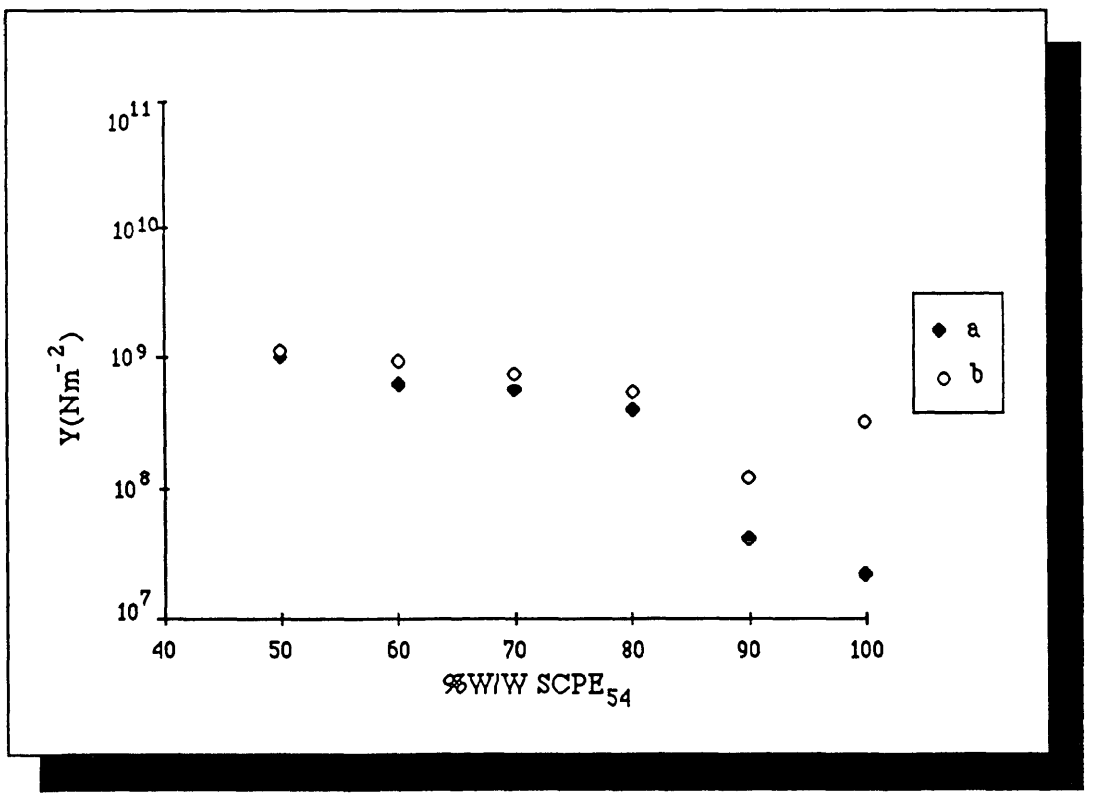

Figure 4.80 The tensile Young's moduli (Y(Nm^{-2})) of (a) blend C and (b) blend C_{DETA} as a function of composition at a crosshead rate of 0.05 mm-min^{-1}.

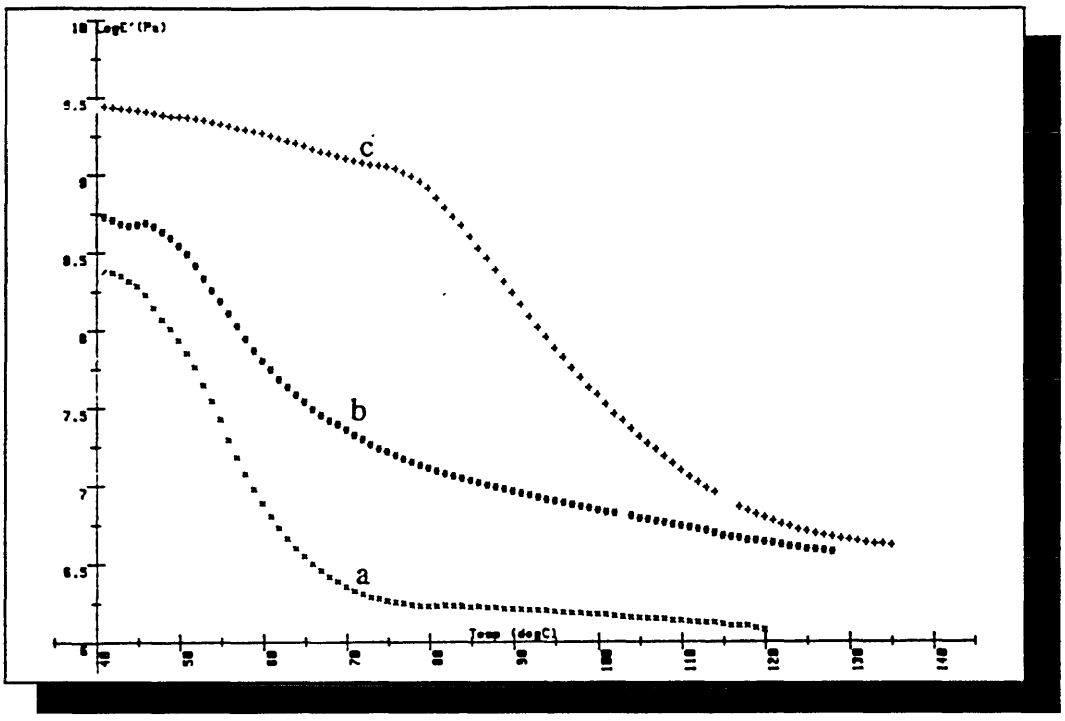

Figure 4.81 Values of logE' vs temperature for: $SCPE_{54}$ (ax), $SCPE_{54DETA}$ (b*) and PMMA1.4 (c+).

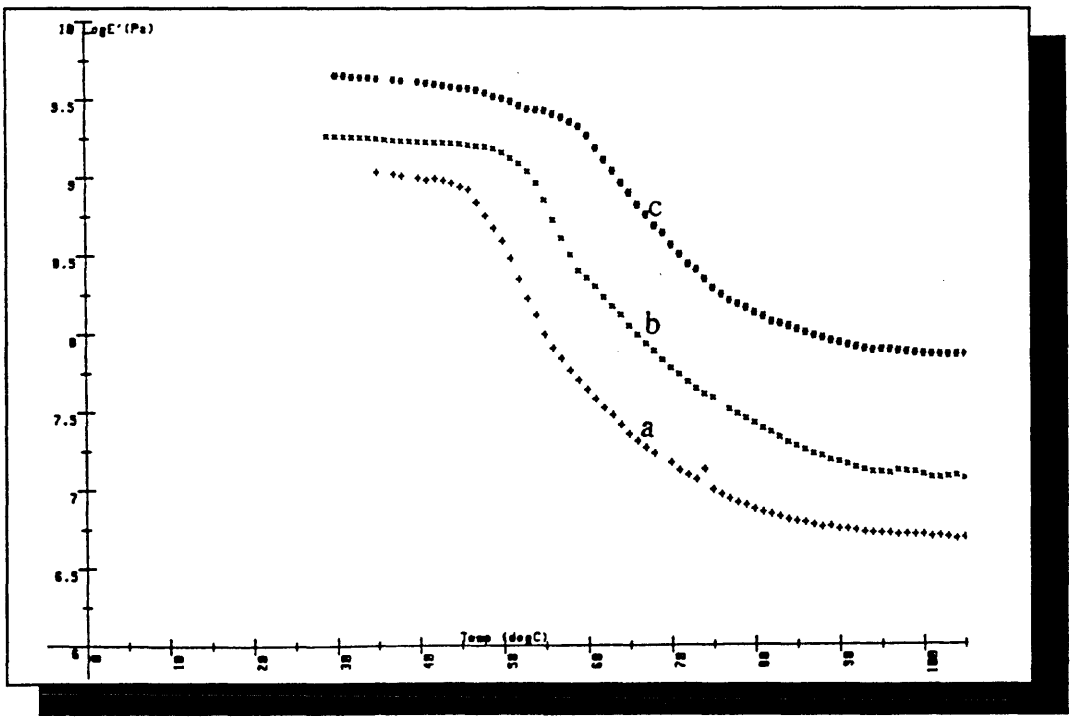

Figure 4.82 Values of logE' vs temperature for some compositions of system *C* ($SCPE_{54}$/ $PMMA_{1.4}$). C_{70} (a+), C_{60} (bx) and C_{60} (c*).

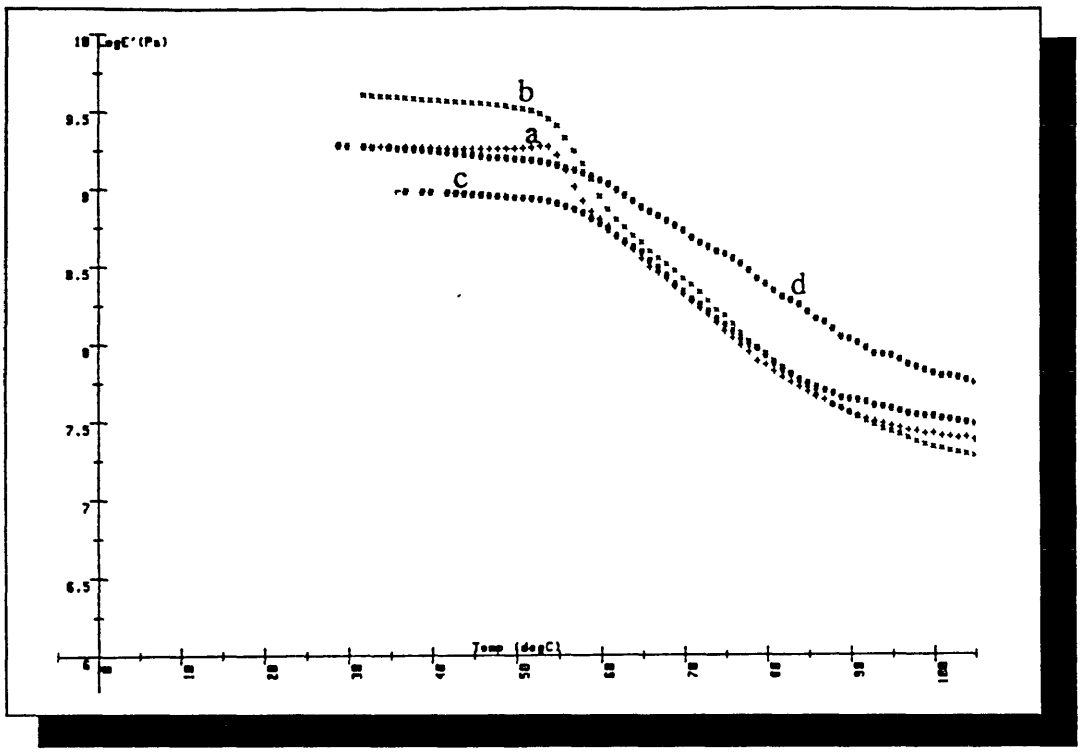

Figure 4.83 Values of logE' vs temperature for some compositions of system C_{DETA} ($SCPE_{54DETA}$/$PMMA_{1.4}$). C_{70DETA} (a+), C_{60DETA} (bx), C_{40DETA} (c*) and $C_{20\,DETA}$ (d*).

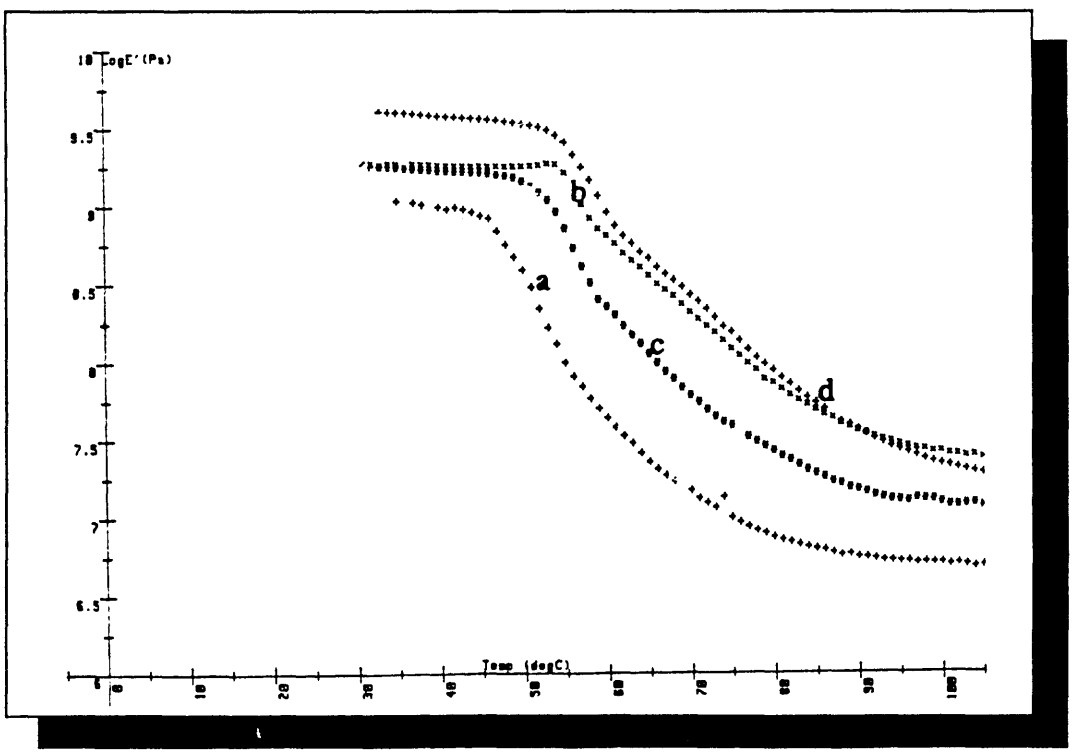

Figure 4.84 Comparison of logE' vs temperature for some compositions of C and C_{DETA}. C_{70} (a+), C_{70DETA} (bx), C_{60} (c*) and $C_{60\,DETA}$ (d+).

4.6.4 CLOUD POINT MEASUREMENTS

Although attempts were made to measure CP temperatures by turbidimetry, laser-SALS, DSC, Rheovibron and Phase Contrast microscopy none of these methods was successful in practice. It was proposed to observe phase separation *insitu* using a TEM which provided a heating stage facility. However this technique did not provide satisfactory results either because the temperature of the heating stage was very difficult to control and the polymers forming the blend degraded very quickly under the electron beam. Despite these limitations, it was possible to observe some samples phase separating. Figures 4.85 (a) and (b) show C_{60} at room temperature and at 270°C. As may be seen at room temperature there is no evidence of domains while at 270°C it is possible to see an interconnected structure, which corresponds to a sample phase separating by spinodal decomposition. Figures 4.86 (a) and (b) correspond to C_{80DETA} at room temperature and at 210°C. Once again no domains were observed at room temperature while at 210°C the presence of domains is quite clear.

Figure 4.85(a). Electron micrograph of C_{60} at room temperature.

Figure 4.85(b). Electron micrograph of C_{60} at 270°C.

Figure 4.86(a). Electron micrograph of C_{80} at room temperature.

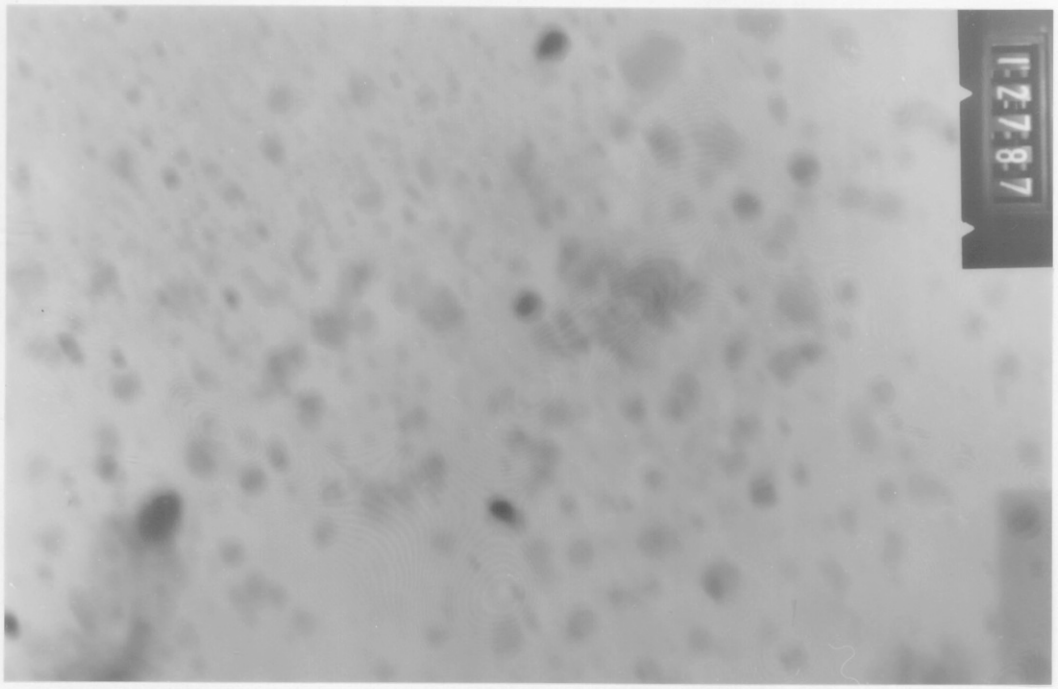

Figure 4.86(b). Electron micrograph of C_{80DETA} at 210°C.

As a last resort SAXS was used. The apparatus was available for a very brief period at Unilever Colworth House and so was used to study only some of the samples. In these experiments [138], samples were quenched at different temperatures. The data obtained from the computer linked to the source were analyzed in a similar way to those obtained by the laser-SALS. All blend compositions before being temperature treated were studied and shown to be one phase. C_{20} and C_{40} showed phase separation around 160°C and 150°C respectively and C_{40DETA} at 160°C. Figure 4.87 shows the intensity of the scattered X-rays vs Q for C_{40} and C_{40DETA} at room temperature and at the temperatures of phase separation. Peak (a) corresponds to parasitic scattering measured in the equipment with no sample present. Peaks (b) and (c) correspond to C_{40} and C_{40DETA} at room temperature. The intensity of the scattered rays in these two blends is very low. This suggests that the samples are one phase. Peaks (d) and (e) correspond to C_{40} and C_{40DETA} at 150 and 160°C respectively. The intensity of the scattered radiation in these two samples had increased considerably which suggests that at those temperatures the samples are phase separating.

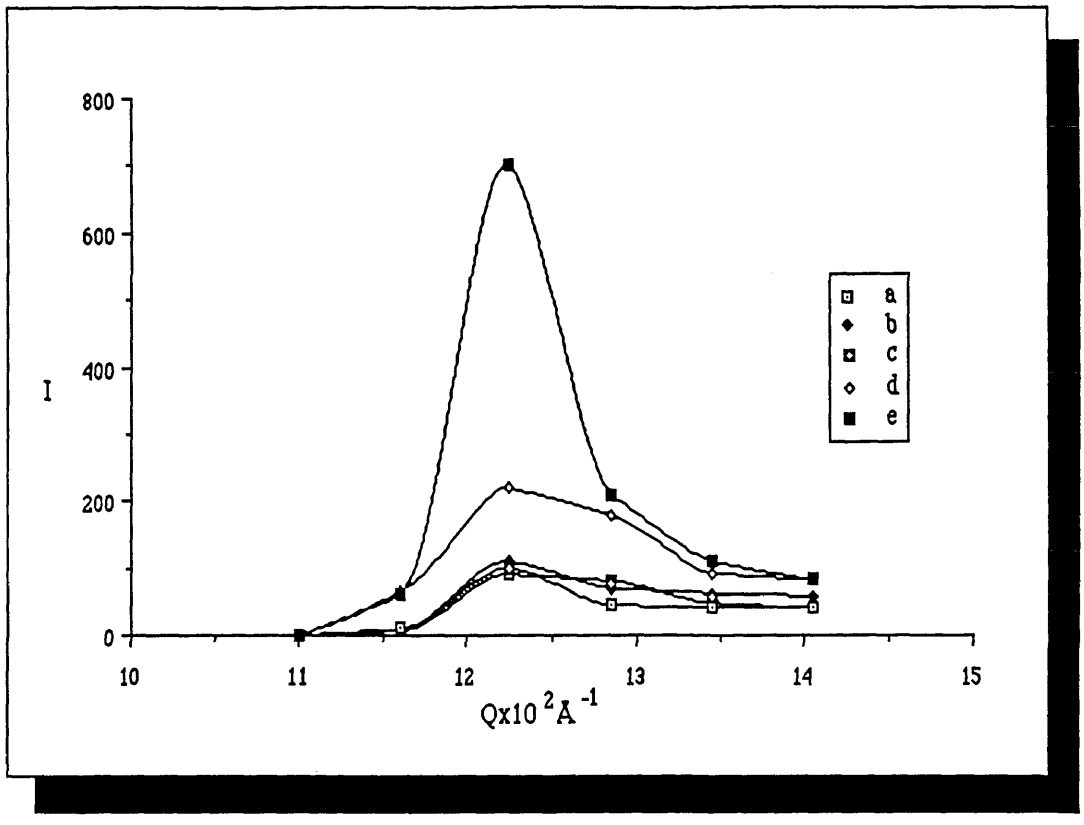

Figure 4.87 Intensity of scattered X-rays vs Q for: (a) an empty cell, (b) C_{40}, (c) C_{40DETA}, (d) C_{40} at 150°C and (e) C_{40DETA} at 160°C.

CHAPTER 5
DISCUSSION

The experimental results will be discussed for each of the systems studied following the same order of presentation and layout of chapter 4.

5.1 $SCPE_{43}$/PVC 50/50 (E_{50})

5.1.1 DEGREE OF CROSSLINKING

Ammonia solution did not proved to be an efficient crosslinking agent for E_{50}. In order to achieve an appreciable degree of crosslinking, it was necessary to employ extreme conditions such as the use of fractionated $SCPE_{43}$ in the blend and immersion of the sample for long periods in the curing media at 50°C, followed by postcuring between 75° to 100°C (figure 4.1 and 4.2 (p. 93)). Fractionation of $SCPE_{43}$ prior to curing increased crosslinking because the smaller chains in the polymer were removed; if present, these chains may have formed branches on larger molecules reducing the number of sites available for crosslinking. The use of curing temperatures above ambient,was necessary since the crosslinking reaction depends on the rates of diffusion and reaction of ammonia in the sample and the degree of crosslinking is a function of the final concentration of ammonia, in the sample and increases with temperature. By postcuring, the remaining ammonia in $SCPE_{43}$ was allowed to react thus increasing the degree of crosslinking. The drop in weight of undissolved $SCPE_{43NH4OH}$ observed in figure 4.2 after the sample was immersed for 144 h in ammonia solution is probably due to the hydrolysis of some sulphonamide crosslinks caused by the alkaline ammoniacal conditions. This side reaction would give a rise to an ammonium sulphonate salt.

As mentioned in sect 4.1.1 (p 94) $SCPE_{43}$ crosslinked less efficiently after being blended with PVC. This suggests that the presence of PVC, which has a T_g 63° higher than that of $SCPE_{43}$, decreases the diffusion rate of NH_4OH in the polymer, therefore influences the final concentration of this curing agent and the degree of crosslinking.

It is interesting to point out that after crosslinking one of the polymers in the blend, the resulting product may be classified[4, 13] as a semi-IPN (sect. 2.4.3.1, pp 38-9). This classification is applicable to E_{50} and to all the blends studied in this work.

5.1.2 MISCIBILITY

As E_{50} could be prepared either by solvent casting or *insitu* blending, it was possible to see the important role which the method of preparing a blend plays in its miscibility behaviour. Microscopy, Rheovibron and DSC results (figures 4.3 to 4.6 and tables 4.1 and 4.2 (see section 4.1.2 pp 94-7) showed that while the solvent cast blend composition E_{50} was phase separated (two well defined peaks were observable in the Rheovibron and DSC (curves b and c in figures 4.5 and 4.6 respectively (p. 95-6) and domains were clearly visible in the Phase Contrast microscope (see figure 4.3, p. 94)) the *insitu* blend $E_{50insitu}$ was partially miscible (a broad peak was observed in the Rheovibron and a single peak in DSC (see curves c and e in figures 4.5 and 4.6 respectively)). Walsh *et al* [21] attributed the miscibility of PVC and SCPE, which are very similar chemically, to dipole-dipole interactions and London dispersion forces. $E_{50insitu}$ is closer to complete miscibility than E_{50} because *insitu* polymerization leads to higher levels of molecular mixing [3] and avoids spurious results introduced by solvent casting [24]. It is possible that complete miscibility was not achieved in this case due to small amounts of low molecular weight material left in the blend after the *insitu* blending was complete. Curves e and f in fig 4.6 show that the DSC peak moves from -24°C to -4°C after the sample was left 12h at 90°C. This indicates that the plasticizing agent is either lost on heating or reacts further, and may therefore be an oligomer of VCM which polymerizes further on heating. In the case of E_{50}, MEK also interferes with the miscibility of the system. This phenomenon has been previously observed in systems which are well known to be miscible but which phase separate in the presence of a solvent, such as the case of PS/PVME when solvent cast from chloroform [52]. This behaviour named by Patterson [52] as the " $\Delta\chi$" effect (section 2.3 p. 28-9), predicts that phase equilibrium in a ternary system of two polymers and a solvent depends not only on χ_{23} but on the difference in magnitudes of χ_{12} and χ_{13} :

$$|\Delta\chi| = |\chi_{12} - \chi_{13}| \qquad 2.108$$

By simulating spinodals in ternary systems he found that the blend is immiscible if:

$$|\chi_{12} - \chi_{13}| \geq \pm 10\%$$

and

$|\chi_{23}| \cong 0$

Doubé and Walsh [25] gave the following data where 1= solvent, 2= $SCPE_{43}$ and 3= PVC:

$\chi_{12} = 0.74$

$\chi_{13} = 1.22$

and

$0.0006 \geq \chi_{23} \geq -0.009$

(as χ_{23} for the 50% PVC composition was not reported, the χ_{23} values for the 25 and 75% PVC compositions, 0.0006 and -0.009 respectively, were used as limiting values).

Clearly, $\Delta\chi = 0.48 > \chi_{23}$ and χ_{23} is very small which confirms the observed immiscibility.

The Rheovibron result showed that the *insitu* blend was phase separated after crosslinking (curve e in figure 4.5, p. 95). It is believed that this was caused either by water in the ammonia, or the ammonia itself, which was introduced in excess to the sample during crosslinking. E_{50} which was already phase separated before being modified, remained unchanged after crosslinking (curve d in figure 4.5).

Table 4.2 shows the composition and mass balance of the two phases present in the immiscible samples. These results were obtained by substituting the values of the T_gs measured with the Rheovibron into the Fox equation. Examination of these data suggests that the two phases present in E_{50}, $E_{50NH4OH}$, and $E_{50insituNH4OH}$, are themselves blends of the original components. The phase of lower T_g is richer in $SCPE_{43}$ and a second phase of higher T_g is richer in PVC. It is interesting to point out that when $E_{50insitu}$ phase separated after crosslinking with NH_4OH, the two phases produced both contained significant amounts of each homopolymer. In contrast, the other two blends produced almost pure PVC as one phase.

5.1.3 PHASE SEPARATION BEHAVIOUR

As the difference in refractive index (η) between $SCPE_{43}$ and PVC (η=1.52 and 1.54 respectively [24]) is very small, it was not possible to use light scattering techniques to measure the phase separation temperature of E_{50}. As recommended by Doubé and Walsh [24], phase contrast microscopy, TEM and the Rheovibron were used instead. Phase contrast microscopy and the Rheovibron showed that $E_{50insitu}$ phase separated at around 90°C (see figures 4.7 and 4.15 (pp 99 and 103 respectively), a temperature 30° degrees lower than that reported by Doubé and Walsh[24].This technique also showed that $E_{50insituNH4OH}$ was phase separated at room temperature and that domain sizes

increased with temperature. TEM was powerful enough to show the presence of some dispersed phase in $E_{50insitu}$ at room temperature (figure 4.13, p.102). This behaviour would be predicted from the miscibility results which showed the sample to be quite close to complete miscibility (see section 5.1.2, p. 186).TEM again confirmed that these small domains increased in size with temperature (figure 4.14 p. 102). Table 4.3 (p. 104) shows that by heat treating the already phase separated E_{50} and $E_{50NH4OH}$ at different temperatures and time intervals the extent of phase separation could be increased. It is noteworthy that from 110°C, onwards the T_gs of the two existing phases shifted quite quickly towards the values of the pure components. These changes occured faster above the T_g of PVC because the rates of diffusion of the phases are several orders of magnitude greater at temperatures above T_g.

5.1.4 FINAL COMMENTS ON THIS SYSTEM.

It was decided not to continue with the study of the rest of the compositions in this blend because the system and the curing agent used presented the following disadvantages:

(a) PVC is not a very convenient polymer to be used in miscibility studies due to its complex semicrystalline structure.

(b) As light scattering techniques are not applicable in this case, very laborious procedures were needed in order to measure the phase separation temperature.

(c) The *insitu* polymerization method is rather laborious and not very practical for the preparation of the larger samples required for mechanical properties measurement.

(d) Ammonia solution is not a very efficient curing agent for this system and, as it is dissolved in water, it causes phase separation.

5.2 $SCPE_{43}$/EVA (*A*).

5.2.1 DEGREE OF CROSSLINKING

The degree of crosslinking results obtained in this work using swelling, static and dynamic mechanical measurements, should only be interpreted qualitatively and at the most used comparatively for the same system and for the same method of determination.The reasons are: (1) The theories on which these measurements are based are greatly oversimplified, and, as is generally accepted, even when applied to networks behaving ideally, predicted results may differ considerably from the experimental ones

(section 2.4.2 pp 32-7). (2) In the present case the theories were applied to networks which, besides behaving non-ideally, were in the presence of a second unmodified polymer. Although this factor was included in the calculations using the methods described in section 4.2.1 (p. 105), it is not completely understood how the presence of another component may modify the behaviour of the network under those circumstances and so assumptions had to be made.

The swelling results in table 4.4 were obtained with the modified version of the Flory-Rehner equation [1, 71], the James and Guth expression [71] and Hermans equation[71,144]. As explained in sect. 3.5.1 (p. 78-9) the presence of the second unmodified polymer was considered in swelling by basing the calculations on the weight of the deswollen cured polymer. Although the three equations were developed using different expressions for $\Delta S_{elastic}$ the results obtained from them are quite similar because the values of ϕ_2 are small and the term on the right hand side of the three equations is equivalent.

As $SCPE_{43}$ ($\bar{M}_n$=23000) contains 1% S as SO_2Cl groups by weight of polymer, approximate 6 SO_2Cl groups may be present per chain. If all these SO_2Cl entities react during crosslinking, $\bar{M}_c$ values around 3800 should have been obtained. The results in table 4.4 (p. 106) suggest that on average only a few of the ~6S present reacted, yielding, as a consequence, a lightly crosslinked network.

The $\bar{M}_{cMECH}$ data shown in table 4.5 (p. 107) were calculated using values of G_N obtained by the four methods described in section 4.2.1 (p. 105-7). Although the four methods gave, in general, reasonable values of $\bar{M}_c$, the interpretation of those results should be made cautiously. The first method simply uses the shear modulus of the crosslinked blend (G_{XB}). In the second method the contribution of the second component (G_B) is subtracted from G_{XB}; and although this method gives reasonable results the physical interpretation of the difference between G_{XB} and G_B is debatable. In the third method the contribution of the second component is considered for all compositions using the simple rule of mixtures. This approach still has a pitfall; as mentioned earlier, in section 4.2.1 p. 105 the rule of mixtures is applicable to systems which behave as one phase systems[133], and the results in section 4.2.2 (see figure 4.19 (p.109) and table 4.8 (p.111)) revealed that only A_{10DETA} to $A_{50\,DETA}$ behaved as one phase systems, while the rest are two phases. The fourth method takes this into consideration by calculating the contribution of the second component in A_{60DETA}-A_{90DETA} to the moduli using an equation for two phase systems. As is well known, there are many equations which are applicable to phase separated systems, such as those proposed by Kerner [110, 106], Hashin and Strikman [110, 106], Budiansky [106] etc.

This last was chosen here due to its simplicity and because it is applicable to two phase systems with some interaction between the components. In this case, the use of this equation still presupposes that the network is present as a continuous matrix and the second component is included as spherical domains; as will be discussed later on and according to the results in section 4.2.2 (p. 108-15), the results obtained with the Rheovibron and DMTA suggest that the two phase blend compositions have a more complex morphology.

In many cases, though not for A_{DETA}, it was possible to make swelling and static stress-strain measurements only below the T_g or T_gs of the blend composition under study so that the system was not behaving as a rubber. In such cases the use of the relationships developed for crosslink density are debatable. In spite of this many researchers have used swelling measurements at room temperature for crosslinked polymers with high T_gs, such is the case of Bell [143] who studied amine-cured epoxy resins which exhibited T_gs above 100°C. In the case of mechanical measurements, Hermans [145] derived an equation for networks of stiff chains. Unfortunately, the use of such a relationship is difficult as it requires the knowledge of some inaccessible parameters. Determination of swelling or static modulus at higher temperatures was not possible owing to lack of equipment and other experimental difficulties. At this point the use of the DMTA technique provided an attractive alternative, as the method provides the storage modulus E' for a wide range of temperatures. In spite of this, DMTA presents one further problem. As measurements were performed at 10Hz, the rate of deformation of the system is relatively high compared with static tests, giving higher values of storage moduli and, as a consequence, higher values of degree of crosslinking (smaller values of $\bar{M}_c$), than predicted by static mechanical measurements.

The measurements obtained by DMTA for A_{DETA} are shown in table 4.6 (p. 107). As in table 4.5 the same four methods were used to calculate the shear loss moduli of the network (G'_N). Comparing the results in tables 4.4 , 4.5 and 4.6, it may be seen that the three techniques gave different results. The swelling experiments may provide the most accurate values because:

(1) The measurements were performed when the network reached equilibrium, while the mechanic and dynamic measurements did not. As pointed out by Gumbrell *et al*[87], static mechanical measurements on dry rubbers differ widely from the Gaussian theory on which the experiment was based; they recommended that such measurements be carried out on swollen polymers when their behaviour is close to ideal. Unfortunately this condition is difficult to accomplish experimentally.

(2) The swelling results suggest that the degree of crosslinking is low, which agrees

with the fact that the T_gs of the blend compositions did not increase considerably after crosslinking although the E' curve did (see figures 4.18, 4.19 (p. 109) and figures 4.23 to 4.25 (p. 117-8).

At this point it is obvious that the value of $\bar{M}_c$ obtained depends on the technique and conditions used for the measurement. This fact has been previously observed by many researchers, such as Murayama and Bell [146], who determined $\bar{M}_c$ for an epoxy resin using both swelling and DMTA methods.

5.2.2 MISCIBILITY BEHAVIOUR OF (*A*) AND (A_{DETA})

The cloudiness observed in system *A* from A_{50} onwards is a clear indication that above this composition the blend is behaving as two phases. The domains present are of the order of the wavelength of light and therefore capable of scattering light. These visual observations were confirmed by the Rheovibron and DMTA results. As shown in figure 4.18 (p. 109) and table 4.7 (p. 110), for the unmodified blend the compositions ranging from A_{10} to A_{40} presented one T_g; this behaviour suggests that the blend is miscible in this range of compositions. It is important to mention here that although the determination of the T_g is a powerful miscibility criteria, it still does not guarantee completely the state of miscibility of the blend under study. As is well known [153], domains which are too small to be detected by T_g measurements can still be present in blends exhibiting only one glass transition. This point is of equal significance for the rest of the systems studied in this work. At A_{50}, the system starts to show some degree of microheterogeneity, giving as a result a broad peak [6]. From A_{60} to A_{90}, two peaks appear more or less at the same temperatures (-6°Cand 17°C). (It may be noted that in A_{90}, it is not always possible to observe clearly the peak corresponding to the phase at -6°C, therefore it is convenient in these cases to use other criteria of miscibility to avoid erroneous conclusions). These peaks were shifted towards each other with respect to the T_g values of the pure polymers, which suggests that above 60% $SCPE_{43}$ the system is partially miscible. The composition of both phases was calculated using the Fox equation [44,100] (see table 4.9, p. 112). As shown in this table, the blend compositions have an EVA_{45} rich phase (~60% w/w EVA_{45}) and a $SCPE_{43}$ rich phase (~95%w/w $SCPE_{43}$). The small difference in composition between the two phases in A_{60} to A_{90} is probably a result of the conditions followed during their preparation (e.g. evaporation rate, temperature) which play an important role in the case of unstable or metastable systems[52]. Table 4.9 also includes the mass balance in each peak which is based on 1g of the original mixture of polymers. As the original amount of $SCPE_{43}$ is increased a

correspondingly larger quantity of the SCPE-rich phase is formed while the actual composition of the two phases remains relatively constant. Comparison of tanδ with the mass balance shows that the changes in the amount of material within the two phases is reflected in the peak value of tanδ [110].

Similar results to those described for system *A* had been previously obtained by Webb [53] and Rostami [136]. Webb, using DSC, observed two glass transitions for the compositions containing more than 50% w/w $SCPE_{43}$. His permeability results showed that, in that range of compositions, the system was partially miscible. Using a ternary solution method, he was also able to see that the χ values were small in magnitude and the densities of the blends did not indicate strong departures from volume additivity, indicating weak intermolecular interactions. Rostami [136] observed similar miscibility behaviour when analysing this blend which he called H48/EVA45 (figure 4.20 and table 4.10 p. 113 and 114). Subsequently this author, together with Walsh [29], determined the thermodynamic parameters of the system using ΔH_{mix} measurements. They found that the ΔH_{mix} of a model system formed from two oligomers similar to $SCPE_{43}$ and EVA_{45}, was negative for all compositions at 64.5° and 73.08°C. However by presenting the results in terms of χ_{23}/Vo (where Vo is an arbitrary and not specified segment volume) it was clear that the miscibility of both oligomers was less favourable from 50% content of the chlorinated oligomer upwards. As pointed out by these authors, ΔH_m measurements provide an idea of the possible behaviour of the polymer blend of interest, however these results may not always be extrapolated because:

(1) ΔH_m measurements depend only on the enthalpy of mixing and do not include the ΔS contribution from interaction which may render the system immiscible.

(2) Using model systems, the real parameters of both polymers which influence their miscibility (molecular weight, polydispersity, thermal expansion and thermal pressure coefficients) are not taken into account.

(3) For model systems, ΔS_{comb} will differ from the polymer system as the number of chains per unit volume is different.

These limitations were evident in the case of H48/EVA45 as the model oligomers were miscible at 64.5 and 73.08°C, at which temperatures the blend was phase separating. Although not proven experimentally, a possible explanation for the two phase behaviour of A_{60} to A_{90} is the presence, at room temperature, of a phase separated region in the ternary system $SCPE_{43}/EVA_{45}$/THF at certain values of solvent volume fraction (ϕ_1). This behaviour was explained in chapter 2 (see figure 2.2 (p. 29)). As mentioned there, at certain ϕ_1 the tertiary mixture was one phase but as the solvent evaporated the system went through a phase separated region. If the solvent

continued evaporating under quasi-equilibrium conditions, $SCPE_{43}/EVA_{45}$ should have become homogeneous at low ϕ_1 finally yielding a clear film. However it is presumed that due to the high viscosity of $SCPE_{43}$ and EVA_{45} the system remained phase separated. This behaviour once again may be a consequence of the $\Delta\chi$ effect (section 2.3 p. 28-9). In this case it was not possible to evaluate $\Delta\chi$ for $SCPE_{43}/EVA_{45}$/THF, because not all the data was available, however from Doubé and Walsh's [25] IGC determinations of the interaction parameters for the $SCPE_{43}$/PVC blend, it was clear that chlorinated hydrocarbons interact strongly with ketones and ethers. In the case of $SCPE_{43}$/THF and EVA_{45}/THF the interaction between $SCPE_{43}$ with the solvent should be higher as EVA_{45} is a poorer proton donor than $SCPE_{43}$, therefore $\Delta\chi$ must be a significant term. Rostami and Walsh [29] showed that χ_{23} for $SCPE_{43}/EVA_{45}$ is less negative above 50% content of $SCPE_{43}$: it is therefore possible that $\Delta\chi$ is greater than χ_{23} in the composition range 60-90% $SCPE_{43}$.

The miscibility behaviour of *A* is very similar to that observed by Nishi and Kwei[140] for PS/PVME solvent cast from trichloroethylene. They found that at room temperature, in the range of volume fractions 0.30-0.97 PVME, all compositions were separated into two phases, one containing a PVME rich phase (ϕ ~0.30) and the other a PS rich phase (ϕ ~0.97). These workers explained their observations in slightly different terms: they proposed that the ternary mixture has a two phase region as a consequence of the existence of a UCST which crosses the LCST at ϕ ~30 and ~0.97, giving phase separated samples with a PVME rich phase (ϕ ~0.30) and a PS rich phase (ϕ ~0.97) and producing a typical hour-glass shaped phase diagram. If this reasoning is applied to system *A* , the composition of the two phases present in the phase separated specimens (table 4.9 p. 112) suggest, as shown in figure 5.1, that the UCST curve should be crossing the LCST between ~40 to ~95 %W/W $SCPE_{43}$ giving blend compositions containing an EVA_{45} rich phase (~60% W/W EVA_{45}) and a $SCPE_{43}$ rich phase (~95% W/W $SCPE_{43}$). The existence of such a UCST provides a plausible explanation for the behaviour of system *A*. Unfortunately this is difficult to probe experimentally, because at low temperatures phase separation may be impeded by kinetic reasons especially if the T_g of the mixture is high [2]. This proposed phase diagram implies that one phase is present at very high concentrations of $SCPE_{43}$ but this has not been verified by experiment.

As shown in the Rheovibron and DMTA results, (tables 4.7 and 4.8 pp 110-1), the compositions exhibiting one peak prior to crosslinking continue to present only one transition after crosslinking. As is well known, in general IPNs and semi-IPNs are inhomogeneous [4,94,100,157]. However, as demonstrated theoretically by Binder and

Frish[155], semi-IPNs may be thermodynamically stable, as in the case of the IPN and semi-IPN of Poly(2,6-dimethyl-1,4-phenylene oxide)/Polystyrene (PPO/PS).(This system has proved to be miscible when the components are mixed as linear polymers)[154]. Other examples of miscible IPNs include some epoxy/acrylic IPNs prepared by Allard *et al* [153]. The two phase compositions A_{60DETA}-A_{90DETA} gave two transitions before and after crosslinking.

As is well known, increasing the degree of crosslinking increases the T_g of a polymer, and although it was expected to see a shift in T_g over the whole range of compositions in A_{DETA} , only a small increase, or no increment at all was noted. Ellis *et al*[156] observed similar behaviour in some crosslinked polymers and were able to show that as little as 2% of plasticizer may decrease the T_g of a polymer by 12 to 80 deg.

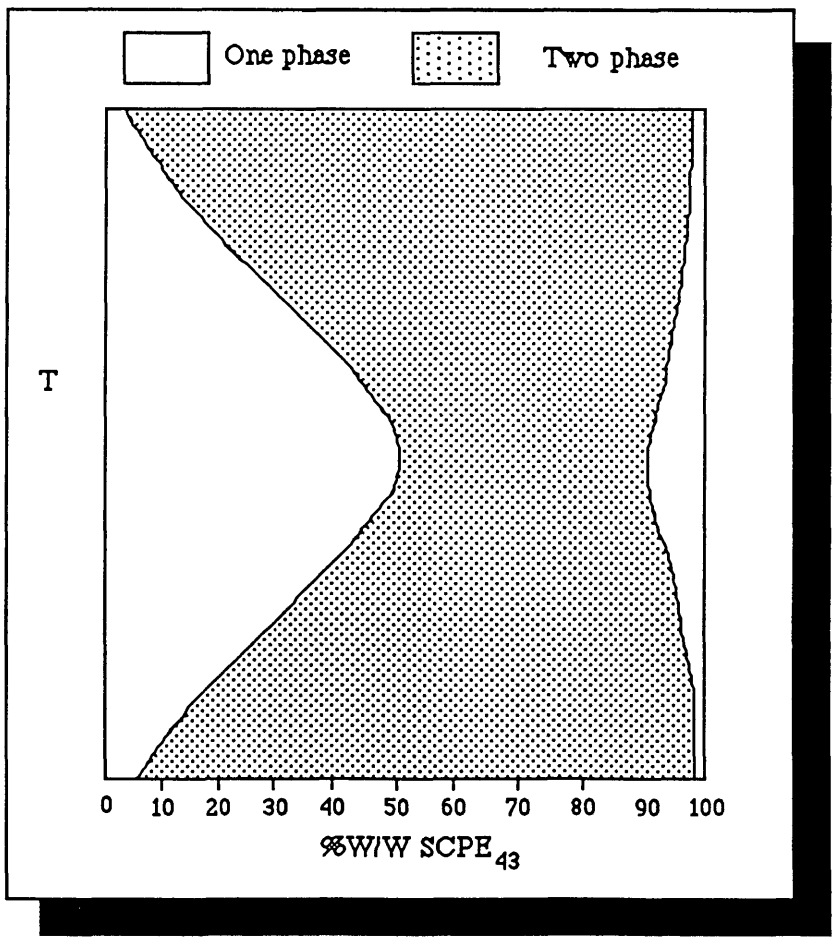

Figure 5.1 Phase diagram showing a LCST curve overlapping with the UCST. This behaviour produces one phase up to 40% composition and two phases up to very high $SCPE_{43}$ content. The single phase behaviour above 90% is hypothetical and it was not verified experimentally.

In the present blend it is quite possible that small amounts of unreacted *DETA* may be plasticizing the whole composition range. In spite of not having been able to observe changes in the T_g, a decrease in the damping peak together with an increment in the values of E' was detected for all samples (sections 4.2.2 and 4.2.3 pp 108-18). Changes in these parameters are sensitive indicators of crosslinking. A decrease in the height of the tanδ peaks have been previously observed in semi-IPNs by Allen and *et al*[105] and by Donatelli *et al* [107]. Allen and coworkers studying the semi-IPN polyurethane/poly(methyl methacrylate), where the polyurethane was crosslinked, attributed this behaviour to an increase in the interaction between the two polymers. This explanation may be applied to the samples in this work, especially after analysing the results in tables 4.9 and 4.11 (pp 112 and 115), where a slight intermixing between the phases present in the sample is observable. For example in A_{70} the amount of $SCPE_{43}$ and EVA_{45} in the phase at -3°C was 0.17/0.24 which decreased after crosslinking to 0.10/0.18, with a simultaneous increase in the amount of both components in the phase of higher T_g from 0.53/0.06 to 0.60/0.10.

5.2.3 STATIC AND DYNAMIC MECHANICAL PROPERTIES

The static and dynamic mechanical properties of *A* and A_{DETA} show a clear dependence on blend composition and on the state of misciblility. The static modulus Y increases smoothly from A_{10}-A_{40}; above this point a definite change in slope was observed. The only difference between the Y values of systems *A* and A_{DETA} is that in A_{DETA} the crosslinked system Y increased for all compositions (figure 4.21 p. 116).

The dynamic experiments (figure 4.22 to 4.25 pp 117-8) provide more information than the static ones just described since a temperature scan was possible. Figure 4.23 shows the logE' curves for A_{10}, A_{30} and A_{40} (curves a to c) which contain a single point of inflexion corresponding to the only T_g present in these compositions. The slope of the modulus curve is steep and it simply shifts up the temperature scale in proportion to the relative concentration of the two components. In A_{50} (curve d) the slope of E' is not so steep and the transition is broadened. Samples A_{60} to A_{90} (curves e to h) show two inflexion points corresponding to the T_gs of the two phases present. The change in slope is less marked than for A_{10}-A_{40}. According to Livingston [151], the behaviour observed in one phase systems, such as A_{10}-A_{40}, resembles that of a homogeneous uniformly random copolymer. The behaviour of the phase separated blends is more complex and is a reflection of the composition, resultant morphology, size of phase separated regions, distribution of those regions, interaction at the interface

and the transitional behaviour of the components in the blend[14, 151].

After crosslinking the blend, logE' (figure 4.24) moves to a higher level but general behaviour is similar to the uncrosslinked blend. As shown in figure 4.25, the increase in E' is more evident above T_g (rubbery plateau). This behaviour is a direct consequence of the restriction of viscous flow caused by the number of crosslinks in the molecule. The relatively high values of E' for A_{60}-A_{90} (curves e-h, figure 4.23) and A_{70DETA}-A_{90DETA} (curve e-g, figure 4.24) and the similarity of these logE' curves to that of $SCPE_{43}$ (curve b in figure 4.22) suggests that in these compositions the SCPE rich phase is the matrix while the EVA rich phase is the dispersed phase [110].

There are a number of theories and equations in the literature which try to simulate the static and dynamic behaviour of two phase systems [113, 152, 153, 154]. Figures 5.2 and 5.3 show a comparison of the experimental values of G' at 0°C with those calculated by (a) the rule of mixtures [133] (b) the inverse rule of mixtures [133] and (c) the Kerner equation extended to viscoelastic behaviour [110, 148] (the G' values were calculated from the E' data obtained with the DMTA). The rule of mixtures and the inverse rule of mixtures are generally considered to be applicable to one phase systems, the Kerner equation to phase separated systems with spherical domains.The rule of mixtures and the inverse rule of mixtures were used to predict the behaviour over the whole composition range and the Kerner equation was used to predict behaviour in the two phase region. The values of G' at 0°C for EVA_{45}, $SCPE_{43}$ and $SCPE_{43DETA}$ were used in the relationships of the rule of mixtures and the inverse rule of mixtures (the calculation of G' for the phase separated samples was performed as if they were one phase). In using the Kerner equation the average properties at 0°C of each of the phases present in A_{60} to A_{90} were calculated. As suggested from DMTA experiments the $SCPE_{43}$ rich phase was considered to be the matrix for these blend compositions.

As shown in figures 5.2 and 5.3 the experimental results are contained in the bounds defined by the inverse rule of mixtures, rule of mixtures and Kerner equations. In both figures the inverse rule of mixtures predictions are closer than those of the rule of mixtures to the one phase compositions; from 50% $SCPE_{43}$ content G' starts to deviate strongly, approaching the rule of mixtures and Kerner predictions as the $SCPE_{43}$ content increases in the mixture. Clearly in this system the Kerner equation and rule of mixtures predict very similar behaviour. Comparing 5.2 and 5.3 it may be observed that in the crosslinked samples E' increases with a more uniform pattern than before being modified. This may be attributed to the greater interaction between the two polymers introduced by curing.

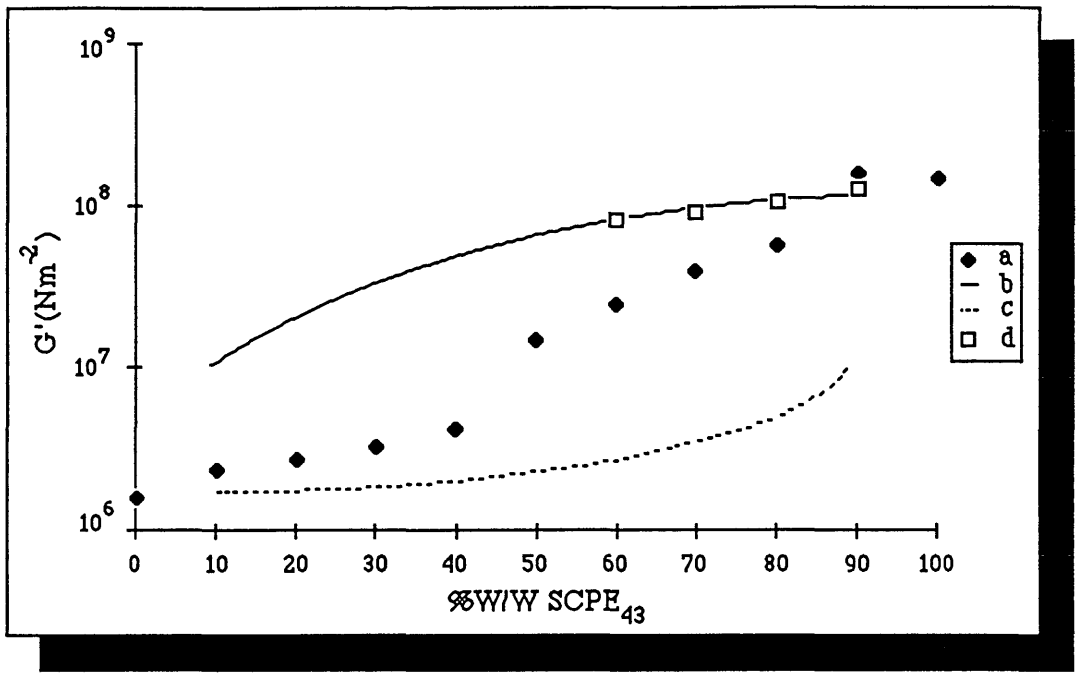

Figure 5.2 Comparison of G' at 0°C for system A obtained: (a) experimentally, (b) with the simple rule of mixtures, (c) using the inverse rule of mixtures and (d) with the Kerner equation.

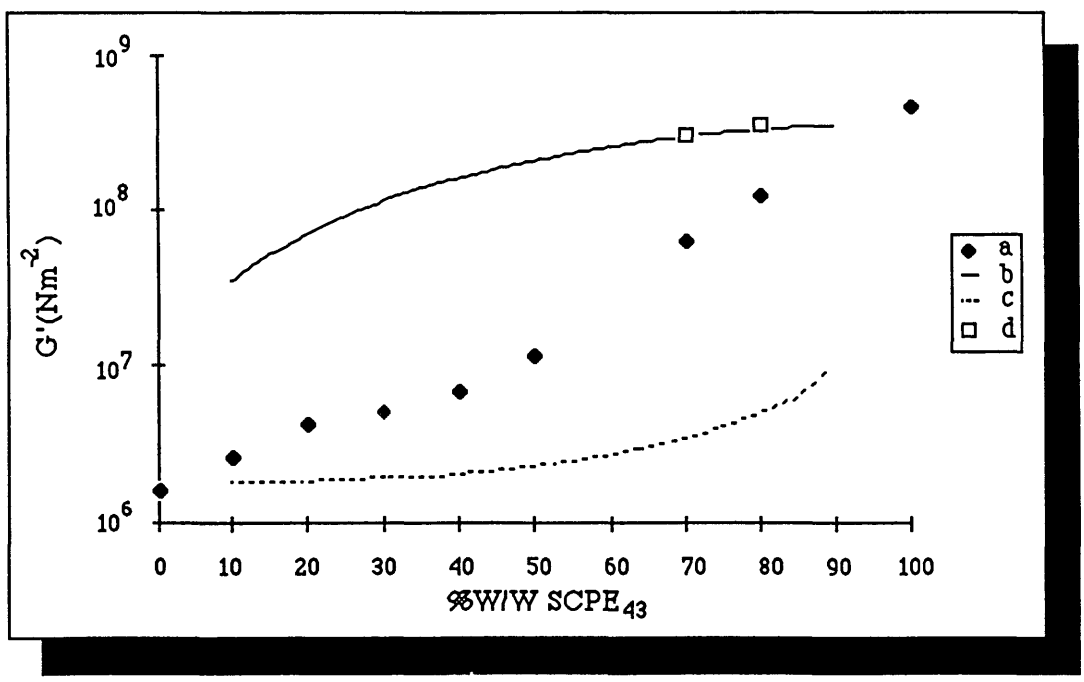

Figure 5.3 Comparison of G' at 0°C for system A_{DETA} obtained: (a) experimentally, (b) with the simple rule of mixtures, (c) using the inverse rule of mixtures and (d) with the Kerner equation.

5.2.4 CLOUD POINT MEASUREMENTS

A comparison between the plots of intensity vs temperature obtained with the turbidimeter for some compositions of system *A* before and after crosslinking (figure 4.26 p. 119) show clearly a decrease in the slope for the crosslinked samples. This suggests that some modification to the way the blend phase separates has taken place due to crosslinking. A possible explanation for this change in the behaviour is that the rate of growth of the domains has decreased due to the crosslinks which hinder their diffusion during phase separation.

The cloud point (CP) curve obtained with the turbidimeter for the whole composition range of *A* (figure 4.27 p. 120) shows the typical LCST behaviour observed in polymer blends. This CP curve lies more or less in the range of values obtained for the same blend (H48/EVA45) by Walsh *et al* [29]. However, as shown in figure 4.27 and later on in the CP curve obtained with the laser-SALS (figure 4.29 p. 121), the CP curve in the present work is practically flat above A_{40}. This part of the CP curve corresponds to the composition range in which the blend is no longer completely miscible and becomes a mixture of EVA_{45} and $SCPE_{43}$ rich phases from A_{60} onwards (see section 4.2.2 p. 108-15). The existence of this flat region in the CP curve agrees with the suggestion of the existence of a two phase region at certain ϕ_1 in system $SCPE_{43}/EVA_{45}$. As explained in section 5.2.2, p. 191-4, this phase separated region may be caused either by: (a) a considerable difference between the χ_{ij} of $SCPE_{43}$ and EVA_{45} with THF or (b) the existence of a UCST crossing at room temperature the LCST at the compositions 40% and 90% w/w $SCPE_{43}$ (see figure 5.1 p. 194), yielding as a result blend compositions that are partially miscible from A_{50} onwards. It is possible to observe a CP in these two phase compositions because each phase (one with approximately 40% $SCPE_{43}$ and the other with 90% $SCPE_{43}$) constitutes a miscible blend which can phase separate at a certain CP temperature. Similar observations were reported by Nishi and Kwei [143]. If, as they suggest, this "mixture of blends" is described as "islands in a sea" (see figure 5.4), where the islands are the EVA_{45} rich phase which constitutes the dispersed phase and the sea is the $SCPE_{43}$ rich phase, then the islands, which have a lower T_g, will become cloudy first while the sea will turn turbid at higher temperatures. (The CP of the second phase is difficult to detect because after the islands phase separate the system becomes too opaque). As may be clearly observed in figures 4.27 and 4.29 (p. 120-1) from A_{40} onwards, the CP was practically constant at 70°C, this CP corresponding to the EVA_{45} rich phase.

The same type of CP curve was observed for system *A* using the laser-SALS, the

only difference being that in this case the curve appears at higher temperatures.This increase in CP temperature may be attributed to two factors:

(1) The laser-SALS was run with a faster heating rate.

2) The turbidimeter was designed to detect the early stages of phase separation (the photodiode was fixed at an angle of 45° (see section 3.7.1.1 p. 86-7)) and as it uses white light (tungsten lamp) it covers a wide range of wavelengths.

It is important to point out that for either of the two scattering techniques used, the CP curves reported in this work may not correspond to the temperatures at which phase separation starts, but to the point at which the domain sizes have grown sufficiently in order to be detected by the technique.

Scatter in experimental CP data is due to the small change in slope in the intensity vs temperature data, particularly for the crosslinked samples, which complicates the determination of the exact temperature at which the CP is observed. Despite this the CP curves obtained for A_{DETA} with the turbidimeter (figure 4.28 p. 120) and the CP temperatures for A_{30DETA} and A_{70DETA} obtained with the the laser-SALS (figure 4.29 p. 121 (see rectangular bars)) were shifted to higher temperatures with respect to the curves of the unmodified blend. In theory, a decrease in the mutual solubility of both polymers with the increase of molecular weight should have been observed as demonstrated by McMaster [40] using a modified form of Flory's "equation of state". However, in agreement with the data obtained in this work, the opposite effect has also been observed. Nishi and Kwei [143] in studies of uncrosslinked PS/PVME noticed that the CP curve decreases until certain values of molecular weight, above which the molecular weight dependence of the CP levels off or even reverses. They observed the same behaviour in the crosslinked blend. In both cases they attributed such behaviour to a kinetic effect (the presence of physical or chemical entanglements hinder the diffusion of the polymers while phase separating) and not to a thermodynamic effect. The same type of kinetic effect would account for the observations reported here.

5.2.5 SIZE OF DOMAINS.

As mentioned in section 4.2.5, (p. 121) all blend compositions for A and A_{DETA} show an exponential decay scattering pattern over the angular range studied even 50°C above the CP temperatures. Figure 4.30 (p. 122) shows this kind of behaviour for A_{30} and A_{30DETA} at different temperatures. Inspection of the data corresponding to each blend shows that as the temperature increases the intensity of the scattered light keeps increasing at low values of θ. This behaviour means that the size of the domains keeps

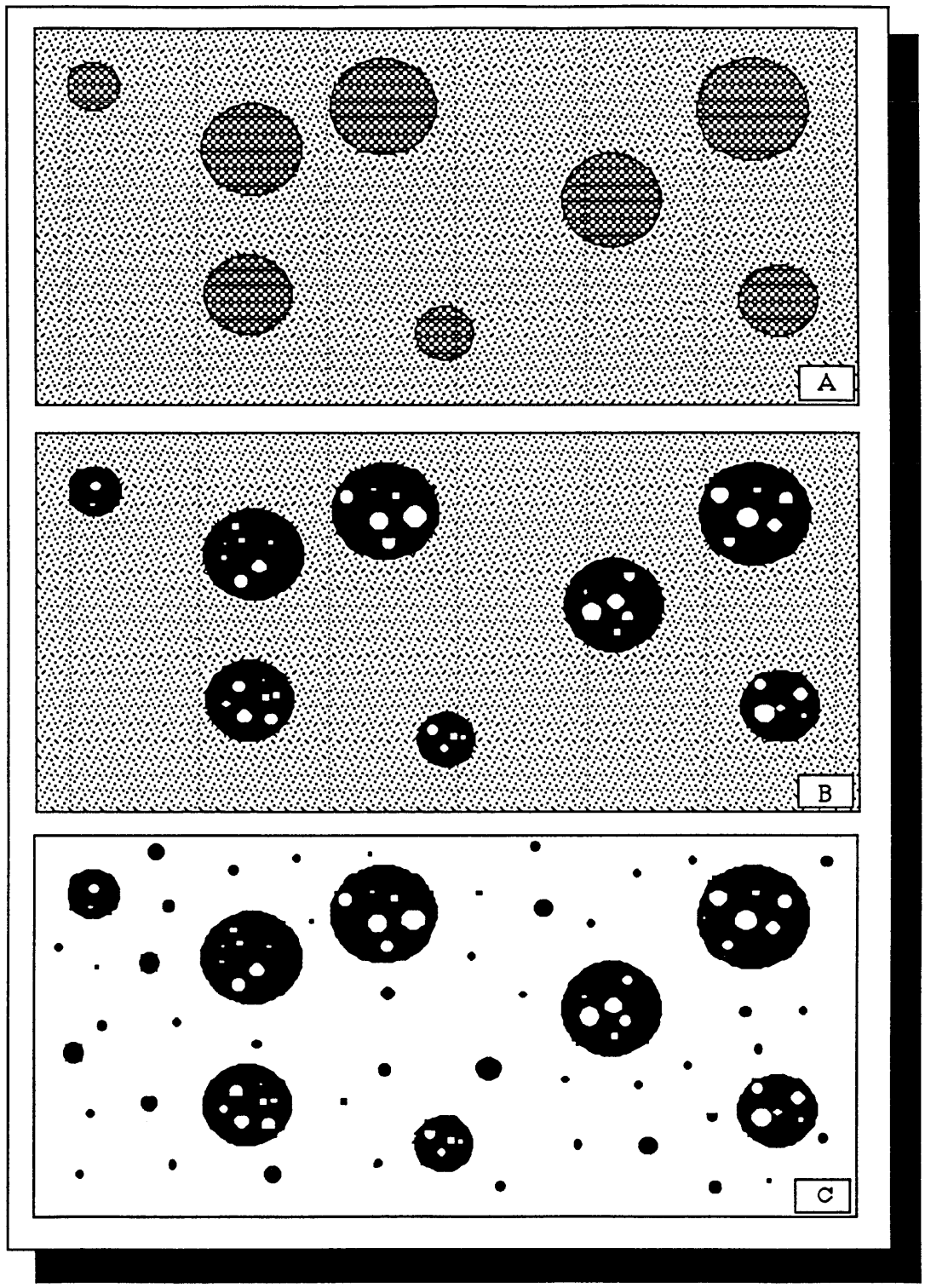

Figure 5.4 Representation of the way in which the phase separated compositions of system *A* undergo further phase separation at their CP temperature: EVA_{45} is represented in black. (A) represents the phase separated blend well below the CP. (B) shows the EVA_{45} phase reaching its CP temperature and (C) shows the $SCPE_{43}$ rich phase reaching its CP temperature.

growing as temperature is increased. Although not conclusive, this behaviour suggests that A and A_{DETA} phase separate by nucleation and growth. Scans were not repeated at larger angles partly because the data showed a clear exponential dependence on angle in this range.

The results for the domain sizes in table 4.12 and 4.13 (p. 123) show the lower and upper limit values for some compositions of systems A and A_{DETA}. The first table contains the data obtained 30°C above the CP obtained with the laser-SALS, the second table shows the data 30°C above the CP obtained with the turbidimeter. The results in both tables were obtained from a plot of lnI vs Q^2 similar to that shown in figure 4.31 (p. 122). In the unmodified samples, no significant variation in the size of the domains was observed throughout the whole range of compositions. After crosslinking the range of sizes and their upper limit were smaller than before curing. The decrease in the size of the domains with crosslinking is consistent with the decrease in slope observed in the intensity vs temperature plots in the CP temperature measurements (figure 4.26, p. 119). This also suggests that during phase separation the crosslinks are acting as barriers to the diffusion of the uncrosslinked component (EVA_{45} in this case), decreasing as a consequence the rate of growth of the domains of this mobile phase [52].

The phase separation for these systems, which as previously mentioned may be considered as semi-IPNs, may be pictured as shown in fig 5.5, where the crosslink cluster is assumed to contain 4 chains. Fig 5.5A shows the blend before phase separation while figure 5.5B pictures the beginning of phase separation; the domains start to grow surrounded by the crosslink cluster which as shown in 5.5C should expand as the domains grow. This growth should reach the limit imposed by the maximum to which the cluster may expand, which is a function of the interfacial energy between the components of the blend, and $\bar{M}_c$. The exponential scattering pattern obtained experimentally in figure 4.30 (p. 122) may be explained in terms of this simple model. If $\bar{M}_c$ were constant this model would imply more or less equal sizes of domains in the dispersed phase giving a Gaussian-like distribution scattering pattern; in practice $\bar{M}_c$ is only an average and the crosslink cluster may contain one, or even, a very large cluster of chains[4], thus a large range of domain sizes is to be expected.

This simple model of phase separation in these semi-IPNs involves small domains of the rubbery phase forming inside "cages" of network links so that each small domain is surrounded by links of the crosslinked network. This would imply that the initial domain size is of the same order as the distance between network crosslinks (see $\langle s^2 \rangle^{1/2}$ values in figure 5.5). The result of this process would be a very large number of small domains having a large total interfacial area. The γ_{ie} would be minimized by the

amalgamation of these domains and the reduction of total interfacial area. This process must proceed by the formation of long cylindrical domains that pass through the links of the network and form into complex clusters. The optical measurements which have been used detect these clusters when they become large enough compared with the wavelength of the light used, and the measured CP temperatures therefore do not necessarily correspond to the point at which small domains were first formed. If SAXS or SANS techniques had been available for the study of all systems discussed in this work, domains might have been detected at earlier stages of phase separation when they were very small. However, as explained in section 5.6.4 p. 225, access to those techniques was very limited, and they were only used for systems *C* and C_{DETA} where all other methods had failed to detect phase separation. It would be very desirable for these techniques to be more readily available when any further work in this area is carried out.The γ_{ie} measured from domain sizes of the system studied (table 4.14, p. 124) are large compared with those of liquids (water/CCl_4 = 45dn/cm at 20°C), which supports the suggestion that a powerful driving force for the amalgamation of small domains exists at the measurement temperature (30°C above the CP temperature of each sample). The large measured domain sizes in this table can therefore seen to be physically reasonable.

5.2.6 SUMMARY

The degree of crosslinking obtained by any of the methods used show that A_{DETA} was lightly crosslinked (on average only a few of the ~6 SO_2Cl groups per chain reacted, producing more than the two links required for network formation). With respect to the miscibility results, the Rheovibron and DMTA data show that the system was miscible in the range A_{10}-A_{50} and clearly two phases above A_{50}. The available techniques can not prove conclusively that very small domains are not present in A_{10}-A_{50}.The miscible compositions remained as such after crosslinking. The two phase samples still showed two T_gs which shifted in position suggesting slight intermixing. As expected the values of E and E' increased in the crosslinked samples.The CP curve for the whole range of compositions apparently increases with crosslinking. This behaviour seems to be a consequence of kinetic effects rather than thermodynamic ones. Finally, in general, it was observed that the sizes of the domains decrease in the cured samples.

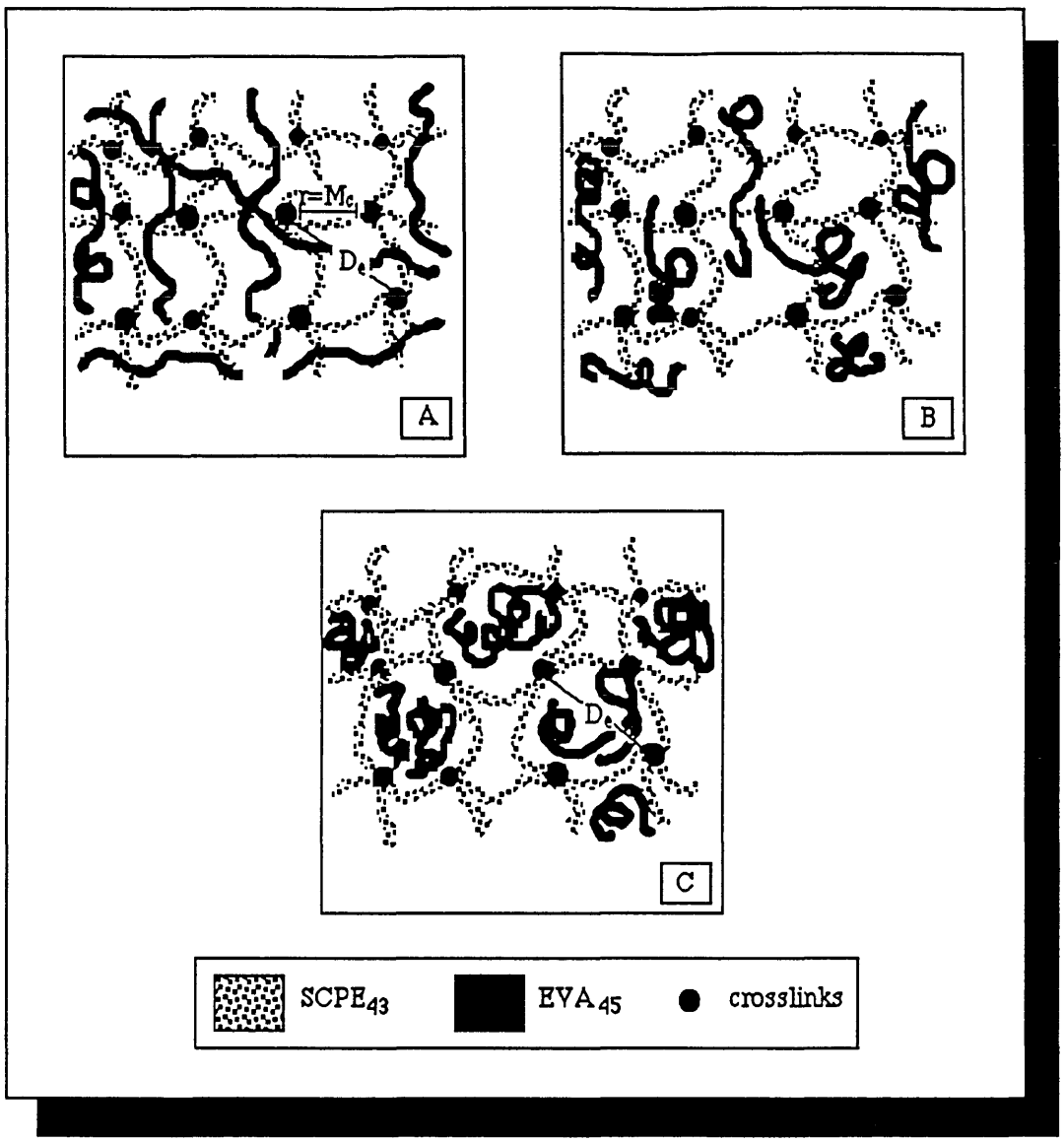

Figure 5.5 Possible phase separation mechanism followed by a semi-IPN. (A) Shows the semi-IPN before phase separation. (B) Illustrates the begining of phase separation. The uncrosslinked polymer (EVA_{45}) is diffusing into domains surrounded by links of the $SCPE_{43}$ network. (C) Shows the semi-IPN completely phase separated.

5.3 $SCPE_{54}/EVA_{45}$ (SYSTEM *D*).

5.3.1 DEGREE OF CROSSLINKING

Although *A* is a rubbery system, discrepancies were observed in the crosslinking results obtained for the A_{DETA} system by swelling, static and dynamic mechanical experiments (see section 4.2.1 p. 105-7). Of the three experiments, swelling is thought

to provide the most accurate results because the measurements are performed when the network reaches equilibrium while the static and dynamic mechanical measurements are not (see section 5.2.1 p. 188-91). In the case of D_{DETA} and the rest of the systems studied in this work, where $SCPE_{54}$ has a T_g 44°C above room temperature, the discrepancy between the swelling and mechanical measurements is even larger. Tables 5.1 and 5.2 provide a good example.

Examination of table 5.1 shows reasonable values of the degree of crosslinking for the compositions with T_g values lower than room temperature. For those samples with T_gs above room temperature the results seem unrealistic, especially for the blends with higher $SCPE_{54}$ content. Dynamic modulus measurements were performed 20°C above the appropriate T_gs but due to the high rates of deformation used in these measurements, the results in table 5.2 gave $\bar{M}_c$ values smaller than those obtained in table 5.1 and differing even more from the swelling data in table 4.15 (p. 125). It is clear, that in these blends, where the behaviour is far from being ideally rubbery, the static and dynamic mechanical measurements are not applicable. Therefore only the swelling measurements were included for D_{DETA} and the rest of the systems studied here.

The $\bar{M}_n$ of $SCPE_{54}$, its S content ($\bar{M}_n$= 33000, S content as SO_2Cl = 0.94%w/w) and the values of $\bar{M}_c$ in table 4.15 indicate that only a few of the ~10 SO_2Cl groups in

	Mechanical measurements $\bar{M}_{cMECH}$ g/mole			
Method*	(1)	(2)	(3)	(4)
Sample				
D_{10DETA}	—	—	—	—
D_{20DETA}	11230	—	—	—
D_{30DETA}	10570	15110	14800	14790
D_{40DETA}	8690	13590	7800	7800
D_{50DETA}	6290	—	4720	4720
D_{60DETA}	2310	7800	1540	1040
D_{70DETA}	2890	6520	2230	1840
D_{80DETA}	1180	3060	970	840
D_{90DETA}	80	270	800	750
$SCPE_{54DETA}$	30	30	30	30

* Methods used for calculation: (1) $G_N = G_{XB}$ (2) $G_N = G_{XB} - G_B$ (3) $G = (G_{XB} - G_U \phi U)$ (4) From D_{10DETA} to D_{50DETA} inclusive method (3) was used ; from D_{60DETA} onwards the Budianski[106] equation was used.

Table 5.1 Values of $\bar{M}_{cMECH}$ for D_{DETA} obtained from stress-strain measurements using four different calculation methods.

Dynamic mechanical measurements $\bar{M}_{cDYN}$ g/mole		
Method*	(1)	(2)
Sample		
D_{10DETA}	610	880
D_{20DETA}	560	770
D_{30DETA}	450	700
D_{40DETA}	680	1130
D_{50DETA}	410	570
D_{60DETA}	1360	2900
D_{70DETA}	910	1350
D_{80DETA}	4040	——
D_{90DETA}	2060	——
$SCPE_{54DETA}$	990	——

* Methods used for calculation: (1) $G'_N = G'_{XB}$ and $G'_N = G'_{XB} - G'_B$

Table 5.2 Values of $\bar{M}_{cDYN}$ for D_{DETA} obtained from the DMTA experiments using four different calculation methods.

the chain were crosslinked. This meant that the $SCPE_{54}$ present in the blend was lightly crosslinked; for 10 SO_2Cl groups reacting, values of $\bar{M}_c$ around 3300 should be expected, but experimentally values around 16000 were obtained. This degree of crosslinking is similar to that found in all the other systems containing $SCPE_{54}$ discussed in later sections.

5.3.2 MISCIBILITY RESULTS

Figure 4.33 (p. 127) shows that *D* is behaving as a miscible system up to a 50% content of $SCPE_{54}$. At 60% content a broad peak was observed. Above this composition the presence of two peaks which are moved towards each other in comparison to the T_gs of the pure polymers is almost always observed. (In the case of D_{90}, the peak at the lower temperature is not clearly observable due to the small content of EVA_{45}). In a similar way to system *A*, using the T_g values and the Fox equation the composition of the two phases present from D_{60} onwards was determined. The calculations showed the presence of an EVA_{45} and a $SCPE_{54}$ rich phases (see table 4.19 p. 131). Once again the two phase behaviour in blend *D* may be explained by the existence of a two phase region for the system $SCPE_{54}/EVA_{45}$/THF between 60 to 90 %$SCPE_{54}$. This two phase

region may be caused by a [$\Delta\chi$] greater that the χ_{23} for SCPE54 /EVA_{45} but this cannot be verified in the absence of χ_{23} data. Rostami [29,117] and Walsh [29] only provide the (χ_{23}/V_2) for the blend CPE3/EVA45 (CPE3=chlorinated polyethylene containing 52.65 w/w Cl) and the required information is not accessible. Alternatively, as in system *A* , it is also possible that a UCST curve exists for this system which crosses the LCST at around 50% to 95 % w/w $SCPE_{54}$.

A comparison between the Rheovibron results for system *D* with those obtained for CPE3/EVA45 [29,117] is shown in table 4.17 (p. 129). As the SCPE used in this blend has a T_g 17°C lower than that of $SCPE_{54}$ the values of the T_gs for all compositions of that blend appear at lower temperatures. Like system *D*, the composition blends containing up to 50% CPE3 showed only one peak. In contrast with system *D*, only one T_g was observed at compositions containing 80% w/w CPE3. A decrease in miscibility with higher content of the chlorinated polyethylene was predicted by Rostami[29,117] and Walsh [29] from IGC and heat of mixing measurements. A second lower temperature transition in the compositions containing 80% w/w of CPE3 may not be detected.The measurements were made with the older Rheovibron instrument which does not resolve weak transitions particularly well. The difference between two transitions in their system would have been smaller as the EVA_{45} used is similar to that in system *D*, and it is possible that a weak transition on the flank of the reported broad transition would be undetectable. Measurements at intermediate $SCPE_{54}$ contents might have revealed two transitions. System *D* does differ chemically from the systems studied by Rostami and Walsh; the SCPE in *D* contains SO_2Cl groups but there is no other evidence that this significantly affects the chain properties.

Comparing the systems *A* and *D* , it may be seen that the polymer with higher chlorine content seemed to be more miscible than *A* which starts to show some phase separation around 50% SCPE while *D* shows it from 60% onwards.

As shown in figure 4.34 (p. 127) and table 4.18 (p. 130), after crosslinking *D* the miscibility behaviour of the whole range of compositions remained very similar, which means that D_{10DETA}- D_{50DETA} showed one T_g and from D_{60DETA} onwards two peaks were always present. The only difference in the T_g results was that after crosslinking the tanδ values decreased considerably. As mentioned previously, semi-IPNs are usually two phase. However it seems that the curing method did not affect the miscibility. Additionally, for the samples with two T_gs, shifts in the temperatures suggested slight intermixing between the phases. This behaviour is clearly shown in tables 4.19 and 4.20 (p. 131) for in D_{60} and D_{90}; the difference between the T_gs of the two phases is clearly reduced by a small significant amount after crosslinking which indicates some

intermixing of the phases.

5.3.3 STATIC AND DYNAMIC MECHANICAL PROPERTIES

As in *A* (section 5.2.3, p. 195-7) the static and dynamic mechanical properties of system *D* show a clear dependence on blend composition, crosslinking and miscibility state (figures 4.35 to 4.39, pp 132-5). Figures 4.35 and 4.36 show, as anticipated, a clear modulus increase with $SCPE_{54}$ content and crosslinking.

In figure 4.38 (p. 134) the logE' curves below D_{60} (curves a to e) show only one inflexion point corresponding to a single T_g. As in *A*, these one phase blends show a rapid change in E' at the T_g. In D_{60} although a second inflexion point is not clear the change of E' through the T_g is less rapid. From D_{70} onwards, the presence of the two T_gs is evident. The great similarity of the logE' curves of $SCPE_{54}$ (curve b, figure 4.37, p. 134), D_{80} and D_{90} suggests that here the $SCPE_{54}$ rich phase is continuous. In all but two cases logE' increases after crosslinking particularly above the rubbery plateau. D_{80DETA} and D_{90DETA} show the opposite behaviour. The reason for this is not clear, but it may be that an excess of crosslinking agent was introduced which may be acting as a plasticizer. Figures 5.6 and 5.7 show a comparison of the experimental values of G'

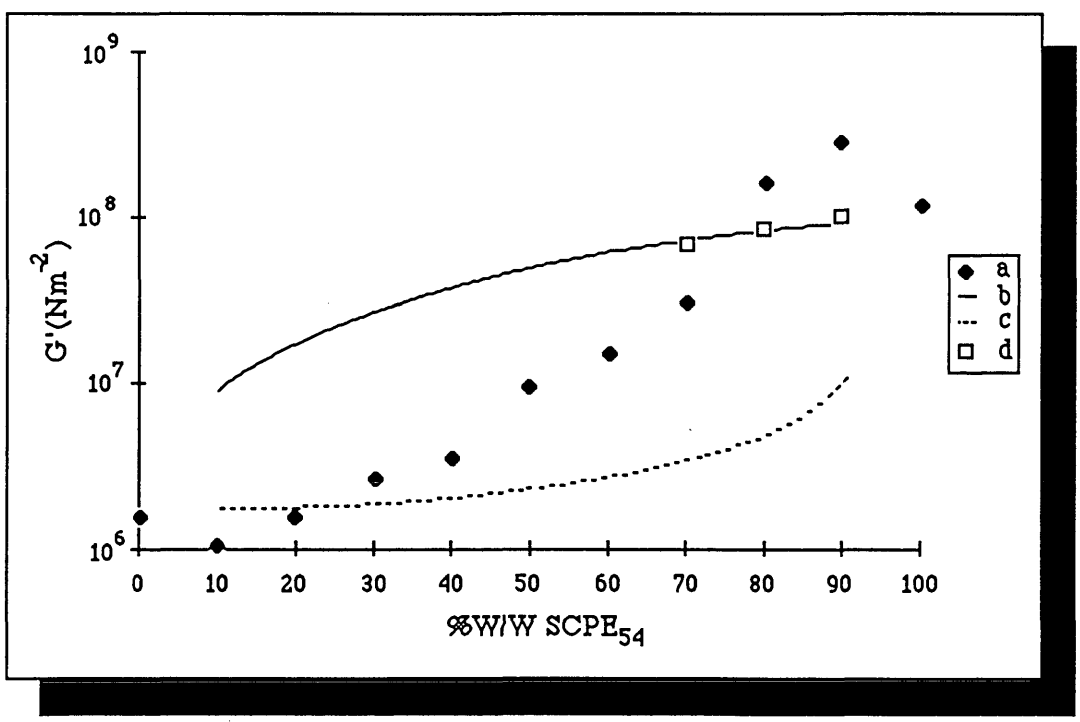

Figure 5.6 Comparison of G' at 0°C for system D obtained: (a) experimentally, (b) with the simple rule of mixtures, (c) using the inverse rule of mixtures and (d) with the Kerner equation.

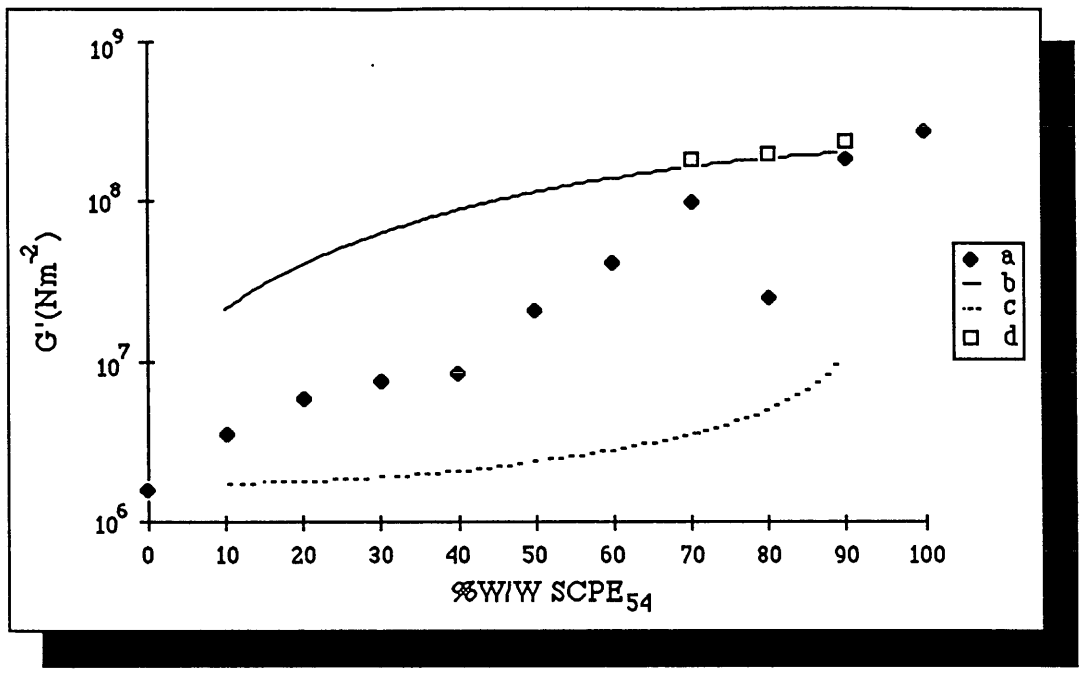

Figure 5.7 Comparison of G' at 0°C for system D_{DETA} obtained: (a) experimentally, (b) with the simple rule of mixtures, (c) using the inverse rule of mixtures and (d) with the Kerner equation.

with those calculated by the rule of mixtures, the inverse rule of mixtures and the Kerner equation.

As may be seen in both figures the inverse rule of mixtures predictions are closer than those of the rule of mixtures to the one phase compositions. From 60% $SCPE_{54}$ content G' starts to deviate strongly approaching the predictions obtained with the inverse rule of mixtures and the Kerner equation. Comparing 5.6 with 5.7 shows that that G' increases in the crosslinked samples with a more uniform pattern than before being crosslinked.

5.3.4 CLOUD POINT MEASUREMENTS

The CP curve for *D* in figure 4.41 (p. 136) is very similar to that reported by Hill [70] who studied a fractionated polyethylene with 50% w/w of chlorine and fractionated EVA with 45% w/w vinylacetate. As with *D* , Hill was also able to observe partial phase separation in the blends consisting of unfractionated material, especially in the compositions rich in $SCPE_{54}$. Figure 4.41 also shows that after crosslinking the CP curve appears to shift upwards.

In spite of the chemical similarity between the SCPEs in *D* and *A* , it may be seen

that their CP curves differ considerably; this behaviour may be attributed to the difference between $SCPE_{43}$ and $SCPE_{54}$ in M_n, polydispersity, thermal expansion coefficient, X_{23} and Q_{23} (see section 2.2 (p. 24)). As mentioned in sec. 5.3.2, p. 206-7, the miscibility with EVA_{45} increases with an increase in Cl in the chlorinated or sulphochlorinated polyethylene, therefore the CP curve for *D* should be higher than that of *A*. However the CP curve of *D* is around 5°C below that of *A*. This effect is probably due to the higher M_n and polydispersity in $SCPE_{54}$.

5.3.5 SIZE OF DOMAINS

Hill[70] observed that a similar system to *D* appeared to phase separate simultaneously by spinodal decomposition and nucleation and growth. In the present work, *D* and D_{DETA} showed exponential behaviour between 5°C to 35°C (figure 4.43 (p. 136)). The measured domain sizes (see table 4.21, (p. 137)) correspond to the lower and upper limit values of the lnI vs Q^2 plot; these results, which were obtained 30°C above the CP, show that after crosslinking the range of sizes is narrower and the upper limit smaller than before curing. As in *A* (sect 5.2.5 (p. 201)) this behaviour suggests that the crosslinks introduced are actually controlling the final size of the domains by restricting the diffusion of the mobile phase during phase separation. A comparison between the experimental domain sizes with those predicted with $\langle s^2 \rangle^{1/2}$, in table 4.22 (p. 137), show that the experimental data is at least four orders of magnitude larger than the results obtained with $\langle s^2 \rangle^{1/2}$, the reasons for this behaviour being the same given in sec 5.2.5 (p. 201-2). The values of γ_{ie} shown in the table were obtained using the Donatelli equation and the experimental domain sizes. Once again, as mentioned in section 5.2.5, these γ_{ie} values may be overestimated as the sizes of the domains when phase separation is taking place initially may be much smaller than those observed with the laser-SALS experiments.

5.3.6 SUMMARY

The main difference between *D* and *A* is that the SCPE in *D* ($SCPE_{54}$) has a higher chlorine content, higher M_n, and is more polydisperse than the SCPE used in *A*. These differences are reflected in the miscibility, mechanical and dynamic mechanical properties and phase separation mechanism. Swelling measurements showed that the whole composition range is lightly crosslinked. As in *A*, *D* behaves as a one phase system from D_{10} to D_{50}; above this composition the blend is partially miscible. *A* is

miscible up to A_{40} ; A_{50} shows some phase separation. The miscibility behaviour of the whole range of compositions of D_{DETA} is quite similar to that of the system prior to being crosslinked, the only difference being that the peaks in the partially miscible systems shift in position suggesting that certain intermixing takes place. Due to the higher values of E and E' for $SCPE_{54}$, the E and E' values for D are higher than those for A. After curing D, the E and E' generally increased.The CP curve in D is different in shape from that of A and appears at lower temperatures than in A, although the higher chlorine content in the $SCPE_{54}$ should have increased its miscibility with EVA_{45}, and raised the CP curve. The CP curve appeared at lower temperatures possibly because the $SCPE_{54}$ has higher molecular weight and is more polydisperse than $SCPE_{43}$. D and D_{DETA} seem to phase separate by nucleation and growth as exponential scattering behaviour was observed. As in A_{DETA} the domains in D_{DETA} decrease in size with phase separation.

5.4 SYSTEM $SCPE_{54}/PBA_{LMW}$ (SYSTEM *F*).

5.4.1 DEGREE OF CROSSLINKING

As PBA_{LMW} is a highly viscous liquid, swelling measurements were performed from the compositions with 40% $SCPE_{54}$ content onwards. Interpretation of these results should consider the limitations explained previously in section 5.2.1 (p. 188-9). The swelling results in table 4.25 (p. 141) were obtained using three calculation methods: Flory-Rehner, James-Guth and Herman equations. The M_c results obtained by any of these equations are similar and range between 16500 to 21800. As in section 5.3.1 (p. 205-6), these results suggest that the blend is lightly crosslinked.

5.4.2 MISCIBILITY BEHAVIOUR

Figure 4.44 (p. 143) and the results in table 4.24 (p. 140) show that F behaves as a one phase system up to 50% w/w $SCPE_{54}$ content. At 60%, although only one T_g is observable, the tanδ falls suddenly to almost half of the value for the previous composition. This behaviour suggests that the sample may have some microheterogeneity and may be quite close to being compatible [6]. From 70% $SCPE_{54}$ content onwards, two peaks inward shifted with respect to the T_gs of the pure components are observable (in F_{90} the peak corresponding to the phase of lower temperature is not clearly observable due to the small PBA content in the sample). As in

previous systems (sections 5.2.2 (p 191-5) and 5.3.2 (p. 206-7)) the semicompatible behaviour of F_{60} to F_{90} is probably caused by the existence at room temperature of a phase separated region in the ternary system SCPE54/PBA_{LMW}/MEK which may be caused by: (1) The stronger interaction of MEK with $SCPE_{54}$ than with PBA_{LMW} ($\Delta\chi$ effect). (2) The existence of an UCST crossing the LCST at room temperature at $\phi \sim$ 0.60 to ~ 0.90 which gives phase separated samples with a phase containing 59% $SCPE_{54}$, and a second phase with 98% $SCPE_{54}$. In spite of the plausibility of either of these two reasons it is not possible to prove them, since the experimental values for χ_{12} and χ_{13} have not been reported.

Chai [27, 137] and Walsh[27] found that the same PBA used here was immiscible with a CPE containing 48% W/W chlorine but miscible with chlorinated polyethylenes with 49.8 and 62.1% W/W chlorine. The first of these two is the most similar to *F*. As the results for this blend were not provided by the authors, a comparison between *F* and the system containing the CPE with 62.1% chlorine content (CPE20) is shown in table 4.25 (p. 141). The T_g values of the different PBA/CPE20 compositions are higher due to a 25°C difference between the T_g values of CPE20 and $SCPE_{54}$. In spite of this, the same behaviour was observed for F_{50}, F_{60} and their equivalents in this work. The results for the samples with 70% and 80% CPE20 were not reported by the authors, who observed only one T_g for the composition with 90% CPE20 content. It is possible that as in F_{90},where a very small hump was observed 50°C below the main T_g, a small transition,which may not have been detected with the Rheovibron, may also have been present 50°C below the T_g of 80°C reported for the 90% W/W CPE20 composition .

By comparing the T_g results for the polymer blend before and after crosslinking (see tables 4.24, 4.26, figures 4.4 and 4.45 (pp 140-144)) it may be seen that the T_g of the crosslinked blend compositions were very similar to those before crosslinking. However, a decrease in the intensity of the damping peak and an increase in E' were clearly observable (see also figures 4.49 to 4.51 (p 147-8). As mentioned in section 5.2.2 (p. 195) the decrease in the tanδ intensities with crosslinking is attributed [105] to an increase in the interaction between the polymers in the blend.

The results in tables 4.27 and 4.28 (p. 144-5) show that the two phases in samples F_{70} to F_{90} and F_{70DETA} to F_{90DETA} are richer in $SCPE_{54}$ than in PBA_{LMW}, containing around 60% $SCPE_{54}$ in the phase of low T_g and around 98% $SCPE_{54}$ in the phase of high T_g. By examining the mass balance results in both tables, it should be noted that intermixing between the two phases with crosslinking is not very obvious in this case.

5.4.3 STATIC AND DYNAMIC MECHANICAL PROPERTIES

As PBA_{LMW} is a highly viscous liquid, it was only possible to measure the Young's modulus (Y) for F from the compositions containing 60% $SCPE_{54}$ onwards and for F_{DETA} from 40% $SCPE_{54}$ onwards. In spite of this limitation in data (see figure 4.46 p. 145), it is clear that a rapid increase in Y occurs from F_{60} to F_{70}. After crosslinking, Y increased at each of the compositions studied. To confirm the behaviour observed in these static measurements, the data in figure 4.46 were compared with a plot of E' versus composition (see figure 4.47 (p. 146)). These data were obtained from the DMTA measurements at 20°C. The results in figure 4.47 show a smooth increase of E' with higher contents of $SCPE_{54}$. This figure also shows a small increase in E' with crosslinking.

Figure 4.48 (p. 147) contains the log E' vs T curves for $SCPE_{54}$ and $SCPE_{54DETA}$ and the logG' (G'= shear modulus) vs T for PBA_{LMW}. The PBA_{LMW} data is a log G' curve (its values are those of the right hand axis) because it was measured using the shearing attachment. Figure 4.48 illustrates the increase of E' for $SCPE_{54}$ after being crosslinked.This increase is most easily seen at the rubbery plateau. The logE' curves for F_{50} and F_{60} (figure 4.49 p. 147) show a rapid change through the only inflexion point present in these samples (F_{50} and F_{60} showed only one T_g). The presence of two inflexion points is quite clear from F_{70} onwards. The similarity between the curves for F_{80}, and F_{90} and $SCPE_{54}$ suggests that, in these samples, the phase containing almost pure $SCPE_{54}$ is the continuous phase. In F_{70} the phase containing 65% $SCPE_{54}$ may be the matrix as it is the phase in greatest quantity (see table 4.27 (p. 144)) and its logE' curve shows a behaviour midway between $SCPE_{54}$ and PBA_{LMW}. The number of inflections and shape of the curves for F_{50DETA} to F_{80DETA} are similar to those before crosslinking (see figures 4.49 and 4.50 (p. 147-8)). F_{90DETA} is similar to $SCPE_{54DETA}$ which suggests that the $SCPE_{54DETA}$ rich phase is the matrix in the sample. The comparison between some compositions before and after crosslinking in figure 4.51 (p. 148) clearly shows that G' increases with crosslinking, the increase being greater for samples with higher $SCPE_{54DETA}$ content.

Figure 5.8 shows that the experimental values of G', for the compositions behaving as one phase, increase rapidly from 10% to 40% $SCPE_{54}$ content and that these values lie within the rule of mixtures and inverse rule of mixture bounds. This indicates that their mechanical behaviour corresponds to that of miscible systems. From 50% $SCPE_{54}$ content onwards, the G' values are above these limits and also above the Kerner predictions for the phase separated compositions. According to Nielsen [133], this

behaviour may be due to a positive interaction between the components which increases with $SCPE_{54}$ content causing the experimental values well in excess of the theoretical predictions. The experimental values of G' for the two phase compositions are higher than those predicted with the rule of mixtures. The Kerner predictions in both figures, which follow closely the trend of the rule of mixtures calculations, are also lower than the experimental data; this difference may be due to: (a) these blend compositions may not meet the condition of being a well defined matrix phase with well defined inclusions and (b) as Dickie [148] points out, the Kerner predictions usually differ from the experimental data because the dependence of the modulus with concentration is always somewhat underestimated. Similar behaviour to that just described is also observed in figure 5.9 for F_{DETA}.

5.4.4 CLOUD POINT MEASUREMENTS

As shown in figure 4.52 (p. 149) the point at which the intensity vs temperature curve changes is very well defined in F and F_{DETA}. This behaviour is possibly due to the greater mobility of the components during phase separation, which may be a result of the relatively low values of M_n and T_g for PBA_{LMW} (M_n= 27000, T_g=-21°C). Of all the systems studied so far F and F_{DETA} give the clearest CP measurements and

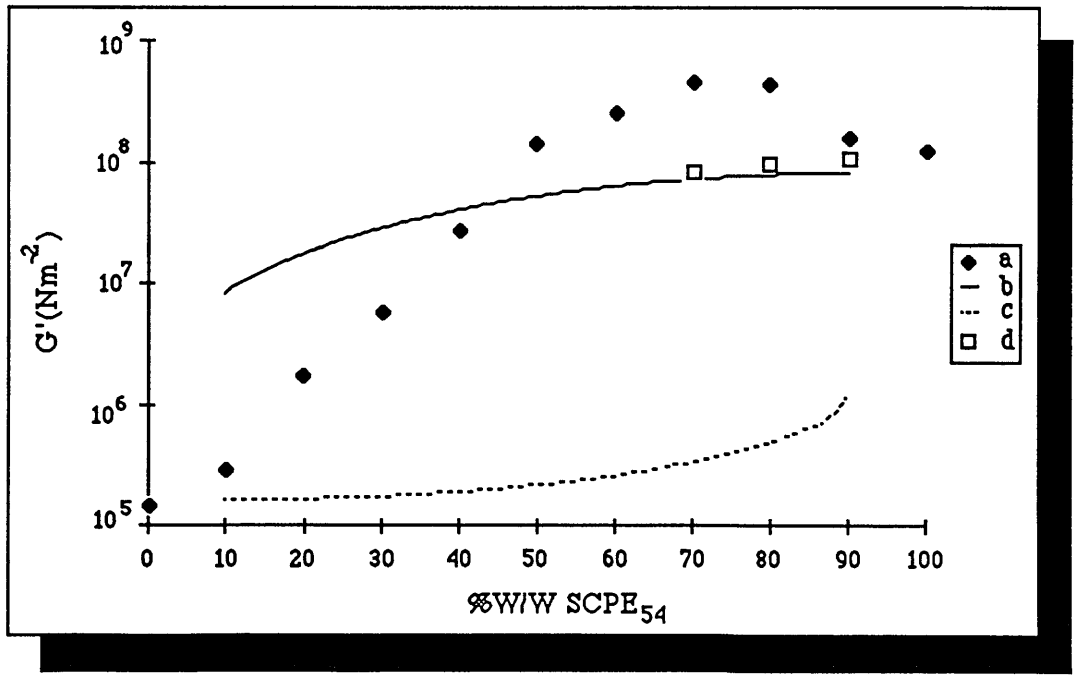

Figure 5.8 Comparison of G' at 0°C for system F obtained (a) experimentally, (b) with the simple rule of mixtures, (c) using the inverse rule of mixtures and (d) with the Kerner equation.

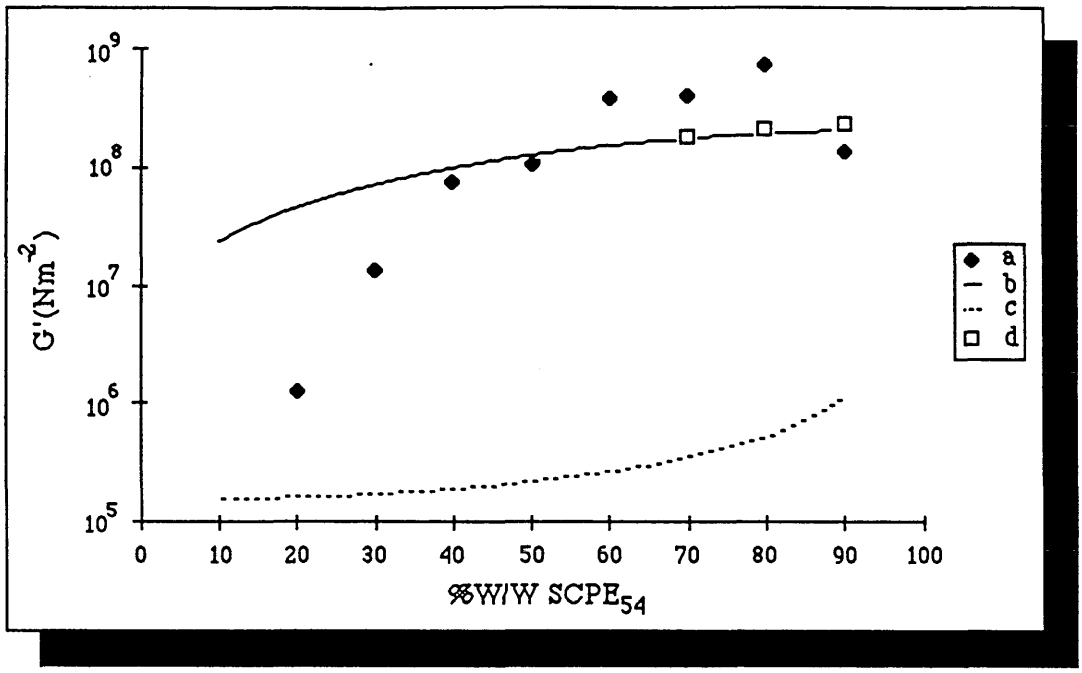

Figure 5.9 Comparison of G' at 0°C for system F_{DETA} obtained (a) experimentally, (b) with the simple rule of mixtures, (c) using the inverse rule of mixtures and (d) with the Kerner equation.

consequently the scatter in the results is somewhat decreased. Figure 4.52 shows once more a decrease in the slope after crosslinking. This behaviour is the same as that observed in section 4.2.4 (p. 119).

The CP curve for F in figure 4.53 (p. 150) is similar to that reported by Chai [27, 137] and Walsh[27] for PBA/CPE17 (CPE17 is a chlorinated polyethylene with 49.8% w/w chlorine content). As may be seen in both cases, as mentioned by Koningsveld et al [44], the skewness of the CP lies towards the polymer with greater polydispersity ($SCPED_{54}$, Z=20; PBA_{LMW}, Z= 6). The curve for F_{DETA} in figure 4.54 (p. 150) is similar in shape to that of F in 4.53 but shows an increase in the CP temperatures at nearly all compositions. Chai [27,137] and Walsh [27] working with PBA of higher $\bar{M}_n$ observed the same increase in the CP curves, an effect that together with the observed effect for F_{DETA} may be explained as in section 5.2.4, (p. 199).

5.4.5 SIZE OF DOMAINS

Figures 4.57 and 4.58 (pp 152-3) exemplified the I vs θ behaviour observed for the whole range of compositions of F. The presence of well defined peaks at certain value of θ indicates that the system phase separates by spinodal decomposition. As may be seen in these figures the peaks move to smaller angles as the temperature increases,

indicating that an increase in the correlation length (d) is taking place. Table 4.29 (p. 156) shows no significant variation in d throughout the whole range of compositions of the unmodified blend.

As shown in table 4.29 and figures 4.59 and 4.60 (p 155), after crosslinking, the preferred d decreases in general. For the samples F_{10DETA} to F_{50DETA} the peaks no longer appear, although they are observed in the unmodified samples 30°C above the CP of each sample. This suggests that d stays below the value of 0.752×10^4 Å that corresponds to the angle of 35°. From F_{60DETA} onwards, the peaks appear at higher temperatures than that of their unmodified counterparts. The decrease in d with crosslinking is consistent with the decrease in slope observed in the intensity vs temperature plots in figure 4.52, (p. 149). As explained in section 5.2.5 (p. 201) this suggests that during phase separation the crosslinks are acting as barriers to the diffusion of the uncrosslinked component (PBA_{LMW} in this case) [52]. It was mentioned earlier that the presence of peaks in the I vs θ plots suggest that F and F_{DETA} phase separate by spinodal-decomposition. To visualize the way F_{DETA} , a semi-IPN, phase separates it can be imagined that the crosslinked component ($SCPE_{54}$),which is already chemically interconnected does not suffer any change, while PBA_{LMW}, the uncrosslinked mobile component, forms an interconnecting second phase. This resulting interconnected phase may eventually break into small domain sizes as temperature increases. The presence of the crosslinks in the $SCPE_{54}$, may control d and eventually the size of the domains formed from this structure.

Comparing the d obtained experimentally with those predicted by $\langle s^2 \rangle^{1/2}$ in table 4.30 (p. 155) it may be seen that the $\langle s^2 \rangle^{1/2}$ values are four orders of magnitude smaller than the experimental values. The optical measurements which have been used, detect d when it has become large enough compared with the wavelength of the light used. The values of γ_{ie}, calculated with the Donatelli equation using the results for d in table 4.14, (p. 124) are large compared with those of liquids (water/CCl_4 = 45dn/cm at 20°C). As mentioned before (section 5.2.5, p. 201-2) this supports the suggestion that a powerful driving force for the amalgamation of small domains exists at the measurement temperature (30°C above the CP temperature of each sample). The large measured domain sizes in this table can therefore be seen to be physically reasonable.

5.4.6 SUMMARY

Swelling measurements showed that the whole range of compositions of F_{DETA} were lightly crosslinked. As in the previous systems, F was miscible up to a content of

50% $SCPE_{54}$, above this composition the blend was partially miscible. With crosslinking the miscibility behaviour was similar to that observed in the unmodified blend. Although expected, an increase in the T_gs of the cured samples was not observed, a possible explanation being that a small amount of unreacted *DETA* is plasticizing the samples. The CP curve for sample *F* obtained with the turbidimeter is similar to that shown previously for an equivalent system. The LCST in *F* is lying towards $SCPE_{54}$, that is the component with the highest polydispersity. After crosslinking, the CP curve shifted to a higher temperature. Equivalent results were also obtained with the laser-SALS. *F* seemed to phase separate by spinodal decomposition as peaks were clearly seen between 5° and 35°. From F_{10DETA} to F_{50DETA} these peaks were no longer observable in this angular range, from F_{60DETA} onwards the peaks appeared at higher temperatures.This behaviour suggests that d decreases after crosslinking *F*.

5.5 $SCPE_{54}/PBA_{HMW}$ (SYSTEM *G*)

5.5.1 DEGREE OF CROSSLINKING

The results in table 4.31 (p. 156) are quite similar to those obtained for the previous systems containing $SCPE_{54}$ (see sect.4.3.1 (p. 124-5) and 4.4.1(p. 138). Once again the M_{cSWELL} values (16400-18800) suggest that the blend is lightly crosslinked. Comparing these results with those for D_{DETA} and F_{DETA} in tables 4.15 (p. 125) and 4.25 (p. 141) the degree of crosslinking of $SCPE_{54}$ seems to be unaffected by the presence of the second component

5.5.2 MISCIBILITY BEHAVIOUR

In spite of having a PBA of higher $\bar{M}_n$ than that used in system *F* the miscibility behaviour of system *G* is quite similar to that of system *F*. Table 4.32 (p. 158) and fig. 4.62 (p. 161), show clearly the presence of only one T_g up to 60% $SCPE_{54}$ content. At this composition the value of tanδ decreases with respect to that of G_{50}, which suggests that the peak is broader or may have a very small peak hidden under one flank. The blend G_{60} is therefore on the boundary of miscibility behaviour. From G_{70} onwards the presence of two peaks which are moved towards each other in comparison to the T_gs of the pure components is clearly defined. Explanations for this semicompatible behaviour are the same as those given in 5.4.2 (p. 211-2). As in *F* a comparison between the results obtained by Chai [27,137] and Walsh [27] for the blend

PBA/CPE_{20} and those of G are presented in table 4.32 (p 158). The conclusions for this comparison are the same as those in 5.4.2.

After crosslinking, the T_gs for the whole compositon range of G_{DETA} remained similar to those of G (see figure 4.64 p. 164 and table 4.34 o 160). As explained before (section 5.2.2 (pp 195), this effect may be caused by unreacted curing agent acting as a plasticizer. As in previous cases a significant decrease in the damping peak together with an increase in E' (figures 4.68 and 4.69 pp 166-7) are clearly observable. This behaviour suggests an increase in the interaction between the polymers in the blend (see section 5.2.2 p.195). Exceptionally, G_{60DETA} gave a very much smaller tanδ peak than expected. This implies that the behaviour of this sample changes significantly on crosslinking and confirms that it happens to be almost exactly on the boundary of miscibility behaviour.

In a similar way to the previous system, tables 4.35 and 4.36 (p 162-3), show that the two phases present in G_{70} and G_{70DETA} onwards are richer in $SCPE_{54}$ than in PBA_{HMW}. The phase of lower T_g contains around 60% $SCPE_{54}$, the phase of higher T_g is almost pure $SCPE_{54}$. Tables 4.35 and 4.36 illustrate that after crosslinking intermixing between the two phases has taken place, for example in G_{90} the amount of $SCPE_{54}$ and PBA_{HMW} in the phase at 12°C increases from 0.07/0.06 to 0.15/10 with a simultaneous decrease of both components in the phase of higher T_g from 0.83/0.03 to 0.75/0.

5.5.3 STATIC AND DYNAMIC MECHANICAL PROPERTIES

As PBA_{HMW} is a highly viscous liquid it was only possible to measure Y for G and G_{DETA} from the compositions containing 60% and 50% $SCPE_{54}$ respectively. In fig. 4.64 (p. 164) a rapid increase in Y from G_{60} to G_{70} is observable. After crosslinking it was possible to see within the scatter that Y increased for each composition.

As in previous blends, the dynamic mechanical properties of G and G_{DETA} are dependent on the miscibility behaviour, and, if phase separated, on the morphology of the blend composition. Figure 4.65 (p. 164) shows the logE' vs T curves for $SCPE_{54}$, $SCPE_{54DETA}$ and the logG' for PBA_{HMW} (the values for logG', measured with the shearing attachment, must be read in the right hand axis). The curves in 4.66 (p.165) for G_{40}, G_{50} and G_{60} show that the logE' curves have a rapid change through the only inflexion point present in these samples. From G_{70} onwards the change is less rapid through the two inflexion points present. The similarity of the logE' curves for G_{80} and G_{90} indicates that in both cases the $SCPE_{54}$ rich phase is the matrix. In figure 4.64 the

logE' curves show again a rapid change through the only T_g present in G_{40DETA} to G_{60DETA}. G_{90DETA} shows a great similarity to $SCPE_{54DETA}$ which suggests that the $SCPE_{54DETA}$ rich phase in this sample is the continuous one. The comparison between the logE' curves for some compositions of G and G_{DETA} in figure 4.65 shows clearly that crosslinking increases E' especially at the rubbery plateau level.

The comparison of the experimental values of G' at 0°C with those obtained with the rule of mixtures, the inverse rule of mixtures and the Kerner equation are shown in figures 5.10 and 5.11. In G and G_{DETA} the experimental values of G' for the samples behaving as one phase are contained between the lower and upper bounds. For the two phase samples in G the experimental G' lie above the bounds predicted by the rule of mixtures and Kerner equation. In the case of the phase separated samples in G_{DETA}, the G'values lie closer to the values predicted by the rule of mixtures and Kerner equations. As mentioned in section 5.4.3 (p. 213-4) these deviations may be due to (a) a positive interaction between the components which increases with $SCPE_{54}$ content causing the experimental values well in excess of the theoretical predictions[133], (b) these blend compositions may not meet the condition of being a well defined matrix phase with well defined inclusions and (c) as Dickie [148] points out, the Kerner predictions usually differ from the experimental data because the dependence of the modulus with concentration is always somewhat underestimated.

5.5.4 CLOUD POINT MEASUREMENTS

Figure 4.69 shows that system G exhibits a very clear change in the intensity of the scattered light at the CP temperature. Similar behaviour was previously observed for system F (figure 4.52, p. 149). After crosslinking, the slope in these curves decreases. As explained before (see section 5.2.5, p. 201) this behaviour suggests that the rate of growth of the domains has decreased due to the crosslinks introduced which hinder diffusion during phase separation.

Figure 4.70 shows that the CP temperatures for system G differ from those obtained with the turbidimeter for F (figure 4.53, p. 150) and for PBA/CPE_{20} and PBA/CPE_{17}[27,137]. The CP curve data for G shifts to higher temperatures and the LCST moves towards the concentrations richer in PBA_{HMW}. As PBA_{HMW} has a higher M_n than the PBA used in blend F, its solubility with $SCPE_{54}$ should be lower and therefore CP temperatures should have occurred at lower temperatures than were observed for blend F. Experimentally, the CP temperatures were greater than those of blend F. This is a direct consequence of the high M_n of PBA_{HMW}, which introduces physical

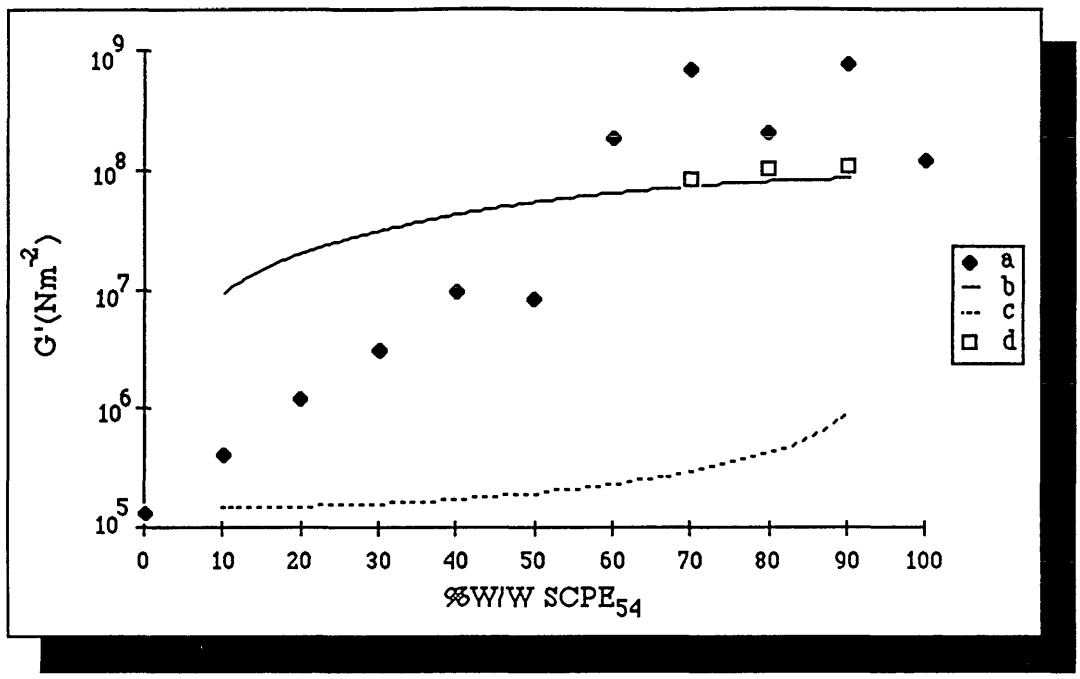

Figure 5.10 Comparison of G' at 0°C for system *G* obtained (a) experimentally, (b) with the simple rule of mixtures, (c) using the inverse rule of mixtures and (d) with the Kerner equation.

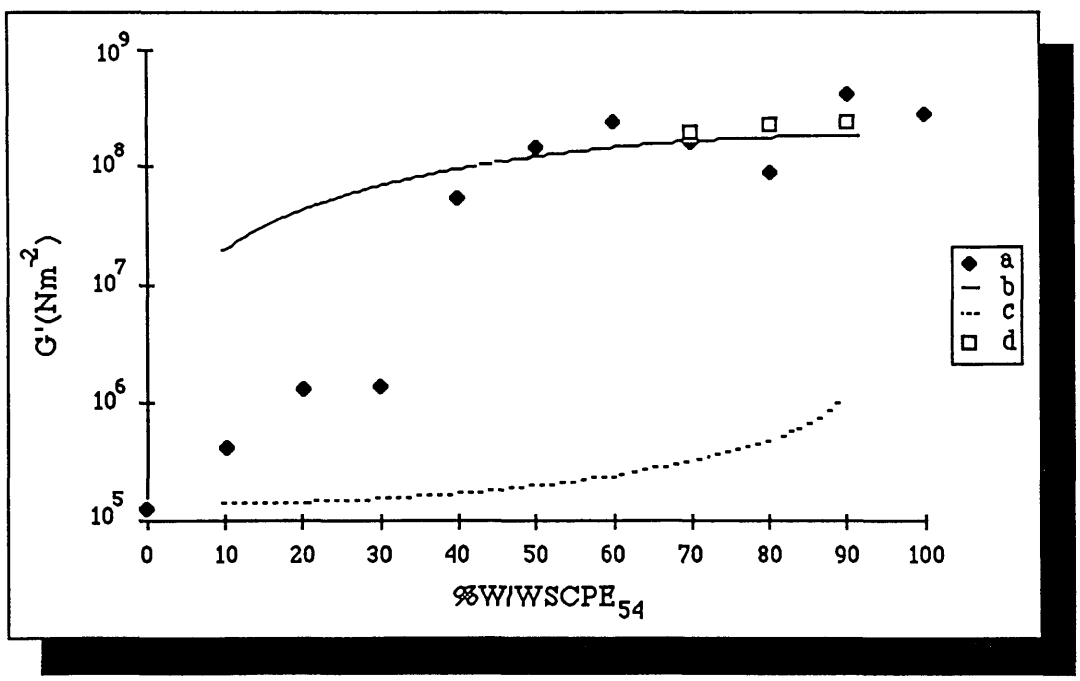

Figure 5.11 Comparison of G' at 0°C for system G_{DETA} obtained (a) experimentally, (b) with the simple rule of mixtures, (c) using the inverse rule of mixtures and (d) with the Kerner equation.

entanglements that hinder the diffusion while phase separation is taking place and completely mask any effect of solubility [52]. The increase in CP observed on crosslinking in other systems, such as *A* and A_{DETA} (section 5.2.4, p. 198) is a consequence of the same process of increasing physical entanglements. The shift of the LCST towards concentrations richer in PBA_{HMW} is due to the higher polydispersity of this polymer compared with that of $SCPE_{54}$; this observation is consistent with the predictions of Flory-Huggins model as extended by Koningsveld and coworkers[44].

Inspection of the data in figures 4.70 and 4.71(p. 167-8) shows that after crosslinking, the CP curve appeared at higher temperatures than before. This behaviour is, as explained before, due to a kinetic effect and not to a thermodynamic one (see 5.2.4 p. 199). The CP curve obtained for *G* with the laser-SALS in figure 4.72 (p. 168) shows a similar shape to that of the turbidimeter.The same figure shows an increase in the CP values for the only two crosslinked samples studied with this technique (G_{30DETA} and G_{40DETA}).

5.5.5 SIZE OF DOMAINS

In general, the whole range of compositions of *G* show a peak at high temperatures between the angular range of 5° and 35°, which suggests that the blend phase separates by spinodal decomposition. Figure 4.73 (p. 169) shows the I vs θ curves for G_{40}. The data at 132°C shows a peak at θ=7°. Although in the crosslinked samples only G_{30DETA} and G_{40DETA} were studied, it was possible to see that even at high temperatures peaks were not present in the angular range studied (see data for G_{40DETA} in figure 4.74, p. 170). It is quite possible, that in both cases, peaks may be appearing at larger angles which suggests that the correlation length decreased with crosslinking. In the absence of measured correlation lengths for G_{DETA}, the $\langle s^2 \rangle^{1/2}$ and the Donatelli equation could not be tested for this system.

5.5.6 SUMMARY

The swelling results for G_{DETA} showed that the whole range of compositions was lightly crosslinked. These results are similar to those obtained for the rest of the systems containing $SCPE_{54}$. In spite of having a PBA of higher $\bar{M}_n$ than that used in *F*, the miscibility behaviour of *G* was similar to that of *F* (the blend was miscible up to 50 %W/W $SCPE_{54}$ content). After crosslinking the miscibility behaviour remained practically the same as that observed in the unmodified blend. The mechanical and

dynamical mechanical properties for G and G_{DETA} are very similar to those previously observed for F and F_{DETA}. In the CP curves it was possible to see considerable differences between G and F : the shape of the curves was different, the CP curves in G shifted to higher temperatures and the LCST moved towards the higher concentrations of PBA_{HMW}. These dissimilarities are certainly a consequence of the difference in $\bar{M}_n$ and polydispersity between the PBA in both blends. After crosslinking it was possible to see an increase in the CP temperatures. The opposite effect was observed if an excess of the curing agent was introduced during the curing reaction. The presence of peaks in the range between 5° and 35° suggested that G phase separates by spinodal decompositon. After curing, peaks were no longer observable in this angular range and it is suspected that they may have appeared at larger angles, which implies that the correlation length decreases with crosslinking.

5.6 $SCPE_{54}$ / $PMMA_{1.4}$ (SYSTEM *C*)

5.6.1 DEGREE OF CROSSLINKING

The determination of the degree of crosslinking for C_{DETA} was performed by measuring the weight of undissolved residue. As figure 4.75 shows the percentage of undissolved material increases with the amount of $SCPE_{54}$ present in each composition, reaching a maximum of 20% for the sample with the highest $SCPE_{54}$ content. Swelling measurements were not used in this blend because, as mentioned in section 2.4.2.2, p. 37, these measurements are based on theories developed for rubbery materials, therefore they are not strictly applicable to C_{DETA} (C_{DETA} shows T_gs above room temperature).

5.6.2 MISCIBILITY BEHAVIOUR

In contrast with the rest of the systems studied in this work,*C* was the only one to show miscibility for the whole composition range. As shown in table 4.38 (p. 173) and figure 4.78 (p. 178) only one T_g was observed for all compositions. The broadness of the peaks for the whole composition range is due to the broad peak for $PMMA_{1.4}$ itself.The DSC data in figure 4.79 (p. 178), confirmed the Rheovibron and DMTA results.

As shown in table 4.38 (p. 173) the miscibility behaviour for *C* is very similar to that of the PMMA1.4/CPE16, system studied by Chai [26,137] and Walsh [26]. The

miscibility results for both systems agree with the negative values of ΔH_m, which they report for the oligomeric analogues chlorinated octadecane and oligomeric methyl methacrylate. As Chai and Walsh[26] suggested, the greater miscibility of $SCPE_{54}$ with $PMMA_{1.4}$ compared with that of PBA is related to the higher concentration of carbonyl groups that provide stronger specific interactions with the acidic hydrogen in the $SCPE_{54}$.

After crosslinking, the whole composition range still shows only one T_g (see table 4.39 and figure 4.79 pp 174 and 178 respectively) which confirms that the blend remains miscible after crosslinking. In contrast with all the previous systems, the values of the T_gs in this blend increased after curing.This may occur because the samples used were thinner than those studied previously and as the CP curve reported for this blend has a LCST around 120°C it was possible to eliminate the excess *DETA* by leaving the samples at 110°C for three weeks.

5.6.3 STATIC AND DYNAMIC MECHANICAL PROPERTIES

Figure 4.80 (p. 178) illustrates how the Young modulus (Y) varies with composition for C and C_{DETA}. As anticipated, an increase of the component with lower modulus ($SCPE_{54}$), causes the overall Y of the blend to decrease. A similar trend was observed for the crosslinked blend but with an overall increase in the Y values. Figure 4.81, p. 179, shows how the logE' curves shift downwards as the content of $SCPE_{54}$ increases ($SCPE_{54}$ has a lower E' than $PMMA_{1.4}$). All these curves show a rapid change of logE' through the only inflexion point, which corresponds to the T_g present at each composition. After crosslinking, figure 4.83, p. 180, shows an overall increase in the logE' curves. This increase was greater for the compositions with higher content of crosslinkable $SCPE_{54}$, so the curves were no longer parallel as shown before in figure 4.82 p. 179. In figure 4.84, p. 180, the comparison between the logE' for some compositions before and after crosslinking shows clearly the increase in E' with curing.

As in all the previous systems studied here, a comparison between the experimental G' values of C and C_{DETA}, obtained from E' at 80°C, with those predicted by the rule of mixtures and the inverse rule of mixtures was made. The results are shown in figures 5.12 and 5.13 for C and C_{DETA} respectively. As expected, in both cases, the experimental results are between the bounds predicted by the rule of mixtures and the inverse rule of mixtures for one phase systems.

5.6.4 CLOUD POINT AND DOMAIN SIZE MEASUREMENTS

As mentioned in section 4.6.4, p. 181, various methods were attempted in order to measure the CP temperatures and size of domains in C and C_{DETA}. Turbidimetry and laser-SALS were not successful. It was thought at the beginning that the reason for this behaviour could be a small difference in the refractive index of $PMMA_{1.4}$ and $SCPE_{54}$ For PMMA, η_{20^oC}=1.545. The η for $SCPE_{54}$ has not been reported in the literature. The most similar system which has been studied is high density polyethylene, η_{20^oC}=1.49. However, it was found that the size of the domains in the blend composition when phase separated was smaller than the wavelength of both radiation sources. DSC, the Rheovibron, DMTA and Phase Contrast microscopy were used in attempts to detect phase separation after quenching the sample. In practice, DSC gave ambiguous traces, the use of the Rheovibron and the DMTA were lengthy procedures and DIC was not powerful enough. TEM was not a very convenient technique because (1) the electron beam proved too intense, degrading very rapidly both polymers in the blend, and (2) it was not easy to control the temperature of the built in heating stage in the TEM. In spite of this, as shown from figures 4.85 and 4.86 (pp 181-183), it was possible to see phase separation occuring, by placing the sample directly onto the heating stage. The temperatures reported in these figures do not correspond to the point of phase separation but to the temperatures at which the heating stage was available. Figure 4.85(a) (p. 182) shows C_{60} at room temperature. Figure 4.85(b) (p. 182) shows C_{60} at 270°C, although the image was fading very fast, it was possible to see an interconnected structure which suggested that the sample was undergoing spinodal decomposition. Figure 4.86(a) (p. 182) shows that C_{80DETA} at room temperature is one phase, while figure 4.86(b) (p. 183) shows that this sample is two phases at 210°C.

The most successful of all the experiments were the SAXS. However as mentioned in 4.6.4 (p. 183), access to the X-ray source was restricted and so few samples were analysed. As shown in figure 4.87, p. 184, the type of information provided by this technique is the same as that obtained with the laser-SALS, however in the case of the X-rays it is possible to detect phase separation taking place when the size of the domains are only a few Å. Figure 4.87 shows the small peaks corresponding to parasitic scattering for C_{40} and C_{40DETA} prior to heat treatment. In contrast, C_{40} at 150°C and C_{40DETA} at 160°C, scattered the X-rays considerably, which is typical behaviour for two phase systems. As discussed in section 3.8, p. 89 a scattering pattern similar to that shown in figure 4.87 is typical for systems undergoing spinodal decomposition. From the position of the peak it was possible to work out the magnitude of the preferred

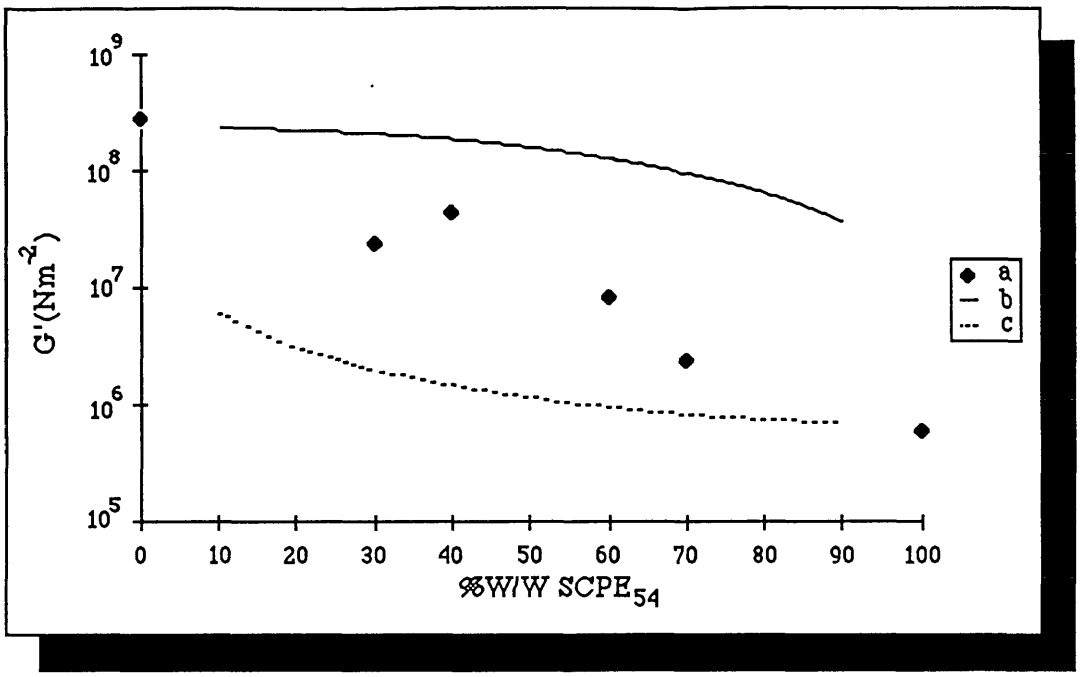

Figure 5.12 Comparison of G' at 80°C for system *C* obtained: (a) experimentally, (b) with the simple rule of mixtures and (c) using the inverse rule of mixtures.

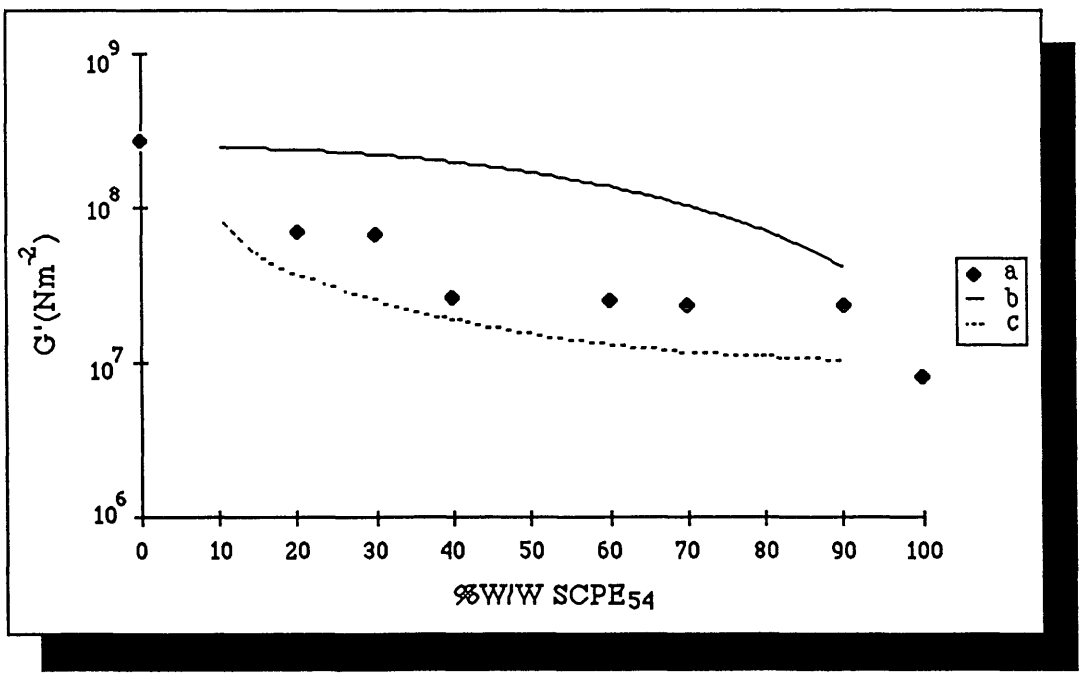

Figure 5.13 Comparison of G' at 80°C for system C_{DETA} obtained: (a) experimentally, (b) with the simple rule of mixtures and (c) using the inverse rule of mixtures.

value of the correlation length of the resultant interconnected structures using equation 3.20, p. 90. For C_{20} at 160°C it was 48Å, for C_{40} and C_{40DETA} at 150°C and 160°C it was 51Å. These results are very small in comparison with those of the other systems reported in this work. There are several possible explanations for this behaviour. The wavelengths of the radiation used for these scattering measurements are very much less than the wavelengths used in the optical scattering experiments previously discussed here, and much smaller correlation lengths are in principle detectable. It is therefore possible that phase separation in these samples is being detected at an earlier stage. Because of experimental limitations, X-ray observations were only made at discrete temperatures, rather than continuously. However, when a system which undergoes spinodal phase separation is heated to temperatures which lie inside the spinodal curve, the correlation lengths decrease as the experimental conditions move deeper inside the spinodal curve. The data collected may therefore be representative of points well inside the spinodal curve, rather than at the temperature of phase separation. Domains in C and C_{DETA} may always remain small: this may be because diffusion processes in this system are inherently slower than in other systems studied because of the side groups on the chains[48].

5.6.5 SUMMARY

Of all the systems studied in this work, C was the only one to show complete miscibility for the whole range of compositions. After curing, the system remained miscible, and in contrast with all previous results, it was possible to observe an increase in the T_g values for almost all compositions. As the system is not rubbery, crosslinking was determined by measuring the percentage of undissolved weight. The static and dynamic mechanical results reflected the state of miscibility in C and C_{DETA}. As the size of the domains of C and C_{DETA} are smaller than the wavelength of light it was not possible to use the Turbidimeter or the laser-SALS to measure the CP curves and so other techniques were employed of which X-rays was the most successful. This method showed the presence of scattering peaks in some samples undergoing phase separation, which suggests that they phase separated by spinodal decomposition.

CHAPTER 6
CONCLUSIONS

The main objective of this work was to study the effect on miscibility and phase separation behaviour when one of the components of a polymer blend is crosslinked.To undertake such a study, miscible blends containing an easily crosslinkable component were selected. The systems chosen were based on sulphochlorinated polyethylene (the crosslinkable polymer) of different chlorine content, mixed with polymers such as PVC, EVA, PBA and PMMA. A total of 6 blends were studied: system E_{50}, system *A* (these two systems are a mixture of an SCPE, containing 48% chlorine and 1% S as SO_2Cl groups ($SCPE_{48}$), with PVC or EVA_{45} respectively) and systems *D*, *C*, *F* and *G* (these blends contain an SCPE with 54% chlorine and 0.98% S as SO_2Cl ($SCPE_{54}$), which was mixed with EVA, PMMA and two PBAs of different molecular weight). All these systems are very similar to those studied by Walsh *et al* previously [24-29, 114, 137], the only difference being that the previous authors used various CPEs instead of SCPEs (CPEs have the same backbone as SCPEs but without the SO_2Cl groups).

Walsh *et al* [28, 29, 114] showed from ΔH_m calculations, that in blends similar to *A* and *D*, the miscibility behaviour was less favourable at 50% W/W of the chlorinated polyethylene and above. They also carried out miscibility experiments and made theoretical predictions on similar systems to *A*, *D* [28,29] and other systems containing different CPEs mixed either with PVC [24, 25], PBA[27] or PMMA[26]. On the basis of this work they concluded that these systems were miscible for the whole composition range [24-29]. In contrast with their results it was found, using a DMTA (a more sophisticated dynamic mechanical analysis instrument than the Rheovibron model used), that with the exception of *C*, all the systems studied in this work were miscible up to a 50 or 60% content of SCPE (only one T_g peak was observed), and partially miscible for the compositions rich in the chlorinated polyethylene. This behaviour was also observed previously by other authors [53, 136]. The disparity in results between the previous and present studies may be explained by the previous use of the older instrument. The model of Rheovibron used has two stages in order to scan temperatures below and above room temperature and so the transitions occurring in the range of 10 to 20°C might have been misinterpreted or not clearly observed. Another possible cause of misinterpretation of

the previous results is the low sensitivity of the older instrument in comparison with the DMTA: it is not always capable of detecting the transitions of phases present in low content, such was the case for the phase rich in EVA present in A_{90}, which was barely detected with the DMTA (see figure 4.19, p.109). It is interesting to mention that in contrast with previous studies [27], the shearing stress attachment of the DMTA allowed the study of the whole composition range of systems containing a viscous polymer such as the blends based on PBA and $SCPE_{54}$ (systems *F* and *G*).

It is thought that a possible reason for the semicompatible behaviour of the samples containing 50 or 60% SCPE in the blends *A*, *D*, *F* and *G*, is the existence at room temperature of a two phase region in the ternary system SCPE/2nd component/solvent. This behaviour may be caused either by : (a) a stronger interaction of the casting solvent (THF or MEK) with SCPE compared with that of the second component ($\Delta\chi$ effect) (previous IGC studies[25] showed that SCPE has a high proton donating strength with ketones, ethers, esters, tertiary amines and tertiary amides) or (b) the possible existence of a UCST curve crossing the LCST curve of these blends at two different weight compositions in the range where the blend is rich in SCPE. (In previous studies Nishi and Kwei [140] observed this behaviour in the PS / PVME system). In accordance with the previous theoretical studies of Walsh *et al* [25, 26, 28, 29], in the absence of a solvent, these blends should be one phase at room temperature for the whole composition range. Therefore after the solvent has been completely evaporated, the partially miscible blend compositions should in theory remix again; this does not occur due to the high viscosity of the components. Using the T_g values obtained with the DMTA and the Fox equation it was possible to estimate the composition of the two phases in the partially miscible samples. The calculations showed that each of these phases was itself a blend with appropriate composition of both polymers.

Using the Instron and the DMTA, the Young's moduli (Y) and the storage moduli (E') of these systems were determined for the whole range of compositions. For the mechanical measurements since no satisfactory extensometer was available to measure strain in these relatively weak specimens, strain measurements were deduced from the movement of the Instron crosshead. Such measurements are liable to a significant degree of error owing mainly to end effects. The Y results may therefore not be entirely precise, but since all specimens from the different materials were treated in the same way, there should be a reasonable basis for comparison. It was observed that the state of miscibility of these systems together with their composition are reflected in the values of E and E'. For the composition range behaving as one phase systems in *A*, *C*, *D*, *F* and *G* it was possible to simulate the experimental G and G' (obtained from the Y and E' results)

using the rule of mixtures and the inverse rule of mixtures.The behaviour of the two phase compositions was approximately predicted by the the Kerner equation which in general agreed with the experimental results to a certain extent but not completely. This reflects the complexity of the morphology in these systems.

The SCPE contained in the blends studied here was cured simply by letting the curing agent (usually diethylenetriamine (*DETA*)) diffuse through the film of the polymer blend. The resultant product may be considered a semi-IPN. As may be seen this method of preparing "semi-IPNs" is not a common one [4], but proved to be efficient and very convenient as it was possible in this way to cure the SCPE when it was already mixed with the other components in their polymeric state.

With respect to the miscibility of these polymers after curing, all the blends showed the same number of transitions as were present before being crosslinked. For the partially miscible compositions, a small shift in the position of the T_gs together with the mass balance analysis may be indicative of slight intermixing between the two phases present. After curing, phase separation was only observed in $E_{50insitu\ NH4OH}$. In this sample immiscibility may be caused by the oversaturation of the sample with NH_4OH and by the water content in this crosslinking agent. This behaviour clearly indicates that the selection of curing agent and of the experimental curing conditions are important as they may interfere with the miscibility of the blend.

The degree of crosslinking of the blends was determined using swelling measurements. Only in the case of system *A*, which behaves like a rubber, the degree of crosslinking was also determined from the G and G' values obtained from the mechanical and dynamical mechanical experiments. In the swelling experiments three different equations were used to calculate the degree of crosslinking: a modified version of Flory-Rehner equation [1, 71], the James and Guth [71] expression and the Herman equation [71, 144]. The effect of the presence of the second polymer in the network was considered by basing the calculations on the weight of the deswollen polymer (see section 4.2.1, p. 105). The results obtained using any of these equations suggested that all the blends studied were slightly crosslinked (large values of $\bar{M}_{cSWELL}$). These results agree with the small number of crosslinkable sites present in the polymer chain. In the static and dynamic mechanical measurements the presence of the second component was considered in the calculation of the shear moduli of the network (G_N or G'_N) using the four procedures explained in section 4.21.

As in the case of homopolymers, the mere fact of crosslinking a blend introduced several changes with respect to its original properties. In the blends studied here, an increase in G and G', a reduction in the viscous flow, and a decrease in the swelling by

solvents were observed. However, in contrast with what was expected, in general the T_g of these blends did not increase a great deal on crosslinking.This may indicate that the samples contain small amounts of unreacted crosslinking agent, which acts as a plasticizer, even though the samples were vacuum dried for a couple of weeks. Unfortunately, the drying process had to be carried out at relatively low temperatures (below T_g) to avoid phase separation in the blend, and it is well known that small molecules diffuse very slowly in polymer systems below T_g. There is no simple way of avoiding this problem, which complicates any chemical manipulation of polymers below T_g.

The phase separation behaviour of these systems was studied by measuring the cloud point temperature with scattering methods (when this method was not suitable for a particular blend, as was the case of $E_{50insitu}$ and C, then indirect methods were used). These measurements were carried out at a controlled heating rate (0.1°C/min using the turbidimeter and 1°C/min using the laser-SALS). In general the rate of increase of the intensity of the scattered light with temperature decreased and the CP shifted to higher temperatures for the crosslinked samples. This behaviour is attributed to a kinetic effect and not to a thermodynamic one. McMaster [39] demonstrated that thermodynamically the mutual solubility of both polymers should decrease with an increase in their molecular weight. However, Nishi and Kwei [140] observed that varying the molecular weight of PS/PVME, lowers the CP curve up to certain values of molecular weight, above which the molecular weight dependence of the CP curves levels off or even reverses; the same phenomena was observed in crosslinked blends. They suggested that in both cases a kinetic effect is causing such behaviour as the physical entanglements or chemical crosslinks introduced are restricting the diffusion of the polymers during phase separation.

Although not a very marked effect, it was possible to see that at least in some cases the size of the domains decreased after curing. For systems *A* and *D*, where a continuous decay as a function of θ was observed, a decrease in the range of the domain sizes was evident after crosslinking. For example, at 103°C, sample A_{70} showed sizes between $2x10^3$-$1x10^4$ Å, while A_{70DETA} showed at 150°C sizes between $3x10^3$-$9x10^3$Å. For blends *F* and *G*, where the presence of a peak was observed before curing, a significant decrease in the domain sizes for some compositions were observed on crosslinking; for example, F_{90} shows domain sizes of $3.70x10^4$ Å before curing, after curing of $2.36x10^4$ Å. This reduction in size suggests that the crosslinks are in some way constraining the diffusion of both components during phase separation (see figure 5.5, p. 203), therefore it is possible that if the cured samples had been left longer phase

separating, the size of the domains may have grown as large as those of the unmodified systems. This suggests that the reduction in size in the crosslinked samples is of kinetic origin. With respect to the phase separation mechanism followed by the blends before and after being crosslinked the following behaviour was observed. In contrast with previous work by Hill [70] in blends similar to *A* and *D*, these systems apparently phase separated before and after being cured by nucleation and growth, as scattering was observed to decay continuously as a function of angle. Scattering measurements in these systems were not taken to very high angles as the results decay smoothly with increasing angle and further peaks were unlikely. For systems *F*, *G* and*C* the presence of such a peak suggested spinodal decomposition. In F_{DETA} and G_{DETA} it was not possible to observe the peaks in the angular range studied, and it is quite probable that the peak may have shifted to larger angles.

Finally, it may be said that although the effects of crosslinking on the miscibility and phase separation behaviour of the systems studied in this work (*A*, *C*, *D*, E_{50}, *F* and *G*) have been studied in great detail, there are still many unresolved problems to consider:

(1) The turbimeter and the laser-SALS instruments used for this work were constructed in the department.The results obtained with this apparatus showed significant and somewhat variable scatter; some runs of particular samples gave much less reproducible results than others apparently because of variations in the performance of the equipment. The turbidimeter in particular suffers from variations in light source intensity and it would be improved by the addition of some means of monitoring these variations. Further refinement of these instruments would clearly improve their performance.

(2) Apart from the technical problems, some of the blends studied here are less suitable than others for optical scattering experiments. For example, the EVA_{45} used in systems *A* and *D* is highly branched [70] and its low mobility slows down the process of domain growth. This in turn causes the light scattering to increase more slowly with temperature and the exact transition point is therefore more dificult to observe (see figure 4.27, p. 120). A similar effect is seen sometimes on crosslinking.

(3) The turbidimeter and the laser-SALS detect phase separation when the clusters of each of the phases present become large enough compared with the wavelength of the light used, and the measured CP temperatures therefore do not necessarily correspond to the point at which small domains were first formed. If SAXS or SANS techniques had been available for the study of all systems discussed in this work, domains might have been detected at earlier stages of phase separation when they were very small. However,

as explained in section 5.6.4 p. 223, access to those techniques was very limited, and they were only used for systems C and C_{DETA} where all other methods had failed to detect phase separation. It would be very desirable for these techniques to be more readily available when any further work in this area is carried out.

(4) Electron microscopy has been widely applied to the study of blends, and undoubtedly provides a very direct method of visualizing morphology. Most of the samples studied in this work had relatively low T_gs and specialized apparatus would be required for sample preparation. In the absence of these facilities very little work has been done on the morphology of the multiphase samples. It is important to point out that any technique for studying miscibility and morphology in polymer blends which uses temperature scanning suffers an inherent limitation. The action of changing sample temperature may modify the miscibility behaviour and morphology of the sample before its initial state has even been determined. In principle microscopes avoid this problem but electron microscopy always involves electron beam heating of the sample. Optical microscopies are not always suitable because the domain sizes are too small.

(5) It would have been desirable to study the same blends using SCPEs of higher content in chlorine and crosslinkable groups. The higher chlorine content should have increased miscibility ; a range of crosslinkable group concentrations would have allowed the effect of various degrees of crosslinking on miscibility and phase separation behaviour to be seen.

(6) A more fundamental problem has been the initial assumptions made about the A, D, E_{50}, F and G systems. These systems were selected for study because it was originally believed that they were miscible and that the effect of crosslinking on a miscible system could be observed. As has been shown all of these systems are in fact more complex than was assumed and the study of each is made more difficult by the sudden change from single phase to partially miscibility at certain compositions. It will still be desirable to study a genuinely miscible system which can be crosslinked so that the effect of crosslinking on phase separation may be observed unambiguously.

All the materials studied in this thesis are examples of polymer blends which have become a very important class of polymer products in recent years. These materials are important because they allow the tailoring of the properties of polymer systems for specific applications. Crosslinking one or both components of a blend, forming semi-IPNs or IPNs, will modify the material properties and improve mechanical performance providing a blend with wider applications. This process also provides an attractive way of modifying the morphology of a system when phase separation occurs. There are many applications for this class of systems which include impact-resistant

materials, tough plastics, pressure sensitive adhesives, ion exchange resins, etc [4, 13]. Commercial SCPEs such as those produced by Du Pont de Nemours ("Hypalon") are used for wire and cable jackets, hoses, chemical resistant materials, etc.[160]: for all these applications the polymer has to be crosslinked. By blending SCPE with materials of lower T_g and retaining the ability to form crosslinked products, the useable range of these useful synthetic rubbers can be extended to lower temperatures: some of the systems reported in this thesis (*A*, *D*, *F* and *G*) show this effect over at least some of their composition ranges.

REFERENCES

1 Flory P.J., "Principles of Polymer Chemistry", Cornell University Press, 1953.

2 Paul D.R. and Newman S., "Polymer Blends", Academic Press, New York, 1978.

3 Olabisi O., Robeson L.M. and Shaw M.T., "Polymer-Polymer Miscibility", Academic Press, New York, 1979.

4 Sperling L.H., "Interpenetrating Polymer Networks and Related Materials", Plenum Press, New York, 1981.

5 Castellan G.W., "Physical Chemistry", Addison-Wesley Inc., Massachusets, 1971.

6 MacKnight W.J., Karasz F.E. and Fried J.R., in "Polymer Blends" (Paul and Newman Eds.), chapter 5 , Academic Press, New York , 1978.

7 Walsh D.J. and Rostami S., Adv. Polym. Sci., **70,** 119 (1985).

8 Krause S., in "Polymer Blends" (D.R. Paul and S. Newman, eds.), chapter 2, Academic Press, New York, 1978.

9 Allen G., Gee G. and Nicholson J.P., Polymer **2,** 8 (1981).

10 Koningsveld R., Kleintjens L.A. and Schoffeleers H.M., Pure Appl. Chem. **39,** 1 (1974).

11 Frisch K.C., Klemper D., Frisch H.L. and Ghiradella H., in "Recent Advances in Polymers Blends, Grafts and Blocks " (L.H. Sperling ed.) p. 375, Plenum, New York, 1974.

12 Huelk V., Thomas D.A. and Sperling L.H., Macromolecules **5,** 348 (1972).

13 Thomas D.A. and Sperling L.H., in "Polymer Blends" (Paul D.R. and Newman S. eds.), chapter 11, Academic Press, New York, 1978.

14 Nielsen L.E., "Mechanical Properties of Polymers and Composites", Dekker, New York, 1974.

15 Manson J.A. and Sperling L.H., "Polymer Blends and Composites", Plenum New York, 1976.

16 Schurer J.W., de Boer A., Challa G., Polymer **16,** 201 (1975).

17 Hammer C.F., Macromolecules **4,** 69 (1971).

18 Koleske J.V. and Lundberg R.D., J. Polym. Sci., Part A 2, **7,** 795 (1969).

19 Walsh D.J., and McKeown J.G., Polymer **21**, 1330 (1980).
20 Walsh D.J., and Cheng G.L., Polymer **25**, 495 (1984).
21 Walsh D.J., Higgins J.S., Doubé C.P. and Mckeown J.G., Polymer **22**, 168 (1981).
22 Grosse G. quoted in Friese K, Plaste Kaut. **12**, 90 (1965).
23 Kosai K. and Higashino T., Nippon Setchaku Kyokai Shi **11**, 2 (1975).
24 Doubé C.P. and Walsh D.J., Polymer **20**, 1115 (1979).
25 Doubé C.P. and Walsh D.J., European Polymer Journal **17**, 63 (1981).
26 Walsh D.J., Higgins J.S. and Chai Z. , Polymer **23**, 336 (1982).
27 Chai Z. and Walsh D.J., Makromol. Chem. **184**, 1459, (1983).
28 Walsh D.J., Higgins J.S. and Rostami S., Macromolecules **16**, 388 (1983).
29 Walsh D.J., Higgins J.S. and Rostami S., and Weraperuma W., Macromolecules **16**, 391, 1983.
30 Prigogine I., "The Molecular Theory of Solutions", North-Holand Publishing Co., Amsterdam, 1957.
31 Billmeyer F., Textbook of Polymer Science, 2nd Edition, New York, Wiley Interscience, 1971.
32 Hildebrand J.H., Ann. Rev. Phys. Chem. **32**, 1 (1981).
33 Flory P.J, J. Chem. Phys. **10**, 51 (1942).
34 Flory P.J., Disc. Faraday Soc. **49**, 7 (1970).
35 Flory P.J., Orwoll R.A., and Vrij A., J. Am.Chem. Soc. **86**, 3507 (1964).
36 Flory P.J., Orwoll R.A., and Vrij A., J. Am.Chem. Soc. **86**, 3515 (1964).
37 Flory P.J., J.Am. Chem. Soc. **87**, 1833, (1965).
38 Eichinger B.E. and Flory P.J., Trans. Faraday Soc. **64**, 2035 (1968).
39 McMaster L., Macromolecules **6**, 760 (1973).
40 Sanchez I. and Lacombe R., J.Phys. Chem. **80**, 2352, (1976).
41 Sanchez I. and Lacombe R., Polymer Letters **15**,71 (1977).
42 Sanchez I., in" Polymer Blends", (Paul D.P. and Newman S., eds.) chapter 3, Academic Press, New York, 1978.
43 Huggins M.L., Ann. N.Y. Acad. Sci. **43**, 1 (1942)
44 Kwei T.K. and Wang T.T., in "Polymer Blends" (Paul D.P. and Newman S., eds.) chapter 4, Academic Press, New York, 1978.
45 Cahn J.W., J. Chem. Phys. **42**, 93 (1963).
46 Cahn J.W., Trans. Met.Soc. **242**, 166 (1968).
47 Cahn J.W., Acta Met. **9**, 795 (1961).
48 Hill R.G., Tomlins P.E. and Higgins J.S., Polymer **26**, 1708 (1985).

49 Shaw M.T. in "Polymer Blends and Mixtures" (Walsh D.J., Higgins J.S. and Maconnachie A., eds.) chapter 4, NATO ASI series E, Applied Sciences-89, Martinus Nijhoff Publishers London, 1985.

50 Runt J. and Rim P.B., Macromolecules **15**, 1018 (1982).

51 Gashgari M.A. and Frank C.W., Macromolecules **14**, 1558 (1981).

52 Robard A., Patterson D. and Delmas G., Macromolecules **10**, 706 (1977).

53 Webb D., Ph. D. Thesis, Imperial College, (1985).

54 Shultz A.R. and Mankin G.I., J. Polym Sc., Polymer Symposia N^{o} 54 ,341, (1976).

55 Hughes L.J. and Brown G.L. J. Appl. Polymer Sc. **5**, 580 (1961).

56 Walsh D.J. and Sham C.K., Polymer **25**, 1033 (1984).

57 Yu H., Adv. Chem. Ser. **99**, 1, (1971).

58 Shaw M.T. in "Polymer Blends and Mixtures" (Walsh D.J., Higgins J.S. and Maconnachie A., eds.) chapter 3, NATO ASI series E, Applied Sciences-89, Martinus Nijhoff Publishers London, 1985.

59 Karasz F.E., in "Polymer Blends and Mixtures" (Walsh D.J., Higgins J.S. and Maconnachie A., eds.) chapter 2, NATO ASI series E, Applied Sciences-89, Martinus Nijhoff Publishers London, 1985.

60 McNaughton J.L. and Mortimer C.T., "Differential Scanning Calorimetry", Connecticut, the Perkin Elmer Corporation, p 2-4[n.d.].

61 Lombardi G., "For a Better Thermal Analysis", V.1, Academic Press, New York (1970).

62 Bair H.E., Polym. Sci. Eng., **10**, 247 (1970).

63 Ferry J.D., "Viscoelastic Properties of Polymers", 3rd Edition, New York, John Wiley and Sons, Inc., 1980.

64 Polymer Laboratories, "Dynamic Mechanical Thermal Analyser", Instruction Manual, Polymer Laboratories Ltd., Shropshire, England (1982).

65 Stein R.S., in" Polymer Blends", (Paul D.P. and Newman S., eds.) chapter 9, Academic Press, New York, 1978.

66 VEB Carl Zeiss JENA DDR, "Pereval Interphako Interference Microscope", Instruction Manual.

67 Nippon Kogaku K.K.,"Nikon Optiphot Labophot Phase Contrast equipment 'Ph'", Instructions, Nippon Kogaku K.K., Tokyo (1982).

68 McMaster L.P., Adv.Chem. Ser. **142**, 43 (1975).

69 Higgins J.S., in "Polymer Blends and Mixtures" (Walsh D.J., Higgins J.S. and Maconnachie A., eds.) chapter 5, NATO ASI series E, Applied Sciences-89,

Martinus Nijhoff Publishers London, 1985.

70 Hill R., Ph.D. Thesis, Imperial College (1985).

71 Miller M.L., "The Structure of Polymers", Reinhold, New York, 1968.

72 Encyclopedia of Polymer Science and Technology, N.Y., John Wiley and Sons, Inc., 1966, V. 4 , pp 331-7.

73 Collins A.E., Bares J. and Billmeyer F.W., "Experiments in Polymer Science", Wiley -Interscience Publication (1973).

74 Stevens M.P., "Polymer Chemistry, and Introduction", Addison-Wesley, Massachusetts, 1975.

75 Maynard J.T., Johnson P.R., Rubber Chemistry and Technology, part 4, **36** 963 (1963).

76 Busse W.F., Billmeyer F.W., J.Polym. Sc. **12**, 599 (1954)

77 McAlevy A., U.S. Patent 2,586,363 (Feb 19, 1952).

78 Brooks R.E., Strain D.E., McAlevy A., India Rubber World **128**, 54 (1953).

79 Busse W.F., Smook M.A., India Rubber World **128**, 348 (1953).

80 Smook M.A., Roche I.D., Clark W.B., Youngquist O.G., India Rubber World **128**, 54 (1953).

81 McAlevy A., U.S. Patent 2,732,257 (Nov 8. 1955).

82 Switzer J.L., U.S. Patent 2, 963, 382 (Dec 6, 1960).

83 Nersasian A., King K.F. and Johnson P.R., Proc. Fourth Rubber Technol. Conf., London (1962) p 124.

84 Walsh D.J., Plastics and Rubber: Materials and Applications, **1,** 17, 1976.

85 Flory P.J., P. Chem. Revs. **35**, 51 (1944).

86 Treloar L.R.G., "The Physics of Rubber Elasticity", Clarendom Press, 2nd Ed., Oxford 1958.

87 Gumbrell S.M., Mullins L. and Rivlin R.S. Trans. Faraday Soc. **39**, 1495 (1953).

88 Mullins L., J. Appl. Polym. Sc., **2**, 257 (1959).

89 Ellis B. and Welding B.N., Techniques of Polymer Science SC1 Monograph 17, 35 (1962).

90 Pinner S.H.," A practical course in Polymer Chemistry ", Pergamon Press, 1961.

91 Moore C.G. and Watson W.F., J. Polym. Sc., **19**, 237 (1956).

92 Flory P.J., Ind. Eng. Chem. **38**, 417 (1946).

93 Flory P.J. and Rehner J., J. Chem. Phys. **11**, p 512, 521 (1943).

94 Sperling L.H., in "Recent Advances in Polymer Blends, Grafts and Blocks (L.H. Sperling, ed.) p 93, Plenum New York, 1974.

95 Yenwo G.M., Sperling L.H., Pulido J., Manson J.A., Conde A. Polym. Eng. Sci., 17(4), 251(1977).

96 Donatelli A.A., Sperling L.H. and Thomas D.A., in "Recent Advances in Polymer Blends, Grafts and Blocks (L.H. Sperling, ed.) p. 375, Plenum New York, 1974.

97 Sperling L.H., Chiu T.W. and Thomas D.A., J. Appl. Polym. Sci. **17**, 2443 (1973).

98 Thouhsaent R.E., Thomas D.A. and Sperling L.H., J. Polym. Sci. Part C **46**, 175 (1974).

99 Kim S.C., Klempner D., Frisch K.C. and Frisch H.L., Macromolecules **10**, 1187 (1977).

100 Scarito P.R. and Sperling L.H. Polym. Eng. Sci. **19**, 297 (1979).

101 Thiele J.L. and Cohen R.E., Polym. Eng. Sci., **19**, 284 (1979).

102 Kim S.C., Klempner D., Frisch K.C., Frisch H.L. and Ghiradella H. Polymer Eng Sc. **15**, 339 (1975).

103 Donatelli A.A., Sperling L.H. and Thomas D.A., J. Appl. Polym. Sci. **21**, 1189 (1977).

104 Allen G., Bowden M.J., Blundell D.J., Hutchinson F.G., Jeffs G.M. and Vyvoda J., Polymer **14**, 597 (1973).

105 Allen G., Bowden M.J., Blundell D.J., Jeffs G.M., Vyvoda J. and White T., Polymer **14**, 604 (1973).

106 Allen G., Bowden M.J., Lewis G., Blundell D.J. and Jeffs G.M., Polymer **15**, 13 (1974).

107 Donatelli A.A., Sperling L.H., Thomas D.A., Macromolecules **9**, p 671,676, 1976.

108 Yenwo G.N., Manson J.A., Pulido J., Sperling L.H., Conde A. and Devia-Manjarrés, J. Appl. Polym. Sci. **21**,1531 (1977).

109 Kim S.C., Klempner D., Frisch K.C., Radison W. and Frisch H.L., Macromolecules **9**, 258 (1976).

110 Dickie R.A. in "Polymer Blends" (D.R. Paul and S. Newman, eds.), chapter 8, Academic Press, New York, 1978.

111 McQueen D.M., U.S. Patent 2,212,738 (August 27 1940).

112 March J., "Advanced Organic Chemistry: Reactions, Mechanisms and Structures", McGraw Hill Kogakusha Ltd., Tokio, 1968.

113 Chai Z., Lianghe S., Sheppard R.N., Polymer, **25**, 368 (1982).

114 Rostami S., Ph.D. Thesis, Imperial College (1983).

115 Tedder J.M. and Nechvatal A., "Basic Organic Chemistry", p 138, John Wiley and Sons, London, 1966.
116 Sham C.K., Ph.D. Thesis, Imperial College (1985).
117 More J.C., J. Polymer Sc.Part A, **2**, 835 (1964).
118 Benoit H, Grubisic Z., Rempp P., Decker D. and Zillioux J., J. Chim. Phys. **63**, 1507 (1966).
119 Grubisic Z., Rempp P. and Benoit H., J. Polym. Sci. B 5, 753 (1967).
120 Du Pont Instruments, Instruction Manual 990, Thermal Analyser and Modules, Wilmington, E.I. Dupont de Nenmours and Co. [n.d.]
121 Walsh D.J., and Cheng G.L., Polymer **23**, 1965 (1982).
122 Walsh D.J. and Singh V.B., Makromol. Chem. **185**, 1979 (1984).
123 Walsh D.J., Rostami S. and Singh V.B., Makromol. Chem **186**, 145 (1985).
124 Singh V.B., Ph.D. Thesis Imperial, College (1985).
125 Graham N.B., Nwachuku N.E. and Walsh D.J., Polymer **23**, 1345 (1982).
126 Rivlin S. and Saunders D., Phil. Trans.Part A 2 **43**, 251 (1951).
127 Rivlin S. and Saunders D., Trans. Faraday Soc. **48**, 200 (1952).
128 Annual Book of ASTM Standards, Part 35, 1978.
129 Prentice P. and Hashemi S., J. Materials Science **19**, 518 (1984).
130 Hodgkinson J.M., Ph.D. Thesis, Sheffield City Polytechnic (1980).
131 Chong C.L., Ph.D. Thesis, Imperial College (1981).
132 Tobolsky A.V., Kotz D., Takahashi M. and Schaffhauser R.J., Polymer Sci. Part A **2**, 2749 (1964).
133 Nielsen L.E., Predicting the properties of mixtures: Mixture Rules in Science and Engineering, Marcel Dekker Inc., New York ,1978.
134 Brandrup J. and Immergut E.H., Polymer Handbook, 2nd Ed., New York, John Willey and Sons., New York, 1975.
135 Dobbin C.J.B., Rudin A. and Tchir M.F., J.Appl. Polym. Sci., **25**, 2985 (1980).
136 Rostami S., Private communication (1986).
137 Chai Z., Ph.D. Thesis, Imperial College (1982).
138 Rueda G. and Hill R (unpublished results).
139 Zeman L. and Patterson D., Macromolecules **5**, 513 (1972).
140 Nishi T. and Kwei T.K., Polymer **16**, 285 (1975).
141 Hsu C.C. and Prausnitz J.M., Macromolecules **7**, 320 (1973).
142 Doubé C.P., Ph.D. Thesis, Imperial College (1979).
143 Bell J., J. Polym Sci. A 2, **6**, 417 (1970).

144 Hermans J., J. Polym. Sci., **59**, 191 (1962).
145 Hermans J., J. Polym. Sci., Part A 2, 4931 (1964).
146 Murayama T. and Bell J.P., J.Polym. Sci. Part A 2, **8**, 437 (1970).
147 Fried J.R., Ph. D. Thesis, Univ. of Massachusetts (1976). As quoted in ref. 60.
148 Dickie R.A., J. Appl. Polym. Sci. **17**, 45 (1973).
149 Nielsen L.E., Mechanical Properties of Polymers and Composites, Marcel Dekker Inc., New York, 1974.
150 Allen G., Bowden M.J., Todd S.M., Blundell D.J., Jefffs G.M., Davies W.E.A., Polymer **15**, 29 (1974).
151 Livingston D.I. and Brown J.E., Proc. 5th Internat. Congr. Rheol., **4**, 25 (1970).
152 Hofmann W., Vulcanization and Vulcanizing agents, Maclaren and Sons Ltd., London (1967).
153 Allard D., Fontanille M. and Prud'Homme R.E., J. Polym. Sci. **22**, 3827 (1984).
154 Frisch H.L., Klempner D., Yoon H.K., Frisch K.C., Macromolecules **13**, 1016 (1980).
155 Binder H. and Frisch H.L., J. Chem. Phys. **81**, 4 (1984).
156 Ellis T.S., Karasz F.E. and ten Brinke G., J. Appl. Polym, Sci. **28**, 23 (1983).
157 Coleman M.M., Serman C.J. and Painter P., Macromolecules **20**, 226 (1987).
158 Sperling L.H. and Ferguson K.B., Macromolecules **8**, 691 (1975).
159 Fujimoto J., Ugo R., Yamamoto Y, Todome K., Proc. ICCMVI and ECCM2 (Mathews F. L., Buskell N.C.R., Hodgkinson J.M., Morton J., Editors) Elsevier Applied Science, London, p 5.134 (1987).
160 Hypalon, information brochure, Wilmington, E.I. Dupont de Nenmours and Co. [n.d.]